Paleolimnology of Lake Iznik (NW Turkey) during the past ~ 31 ka cal BP

Dissertation

zur

Erlangung des Doktorgrades (Dr. rer. nat.)

der

Mathematisch-Naturwissenschaftlichen Fakultät

der

Rheinischen Friedrich-Wilhelms-Universität Bonn

vorgelegt von

Patricia Angelika Roeser

aus

Wiesbaden

Bonn, 2013

Angefertigt mit Genehmigung der Mathematisch-Naturwissenschaftlichen Fakultät der Rheinischen Friedrich-Wilhelms-Universität Bonn

1. Gutachter: Prof. Dr. Thomas Litt / Rheinische Friedrich- Wilhelms- Universität Bonn

2. Gutachter: Prof Dr. Kurt Friese / Martin-Luther-Universität Halle-Wittenberg

Prüfungsdatum der Promotion: 26.03.2014
Erscheinungsjahr: 2014

Index

List of Figures

(Simplified legends)

Chapter 7

Chapter 8

List of Tables

Abbreviations

AD	Anno Domini
AMS	Accelerator Mass Spectrometry
ASi	Amorphous Silica
BA	Bolling/Allerod event
BC	years Before Christ
BSi	Biogenic Silica
CIA	Chemical Index of Alteration
CFB	Carbonate Free Basis
CoDa	Compositional Data
DO	Dansgaard-Oeschger events
ΔGS	Grain Size Difference: parameter that expresses relative changes of ASi
GI	Greenland Interstadial
GS	Greenland Stadial
HE	Heinrich Event layers
HS	Heinrich Stadials
IMF	Iznik Mekece Fault
IZN	Iznik
ka BP	thousand years before present (radiocarbon age)
ka cal BP	thousand years before present (calibrated radiocarbon age)
LC	Long Core (herein retrieved with piston core equipment)
LGM	Last Glacial Maximum
LOI_t	Loss on Ignition at Temperature *t*
MAR	Mass Accumulation Rate
masl	meters above sea level
mcd	meters composite depth
mblf	meters below lake floor
MIA	Mineralogical Index of Alteration

MIS	Marine Isotope Stage
MS	Magnetic Susceptibility
NAF(Z)	North Anatolian Fault (Zone)
NGRIP	North Greenland Ice Core Project
OD	Older Dryas
OSL	Optical Stimulated Luminescence
pdf	probability distribution function
PT	Pre Treatment method
PU	tie points
SC	Short Core (herein retrieved with gravity core equipment)
SEM	Scanning Electron Microscope
Sf	Sediment facies
SI	*Système International d'unités*
SR	Sedimentation Rate
SS	Smear Slides
SU	Sedimentary Unit
TC	Total Carbon
TEFZ	Thrace-Eskisehir Fault Zone
TIC	Total Inorganic Carbon
TOC	Total Organic Carbon
UV	Ultraviolet
VPDB	Vienna Pee Dee Belemnite
XRD	X-ray Diffraction
XRF	X-ray Fluorescence
YD	Younger Dryas event

1.) Introduction

The city of Iznik, situated in the Marmara Region between the Mediterranean and the Black Sea water bodies, was founded by Antigonus in 316 BC, later to be renamed to Nicaea, which remained its name through the Byzantine era (Hellier, 1993). During the early development of eastern church, the city hosted two ecumenical councils (Hellier, 1993). The city of Iznik is also known for its ceramic production, which had prospered during 15th and 16th centuries (Highet, 1999). Many of the tiles produced in Iznik decorate Ottoman buildings and mosques, still to be seen in Istanbul today. The city of Iznik lies at the margins of the lake with same name, Lake Iznik – formerly known as Lake Askania (Akbaygil et al., 2003).

Lake Iznik (Figure 1.1), Pliocene/Pleistocene in age, is located between four geographic realms – namely the Pontic Coast, the Aegean, the Southern Balkans, and the Anatolian Plateau (French, 1967). Lake Iznik has been believed to react sensitively to climate, as the basin shows past lake level stands (Ikeda et al., 1991a). Moreover the sedimentation processes within the lake are potentially related to dry and/or humid phases (Franz et al., 2006). Thus, Lake Iznik sedimentary record is a key paleoclimate archive.

Precipitation distribution over Turkey is strongly affected by local factors, e.g. orography (Sariş et al., 2010), whereas the seasonal rainfall in the Marmara region is mainly controlled by the strength of influence of Mediterranean cyclones (Sariş et al., 2010). Further large-scale atmospheric circulation patterns of the regional climate are directly influenced by the North Atlantic realm (Kwiecien et al., 2009; Lamy et al., 2006), and during winter by the Siberian High Pressure System (Pross et al., 2009). The Northern Hemisphere climate presents instable character (e.g. Dansgaard et al., 1993; Wolff et al., 2010), and typical millennial scale fluctuations known for the North Atlantic have been recognized in the paleoclimate records of the eastern Mediterranean, Pontic Coast and Aegean (Bahr et al., 2008; Fleitmann et al., 2009; Kwiecien et al., 2009; Müller et al., 2011; Stein et al., 2010). Additionally, the Marmara region acts as a bridge for past human migration routes between Europe and Asia, and is a specially interesting site for the debate how farming spread into Europe (Roodenberg et al., 2008).

Open issues for the nature of climatic change through the late Pleistocene to Holocene in the eastern Mediterranean concern specially the synchroneity of events, and the contribution of evaporation and precipitation to the regional hydrology, e.g. effective moisture and

temperatures for the Last Glacial (Roberts et al., 2001; Tzedakis, 2007). Lake Iznik basin holds the geological evidence for past lake level stands (Ikeda et al., 1991a; Öztürk et al., 2009). However, a timely tied history of long-term variations in Iznik lake levels was still missing and might in future contribute to the understanding of regional water balance.

Regional geological records for the Marmara region focus on the Holocene or cover distinct Pleistocene time intervals (Kazanci et al., 2010; Leroy et al., 2002; Mudie et al., 2007; Mudie et al., 2002; Schwab et al., 2009). Further records focus on the adjacent Pontic Coast (Fleitmann et al., 2009; Kwiecien et al., 2009; Shumilovskikh et al., 2012), or Aegean regions (Pross et al., 2009; Pross et al., 2007). A continuous, well dated and high-resolution record for the Marmara region, covering the Pleistocene to Holocene transition, was still missing. In a recent field work, Pleistocene sediments have been recovered from the bottom of Lake Iznik for the first time, and these are also under investigation within the present thesis. In order to identify and differentiate site specific signals from responses to climatic forcing it is essential to gain a detailed understating on the functioning of the lacustrine system.

The alkaline Lake Iznik is subject to endogen carbonate production during the dry summer periods, most likely triggered by aquatic productivity (Franz et al., 2006; Ülgen et al., 2012; Viehberg et al., 2012). A correlation between the carbonate accumulation within sediments deposited in the lake and relative dry climatic periods was established for the last century (Franz et al., 2006), and recently extended to the late Holocene (Ülgen et al., 2012). A reconstruction of evolution of limnological processes and geochemical conditions of Lake Iznik for middle to early Holocene, and specially the late Pleistocene, was missing. Such a paleoenvironmental reconstruction can be inserted into a climatic frame, and contribute to the understanding of past climate in the Marmara region.

1.1) Objectives

The overall objective of this thesis is to obtain a paleoenvironmental reconstruction in terms of climatic forcing for the Marmara Region, during the late Pleistocene and Holocene. To achieve such objective it is indispensable to gain independent knowledge on the significance of geochemistry and mineralogy in the limnological context.

Thus, main aspects considered in the present work are (1) lake evolution under the light of sedimentary, geochemical and mineralogical processes, (2) endogen lacustrine carbonate production/formation, and (3) association between limnological evolution and the climatic

forcing. The main hypothesis is that the endogen carbonate production in Lake Iznik is registering climatic signals throughout the late Pleistocene and Holocene.

Figure 1.1: Lake Iznik and Marmara region (a) location in continental context and main hydrological systems for Black Sea and northeastern Mediterranean, black triangles label volcanoes Vesuvius and Santorini; (b) and (c) LANDSAT image, zone 35T, composite TM3 (Blue), TM4 (Green), TM5 (Red). Satellite images obtained from USGS Landsat gallery and processed digitally with software SPRING v5.2 (Camara et al., 1996); (b) yellow lines indicate northern, central and southern branches of North Anatolian Fault – NAF, after Yilmaz et al. (2010) (c) main inflow rivers and outflow from Lake Iznik in white; grey dashed lines indicate wave cut scarps after Ikeda et al. (1991a), for details see section 2.2; yellow circles and dots indicate main cities, and villages surrounding the lake: Keramet, Boyalica, Cacirka, Narlica, Sölöz and Gölyaka; white dots indicate coring locations.

1.1.1) Project frame

This work is inserted in the Collaborative Research Centre – CRC 806 / Our way to Europe, which is founded by the German Research Foundation – DFG. The CRC 806 is concerned with human mobility in the late Quaternary, and possible climatic driving forces. Hence, the sub-projects of CRC 806 are clustered geographically along potential human migration routes, and have climatic and/or archeological motivations[1]. Within this framework, this thesis is inserted in the overhead project 'B4 – Climatic evolution of the Marmara Region during the past 50,000 years'.

An independent complementary investigation was conducted during a scientific stay at Istanbul Technical University – ITU, at the division for Eastern Mediterranean Centre for Oceanography and Limnology – EMCOL, between June and August 2012. This investigation was supported by a scholarship from the German Academic Exchange Service – DAAD (Reference D12/40880). This study focused on methodic aspects of grain size analysis and the interference of amorphous silica on the determination of siliciclastic grain size for lacustrine sediments. The outcomes of this complementary investigation (chapter 7) proved essential to the paleoenvironmental reconstruction within this thesis.

1.2) Thesis Outline

This thesis is divided into four main Parts, which contain (I) a description of state of the art and methods, (II) presentation of the results and their discussion, as well as discussion of methodic aspects, (III) interpretation of results in a limnologic context and (IV) a synthesis under the light of a paleoenvironmental reconstruction. Within these four parts, the individual chapters are outlined as follows.

Chapter 2 is a literature review that contextualizes Lake Iznik from a geological and limnological point of view.

The materials and methods are presented in *chapter 3*. An important milestone presented in this chapter is a composite profile which was defined through lithofacies and chemostratigraphy. Building on this composite profile, the lithology and geochronology as framework for this thesis are set within *chapters 4* and *5*, respectively. The composite profile, as well as selected results from chapters 4 and 5 have been partially published (Roeser et al.,

[1] www.sfb806.de

2012). Still, *chapter 5* presents an improved and discussed age model, which further adds eight novel radiocarbon ages to the previously published model.

For the chapters within parts II and III, the scientific goal is to resolve how sedimentological and geochemical aspects in question register environmental changes.

Thus, *Chapter 6* outlines in detail the basic geochemical and the mineralogical evolution of Lake Iznik sediments, using compositional data analysis (CoDa) as major tool, therefore CoDa analysis is briefly introduced and reviewed.

Chapter 7 is the outcome of a two month scientific stay at EMCOL - Istanbul Technical University. The chapter deals with the grain size analysis for the sediments of the investigated profile. One significant methodic aspect is the evaluation of the interference of amorphous silica in siliciclastic grain size analysis for lacustrine carbonate sediments. From a paleoenvironmental perspective the aim of the chapter is to determine how grain size can be used to infer on past lake levels.

Chapter 8 deals with paleolimnological aspects from Lake Iznik, such as productivity, early diagenetical processes and water column mixing.

Within *Chapter 9* the carbonate accumulation expresses the unique character of Lake Iznik as aragonite depositing milieu. The origin of the carbonate phases is discussed, and stratigraphic changes in their concentrations and occurrence are associated to specific stages of lacustrine physical processes and hydrology.

Chapter 10 synthesizes the key aspects from sedimentology, mineralogy and geochemistry, which are inserted into the millennial climate event stratigraphy for the Northern Hemisphere, and correlated to regional records.

2.) Iznik basin and the Marmara region

2.1) Geological settings

Turkey consists of a number of tectonic blocks or microcontinents, which are separated by suture zones of different ages. The juxtaposition of three tectonic units makes up the Pontide mountain region. These are the Istranca Massif, located at Thrace; the Istanbul Zone and the Sakarya Zone (Okay, 1989) (Figure 2.1). Lake Iznik locates in the central zone of the Sakarya continent, adjacent to the Armutlu peninsula (Figure 2.2 b) – an elevated and southward tilted fault block, which is margined by the gulf of Izmit to the north, and the gulf of Gemlik to the south (Yilmaz et al., 2010). The Sakarya and the Istanbul zones have independent pre-Jurassic histories and are separated by the Intra-Pontide suture; the Paleozoic of the Istanbul Zone being located to the North, and the Karakaya Complex of the Sakarya zone to the south (Okay, 1989). They probably were juxtaposed at pre-Santonian times (Özcan et al., 2012). The Paleozoic section of the Istanbul zone extends without major brakes from the Ordovician to the Carboniferous; consisting of sedimentary rocks deposited on an Atlantic-type passive continental margin (Okay, 1989). While the Istanbul zone is marked by the absence of metamorphism and major deformation, the Sakarya Complex was subject to variable metamorphism, and has a strongly deformed Triassic basement – the Karakaya Complex (Okay, 1989).

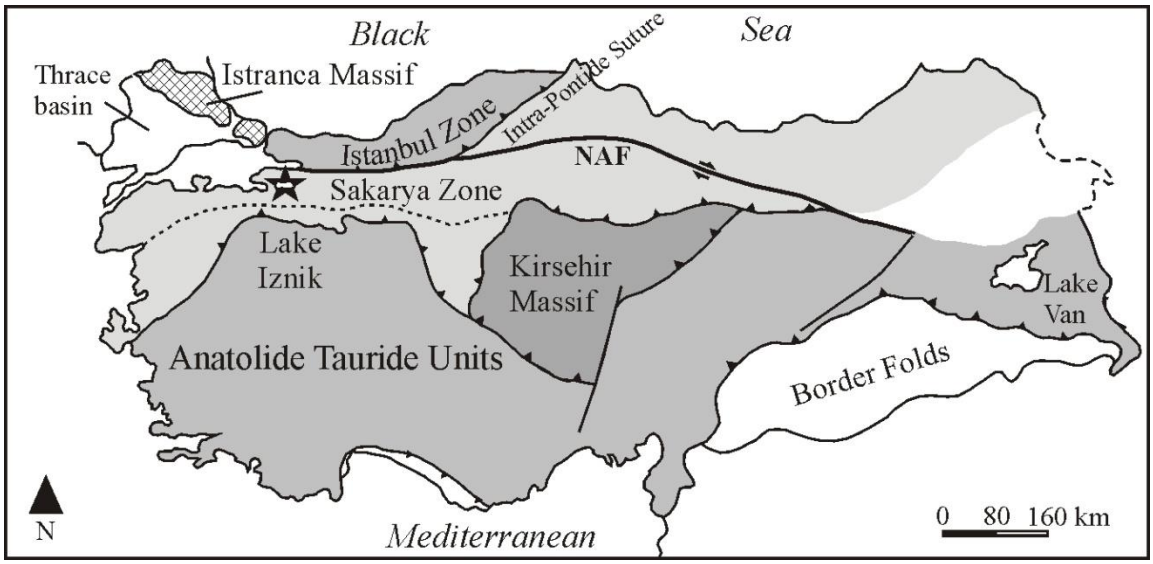

Figure 2.1: Turkey subdivided in its main tectonic blocks, after (Okay, 1989). Black star indicates location of Lake Iznik.

The Pre-Miocene basement of the region is formed by Late Paleozoic, Mesozoic and Paleogene formations. Miocene sediments unconformably overlay basement rocks, and are covered by Pliocene and Quaternary units (Öztürk et al., 2009). The evolution of Iznik Lake basin is contemporary to the Pontides fold orogenesis (Appendix A2.1), and the tectonic Iznik Lake basin was filled with Tertiary marine sediments (Wester, 1989). Non-marine sediments of Pliocene age occur in the northern part of the Orhangazi plain, but these are unrelated to the present regime of Lake Iznik (Ikeda et al., 1991a). The complete basin has been lifted to circa 80 m above sea level (Yaltirak et al., 2011).

Two mountain ranges limit the Iznik Basin; the Samanli mountains to the north, east and west, and the Katirli mountains to the south. The Samanli mountains consist of Paleozoic shales (Figure 2.2), with general low permeability and isolated lenses or layers of crystalline limestone (marble) (Wester, 1989). The Katarli mountains at the south consist mainly of Eocene flysh – conglomerates of sandstone, claystone, limestone, and marl – with low permeability (Wester, 1989). At the western and eastern edges of the Lake there are the Orhangazi Plain, and Iznik Plain respectively. These Tertiary and Quaternary plains consist of up to 250 m deposits of gravel, sands and clays (Wester, 1989).

2.1.1) North Anatolian Fault

Two different fault systems formed the present structural configuration of the Marmara region, during two different periods. In the early neotectonic period (early Miocene-early Pliocene) the Thrace-Eskisehir Fault Zone (TEFZ) was active, and during the late neotectonic period (Pliocene-Recent) the North Anatolian Fault (NAF) and its segments emerge. The basins in the Marmara region which were opened by the NAF (Figure 1.1) also have the features of the former fault zone (Leroy et al., 2002; Yaltırak, 2002; Yaltirak and Alpar, 2002).

The NAF extends from the town Karliova, eastern Turkey – in the vicinities of Lake Van (Figure 2.1), as a parallel contour to the southern Black Sea coast, reaching the Gulf of Saros in the northern Aegean Sea in the west, passing through the Marmara region where it subdivides into three segments (Figure 1.1 b) (Şengör et al., 2005; Yaltirak and Alpar, 2002). The Marmara region was subject to North Anatolian shear related deformation in a wide zone already in the late Miocene. Although having its onset in west Turkey at about 11 Ma, the NAF reached the region not earlier than circa 200 ka ago (Şengör et al., 2005; Yilmaz et al., 2010).

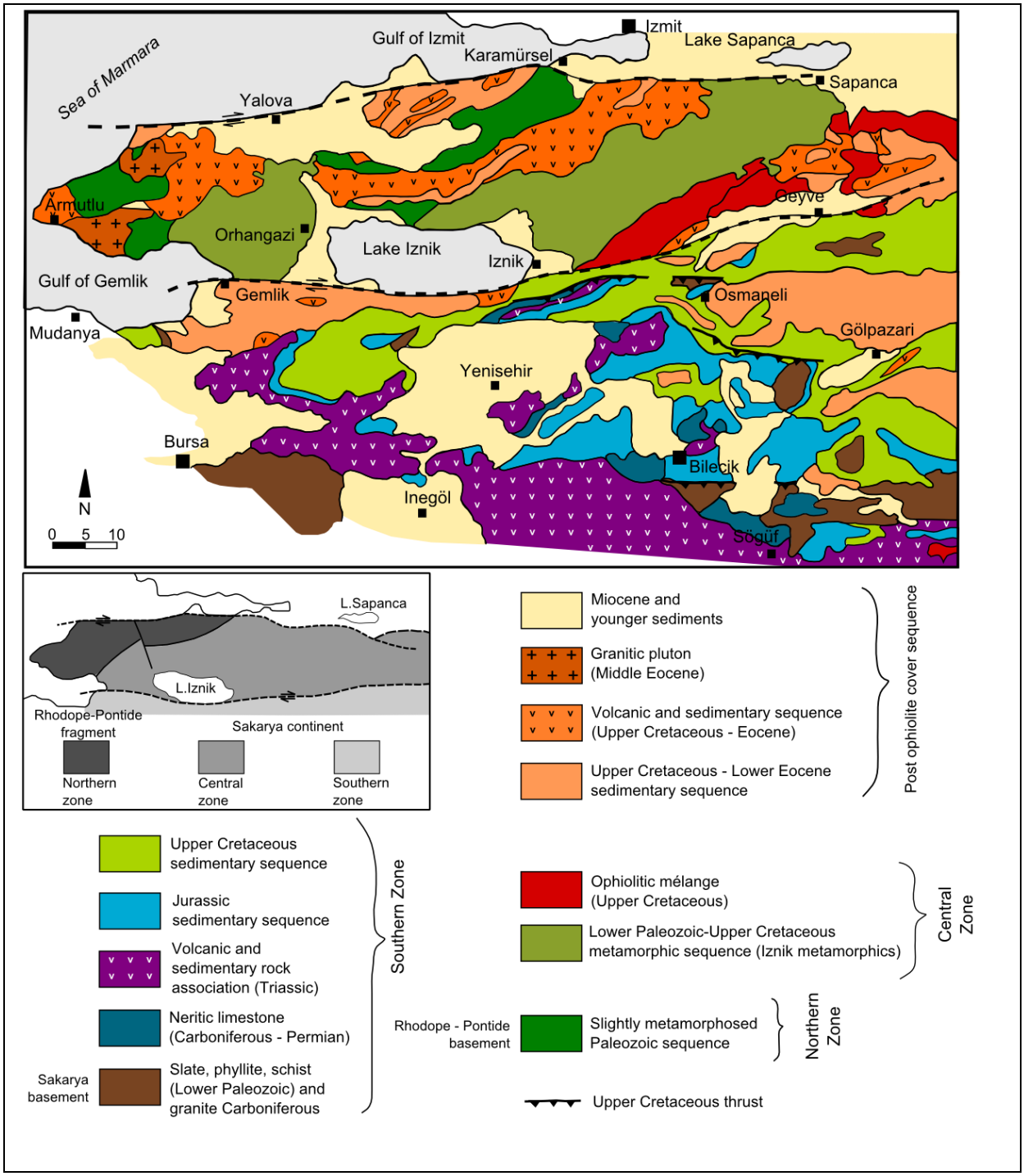

Figure 2.2: (a) Geological map of the Iznik Lake Basin and surroundings (b) main tectonic zones from the region. Original figure modified after (Yilmaz et al., 1995).

The NAF represents the seismically active boundary between the Eurasian (or Black Sea) plate to the north and Anatolian plate to the south (Şengör et al., 2005). Its activity in the Marmara region is reflected by historical[2,3] and recent earthquakes (Ikeda et al., 1991b;

[2] Historical earthquakes that had direct impact on the town of Iznik, former Nicea, happened in the years of AD 123, between AD 358 and AD 368, AD 740, and AD 1065 (Nagels, 1970).

Nagels, 1970), for example registered in sediments of Hersek coastal lagoon, in the gulf of Izmit[4] (Bertrand et al., 2011). Recently, the earthquakes of August and November AD 1999 in Izmir (Schwab et al., 2009; Şengör et al., 2005; Yilmaz et al., 2010) loaded the Marmara segment of the fault, thus a major event is expected for the next half century (Şengör et al., 2005).

The Iznik Lake basin has subsided under the control of the middle strand of the NAF, which limits the southern shore line of the lake, namely the Iznik-Mekece fault – IMF (Ikeda et al., 1991a; Yaltirak and Alpar, 2002). Geomorphological evidence indicates that the basin has been tilting progressively, most likely to slip on the Iznik Mekece Fault (Ikeda et al., 1991a).

2.2) Geomorphology and Iznik past lake levels

A narrow valley separates the Iznik Lake Basin from the southeastern bay of the Sea of Marmara (gulf of Gemlik). This valley conducts the Karsak river, outlet of the lake, flowing westwards. Along the shores of Lake Iznik, quaternary alluvial fans occur in front of the faults, especially in the Iznik plain, in the south of the Orhangazi plain, and along the southern coast of the lake (Ikeda et al., 1991a; Yaltirak and Alpar, 2002).

At least three wave-cut scarps mark the northern shoreline margin of the basin (Figure 1.1 c) (Ikeda et al., 1991a). Their heights vary in the different sections (east, central, western) of the shore, between 15 – 25 meters for the lowest scarp, 65 – 80 meters the middle scarp, and 115 – 125 meters for the highest one (Ikeda et al., 1991a). Due to southward tilting of the basin during the Quaternary, the height difference in between the scarps does not imply progressive lowering in the amplitude of lake level variations, on the contrary, a differential uplift could lead to progressively higher wave cut scarps with increasing age (Ikeda et al., 1991a).

The wave-cut scarps relate either to past high lake level stands or to individual slow transgression epidoses (Ikeda et al., 1991a). Considering lake level variations described for the Konya basin in central Anatolia, and under the assumption that there is a regional relationship between these two sites, it was inferred that the lowest wave-cut scarp from Lake Iznik is of circa 18 ka BP in age (uncalibrated), corresponding to the last high stand at the former mentioned basin during the Last Glacial Maximum – LGM (Ikeda et al., 1991a). In contrast to this suggestion, a second hypothesis is that the LGM lake level of Lake Iznik was a

[3] Ikeda et al. (1991) correlated a surface rupture zone in the Mudurnu Valley to a historical earthquake of AD 1668 which caused severe damage between the cities of Bolu and Erzincan in an area of circa 100 km x 600 km. Relative more recent events happened AD 1939 and AD 1967.
[4] These are the events of AD 740, AD 987, AD 1509 and AD 1719.

low stand at circa 40 meters below the present lake level, characterized by a submarine terrace (Öztürk et al., 2009). However, both hypotheses lack corresponding age measurements.

Additionally, lacustrine sediments in the form of terraces (including marked cross beddings) exist up to 80, and 120 meters above the present lake level (Ikeda et al., 1991a; Öztürk et al., 2009). Öztürk et al. (2009) suggest that the changes in lake level have more influence on the elevation of the terraces, than the faults observed around the lake with their morphological influence on the depositional sequence. Also Nümann (1960) assumes that the lake level must have reached 30 up to 35 meters higher in relation to the present, sometime during the Quaternary. However, given the tectonic influence on the basin, it is possible that the lake level was never much higher relatively to the level it presents today (Niessen, 2010).

Along with the wave cut scarps and lake level terraces, a third feature described in detail by Ikeda et al. (1991a) is a sequence of subparallel beach ridges, formed by reworking of sediments on the western coastal plain of the lake. They are located below the lowest wave-cut scarp, which represents the last high stand (or slow transgression) of the lake. Hence, the beach ridges were formed during the regression after the last high stand, and are inferred to be of postglacial age (Ikeda et al., 1991a).

Besides the observation of submarine terraces pointing to lake level lowstand in a geological timeframe (Öztürk et al., 2009), lower lake levels in historical times are evidenced in marginal regions by Roman ruins, which become visible on certain lowstands (Nümann, 1960). Furthermore, recent investigation on beach rocks[5] at the lake's southern margins, dated different formation strata of these beach rocks to a range of Holocene times[6] via Optical Stimulated Luminescence - OSL dating (Erginal et al., 2012a). Additionally two ages in a parallel study yielded two Pleistocene glacial to postglacial ages, of 18.48 ± 1.93 ka BP and 20.29 ± 2.07 ka BP (Erginal et al., 2012b). Even with an uncertainty of about 10% for the OSL ages; given the specific coastal environment required for the formation of these beach rocks one can only conclude that the lake level was at a level similar as today.

2.2.1) Timing for a Iznik-Marmara connection

The geomorphological and structural settings of the region make it tempting to infer on possible alternative paleo-connections between the Black Sea and the Sea of Marmara, through the pathways of the basins of the modern Lake Iznik or Sapanca. For instance, at

[5] polygenic conglomerates cemented with carbonate
[6] The lowermost level was dated to 4.23 ± 0.57 ka BP and the uppermost to 0.706 ± 0.081 ka BP

circa 250 ka BP - before tectonic uplifting, particularly the lowlands such as Lakes Iznik and Sapanca were invaded by sea waters (Pfannenstiel, 1944). One possible connection between the Black Sea and the Marmara Sea, alternative to the Bosphorous, would pass trough part of the Sakarya valley, and then the Sapanca basin (Gürbüz and Leroy, 2010).

A late Quaternary/Holocene connection between the Iznik Basin and the gulf of Gemlik has been proposed by Nazik et al. (2011), based on the findings of foraminifera in the superficial sediments of these lakes. However, Yaltirak et al. (2011) exclude any possible connection between the gulf of Gemlik and Lake Iznik crossing the Karsak sill (85 masl) during the late Pleistocene until present. This conclusion is reached by extrapolating the present tectonic uplift rates in the region, associated with the global sea level changes for the past half million of years. If at some point in geological times such connection existed, it was not possible before at least 380 ka BP (Yaltirak et al., 2011). However, the consideration of an average tectonic uplift for such long time frames has to be considered with caution (Nazik et al., 2012). Still, according to this discussion, for the time frames under investigation within this work, the sedimentary record of Lake Iznik is not directly influenced by a water connection to the Sea of Marmara or Black Sea.

2.3) Regional climate

The Marmara region lies in between four different environments and climatic zones: the Pontic Coast, the Aeagean, the Southern Balkans, and the Anatolian Plateau (French, 1967). Regarding its general humidity, the region is subject to higher precipitation than the Aegean, but lower rates than in the southern Black Sea coast (French, 1967; Gokturk et al., 2011; Sariş et al., 2010). While the Pontic Coast is subject to precipitations of circa 1000 to 1200 $mm.year^{-1}$ due to the humidity originated from the Black Sea, the rainfall over Lake Iznik is in the order of 600 $mm.year^{-1}$ (Fleitmann et al., 2009; Gokturk et al., 2011; Türkes, 1996). On a rather regional scale, moisture of the Black Sea-Marmara complex is derived from evaporation of the Mediterranean and Atlantic seas, and the rainfall distribution is controlled by orographic cooling (Mudie et al., 2002).

The Marmara region presents typical Mediterranean type climate, expressed by an inverse pattern between averages in humidity and temperature. For instance, in Figure 2.3 the bars indicating the rainfall in the region show that most of the precipitation falls during the colder seasons - from October to April, peaking in December with a rapid onset of a wet winter. During the hot summer, when average temperatures are higher than $20^{o}C$, rainfall decreases

gradually, reaching its minima in July and August (Sariş et al., 2010; Wester, 1989). Within the Iznik Lake Basin, there is a difference of about 20 mm in monthly average rainfall between the cities of Orhangazi (west) and Iznik (east), the west basin being subject to higher amounts of precipitation (Wester, 1989). This is observed also in long term meteorological time series (Franz et al., 2006). In relation to Turkey, the Marmara region presents a moderate to high magnitude precipitation regime, which is the combined result of frontal and orographic rains (Sariş et al., 2010). In winter, the prevailing northeast winds, bring Black Sea humidity (Appendix A2.2). After passing over the Naldöken elevation, the air currents which lost part of their humidity bring solely slight amount of precipitation to the northeast region of the basin. Passing over the lake, the air masses regain humidity, which is then precipitated on the western Orhangazi region (Wester, 1989). But, besides local factors, precipitation patterns across Turkey seam to depend on the strength of influence of Mediterranean cyclones. Such large-scale atmospheric circulation patterns are responsible for controlling precipitation in the winter months also for the Marmara region (Sariş et al., 2010).

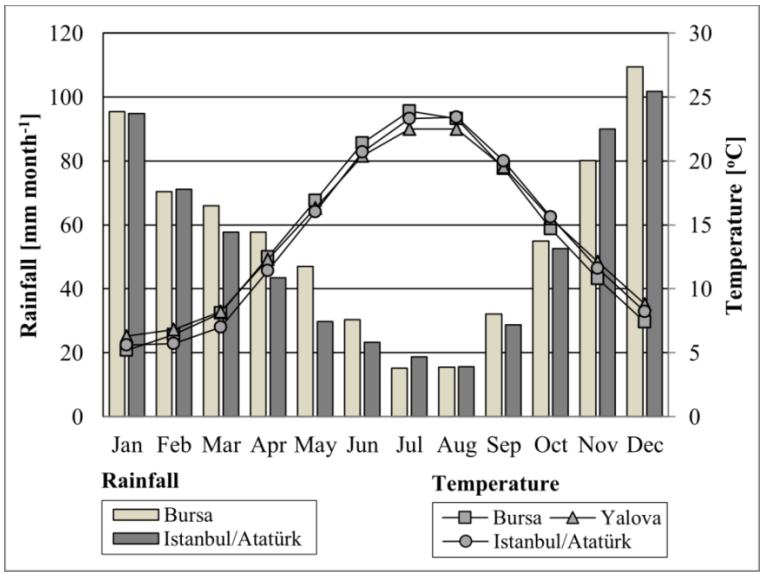

Figure 2.3: Average Rainfall [mm; bars] and average 24h temperature [°C; dots connected by lines] for three meteorological stations from Marmara region, Bursa being the closest to Lake Iznik. (Data from the World Climate Data Center, between 356 and 477 month of observation from 1951 to 1990).

2.4) Basin hydrology

Inflows to the lake are from fluvial and groundwater nature. The surface runoff is subject to extreme seasonal, long and short term variability – peaking only a few hours after heavy rainfall (Wester, 1989). Up to 30 small surface streams feed the lake, originating from the two mountain belts that delineate the basin (Nümann, 1960). They account for a fast runoff into the lake, as in their upper parts the flowing gradient of the streams reaches more than 50 % – in the catchment mountains reach 1280 masl (Franz et al., 2006; Wester, 1989). The main fluvial inputs to Lake Iznik are the Kara and Söloz (alternatively called Koca) rivers. The prominent Söloz delta can be observed on the southern shore near the village of same name, and the Kara inflow is located on the northeastern shore, at the village Cakirca (Figure 1.1 c). Given the intermittent nature of surface drainage, even the Kara river, as main inflow, nearly dries out during summer (Wester, 1989).

Geographically, Lake Iznik is situated in an area that reunites meteorological conditions for closed lakes (Langbein, 1961). In fact, from the water drained into Lake Iznik, circa 80 % is lost again due to evaporation, and in the lake the water the hydraulic residence time is of 25 up to 150 years (Franz et al., 2006; Wester, 1989). The characteristics of the basin have significant influence on how a lake responds to climate, and models show that deep lakes in small basins with steep slopes, such as Lake Iznik, are usually better recorders of high-amplitude and low frequency climatic changes (Lerman et al., 1995).

At the northern Iznik basin, i.e. Samanli Mountains, the seepage water from the shales to the limestone layers leads to carst formation, and springs outflow locally at this contact layers (Canık and Rosen, 2004). The high transport and erosion capacity of the northern rivers prevent considerable groundwater storage (Wester, 1989). For the southern Katirli mountains there are no cleavage surfaces and the sub-surface water outflow is relatively low (Wester, 1989). The Orhangazi and Iznik Plains retain the groundwater occurrences in the lowlands around the lake (Wester, 1989).

The outlet from the basin is the Gölayagi stream, which after circa 8 km from the lake, receives the waters from the Karsak stream, changing its name to Karsak, flowing with relative steep slope into Gemlik Bay (Wester, 1989). The outflow of the lake is dammed since the 60’s, regulating the maximum lake level. The damn is maintained by the General Directorate of State Hydraulic Works - DSI. In our days, water level is highly influenced by water exploitation for irrigation of crops, with variations of up to 2 m in a few years

(Appendix A2.3), as the plains around the lake, and the Solöz delta are intensively used for agriculture.

Altinsaçli (1999) observes that the lake does not discharge into the bed of the Karsak river directly but that '*the water coming through the bottom at the west of the lake creates the source of the Karsak Stream*' *(sic)*. Although the direct outflow would be named Gölayagi, it is noteworthy that also in the 50's a percolating outflow has been described through this sandy gravel deposits on the western shore (Nümann, 1960). Therefore, the still active alluvial processes in the western part of the basin, might have temporarily closed the lake in geological times, e.g. filling the water outlet with sands (Ikeda et al., 1991a).

2.5) Lake Iznik limnology

Lake Iznik (40°26'N, 29°32'E) has a surface area of circa 313 km^2, which is proportionally circa ⅓ of the catchment terrain (920 km^2). The mean water depth is of 40 meters and the maximum depth is of 80 meters in the southern basin (Figure 1.1) (Franz et al., 2006). The annual seasonal lake level variation is of about half a meter, and is in accordance to the hydrological regime.

The Iznik waters are clear and transparent, occasionally turbid at coastal regions after storms or heavy rainfall (Nümann, 1960). At first sight from the hills around the lake, any observer would deduce an oligotrophic lake, due to its clear and deep blue waters (Nümann, 1960) resultant from the low algal production.

In relation to its zooplankton fauna Lake Iznik is oligotrophic, but nutrient concentrations point towards mesotrophic-eutrophic status, vulnerable to eutrophication (Yagci and Ustaoglu, 2012). In fact, the lake has become increasingly eutrophic for the past 20 years, as shown by nutrient content in surficial sediments, as well as characteristic diatom association (*Cyclotella meneghiniana, Cyclotella ocellata, Fragilaria brevistriata, Fragilaria crotonensis* and *Stephanodiscus hantzschii*), and abundant occurrence of cladoceran remains (carapax residuals of *Bosmina sp.*) (Franz et al., 2006). Comparing to other Anatolian lakes, Lake Iznik has a relatively rich plankton assemblage covering *Diaptomus*, *Cyclops*, *Daphnia*, *Bosmina*, and *Diaphanosoma* each of which present maxima at different seasons (Nümann, 1960).

2.5.1) Hydrochemistry and lake mixing

Lake Iznik has a pH of 8.8, CO_3^{+2} concentration of ~111 mg/L, HCO_3^- ~341 mg/L, Ca^{+2} ~16 mg/L and Na^+ ~100 mg/L (annual mean values) (Franz et al., 2006). Due to the characteristic

hard water hydrochemistry (Table 2.1) – bicarbonate rich and alkaline, the lake is subject to characteristic endogen carbonate production. This has been observed in the field in the summer of 2010, as a whiting event, after an interval of three weeks without precipitation and average air temperature of 23^{o}C (Viehberg et al., 2012). The whiting was identified in satellite images from the period, and the dispersion of the carbonate plume additionally exposes the complex dynamics of epilimnion mixing (Viehberg et al., 2012). As a result, ionic concentrations measured from sample points near the lake's margins (Table 2.1, line C), are somewhat higher than concentrations of surface water in the center of the lake (Table 2.1, line B).

The seasonal record of depth profiles for water temperature, pH, electrical conductivity, and dissolved oxygen, for the northern and southern basin, delineate the development of a thermocline for Lake Iznik during summer at circa 15 to 20 meter depth (Viehberg et al., 2012; Wester, 1989). During autumn and towards the winter, the thermocline moves to a depth of ca. 20 to 30 meters. At some point between January and April, the lake has been subject to a complete mixture of the epilimnion and hypolimnium (Nümann, 1960; Viehberg et al., 2012). Ice cover is not observed during winter; hereafter the lake would be classified as a warm-monomictic lake (Boehrer and Schultze, 2008). The minimum temperatures in winter lie between 5 ^{o}C and 8 ^{o}C, the former value being measured after a severe winter in the years of 1953/1954 (Nümann, 1960).

It is not trivial task to classify the type of waters of a lake, especially when the concentrations change seasonally, or across the borders of formal definitions. Moreover, there is a variety of terminologies for different levels of salinity in the different fields of science (Last and Ginn, 2009), and additionally definitions might disagree. For instance, lake water is referred to as saline when the salt content is above 3 ‰, or 5 ‰ (Boehrer and Schultze, 2008; Eugster and Hardie, 1978).

The present waters of Lake Iznik have a calculated salinity between 0.5 ‰ and 1 ‰ (one gram salt per kilogram of water), according to the minimum and maximum values for ionic concentrations, respectively (Table 2.1, line A). This classifies Lake Iznik as fresh, brackish or subsaline, as the value lies in between 1 mg.l^{-1} and 10^{4} mg.l^{-1} (Jones and Deocampo, 2003; Last and Ginn, 2009). Interestingly, literature registers that Iznik waters have been described as brackish in the past (Devedjian, K. 1926, Pêche et pêcherie en Turquie) *apud* (Nümann, 1960). Salt can be tasted by humans from a concentration of 3 ‰ (Boehrer and Schultze, 2008), therefore in historical times variations of salinity from Iznik waters took place possibly

resulting from evaporation, during phases of no discharge to the Gölayagi stream. Finally, the salinity, i.e. the chemical composition of lakes, influences density and is therefore a controlling factor in lake mixing processes (Imboden and Wüest, 1995). For lakes with low salinity, such as Lake Iznik, the influence of chemical stratification is pronounced when temperatures are near to 4^{o}C – when water has a thermal expansion coefficient of nearly zero, and can strongly influence vertical mixing processes (Imboden and Wüest, 1995).

2.5.2) Sediments and deposition processes

From the lake's morphology and bathymetry, a sedimentary ridge elongated in the E-W direction separates the northern and the southern basins, with 60 and 80 meters water depth, respectively (Figure 1.1 c). The deepest southern basin exhibits the steepest slopes, reflecting the tectonic settings, as the NAF outlines the southern margin of the lake (Franz et al., 2006). As shown by seismic investigations, despite the tectonic origin of the lake, the reflector geometry suggests undisturbed horizontally layered and continuous sediments in the centre of the lake, being appropriate for paleoclimatic research. They have a total thickness of more than 1000 m, overlaying a bedrock of sedimentary rocks, deposited in a half graben structure along the Iznik Mekece Fault (Niessen, F. and Franz, S. O.; personal communication).

Sediments of Lake Iznik are homogeneous silty-clays, rich in biogenic components reflecting the lakes rich fauna, ranging from diatoms, cladocerans, chironomids, pollen and 27 species of ostracods (22 genera), and oligochaetes (Altinsaçli, 1999; Franz et al., 2006; Nümann, 1960). The mineral assemblage of the Iznik sediments is composed mainly of quartz, feldspar (plagioclase), carbonates (aragonite and calcite) and clay minerals (smectite, illite, kaolinite/chlorite) (Franz et al., 2006; Ülgen et al., 2012; Viehberg et al., 2012).

The surface sediments of Lake Iznik have been described as a soft black mud, which is partly interlayered by yellow laminations (Nümann, 1960). These still undisturbed carbonate laminae, resulting from the endogen carbonate production, are also observed on the uppermost centimeters of some short gravity cores, when they do not have been bioturbated.

Table 2.1: Physicochemical properties and average composition of Lake Iznik waters

	T [°C]	**pH**	**Cond. [µS/cm]**	**Secchi Depth [m]**	**Na^+ [mg/l]**	**K^+ [mg/l]**	**Ca^{2+} [mg/l]**	**Mg^{2+} [mg/l]**	**Cl^- [mg/l]**	**HCO_3^- [mg/l]**	**CO_3^{2-} [mg/l]**	**SO_4^{2-} [mg/l]**	**PO_4^{2-} [mg/l]**	**NO_3^- [mg/l]**	**Si [mg/l]**	**D.O. [mg/l]**	**Sr [µg/l]**
A		9.2 – 8.5	1100 – 900		23 – 155	11 – 15	7 – 42	48 – 78	62 – 74	240 – 466	63 – 151	15 – 33	0.04 – 0.84				
B	**10** **–** **29.3**[a]	9.0 – 9.3	966	5.5 – 0.2[a]	111.5 – 127	10.6 – 11.1	7.5 – 9.4	60.2 – 69.8	66.3 – 72.2			27.7 – 30.4				8 – 9.3	23.8 – 30
C	**7.2** **–** **28.4**	7.7 – 9.1	927 – 999	4.9 – 1.3			18 – 53.1	80.8 – 100.9				12 – 239.6	0 – 0.1	0 – 1.3	0.1 – 0.4	4.1 – 13.5	
D	**5.3**[b] **–** **24.5**	8.6 – 9.0														7.9 – 12.5	

[a]*Maximum temperature and minimum secchi depth refer to whiting event during summer 2010*
[b]*Minimum temperature refers to surface waters after a strong winter in 1953*
A) max. and min.values compiled from several sources (Wester 1989, Akkoyunlu 2003, and the Turkish Water Resources Division Bursa), by (Franz et al., 2006)
B) selection of max. and min. values for surface waters for northern and southern basin in a seasonal investigation from 2011 (Viehberg et al., 2012)
C) whole year monthly investigation during 2006 (Yagci and Ustaoglu, 2012)
D) values from (Nümann, 1960)

Surface sediments are differentiated between marginal and basin deposition. The margin deposition reflects fluvial input, which is delineated by quartz deposition (Ülgen and Franz, 2006; Viehberg et al., 2012). In the marginal regions of the lake, up to 25 meters in depth, the sediments consists of sand (Nümann, 1960). From the carbonate minerals, aragonite is deposited in the center of the basin, and calcite, being enriched in the center, also presents a influence of the margins at the vicinities of the inflows (Ülgen and Franz, 2006; Viehberg et al., 2012). It has been noted that calcite is of autochthonous and detrital origin (Franz et al., 2006), making out circa 12% of the mineral assemblage. Aragonite, on the other hand, is solely endogen and represents circa 30 % of the surface sediments.

3.) Materials and methods

3.1) Field work and core recovery

New sediment cores were recovered from Lake Iznik in autumn 2009. Two different coring locations were selected based on a detailed seismic investigation in 2005 (Franz, S.O., personal communication), and in total three long cores were collected. The two coring locations are situated on the sedimentary ridge that separates the lake's southern and northern basins. Two different coring devices were used from a floating platform (UWITEC, Austria). A gravity corer was used to ensure recovery of the sediment water interface at each location. The long cores were collected in succeeding two meter sections with a piston corer. At the first location (N 40° 26.57', E 29° 32.35') two parallel cores were retrieved, IZN09/LC1 (10 meter core length) and IZN09/LC2 (14 meter core length), at a water depth of 50 m. According to the geophysical reconnaissance studies, this is the region with the lowest deposition rates (Figure 3.1). At the second location (N 40° 26.92', E 29° 32.61') core IZN09/LC3 (14 meter core length) was recovered at a water depth of 50 m. The collected two meter long core sections were cut in one meter long segments, for transportation and storage purposes.

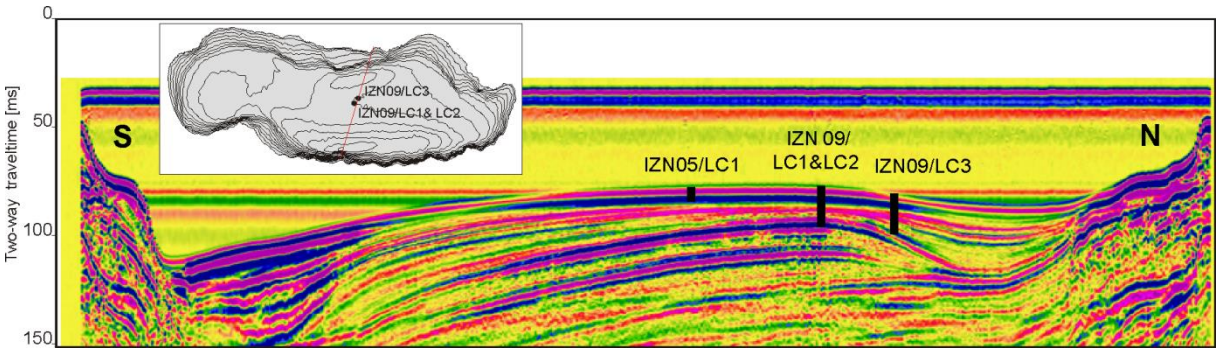

Figure 3.1: Seismic profile nr. 5 from the field campaign 2005 and coring locations. IZN05/LC1 refers to a 5 meter core retrieved in the campaign from 2005. IZN09/LC1, LC2 and LC3 refer to the cores retrieved in the campaign from 2009

3.2) Core documentation and storage

Core halves were documented photographically, and additional digital images and X-ray images were acquired with the Itrax core scanner located at the Eastern Mediterranean Centre for for Oceanography and Limnology – EMCOL, at Technical University of Istanbul – ITU. Core description was undertaken on fresh sediment immediately after core opening and a few

weeks later compared to the oxidized state. Archive core halves are stored at EMCOL, and working core halves are stored at the Steinmann Institute, University of Bonn. Additional digital image documentation was undertaken in the University of Bonn of working halves in the oxidized state. Cores were maintained at cool temperatures during handling, and transportation in thermic boxes. They are stored in a cold room at 6^{o}C.

3.3) Composite profile

In order to obtain a continuous record the construction of a composite profile is obligatory. The composite profile for the cores obtained in 2009 was presented in (Roeser et al., 2012). To build the composite profile parameters were chosen that can be systematically correlated throughout the different cores and that represent the sedimentation processes occurring within the lake. Experience shows that for the Iznik lake the Ca/Fe ratio and other geochemical proxies can be precisely correlated throughout short cores for several transects within the lake (Ülgen et al., 2012). This was extended also to the long cores, and the correlation 'tool', the Ca/Fe ratio, is supported by lithology. As the sampling location of IZN09/LC2 is subject to low sedimentation rates, this core location is chosen as main constituent for the composite profile. To fulfill the intervals between piston core sections from IZN09/LC2, the above mentioned correlation has been undertaken to the undisturbed sequences of IZN09/LC3. Applicable correlation points between the two locations are given by twenty seven defined tie points (PU's). From these, six points were chosen to build the composite profile. It is made of a continuous record until 12.09 m of composite depth (mcd; Table 3.1; Figure 3.2), and reaches a total virtual composite depth of circa 18 meters. It is noteworthy that the core length is of 14 meters, and expected core depth in meters below lake floor reaches approximately 16.9 meters (Table 4.1), according to correlations to seismic profiles. The location of the additional core IZN09/LC3 is subject to eventual mass movements that can be delineated within seismic profiles (F. Viehberg, personal communication), which is also evidenced lithologically by the doublet appearance of a tephra marker layer.

A continuous sedimentary record from the late Pleistocene towards present day, can be achieved by the extension of the composite profile IZN09/LC2&LC3 to the water-sediment interface, by correlation to the profile presented in Ülgen et al. (2012). This sedimentary sequence corresponds to one continuous 5 meter core, IZN05/LC1 (Figure 3.1), which holds from recent sedimentation to the middle Holocene. The point chosen for emending a future extensive profile is tie point PU8 (4.58 mcd) (Figure 3.2), which has been identified as a tephra layer, therefore representing definite chronological synsedimentation (section 4.2).

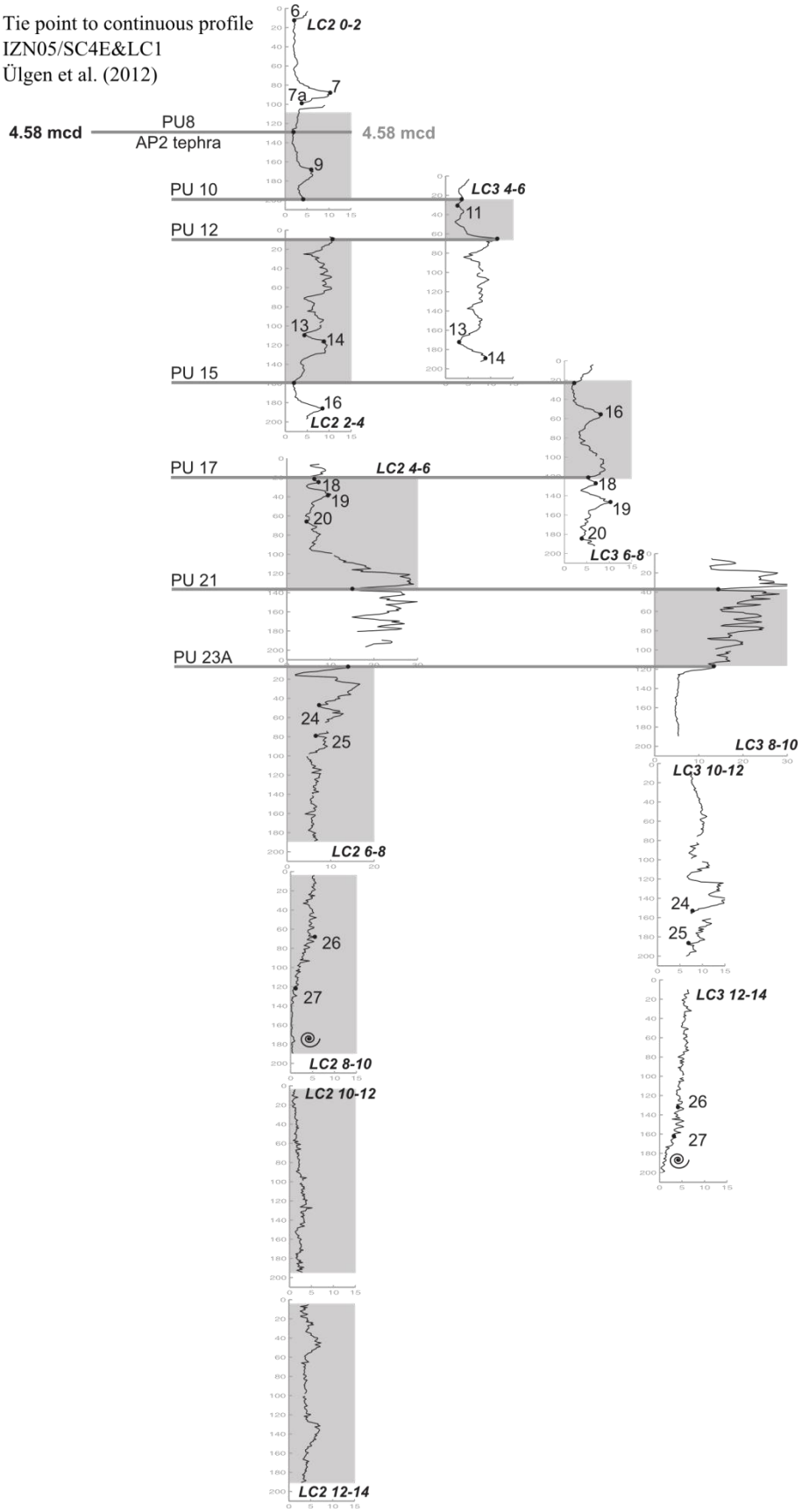

Figure 3.2: Chemostratrigraphical correlation between cores IZN09/LC2&LC3 based on the Ca/Fe relation. Tie points (PU's) are numbered from top downwards and indicated by black dots. Gray horizontal bars indicate tie points (PU's) used to construct the composite profile IZN09/LC2&LC3 (Table 3.1). Numbers marked at only one core, in the upper three meters, represent tie points to IZN05/LC1. Spiral indicates first appearance of shell in the profile (from top to bottom). Modified after (Roeser et al., 2012).

Table 3.1: Correlation table for the presented composite profile IZN09/LC2&LC3. Tie points were defined based on chemostratigraphy using the Ca/Fe ratio (which behaves the same as Ca /Ti), supported by lithology. From Roeser et al. (2012).

Core, Segment, Section, Interval [cm]	Depth [mblf][a]	Depth [mcd]		Core, Segment, Section, Interval (cm)	Depth [mblf][a]	Depth (mcd)
IZN05/LC1(5), 29	**4.6**	4.58	Tie	IZN09/LC2 (0-2)II, 25	**2.9**	4.58
IZN09/LC2 (0-2)II, 99	**3.6**	5.32	Tie	IZN09/LC3(4-6)I, 22	**5.4**	5.32
IZN09/LC3(4-6)I, 65	**5.8**	5.75	Tie	IZN09/LC2(2-4)I, 11	**4.4**	5.75
IZN09/LC2(2-4)I, 100.5	5.3	6.65	Tie	IZN09/LC2(2-4)II, 0	5.3	6.65
IZN09/LC2(2-4)II, 66	**6.0**	7.31	Tie	IZN09/LC3(6-8)I, 26.5	**7.5**	7.31
IZN09/LC3(6-8)I, 100.5	8.3	8.05	Tie	IZN09/LC3(6-8)II, 0	8.3	8.05
IZN09/LC3(6-8)II, 21.5	**8.5**	8.26	Tie	IZN09/LC2(4-6)I, 20	**7.0**	8.26
IZN09/LC2(4-6)I, 100	7.8	9.06	Tie	IZN09/LC2(4-6)II, 0	7.8	9.06
IZN09/LC2(4-6)II, 37	**8.1**	9.43	Tie	IZN09/LC3(8-10)I, 38	**10.0**	9.43
IZN09/LC3(8-10)I, 100.5	10.6	10.06	Tie	IZN09/LC3(8-10)II, 0	10.6	10.06
IZN09/LC3(8-10)II, 18	**12.9**	10.24	Tie	IZN09/LC2(6-8)I, 6	9.0	10.24
IZN09/LC2(6-8)I, 100.5	10.0	11.18	Tie	IZN09/LC2(6-8)II, 0	10.0	11.18
IZN09/LC2(6-8)II, 91	10.1	12.09	Tie	IZN09/LC2(6-8)CC, 0	10.1	12.09
IZN09/LC2(6-8)CC, 10	**10.9**	12.19	Tie	IZN09/LC2(8-10)I, 2.5	**10.9**	12.19
IZN09/LC2(8-10)I, 100.5	11.8	13.17	Tie	IZN09/LC2(8-10)II, 0	11.8	13.17
IZN09/LC2(8-10)II, 92	12.8	14.09	Tie	IZN09/LC2(8-10)CC, 0	12.8	14.09
IZN09/LC2(8-10)CC, 10	12.9	14.19	Tie	IZN09/LC2(10-12)I, 2.5	12.9	14.19
IZN09/LC2(10-12)I, 100.5	13.8	15.17	Tie	IZN09/LC2(10-12)II, 0	13.8	15.17
IZN09/LC2(10-12)II, 98	14.8	16.15	Tie	IZN09/LC2(10-12)CC, 0	14.8	16.15
IZN09/LC2(10-12)CC, 10	14.9	16.25	Tie	IZN09/LC2(12-14)I, 3.5	14.9	16.25
IZN09/LC2(12-14)I, 100.5	15.9	17.22	Tie	IZN09/LC2(12-14)II, 0	15.9	17.22
IZN09/LC2(12-14)II, 94.5	16.8	18.17	Tie	IZN09/LC2(12-14)CC, 0	16.8	18.17
IZN09/LC2(12-14)CC, 10	16.9	18.27			16.9	18.27

[a] *bold values are derived from geophysical interpretations (F. Viehberg, personal communication)*

3.4) Sampling Strategy

Firstly, sampling was focused on the main constitute of the composite profile, core IZN09/LC2, and later completed for the segments from the core IZN09/LC3 which belong to the composite profile. For the sedimentological investigations, the composite profile was sampled systematically in 5 cm resolution. Samples for pollen, ostracodes, and water content were taken with syringes (diameter 2 cm) for estimated volumes, and samples for geochemistry and mineralogy consisted of an integration of 4 cm or 2 cm depth interval, in alternation (Appendix A3.1). Sediment in direct contact to the liner was avoided due to possible carriage of sediment from other depths during the field coring. Also, smear slides were prepared for every 10 cm. For that, a small amount of fresh sediment was carefully smeared on glass slides with wooden sticks and distilled water. After drying at low temperature the slides were embedded with a thin layer of '*Bohle*' UV Adhesive (2-

hydroxyethylmethacrylate, acrylic acid), and cured for 4 minutes under ultra violet light. Further taken samples include detailed sampling for chronology (section 3.10) and selected samples for further purposes, e.g. SEM analysis, or grain size in higher resolution (e.g. section 3.6.3.1).

Table 3.2: Summary of the main applied methods

Sedimentology			
Parameter	**Method**	**Location**	**Sample Series Identification**
Lithology	Visual Description, Optic Microscopy	University Bonn	(2010.158)
Physical properties	Gravimetry	University Bonn	(2010.158), (2011.226), (2010.154)
Physical properties	Multi Sensor Core Logging (MSCL)	ITU	core segments
Geochemistry Major elements / relative measurements	X-ray Fluorescence, Itrax core scanner	University Köln, ITU	core segments
Geochemistry Major and Trace elements Bulk Sediment Absolute measurements	X-ray Fluorescence, discrete sampling (fusion discs and powder pellets)	University Bonn	(2010.158), (2011.218), (2011.226), (2010.154)
Geochemistry Major elements Fraction <63µm Absolute measurements	X-ray Fluorescence, discrete sampling (fusion discs)	University Bonn	2010.158 unit IV samples
Geochemistry 'C,N,S' and 'TOC'	purge and trap Chromatography, elemental analyser	University Bonn	(2010.158), (2011.218), (2011.226), (2010.154)
Loss on Ignition	gravimetry	University Bonn	(2010.158), (2011.218), (2011.226), (2010.154)
Mineralogy Bulk Fraction	X-ray Diffraction on powder mounts	University Bonn	(2010.158), (2011.218), (2011.226), (2010.154)
Mineralogy Fraction <63µm	X-ray Diffraction on powder mounts	University Bonn	2010.158 unit IV samples
Mineralogy Clay size fraction	X-ray Diffraction on oriented aggregates	University Bonn	2010.158 alternate samples
Mineralogy Microfacies characterization	Scanning Electron Microscopy	University Bonn	Selected samples
Grain size	Laser Diffraction	University Bonn	(2010.154)
Grain size (including: Assessment between chemical pre-treatmens)	Laser Diffraction	Istanbul Technical University - ITU	(2010.158), (2011.226) and selected samples
Stable isotopes ($\delta^{13}C$ and $\delta^{18}O$)	Mass Spectrometry	Leibniz Laboratory Kiel	(2010.158)
Chronology	Radiocarbon	Leibniz Laboratory Kiel Beta Analytics	see chapter 5
Chronology	Optical Luminescence Method (OSL)	University Köln	see Roeser et al., 2012
Chronology	Tephrochronology	GFZ Potsdam	see Roeser et al., 2012

3.5) Overview on analytical methods

The methods applied within this study, and applicable sample processing, are summarized in Table 3.2. They are briefly explained in the subsequent topics. Additional information on sampling and methods procedures can be found in the appendices (A3.1, A3.2).

3.6) Physical properties

3.6.1) Water content and dry bulk density

In soil mechanics dry bulk density is commonly used to evaluate soil compaction. It is given by the division from the mass of dry soil – after drying to constant weight – by its moist volume (Eq. 3.1). The water content (or moisture content) of soils or sediments is generally expressed as the ratio between the mass of water, and the mass of dry sediment after drying at 110°C (Eq. 3.2) (Suguio, 1998). This value corresponds to the gravimetric water content (θ_m). The volumetric water content, or sediment porosity, can be expressed as a function of wet bulk density (Eq. 3.3), or dry bulk density (Eq. 3.4) (Lukas et al., 2012).

$$\rho_{bd} = m_s / v_{ws} \qquad \textit{(Eq. 3.1)}$$

$$\theta_m = (m_{ws} - m_s)/m_s \qquad \textit{(Eq. 3.2)}$$

$$n = (\rho_{bw} - \rho_s)/(\rho_w - \rho_s) \qquad \textit{(Eq. 3.3)}$$

$$n = 1 - (\rho_{bd}/\rho_s) \qquad \textit{(Eq. 3.4)}$$

where:

ρ_{bd}: dry bulk density [g.cm^{-3}]

m_s: mass of dry sediment [g]

m_{ws}: mass of moist sediment [g]

v_{ws}: volume of moist sediment [cm^{-3}]

θ_m: gravimetric water content (wet/dry) (*100) [%]

ρ_{bw}: wet bulk density [g.cm^{-3}]

ρ_s: density of solids (sediment) [g.cm^{-3}]

ρ_w: density of water [g.cm^{-3}]

n: porosity

In order to maintain water content of cores preserved after field work, these were air sealed after core opening. When removing the seal for sampling, first sample taken was the 5 cm^3 sample for measuring the gravimetric water content on discrete samples. Humid samples were dried at 105^oC to constant weight.

3.6.2) Magnetic susceptibility

Additional physical sediment properties were measured by the cooperation partners on the closed cores using a MSCL core logger (Geotek Corp., United Kingdom) located at Istanbul Technical University (ITU), in a resolution of 0.6 cm. The measured properties are p-wave amplitude, p-wave velocity, density, magnetic susceptibility, impedance, fractional porosity and resistivity. From these parameters, the degree of magnetization of material in response to an applied magnetic field is sensitive enough to be frequently and successfully applied to paleo-environments, related to a variety of influencing factors, e.g. carbonate accumulation, erosion signals, anthropogenic impact, earthquake identification or tephra deposition (Litt et al., 2009; Nowaczyk et al., 2007; Schwab et al., 2004; Schwab et al., 2009; Ülgen et al., 2012; Wagner et al., 2008).

3.6.3) Grain size

Grain size analyses were conducted at the facilities from EMCOL at Istanbul Technical University, during a two month research stay during July/August 2012 financed by the German Academic Exchange Service - DAAD (*Doktorandenkurzstipendium Referat 314 Kennziffer D12/40880*).

3.6.3.1) Sampling and analysis

For grain size, the profile IZN09/LC2&LC3 was sampled from the archive cores at the storage at ITU. The core halves were carefully sampled with a glass tile from the sediments surface to assure preservation of the sedimentary structures. Sampling was conducted in correspondence to the previous sampling of the composite profile (section 3.4), in 10 cm resolution. Additionally, sampling density was increased for some intervals. In total, circa 250 samples were analyzed for the grain size distribution; 150 of which were subjected to two different pre-treatment methods, resulting in a total count of 400 analyzed samples. Each analysis consisted of double to triple measurements of the grain size of one sample.

3.6.3.2) Pre-treatment procedures

To obtain the grain size information of the solely siliciclastic fraction of sediments, these undergo a series of pre-treatments to remove non siliciclastic components. Traditionally organic material is digested means hydrogen peroxide or sodium hypochlorite. Sediments with a certain content of carbonate usually present a poor reproducibility of grain size analysis (Murray, 2002), therefore it is common practice to remove the carbonate fraction as well. Traditional removal of carbonates is undertaken by a pre-treatment with diluted acids, specially hydrochloric or acetic (Müller, 1967).

A protocol for pre-treating the samples of Lake Iznik was adapted from literature (Murray, 2002; Vaasma, 2008) and based on empirical work. It can be extended to other sediment samples with the necessary adaptations, and is already being implemented at EMCOL. The generation of a solely siliciclastic sample, consisted mainly of three steps in the following order: (1) removal of carbonates, (2) removal of organic material, (3) removal of amorphous silica (Appendix A3.2). In order to assess the influence of amorphous silica in the measurements, two distinct pre-treatment methods were applied. The first pre-treatment (PT1) consisted of steps (1) and (2). And the second pre-treatment method (PT2), added the step (3). Small sample amounts were used, approximated volume of 1 cm^3, which considerably reduced pre-treatment reaction times.

Carbonate and organic matter were removed according to the attached protocol, via treatment with diluted HCl and H_2O_2 respectively, in subsequent steps, until the point of no more observed reaction. Afterwards representative samples from the sedimentary profile were measured for their total inorganic carbon and total organic carbon contents, assessing the value of these steps of the treatment methods for the Iznik sediments. Measurements were conducted on selected samples, using a Shimadzu total organic carbon analyzer (TOC – V_{CPH}), equipped with a Solid Sample Module SSM – 5000A. Sample mass varied from 10 to 30 mg. Total inorganic content for all measured samples were under the detection limits of the equipment. Results for total organic carbon are summarized in the table. The value of the organic matter removal was between 70 and 95%, and absolute total organic carbon concentrations after the treatment with H_2O_2 are nearly zero.

Table 3.3: Total organic carbon for representative Iznik sediment samples after PT1

Sample ID	TOC removal [%]	TOC [%]	Sample ID	TOC removal [%]	TOC [%]
2010-158-022	83,2	0.24	2010-158-071	74,2	0.60
2010-158-039	95,8	0.07	2010-158-082	84,1	0.15*
2010-158-049	82,8	0.20	2010-158-098	90,1	0.08*
2010-158-054	73,9	0.46	2010-158-105	70,9	0.23*
2010-158-066	75,1	0.63	2010-158-121	80,9	0.05*
2010-158-139	84.7	0.11			

** When enough sample material was available, replicate measurements*

Amorphous and biogenic silica is soluble in alkaline milieu (Demaster, 1981), therefore a pre-treatment with sodium or potassium hydroxide is expected to remove diatoms from the sediment samples. Reynolds and coworkers (2004) report a tendency of decreasing grain size after diatom dissolution, which they assessed for nine lacustrine samples. A relative recent study which investigates lake sediments with a high organic content (up to 50%) also reports a tendency of grain size to present relative finer values after diatom removal (Vaasma, 2008). Systematic investigations of this nature on carbonate lacustrine sediments are still pending in literature. Discussion is deepened in chapter 7, along with an estimation of the amorphous silica, which is possible given the appliance of the two distinct pre-treatment methods.

3.6.3.3) Control group

A general difficulty that arises from high carbonate and organic contents in sediments is to obtain good reproducibility of results for grain size analysis. In order to test the reproducibility of the method, including the reproducibility of the two applied pre-treatment methods, standard samples were inserted into the procedures. The standard samples were prepared from left over material collected along the whole profile during sampling. The collected sediment was thoroughly homogenized on a glass plate, using traditional quartering techniques from soil science, and split into ten samples that make out a control group. From these samples, five were treated for pre-treatment PT2. The other five samples were treated for PT1 and PT2. In the latter case, the PT2 was accomplished after an 'interruption' for grain size analysis on the 'after PT1 state', and then adding the last pre-treatment step (removal of ASi), on the same samples. The results for the final pre-treatment (PT2) of the ten samples is shown in Figure 3.3. This comparison shows that the results are identical (*a*) within both groups of five samples, and (*b*) between the groups. This implies a good reproducibility of both (*a*) the grain size measurement per se, and (*b*) the developed pre-treatment method PT2, with or without the 'interruption' step.

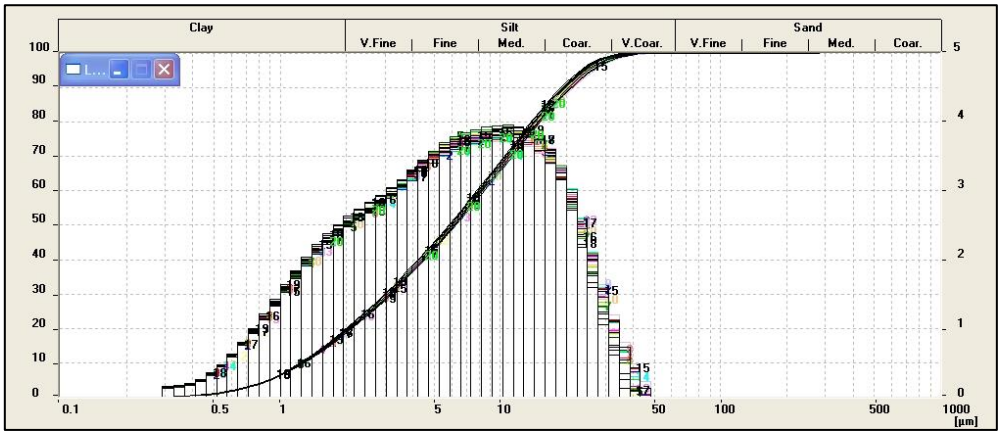

Figure 3.3: Grain size distribution of ten different standard samples, in replicate. One set of five samples directly treated with HCl + H_2O_2 + KOH pre-treatment. Second set of five samples treated in two stages, firstly HCl + H_2O_2 followed by KOH (results of first stage are not presented herein). Frequency distributions (bars) and cumulative frequency distribution (lines) are scaled on left and right axis respectively, i.e. $dq_3(x)$ and $Q_3(x)$. The bottom x-axis represents the grain size intervals and classes in µm.

3.7) Loss on ignition

Loss on ignition (LOI) at 550^{o}C is traditionally applied for estimating the organic content in sediments, and at 950^{o}C it gives an estimate on the inorganic carbonate content (Heiri et al., 2001; Santisteban et al., 2004). Factors as sample size, exposure time, position of samples in the furnace and measurements in different laboratories affect the reproducibility of results (Santisteban et al., 2004). The sedimentary composition (for example clays, salts, and diverse content of organic carbon) can affect the relationship between LOI_{550} and organic carbon, as well as between LOI_{950} and inorganic carbon (Santisteban et al., 2004). Digerfeld et al. (2000) use the loss on ignition at 1000^{o}C as a gravimetric estimation of the inorganic non-carbonate fraction (or minerogenic matter, or mineral residue) of the bulk lacustrine sediment.

In the present study, the percentage of mineral residue LOI_{1100} is used for the normalization of the major elements oxides, quantified via X-ray fluorescence (XRF) (section 3.9.1). The temperature of 1100^{o}C is determined by empirical analytical experience (R. Hoffbauer, personal communication). It is the temperature the fused discs for the XRF analysis are manufactured. Hence, LOI_{1100} assures that the minerogenic residue is representative for the phase for which the major element composition has been determined.

For estimating the LOI_{1100}, circa 1 g sample material was weighed into crucibles, which were previously heated up to 1100^{o}C for at least one hour. The crucibles containing sample material were heated at 1100^{o}C for two hours. After burning they were allowed to cool in an

exicator and the remaining mass was weighed. The estimation for LOI is then given by the calculation of the gravimetric difference between the mass before and after burning.

3.8) Mineralogy

3.8.1) Bulk sediment

Bulk mineralogy from powdered bulk sediment samples was qualitatively assessed on selected samples (series 2010.158, Table 3.2) by X-ray diffraction (XRD) using a Bruker AXS D8 Advance with automatic slit and Ni-filtered Cu-*K*α radiation. Samples were homogenized properly, generally smaller than 50 μm, and prepared into the sample holder through the back loading method, to avoid preferential orientation on the surface subject to the X-ray beam. Operating conditions were: voltage (kV): 40, current (mA): 30, scan range (^{o}2θ): 3-60, step size (^{o}2θ): 0.04, counting time (s): 1, divergence slit: 1^o, anti scatter slit: 1^o, mask fixed: 0.1mm.

Semi-quantitative mineralogy for the profile IZN09/LC2&LC3 was obtained from the powdered bulk fraction measured a Siemens D5000, equipped with a CuKα1,2 target tube, under following operation conditions: voltage (kV): 40, current (mA): 30, scan range (^{o}2θ): 4-70, step size (^{o}2θ): 0.02, counting time (s): 1, divergence slit: 1^o, anti scatter slit: 1^o, mask: 0.15^o mm . The diffractograms were evaluated with the application of the full pattern Rietveld method.

3.8.2) Clay fraction

Oriented aggregates were obtained through the glass slide method. The steps from concentration of the clay fraction (<2 μm) up to the preparation of the glass slides were optimized for the Iznik sedimentary samples, based on literature, and empirical experience. Iron oxides, organic matter, and also carbonates can influence the XRD diffractogram by elevating background values, or masking *001* reflections of some clays. To avoid this, they are often removed chemically from the samples. However, the need of this removal has to be assessed in first place, as some of the methods can potentially change the X-ray response of the phylosilicates in the clay fraction, and should be used only as last resort (Moore and Robert C. Reynolds, 1997).

For the Iznik sediments, clay fraction was concentrated via centrifugation after dispersion with sodium hexametaphosphate. A good dispersion is obligatory to avoid flocculation of clay

particles during the concentration, which could lead to selective segregation. The sodium released by the hexametaphosphate aggregates on the clays surface increasing their surficial charge, consequently reducing their aggregation character. Oriented clay mounts allow a qualitative and semi-quantitative assessment of the minerals and clay-minerals present in the clay fraction. Oriented clay mounts were measured after undergoing different procedures: (1) air drying, (2) glycolization, (3) heated to 350^{o}C and (4) heated to 500^{o}C. X-ray diffraction measurements of the prepared glass slides were conducted on the Bruker AXS D8 Advance equipment with Cu-*K*α radiation. Measuring conditions were: voltage (kV): 40, current (mA): 20, scan range (^{o}2θ): 3-30, step size (^{o}2θ): 0.017, counting time (s): 1, divergence slit: 1/2^{o}, anti scatter slit: 1/2^{o}.

The identification of the clay mineral assemblages is traditionally based on the evaluation of the measurements after the four different procedures (air dried, glycolized, two heating steps), for the same sample. Generally, this first evaluation allows the identification of the clay minerals belonging to the four major groups: kaolinites, illites, smectites and chlorites. A semi-quantitative evaluation of the relative changes in between the clay assemblages is conducted on the diffractograms of glycolyzed slides based on peak areas and intensities.

3.9) Geochemistry

3.9.1) Major and trace elements

The inorganic geochemistry was analyzed with the use of X-ray fluorescence spectrometry for the sediment cores, using and Itrax core scanner, and additionally for discrete samples.

Split core halves were analyzed in 1 cm resolution using an Itrax XRF core scanner (Cox Analytical Systems, Sweden) at University of Cologne, equipped with a Cr X-ray source, operated under following conditions: voltage (kV): 30, current (mA): 30 and exposure time (s): 10. The Itrax offers the possibility of relatively rapid and continuous analysis of split sediment cores, however data quality in this direct analysis is subject to interference of physical (e.g. grain size, wet bulk density) or compositional (e.g. mineralogy) variations (Croudace et al., 2006; Tjallingii et al., 2007).

Quantitative information was obtained from measurements on discrete samples in 5 cm resolution using a PANalytical Axios 3 kW, at the University of Bonn. Trace element composition was measured from powder pellets. The major element composition, i.e. for their respective oxides, was measured from fused discs. Methods used for the preparation of pellets

and fused discs followed the laboratory procedures from the Steinmann Institute for Geology. Samples were dried at 105^{o}C overnight.

For the preparation of powder pellets, 5 g of sediment were thoroughly homogenized with 1 g micropowder wax as a binding agent. The homogenization is undertaken in two steps, manually and using a sample shaker. The sediment-wax mixture is then pressed into a pellet using a metal mold, subject to a pressure of 20 Pa, for 3 minutes. Measured trace elements are obtained in concentrations of parts per million (ppm).

The fusion method produces a solid solution in the form of a glass bead by melting a mixture of a smaller amount of sample material in a flux (Di-lithiumtetraborate) at 1100^{o}C. The fusion eliminates matrix effects such as particle size and mineralogical effects, which are typical for powdered press pills (Hahn-Weinheimer et al., 1995). A relation of 1:10 (sample to binding agent) was preferred (0.4 g of dried sediment mixed to 4 g of flux, weighed with a precision of 10^{-3} g). A 'pinch' of ammonium nitrate is added as oxidizing agent. The mixture is fused in platinum crucibles, in a sequence of four gradual heating steps, up to 1100^{o}C. The fusion fluid is homogenized during the process, through mixing of the melt fluid by inclining the platinum crucibles. After 10 minutes in each heating step, the fluid is then given into a metal mold, in which it is allowed to cool forming the glass disc. The measured major elemental composition is given as the percentage of the respective oxide in the mineral matter remaining after heating to 1100^{o}C. The oxide composition (w%) and its respective LOI_{1100} (w%) are closed to sum 100%, maintaining LOI values constant. Afterwards, proportional atomic weight is used to obtain elemental concentrations.

The detection limits for the wave length dispersive XRF is of about 100 ppm for the lighter elements (Na, Mg, Al, Si, P); about 10 ppm for S and Cl, and for all the other elements (from K to U) the values range between 1 and 10 ppm (Hahn-Weinheimer et al., 1995). The values presented in Boyle (2001) are somewhat higher for the detection limits of the lighter elements (E.g.: 400 ppm Na; 300 ppm Mg; 500 ppm Al; 900 ppm Si; 30 ppm P) however, these relative high values are not of concern, as the observed concentrations are at least about thousand times above these limits for Iznik sediments.

3.9.2) Organic and inorganic carbon, nitrogen and sulfur

For a basic characterization characterization of organic components, carbon, nitrogen and sulfur were determined with an elemental analyser vario EL cube (Elementar Analysensysteme GmbH, Germany). The equipment works with the established principle of

the purge and trap chromatography, which is based on separation of gaseous components on up to three specific columns for segregation without overlap, followed by thermal conducting detection[7].

For the determination of total carbon, nitrogen and sulfur contents, 20 mg from the homogenized sediment are weighted directly in a tin receptacle (boat). The same mass of wolfram oxide is added to bind earth alkaline ions. The folded tin boats were burned into the vario EL cube equipment, under following analysis conditions: combustion unit (^{o}C): 1150, reduction unit (^{o}C): 850, carrier gas flow (ml/min): 192.

Most of the carbon content in sediments is inorganic. To differentiate between the organic and inorganic fractions, also the total organic carbon content was directly determined. Total inorganic organic carbon is then given by the difference between the measured total carbon and total organic carbon. Additionally, calcium carbonate content of the sediment can be estimated by TIC*8.33 assuming that all the inorganic carbon is in that phase, or alternatively carbonate content can be estimated by TIC*5.

Total organic carbon measurements were conducted directly on an acidified aliquot of the sediment. From the homogenized sediment, 10 mg were weighed into silver boats and acidified through addition of drops of HCl (3.7%) directly into the boat. Afterwards the sediment was dried at 90^{o}C for 4 hours and tested for reaction with HCl (10%). If there was still reaction, further drops of acid were added and the steps were repeated. The folded silver boats were burned into the same equipment. The given detection limits for the vario EL cube, for a sample mass of 20 mg, are of 0.04 wt% N, 0.23 wt% C, 0.11 wt% S.

3.9.3) Stable isotopes

Stable isotopes, $\delta^{13}C$ and $\delta^{18}O$, were measured at the Leibniz Laboratory/Kiel, with two different sets of equipment. The first batch of samples was measured with the system Kiel I (prototype) in association with the Finnigan MAT 251 mass spectrometer, and the second batch was measured with the Kiel IV in association with the Finnigan MAT 253 spectrometer. The two sample batches were composed of circa 75 samples each, in alternation with each other, covering the sedimentary profile under investigation in 10 cm resolution. If plotted separately the results of both batches present identical variations, which reaffirms the direct comparability between the measurement systems. The comparability and the fact that both

[7] www.elementar.de

measurement systems deliver identical results have been controlled on different sets of samples in internal analysis from the Leibniz Labor (Andersen, N. personal communication).

For the measurement of the stable isotopes the samples are digested with 100% orthophosphoric acid at 75°C, in pre vacuum conditions. Carbonate within the samples reacts with the orthophosphoric acid releasing CO_2. The reaction time is of circa thirty seconds to two minutes; as a safety interval the system works with a four minute treating interval. It is assumed that there is no liberation of CO_2 due to reaction with organic material, for that the reaction time is too short. Additional CO_2 could be released in the presence of specific phosphate compounds. Reaction of orthophosphoric acid with clays or other minerals can potentially release H_2O. Therefore the complete gas liberated during reaction is passed by a two-step system. The first step consists of a trap, freezing the gas means liquid nitrogen, followed by a stepwise heating, which achieves a maximum of minus 45°C. This ensures the separation from the CO_2 and H_2O molecules. The next step consists of a concentration of the CO_2 to be measured within the mass spectrometer. The Leibniz Laboratory Kiel works with gas standards for comparable measurements, and sample material is analyzed up to ten times to define the internal error of the mass spectrometer, which is relatively small when compared to the potential deviations caused during the reaction time and trap systems (Andersen, N. personal communication). The results are standardized to the VPDB isotope scale, standard material NBS 19 (Friedman et al., 1982), and have a precision of circa 0.07 ‰.

3.10) Chronology

In order to obtain first guidance on the age of the sedimentary profile, samples were chosen for selected depths to be analyzed with Optical Luminescence Method (OSL) in cooperation with the Geography Department/University of Cologne. The samples consisted of core segments of 20 cm, which were cut off from the 2 m core segments. These 20 cm sections were opened under dimmed red light conditions in the laboratory, and just the sediment from the inner core portion was recovered for dating - considering that the sediment portion in contact with the liner protected the inner sediment from contact to sunlight. Results and discussions on the OSL age determinations have been published elsewhere (Roeser et al., 2012).

Ash layers macroscopically observed and identified on smear slides were investigated in cooperation with the the Geoforschungszentrum – GFZ/Potsdam, in order to determine the major glass composition to allow correlation of the tephras with known eruptions (section

4.2). The sampled material was wet sieved, and the fraction >63 µm for each sample was prepared as polished thin sections for electron probe microanalysis (Roeser et al., 2012).

Further effort was applied to obtain appropriate material for radiocarbon age determinations. The two sedimentary profiles for the first coring location (IZN09/LC1 and IZN09/LC2) are identical (Roeser et al., 2012), and hence IZN09/LC1 was used exclusively for dating purposes. An interval of approximately 4 meters core length, representing the Pleistocene to Holocene transition, was sampled for 36 samples of 5 cm slices each (circa 70 cm^3). They were wet sieved into five size fractions. Organic plant remains and ostracodes were sorted from the fractions >250 µm. From these, seven samples offered enough material for reliable radiocarbon age determinations. For the Pleistocene interval further samples were taken from shell horizons and bulk sediment. For the Holocene interval additional bulk sediment was sampled. Details on sample material and implications are presented in the chapter about the chronology of the sediment profile, along with the results for age determinations (Table 5.1). Radiocarbon datings were performed by accelerator mass spectrometry (AMS), by the Leibniz-Laboratory for Radiometric Dating and Isotope Research, Kiel/Germany and by Beta Analytics, London/GB.

4.) Lithology, Physical Properties and Stratigraphy

Lake Iznik's sediments are silty clays, mainly homogeneous, and consist mainly of three components: a clastic fraction, a carbonate fraction and biogenic components. The clastic fraction is mainly detrital in origin. It is made out of quartz, feldspar (plagioclase), kaolinite/chlorite, illite/muscovite, and smectite (Franz et al., 2006; Viehberg et al., 2012). The carbonate fraction is composed of calcite and aragonite. Aragonite is primary in origin, i.e. produced in the lake. Calcite is expected of detrital origin, from carbonate rocks in the catchment (Franz et al., 2006; Viehberg et al., 2012).The biogenic fraction consists of pollen and other plant residuals, diatoms, cladocerans, chironomids, and ostracods (Franz et al., 2006).

4.1) Magnetic Susceptibility and Sedimentary Units

The magnetic susceptibility of the sediments, being a proxy measure for the mineral matter, is in inverse correlation to the carbonate accumulation. Previous investigations have shown that the total clay content – calculated from bulk X-ray diffractograms – is in positive correlation to the measured magnetic susceptibility (Ülgen et al., 2012). Hence, there are two factors controlling the fluctuations observed for magnetic susceptibility along the sedimentological profile: the detrital input and the carbonate accumulation. Based on variations for the magnetic susceptibility and the core lithology, five sedimentary units (I to V) were defined within the sedimentary record from Lake Iznik, see Table 4.1 and Figure 4.2 (Roeser et al., 2012).

4.1.1) Unit I

Unit I consists mainly of a homogeneous, moderately organic (average 3% organic carbon), black-grayish clayey-silt. Magnetic susceptibility values fluctuate between 2 and 10 [SI]. The unit is often spotted with black dots, with <1 mm in diameter, which occur grouped in beds from a few centimeters to approx. 20 cm thickness. The dots are most likely related to organic material, and to a lesser extend originate from post burial formation of iron sulfides, in contrast to the lowermost units.

Unit I presents an alternation of beds with varying thicknesses (from 3 up to 20 cm) with subtle color changes in gray colors. These beds are the result of a temporal change of

dominance of primary carbonates and clastic sedimentation. Carbonate-rich beds are associated with brighter shades of gray. After core opening these beds oxidize to an olive color (in Munsell color system: 5Y 5/2), which is subtle different from the intervals with clastic dominance, which oxidize from a rather dark gray/black to a grayish brown/light brownish gray (in Munsel color system: 2,5Y 5/2). Primary carbonates are characterized by aragonite needles smaller than 1 up to 4 µm.

Further distinguishable in Unit I is an interval consisting of sub-millimeter laminations, containing white aragonitic laminae (Sf1,4.38 mcd), in alternation with dark brownish laminae, consisting of detrital clay. This interval can be observed and correlated in both investigated sites (IZN09/LC1&LC2 and IZN09/LC3 – Figure 1.1), and hence is related to a particular sedimentological/hydrochemical regime within the lake.

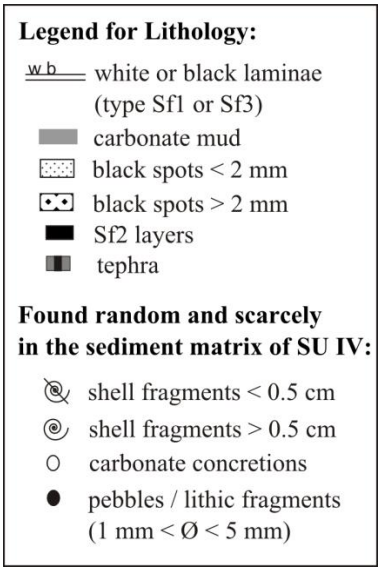

Figure 4.1: Legend for Lithology

4.1.2) Unit II

Unit II is characterized by an olive gray carbonate mud with dominance of aragonite needles (3-10 µm). Magnetic susceptibility values close to zero (<2 [SI]) are the lowest in the entire profile, reflecting high carbonate accumulation. At the base of Unit II, overlaying the event layer Sf2, there is a 15 cm thick bed of a black homogeneous mud which turns to a dark brown color after oxidation, indicating a higher organic and/or iron content. Diatoms are more abundant than in the other units. Smear slides contain terrestrial organic matter, e.g. fibrous plant remains. Also gypsum needles were found. Because gypsum has similar optic characteristics as aragonite – transparent colorless, and birefringence – its presence was only distinguished after treatment of samples for removing carbonates. It was confirmed through XRD measurements on freeze dried bulk sediments. Furthermore, Unit II shows interbedded

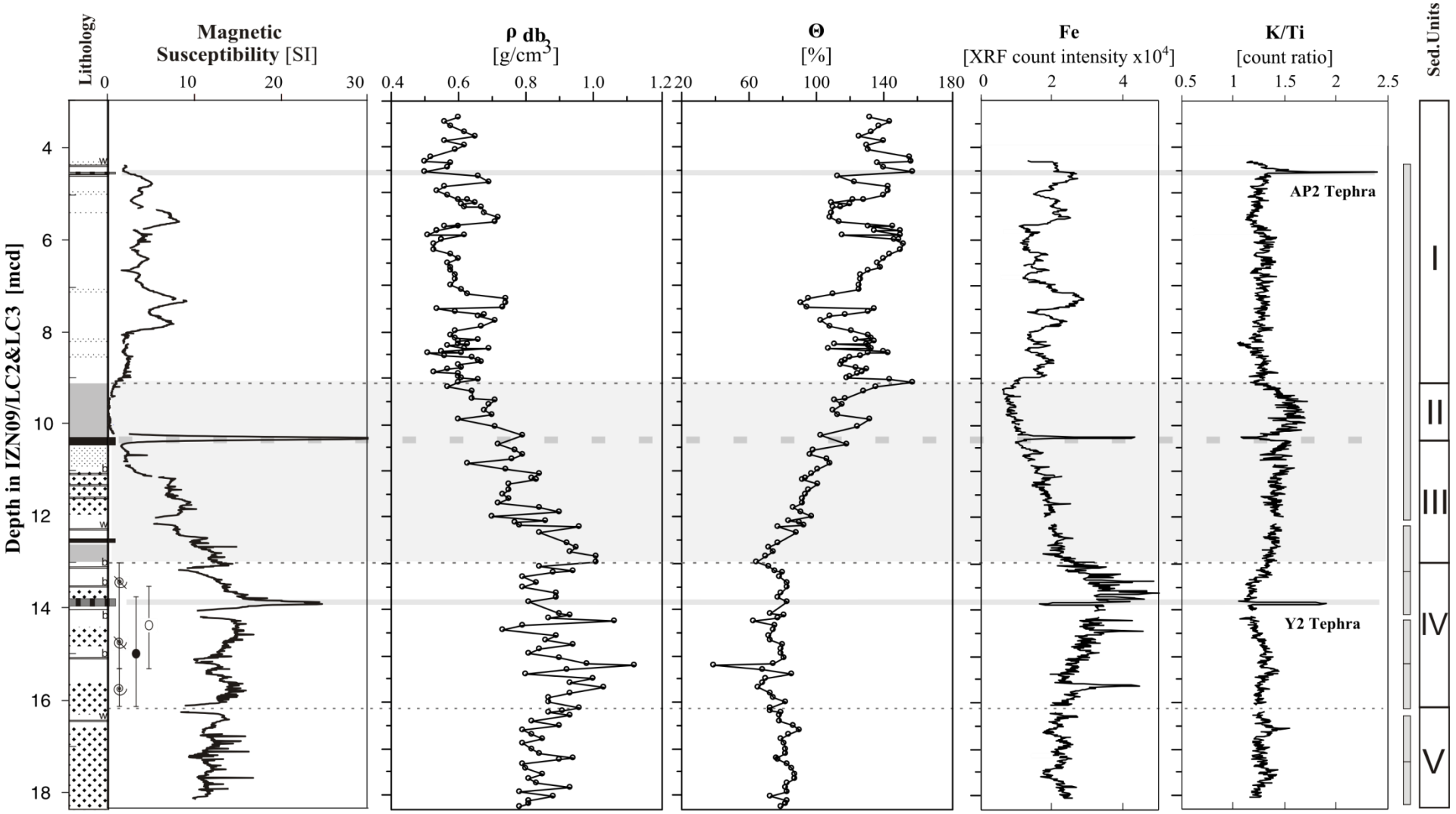

Figure 4.2: Definition of the sedimentary units for Lake Iznik, based on lithology and magnetic susceptibility for the composite profile IZN09/LC2&LC3. Gray vertcal bars indicate continuous section from composite correlation, and the cored two meter sections, and cut one meter segments.

sequences which are slightly darker in color than the carbonate mud. These layers show sharp color boundaries at their base and a gradual change to lighter colors towards their top.

Table 4.1: Summary of the features that define the sedimentary units for the composite profile IZN09/ LC2&LC3. Modified after (Roeser et al., 2012)

Sedimentary Unit	Main lithological character	Magnetic Susceptibility (MS) Values in [SI]	Record of Events[b]	Lower limit in composite [mcd]
I	Homogeneous, moderately organic, black to grayish clayey-silt Alternation of beds with varying thickness (from 3 up to 20cm) with subtle color changes in gray tones Sporadic layers with reduced spots < 1mm in diameter	Fluctuations 2 < MS < 10	Tephra from Vesuvius' AP2 eruption	9.12
II	**Olive gray carbonate mud**, aragonite and diatom rich	**Lowest values**[a] MS < 2	-	10.31
III	Silty clay matrix, overprinted by abundand reduced spots (>2 mm in diameter), sporadic black laminae	**Decreasing upwards**[a]	Distinct iron sulfide layer at top, with MS > 30 Small iron sulfide layer at 12.5 mcd	13.02
IV	Sporadic presence of **shell horizons**[a] as thin event-layers of **shell fragments**[a] with shell fragment grain size fining upwards Sporadic presence of **detrital lithic fragments**[a] (1 ~ 5 mm) Sporadic presence of carbonate concretions	Highest values/ Average: 10 < MS < 15	Tephra from Santorini's Y2 eruption MS > 20	16.11
V	Overprinted by several bands with reduced spots > 2 mm in size	Lithology with Highest values/ Average: 10 < MS < 15	-	18.2

[a] *Bold text highlights the decisive characteristic for boundary setting between units;*
[b] *See section 4.2*

4.1.3) Unit III

The mottled Unit III generally consists of a silty clay matrix with different varying shades of gray. The unit is overprinted by abundant black spots (> 2 mm in diameter), and black and white laminae (Sf3, upper half; Sf1, 12.39 mcd). The black concretion-like spots have silty

texture in contrast to the clayey matrix. The black laminae and the spots turn into a brownish rusty color after oxidation, indicating mineral instability under aerobic conditions. They are most likely related to remobilization of redox sensitive elements, and further occur in Unit IV and V. On top of Unit III (i.e. base of Unit II), there is a distinct black layer (Sf2, 10.33 mcd) of silty to sandy grain size, with 2 cm thickness. This layer is characterized by high concentrations of Fe and S, as well as high magnetic susceptibility values (Figure 4.2). A further layer of the same type (0.5 cm thin) occurs in deeper parts of Unit III, at 12.5 mcd. These layers are related to post burial formation of iron-sulfides, intermediary to the diagenetical formation of pyrite. Based on mineralogical and geochemical information, unit III was subdivided into unit IIIa (10.31 to 11 mcd), and unit IIIb (11 to 13.02 mcd) (details in section 6.3.2).

4.1.4) Unit IV

Unit IV is characterized by a clay-sized matrix and the repeated presence of *Dreissena* sp. and other shell fragments, e.g. gastropods. The shell fragments show size fining upwards, with entire shells appearing only at the base of the unit. Unit IV contains some pebbles (<5 mm) with subangular to subrounded shape, being characteristic for short-distance fluvial transport. The exact depth of the pebbles is depicted in association to geochemical information (e.g. Figure 8.4). In general, the magnetic susceptibility values for this unit indicate a high terrigenous content. In the upper half (~14 to 13 mcd) the unit has black laminae (Sf3). In its lower half (~16 to 14 mcd) unit IV is spotted with black dots (>2 mm). Unit IV is further characterized by the almost complete absence of aragonite needles in the interval from ~ 15 to 13.5 mcd. The lower half contains some aragonite needles (6-12 µm). Because of the presence of a few carbonate concretions the possibility of diagenetical dissolution of aragonite cannot be excluded. Based on mineralogical and geochemical data analysis, unit IV was subdivided into unit IVa (13.02 to 15 mcd), and unit IVb (15 to 16.11 mcd) (details in section 6.4.2), intervals which coincide with the observed differences in lithology. Moreover, for unit IV the wet sieved fraction <63µm is additionally investigated for geochemistry and mineralogy. (e.g. Figure 6.7), to exclude the influence of observed shell material on bulk geochemistry.

4.1.5) Unit V

The most basal Unit V is characterized by clay of a binding and sticky texture. It is overprinted with mottled spots (>2 mm) which tend to occur in bands (2-10 cm). Notably aragonite laminae are preserved at the top of the unit (16.36 mcd). These laminae are

somewhat discontinuous likely due to pos-sedimentary bioturbation. Still, the conservation of the laminae in the sedimentary profile is favored by bottom water and/or sediment-water interface anoxia. The laminae are characterized by well crystallized aragonite needles (10-12 μm). Further characterization on the carbonate phase, is given in chapter 9 (Figure 9.2).

4.2) Tephra Layers

Two tephra layers were found in Lake Iznik. The uppermost of them (Unit I, 4.58 mcd) can be found at both coring sites from 2009 field campaign, and the site IZN05/LC1 from 2005 field campaign (Ülgen et al., 2012). The second tephra is deeper in the sediment profile (Unit IV, 13.89 mcd), sediment depth which was reached only within IZN09/LC2. Both layers were first macroscopically identified within this core. The geochemical identification of the tephra layers, and details on glass composition, are depicted by Roeser et al. (2012). The uppermost tephra can be correlated in between the different cores. Furthermore, this tephra represents the tie point between the composite profile IZN09/LC2&LC3 (this study) and stratigraphically overlaying core IZN05/LC1 (Ülgen et al., 2012). Both tephras can clearly be identified by their characteristic high K/Ti ratio (Figure 4.2).

"The tephra at 4.58 mcd is fine gray layer of circa 1cm thickness, overlying a thinner black layer. It contains abundant microcrystal-rich, high-vesicular micro-pumices which are phonolitic to tephriphonolitic. Sanidine, plagioclase, biotite, amphibole, clynipiroxene, apatite and rare limestone clasts occur as phenocrystals. The mineral assemblage, as well as the major element composition of glass shards most probably match the tephra to originate from the Avellino AP2 eruption of Vesuvius, which has a radiocarbon age of 3.50 ± 0.04 ka cal BP, (Rolandi et al., 1998; Santacroce et al., 2008; Terrasi et al., 1999; Vogel et al., 1990). The AP2 tephra has been identified in various sites (marine and lacustrine) of the Italian Peninsula and the Adriatic Sea. In the Lago Grandi di Monticchio it was assigned a varve age of 4150 years (Wulf et al., 2004). To date, Lake Iznik is the most distal site where the AP2 tephra is identified."(Roeser et al., 2012)

"The tephra at 13.89 mcd is a vitric ash layer of 7 cm thickness and well defined boundaries. It is further characterized by a strong peak in magnetic susceptibility, observed within unit IV. The glass shards have maximum grain size of 100 μm and are rhyolitic in composition. Few feldspars are the only phenocrystals. Their major element composition matches best the Cape Rive eruption of Santorini, at circa 22.0 + 0.854/-0.902 ka cal BP (Eriksen et al., 1990; Pichler and Friedrich, 1976). The so called Y2 tephra is widely documented in the

Mediterranean region (Aksu et al., 2008; Günther and Pichler, 1973; Kwiecien et al., 2009; Margari et al., 2007; Wulf et al., 2002)."(Roeser et al., 2012)

At the coring site IZN09/LC3 two layers with circa 1cm thickness were assigned to the same tephra (AP2) (core IZN09/LC3(2-4)II, at 52 and 67 cm segment depth). This suggests that this site is subject to eventual deposition of reworked material.

4.3) Water content and dry bulk density

Per definition, the dry bulk density (ρ_{db}) is directly proportional to the dry sediments mass, whereas the gravimetric water content (θ_m) is inversely proportional to the dry sediment mass (section 3.6.1, equations 1 and 2). Therefore these two parameters are inversely correlated to each other (Figure 4.3). Water content is closely related to sediment composition (Koczy, 1951; Menounos, 1997), and can have significant influence on XRF measurements with core scanners (section 6.3.1.1), e.g. by reducing the count intensities of light elements such as Al or Si (Tjallingii et al., 2007). The gravimetric water content is directly proportional to porosity. Porosity, which for subaqueous sediments equals the volumetric water content, is closely related to the sediments' particle size, and the density of the particles (minerogenic and organic) (Lukas et al., 2012; Menounos, 1997).

The stratigraphic variation of gravimetric water content (θ_m) and dry bulk density (ρ_{db}) along the sedimentary profile allows the following observations. For the basal units V and IV, both properties present a relatively constant trend (Figure 4.2). The gravimetric water content is generally low (60% - 100%) and dry bulk density is generally high (up to 1 g cm^{-3}). For unit III and II, water content is increasing upwards (60% to 160%), and dry bulk density decreases upwards (1.0 g cm^{-3} to 0.6 g cm^{-3}). For unit I values oscillate around an arithmetic average, of 128% for water content and 0.6 g.cm^{-3} for dry bulk density.

The expected inverse correlation between (θ_m) and (ρ_{db}) can be observed from the scatterplots in Figure 4.3. For Lake Iznik sediments the gravimetric water content and the organic carbon (TOC) have a positive correlation (R^2=0.75, linear). Inverse correlation is observed from the dry bulk density, with the other parameters, θ_m and TOC, respectively. Noteworthy is that for the plots relating ρ_{db}, two distinct regression slopes are observable. The 'cut point' or slope change is around 0.7 g cm^{-3}, which represents the bimodal distribution for the dry bulk density. When applied to the sediment profile, the 'cut' point (0.7 g cm^{-3}) is at the transition between Units II and I.

In general, the inverse relation between the bulk density and water content can be a reflection of sedimentary compaction, resultant from a decrease in porosity and consequent expulsion of water. One could expect a correlation between the water content and grain size, however no clear correlation was observed between these parameters and the grain size.

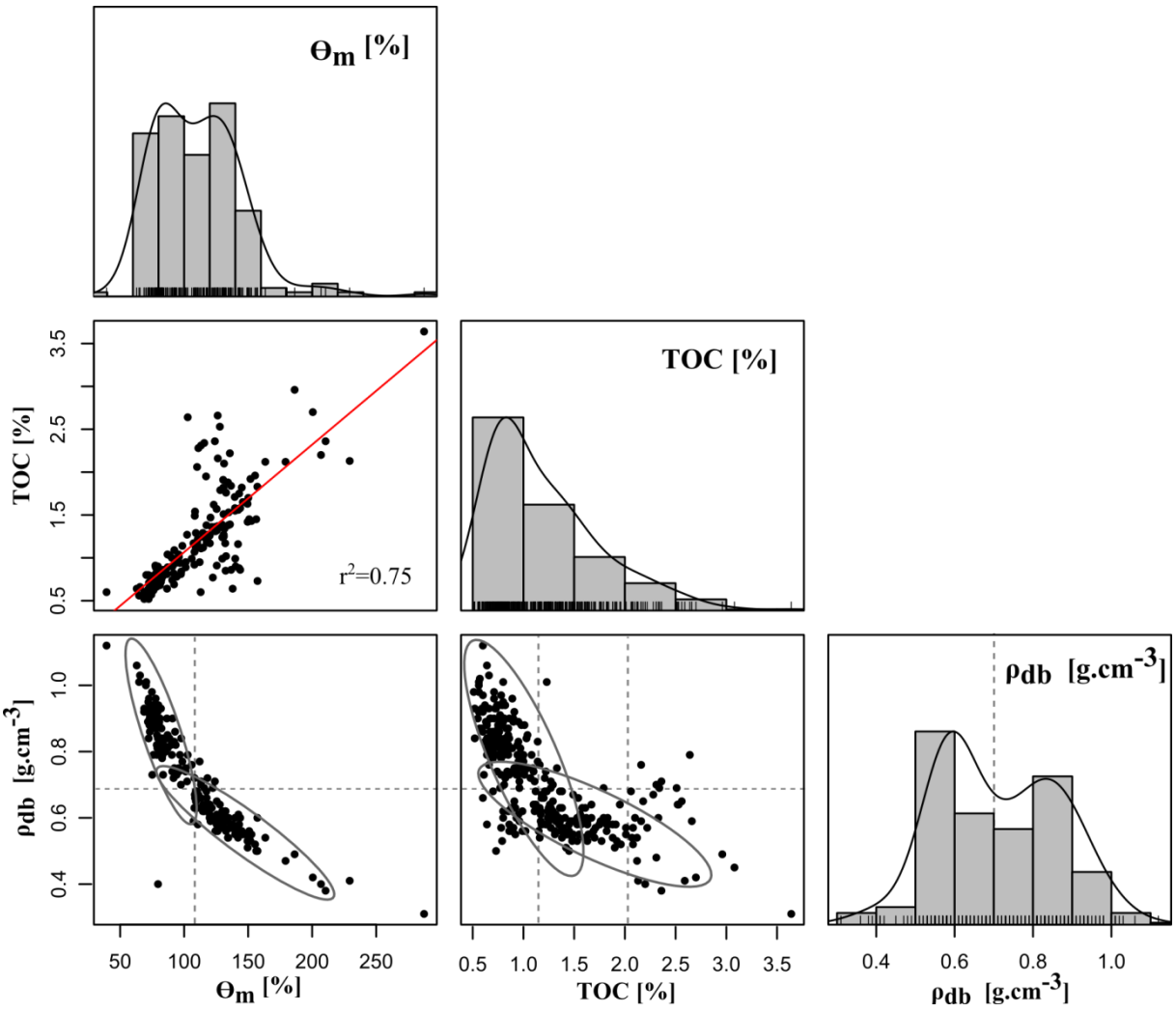

Figure 4.3: Scatter plots and histograms for the gravimetric water content (θ_m), total organic carbon (TOC), and dry bulk density (ρ_{bd}). Ticks on the bottom of frequency distributions represent the sample density. Linear regression is calculated for (TOC vs. θ_m). Distinct slopes of the scatter plots (ρ_{bd} vs. θ_m) and (ρ_{bd} vs. TOC) are indicated on the bottom graphik.

5.) Chronology

The stratigraphic profile constructed and discussed so far had a first age model presented in Roeser et al. (2012). This model gave the sedimentary record a total age of circa 36 ka cal BP. Herein, this model is improved adding novel dated levels, and new considerations are made in the following discussion. Eight new radiocarbon measurements were obtained for the composite section, all on bulk organic material. Four of the new dated samples are located within the middle Holocene and the other four within the Pleistocene interval of the profile. The new measurements complement the pre-existing investigations and data set (Roeser et al., 2012). One aim was to improve past uncertainties regarding the bottom profile. The final model relies basically on ages obtained on organic material, either terrestrial material – sorted under a binocular – or bulk organic. Additionally, the tephra layers are important chronological markers. Especially the Y2 tephra confirms that the record encompasses the LGM. Ages obtained based on carbonate material – either shells, ostracods, or bulk – were not included in the calculations of the final model.

5.1) Samples and dating results

In total, there are **22 age determinations** available for the composite profile IZN09/LC2&LC3 (for labeling see Table 5.1). The age of sample no. 1 refers to a radiocarbon dating from the base of the short core IZN09/SC1B which does not belong to the composite profile, and is listed as age reference. Considering measurement and calibration uncertainties, all obtained ages are in chronological order.

Two dated samples refer to tephra layers and all others refer to radiocarbon determinations. The two tephras (samples no. 2 and no. 17) were identified by means geochemical fingerprinting to originate from eruptions of Vesuvius and Santorini (3.50 ± 0.4 ka cal BP and 22.00 ± 0.9 ka cal BP), respectively (see section 4.2).

Four radiocarbon determinations were carried out on segregated organic material (samples no. 7, no. 9, no. 11 and no. 13) - obtained as described in section 3.10. From these, three samples refer to terrestrial plant remains, and one (sample no. 13) to aquatic plants (most likely moss). The $\delta^{13}C$ values for sample no. 13 are consistent with an organic origin.

Nine of the radiocarbon ages from the composite profile IZN09/LC2&LC3 were obtained from bulk sediment: eight from bulk organic material and sample nr. 8 from bulk carbonate.

The bulk organic samples for measurement of ^{14}C activity, were pre-treated with acid washes, and hence contain the terrestric organic matter originated from the basin, as well as the accumulated limnic organic matter. **Five** radiocarbon ages were carried out on shell fragments, mainly *Dreissena*, and additional **two** age determinations refer to ostracode samples.

5.1.1) Reservoir effect and hardwater effect

The *reservoir effect* results from a lack of CO_2 exchange between the lake waters and the atmosphere, and consequently a lack of atmospheric ^{14}C in the lake. Radiocarbon from the waters continues to decay increasing the age of the reservoir, e.g. during long-term isolation of a water mass (Stein et al., 2004). Additionally, in alkaline lakes, dissolved inorganic carbon is constantly recycled, and therefore older than the age of the water, resulting in the *hardwater effect* (Meyers and Lallier-Verges, 1999). Also detrital carbonates from the bedrock (*dead carbon*) potentially affect the radiocarbon concentration in the lacustrine system (Ramsey, 2008). For practical purposes, the offset between bulk age determinations and ages of organic material, is generally named the reservoir effect. Bulk limnic sediment might be subject to a reservoir offset on the order of thousands of years, which might result from lacustrine organic matter being in ^{14}C equilibrium with waters, or occurrence of some proportion of reworked organic material (Meyers and Lallier-Verges, 1999; Neumann et al., 2007).

Corrections are not always straight forward, and moreover, given system dynamics the reservoir effect might change over time (Stein et al., 2004). Still, in general, a reservoir effect can be accounted for in age modeling, if the offset between the sedimentological age and the measured ^{14}C activity can be estimated (Blaauw, 2010).

The reservoir offset resulting from hardwater effect and lacustrine dynamics can be estimated between endogenic carbonates and the respective syndepositional terrestrial organic matter, for the depths 9.78 mcd and 10.89 mcd (see Table 5.1). Samples no. 9 (organic) and no. 10 (biogenic carbonate) yield a reservoir offset of 370 (-80, +100) years. Samples no. 11 (organic) and no. 12 (biogenic carbonate) yield a reservoir offset of 250 (±190) years.

The offset between samples no. 7 (organic) and no. 8 (bulk carbonate) ranges from 725 years to 945 years. This is considerably higher than the previous doublets. Since sample nr.8 contains at least 50% of endogenic carbonates, this elevated reservoir offset is most likely due to a mixture of hardwater effect on the primary carbonates (chemically precipitated) and possibly minor amounts of incorporated carbon from detrital origin.

Table 5.1: Tephra and radiocarbon ages obtained for the composite profile IZN09/ LC2&LC3

No.	Sample I.D.	Core /Segment	Depth in Profile [mcd]	Material	$\delta^{13}C$(‰)	Radiocarbon age [ka BP]	Min [b] [ka cal BP]	Max [b] [ka cal BP]	Probab.[b] [%]
1	Beta 320052	SC1 BII	*n.i.c.*	bulk sediment[g]	-24.7	2.84 ± 0.03	2.87 3.01 3.05	3.01 3.04 3.06	87.5 5 2.4
2	Beta 320054	LC1 (0-2) II	4.34	bulk sediment[g]	-25.4	3.55 ± 0.03	3.72 3.81 3.95	3.8 3.92 3.96	27.4 67 0.6
3	AP2 Tephra	LC2 (0-2) II	4.58	-	-	3.52 ± 0.04[d] *(ka calBP)*	3.46	3.54	95
4	Beta 320053	LC1 (0-2) II	5.26	bulk sediment[g]	-24.8	4.72 ± 0.03	5.33 5.45 5.51	5.41 5.49 5.58	39.7 20.4 34.7
5	Beta 320056	LC1 (2-4) II	6.66	bulk sediment[g]	-24.6	5.66 ± 0.04	6.32 6.39	6.37 6.54	10.3 84.6
6	Beta 320055	LC1 (2-4) II	7.58	bulk sediment[g]	-23.9	6.76 ± 0.04	7.57	7.67	95
7	KIA 44582	LC1 (4-6) II	9.28	terrestrial plant remains[c]	-25.43 ± 0.20	8.23 ± 0.06	9.03 9.35	9.33 9.40	86.2 8.7
8	KIA 44584	LC1 (4-6) II	9.28	bulk sediment[a c h]	1.58 ± 0.21	9.065 ± 0.05	-	-	-
9	KIA 44585	LC1 (4-6) II	9.78	terrestrial plant remains	-26.75 ± 0.17	9.07 ± 0.05	10.17 10.32 10.35	10.3 10.34 10.38	90.2 2.1 2.7
10	KIA 44586	LC1 (4-6) II	9.78	ostracodes[a c]	-4.86 ± 0.17	9.44 ± 0.05	-	-	-
11	KIA 44588	LC1 (6-8) Ic	10.89	terrestrial plant remains[c]	-22.93 ± 0.14	12.34 ± 0.13	13.95	15.00	95
12	KIA 44589	LC1 (6-8) Ic	10.89	ostracodes[a]	-5.61 ± 0.18	12.59 ± 0.06	-	-	-
13	KIA 44591	LC1 (6-8) IIa	11.69	plant remains[c]	-23.41 ± 0.22	13.45 ± 0.1	15.98	16.9	95
14	KIA 44594	LC1 (8-10) IIa	13.28	shell fragments[a f]	1.63 ± 0.23	15.02 ± 0.08	17.26 17.36	17.34 17.97	3.9 91.1
15	Beta 324496	LC2 (8-10) II	13.37	bulk sediment[g]	-25.7	16.63 ± 0.07	19.48	20.09	95
16	KIA 44901	LC3 (12-14) II	13.58	shell fragments[a]	1.42 ± 0.20	16.91 ± 0.1	19.4 19.65	19.63 19.9	62.4 32.6
17	Y2 Tephra	LC2 (8-10) II	13.89	-	-	22.00 ± 0.9[e] *(ka calBP)*	20.97	22.93	95
18	Beta 324497	LC2 (10-12) I	14.52	bulk sediment[g]	-25.5	21.32 ± 0.10	25.01	25.88	95
19	KIA 42968	LC2 (10-12) II	15.27	shell fragments[a]	7.17 ± 0.27	25.5 ± 0.24	29.44	30.35	95
20	KIA 42969	LC2 (10-12) II	15.67	shell fragments[a]	4.46 ± 0.18	25.81 ± 0.25	29.54	30.63	95
21	KIA 42970	LC2 (10-12) II	16.11	shell *Dreissena*[a]	3.44 ± 0.16	27.33 ± 0.31	30.92	31.63	95
22	Beta 324498	LC2 (12-14) II	16.47	bulk sediment[g]	-25.5	27.14 ± 0.16	31.15	31.59	95
23	Beta 320057	LC2 (12-14) II	18.01	bulk sediment[g]	-24.5	27.4 ± 0.14	31.25	31.85	95

[a] *radiocarbon determination on carbonates: Dreissena, ostracode shells and bulk carbonate were not directly used to determine 'age depth' relation for the model*

[b] *calibrated age interval of ^{14}C analysis with 2 sigma standard error, after using the IntCal09 calibration curve (Reimer et al., 2009)*

[c] *these samples had an amount <1mg of C, nevertheless the results are reliable and in correspondence to those of the same depth on different material*

[d] *preferred age according to Santacroce et al. (2008), based on discussion and averaging of four radiocarbon datings (Rolandi et al., 1998; Santacroce et al., 2008; Terrasi et al., 1999; Vogel et al., 1990), and comparison to the varve age of 4150 yr BP from the Monticchio record (Wulf et al., 2004).*

[e] *equivalent weighted calibrated mean age of four radiocarbon dates (Eriksen et al., 1990; Pichler and Friedrich, 1976)*

[f] *a further age obtained on organic remains for the same depth yielded a radiocarbon age of ca. 14.8 ka BP. It's not presented in the table, or further used, as for small sample amount and additional technical problems during measurement it is considered a non-reliable age.*

[g] *radiocarbon content determined on bulk organic fraction*

[h] *radiocarbon content determined on bulk carbonate fraction*

5.2) Age-depth model

The age-depth model for the profile IZN09/LC2&LC3 of Lake Iznik is calculated using the code 'classical age modeling - clam' (Blaauw, 2010). For a first approximation of an age-depth model, a linear regression is assessed (Figure 5.1), considering all the dated levels. An 'average' sedimentation rate for the composite profile resulting from this linear regression is of 0.47 mm.yr^{-1}. This value gives a rough approximation of what is expected from the sedimentation rates for the profile. Furthermore, the average sedimentation rate generates an age of circa 31ka calBP for the sedimentary profile.

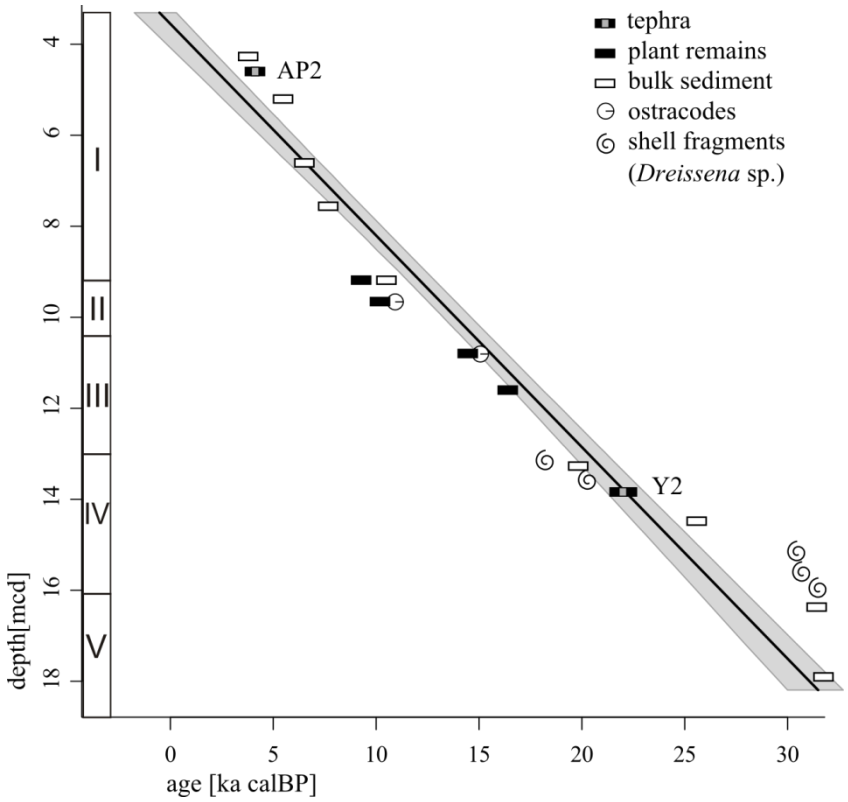

Figure 5.1: linear regression calculation considering all ages in the composite. No reservoir correction applied. Roman numerals on the left refer to sedimentary units. Grey shaded area refers to calibrated probability distribution.

A linear interpolation forces the 'best age estimate' (given by the black line in the plots) to pass through the dated levels. Hence, the changes in sedimentation rate within the profile IZN09/LC2&LC3 are delineated (Figure 5.2) (Telford et al., 2004). The code clam operates a Monte Carlo sampling on each calibration curve, meaning that all possible ages are considered for each dated layer, therefore a point estimate from the calibrated ages is not necessary and the uncertainties that it would implicate are considered within the model (Blaauw, 2010).

The calculated age-depth model is based on age determinations from organic samples no. 7, no. 9, no. 11, and no. 13; from bulk organic samples no. 2, no. 4, no. 5, no. 6, no. 15, no.18, and no. 23; and from tephras AP2 and Y2. Sample no. 18 is in chronological order with the Y2 tephra after calibration to calendar years. Ages excluded from the age-depth model are discussed in the following section. All ages were calibrated using the IntCal09 calibration curve (Reimer et al., 2009). The reliability of models' presented herein was enhanced with up to 10,000 iterations.

Organic matter deposited in Lake Iznik has an imprinted autochthonous character (section 8.2.1), i.e. most of organic material is in ^{14}C equilibrium with lake waters, and therefore a reservoir offset should be accounted for the limnic bulk organic matter. The maximum reservoir offsets estimated at three different depth levels within the sediment profile were of 440 yrs, 470 yrs, and 945 yrs. Assuming that these offsets represent the difference between the ^{14}C age of lake waters as registered within the biogenic and endogenic carbonates, and the atmospheric ^{14}C, an estimation of maximum 1000 years offset was applied to the bulk organic samples (Figure 5.2 and Figure 5.3).

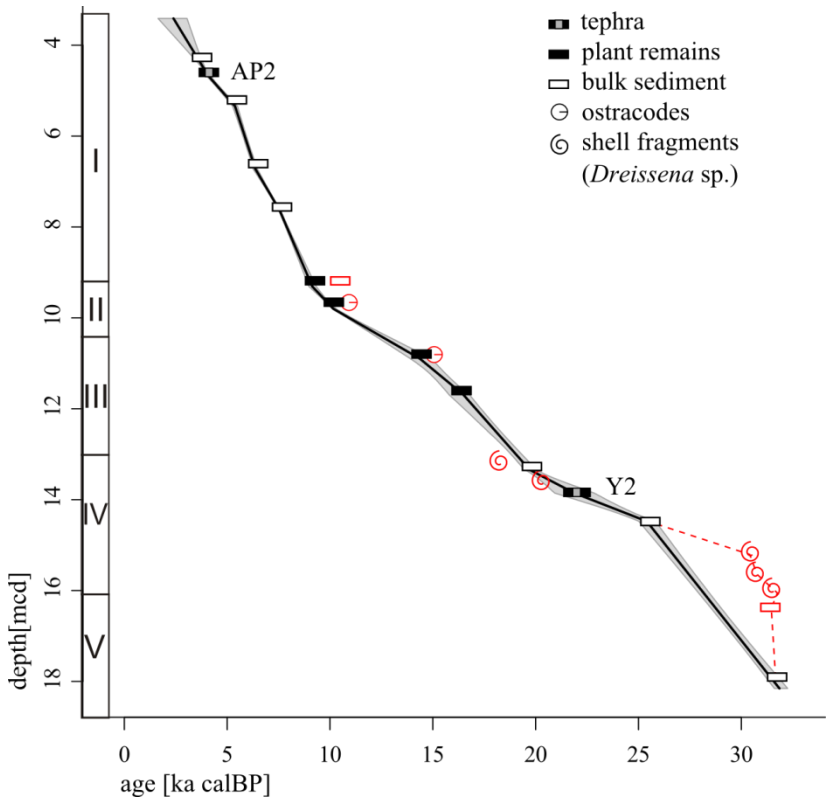

Figure 5.2: linear interpolation between the dated levels. No reservoir correction applied. Roman numbers on the left refer to sedimentary units. Grey shaded area refers to calibrated probability distribution. Red marked symbols refer to datings not included in calculation. Red dashed line indicates linear interpolation for the bottom profile if samples no. 19 to 22 were considered.

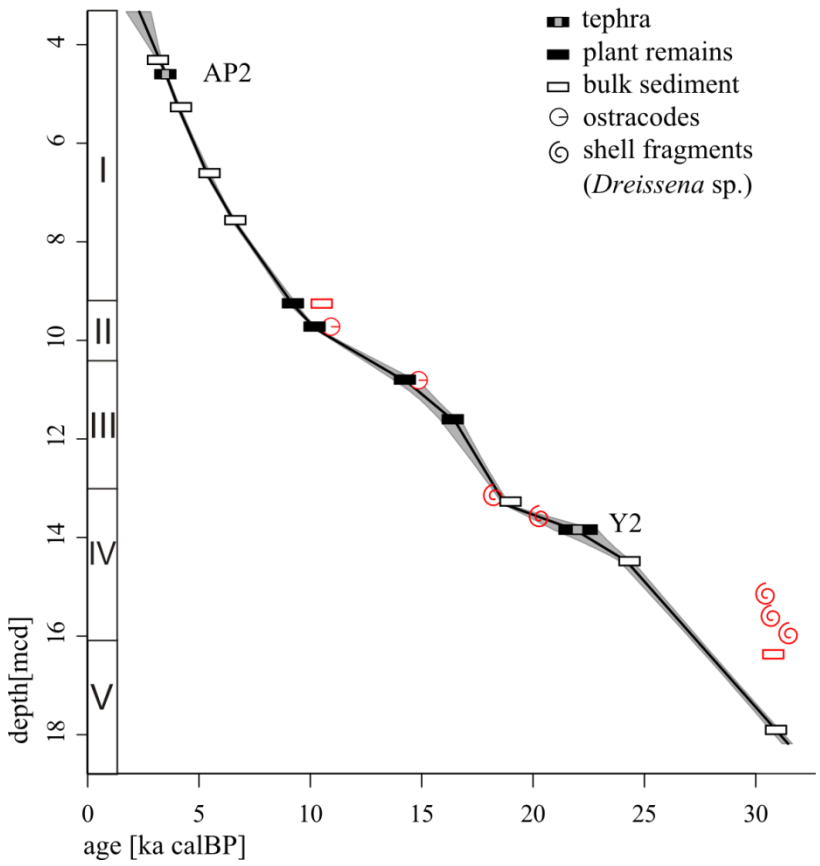

Figure 5.3: linear interpolation between the dated levels. Reservoir correction applied. Roman numbers on the left refer to sedimentary units. Grey shaded area refers to calibrated probability distribution. Red marked symbols refer to datings not included in calculation.

The new age-depth model calculates the Iznik profile to reach ~31 ka cal BP, which is circa 4000 years younger than a first proposed age model (Roeser et al., 2012). The new bottom age lies in the confidence range of the previous model, which presented high degree of uncertainty for the bottom profile.

5.2.1) Considerations on datings rejected for age depth model

During interpolation, samples no. 3 (AP2 tephra) and no. 2 (bulk organic) might present some age inversions, depending on one hand on the type of function used for the model and on the other hand on the considered age for the Vesuvius tephra. Hence, the radiocarbon mean age for AP2 was preferred over the varve age (section 4.2), especially when including corrections for the reservoir effect of the bulk ages (Figure 5.3).

Between 14.5 and 15.6 mcd, three different shell layers have almost the same age (samples no. 19, no. 20 and no. 21), partly with an age difference of only 300 years between ages 19 and 20. Despite the ages of these shells being older than the underlying bulk sediment, there is

no evidence from geochemical detrital input (e.g. Ti/Al), neither from grain size, that this interval could be one massive slump deposit of 1 m thickness. This is improbable given the location of the profile in the center of the lake. Instead, the *Dreissena* bivalves are expected to be (a) reworked, and/or (b) subject to a reservoir effect, as the shells live in ^{14}C equilibrium with the water body. For instance, *Melanopsis* shells from the modern alkaline environment of Lake Kinneret and surrounding waters have reservoir effects from 1000 up to 7200 years (Lev et al., 2007). Therefore, the age determinations on the *Dreissena* shells are no longer considered in the new age model. Also the ages of the endogen carbonates (samples no. 10 and no. 12) are not included in calculations, since for the same depth there are determinations on organic material. The latter also applies to bulk carbonate sample no. 8.

Samples no. 22 and no. 23, both conducted on bulk organic, present a radiocarbon age difference of less than 300 years for a cored interval of ~1.5 m. This would imply a sedimentation rate of 5 $mm.yr^{-1}$ which is improbable. The highest sedimentation rate for the sedimentary profile during the Holocene is of circa 1.1 $mm.yr^{-1}$, and an 'average' sedimentation rate can be considered to be 0.47 $mm.yr^{-1}$ (Figure 5.1). Considering a 'best case' scenario, in which the uppermost of these two levels has the minimum age value from its probability distribution function (pdf), 31.15 ka calBP, and the lowermost level the maximum age value of its distribution after calibration, 31.85 ka calBP (Table 5.1) the obtained sedimentation rate is ~2.1 $mm.yr^{-1}$, which is still relatively high. The occurrence of a slump, or mass movement deposition of 1.5 m thickness, is not conceivable. Both samples, at 16.47 mcd and 18.01 mcd, are placed in segments of the profile for which the geochemical and mineralogical data present smooth variations in accordance to each other. Additionally, grain size for this interval remains rather constant. The small amount of total organic carbon concentrations at this part of the profile, of about only 0.8% could be regarded as an issue for reliable radiocarbon measurements. However, circa 160 mg of dry material were measured for each sample, resulting in at least 1.3 mg of TOC, which is in the normal range for concentration of carbon for AMS measurements (1 to 2 mg C). Moreover, the given $\delta^{13}C$ ratios for the organic matter of samples no. 22 and no. 23, obtained along with the radiocarbon measurements are in agreement with the expectations for organic material, and also with all the other bulk organic ages in the profile (~ 24‰). The TOC/N rations of both samples are similar, 8.05 (at 16.5 mcd) and 7.59 (at 18 mcd), demonstrating that the quality of the organic matter has not changed dramatically in the interval, and has a predominant limnic origin.

Hence, one explanation for the apparent age inconsistency between samples no. 22 and no. 23 is that the bulk organic material from these samples is subject to different reservoir ages, sample no. 22 being subject to a higher offset than sample no. 23. These different reservoir offsets cannot be quantified through the available information. So it is reasonable to consider these ages as maximum ages for the levels in which they are located in the profile, which is ~31 ka calBP. Therefore, it is most reasonable to consider only the lowermost from the two dated levels with the given maximum age. Thus sample no. 22 is not further included in the calculations of the final age model. Moreover, such a divergence in the reservoir offsets for the bottom profile might be indicating profound changes in the limnological system for the Pleistocene.

5.3) Mass accumulation rates

The calculation of mass accumulation rates (MARs), or fluxes, avoids the issue of 'dilution' of sedimentary components, i.e. the compositional nature of data. Mass accumulation rates of the total accumulating sediment can be estimated by:

$$MAR = SR.\rho_{db}.10^3 \qquad \textit{(Eq. 5.1)}$$

ρ_{db}: dry bulk density [g cm^{-3}]

SR: sedimentation rate [mm $year^{-1}$]

MAR: mass accumulation rate [g m^{-2} $year^{-1}$]

However, the estimation of mass accumulation rate models is constrained by several factors. Sedimentation rates are much less precise than the measured concentrations of elements, which record slight compositional changes. For this reason, the application of the MARs to individual components can result in a loss in precision. The uncertainty further increases with the interpolation of unknown dated levels (Boyle, 2001). Another constriction in the determination of mass accumulation rates arises from the sedimentary dry bulk density. As this value is an estimate of the average sediment density, it does not reflect the different densities of the single components (e.g. carbonates, siliciclastics, organic material). Hence, the MAR signal modulates all components equally (Figure 5.4), and a distinction between which is the component responsible for the increase/decrease in the accumulation rate is not possible. Therefore, for the further chapters within this document, ratios of measured element concentrations are favored due to its higher precision. Additionally, a compositional analysis is undertaken.

The sediment accumulation in Lake Iznik fluctuated between circa 300 g m $^{-2}$ year^{-1} to 900 g m^{-2} year^{-1}. A whole lake extrapolation should be considered with care from a single core (Boyle, 2001). The calculated values allow first approximations with the magnitude of deposition in other lakes. In Lake Baikal, for instance, the sediment accumulation rates are in the order of 68 g m $^{-2}$ year^{-1} to 248 g m $^{-2}$ year^{-1} for different locations in the lake (Müller et al., 2005).

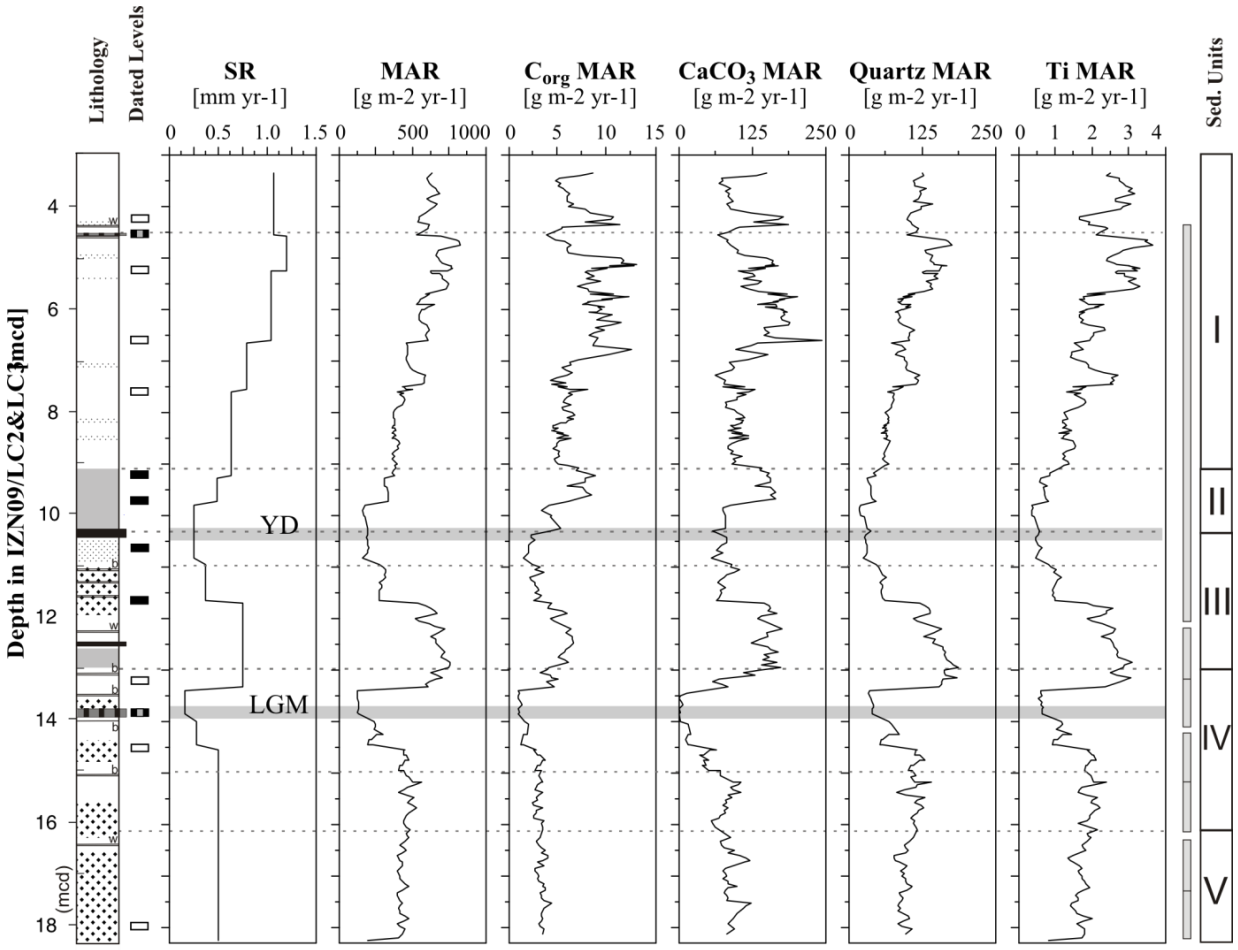

Figure 5.4: Sedimentation rates based on final age model and associated mass accumulation rates versus depth, in association to dated levels used in the age model. Example of estimation of the MARs to individual sedimentary components.

6.) Sedimentary geochemical and mineralogical evolution: a compositional approach

6.1) Introduction

Minerals and geochemical elements, as essential building blocks of sediments and its components, are powerful and indispensable tool for understanding evolution of a lake and its catchment, providing understanding for sedimentation processes. The nature of the mineralogical and geochemical sedimentary compositions asks for proper methods to explore and interpret the data.

This chapter investigates Lake Iznik's mineralogical and geochemical evolution over studied sediment profile using compositional data (CoDa) analysis and chemostratigraphy. CoDa is used for grouping of the chemical elements and minerals according to their environmental meaning, and to interpret and discuss processes controlling sedimentation. At beginning, an example of direct application of CoDa analysis to the Itrax corescanner data is given. The major conclusions are confirmed and extended by using CoDa analysis on an wider selection of elements – which have available values of concentrations – and the major mineral assemblage. Minerals that occur in trace amounts are inserted in a stratigraphic frame.

Based on the geochemical groups identified with CoDa analysis, the discussion of sediment geochemical evolution divides into (a) changes in the catchment (this chapter), (b) organic sedimentation and redox processes (chapter 8), and (c) carbonate accumulation (chapter 9). Herein, sediment geochemical evolution is discussed as reflecting evolving weathering intensity. For this, the applicable ratios identified within this study are compared to the conventionally applied chemical and mineralogical alteration indexes.

6.2) Nature of compositional data and brief history

An inherent issue regarding geochemical information or data, which deals with parts of a whole, is the relative interdependence of these parts (Aitchison, 2003b; Rollinson, 1993; Rollinson, 1992). The negative bias encountered within compositional data sets, was termed *spurious correlation* already in the nineteenth century by K. Pearson (Pawlowsky-Glahn et al., 2011 and references therein). Given this *closed* nature of the information, Euclidian geometry is not satisfactory for statistical data analysis within the natural sampling space of

compositional data, the so called *simplex* (Aitchison, 1982). The usage of standard statistical methods to raw compositional data might lead to inconsistent results, and even if the results seem reasonable, it remains open whether more information can be gained out of the data (Tolosana-Delgado et al., 2005). Already the calculation of univariate statistic parameters (e.g. mean, standard deviation) should regard the compositional nature of the gained data (Filzmoser et al., 2009). Compositional vectors provide information about relative values of the parts and every statement about a composition can be stated by a ratio of parts (Pawlowsky-Glahn et al., 2011). Realizing this, in the 80's John Aitchison develops a methodology based on logratio transformations to work with compositional data (CoDa). The use of logratio transformations bases on the fact that there is a direct correspondence between the compositional vector and the transformed logratio vector, thus allowing the unconstrained application of standard multivariate statistic methods to the transformed, *opened* data (Aitchison, 1982; Aitchison, 1983, 1984a; Aitchison, 1984b; Aitchison and Egozcue, 2005). Today, the compositional geometry, also *C-geometry* or *Aitchison geometry*, and operations therein, have been further improved. Novel developments on CoDa allow the investigation of compositional problems with a 'staying-in-the-simplex' approach, proposing the representation of the compositions by their associated Euclidian space coordinates (Pawlowsky-Glahn et al., 2011 and references therein). A review on the concepts that underlie the compositional data analysis within this chapter, as well as details corresponding to the applied methods, can be found in the supplementary material for the chapter (Appendix A6.1).

6.3) Bulk Geochemistry

6.3.1) CoDa Analysis

6.3.1.1) Major elements – Itrax core scanner

To come up with a first approximate characterization of sediments, a reduced selection of elements was made from those measured with the Itrax corescanner. This first discussion focuses on Ti, Al, Fe, Si, Ca, K, S and Sr; elements which fulfill the following criteria: count rates are in average minimum 150 counts per 10 seconds; the data scattering is low[8]; and the counted data contains only a few zeros[9]. The resulting sample size for scanning in 1 cm

[8] The absolute difference between subsequent values for element counts is proportionally less than 7% of the average of total counts for Ti, Fe, Si, Ca, K and Sr; 14% for Al; and 24% for S.
[9] The selected elements have less than 0.5% of zeros, hence the respective sample depths could be ignored.

resolution is of 1365 depths; which were computed for a compositional statistical summary. The centers for each of the elements, i.e. the proportion of the geometric mean of the number of counts, are Ca (0.6750), Fe (0.1600), K (0.0808), Ti (0.0615), Si (0.0151), Sr (0.0045), S (0.0018), and Al (0.0013)[10]. Physical properties such as water content of the sediments might influence the count intensities, especially for the relative light elements Si and Al (Tjallingii et al., 2007). In fact, this is reflected in the deviation between the counts in relation to the absolute concentrations as measured on discrete samples. Regarding the latter, the most abundant major elements are Si (19.55%) and Ca (8.10%), followed by Al (7.06%) and Fe (3.79%).

The clr-biplot of the selected subcomposition (Ti, Al, Fe, Si, Ca, K, S and Sr) shows that there is one set of elements which have very small variance between each other (Figure 6.1), and hence are strongly correlated. These are Ti, Al, Fe, Si, and K, all of them characterizing the siliciclastic sedimentation. In the clr-biplot the distances between vertices, i.e. the lengths of links, are proportional to the variances between the elements. The siliciclastic elements have nearly coincident vertices. This means that the variance in-between them is zero, or nearly zero, and consequently the ratio in between them is nearly constant. The vertices for K, Ti and Si are nearly coincident for any chosen projection of principal components, (1^{st} vs. 2^{nd}), (3^{rd} vs. 2^{nd}) and (1^{st} vs. 3^{rd}), (the two latter projections not illustrated herein). The distribution of siliciclastic elements is mainly controlled by the same process, i.e. the detrital input. However, the projection (1^{st} vs. 3^{rd}) separates Al and Fe from the further siliciclastic elements (Ti, K, Si), indicating that Al and Fe are additionally influenced by some other processes, for instance Fe can be subject to redox mobility in the sedimentary column after deposition and consequently precipitated as iron-monosulfides. Therefore, the elements which are most representative for the detrital supply are K and Ti, titanium because of its immobile geochemical character in sedimentary environments, and potassium due to its association to the detrital mineral muscovite and/or its clay counterpart illite. The same conclusion is derived from the computed variance table (Appendix A6.1).

The elements Ca, and Sr, as alkaline earth metals, present low variance in between each other, and characterize the carbonate sedimentation (chapter 9). Nevertheless, the (3^{rd} vs. 2^{nd}) projection of the clr-biplot (not illustrated) indicates some variance in-between them. Sulfur belongs to neither of the identified groups, and presents one-dimensional variability in

[10] These centers represent the closed geometric mean of the counts obtained for each element by the Itrax core scanner. For instance, the order of magnitude of counts of Ca and Fe, [$x10^5$], is one order higher than the counts of K, Ti, and Si, which otherwise have counts one order of magnitude higher than Sr, S, and Al.

relation to each of these groups. Sulfur is most likely related to organic input and/or a diagenetic component (further discussion in section 8.2.3).

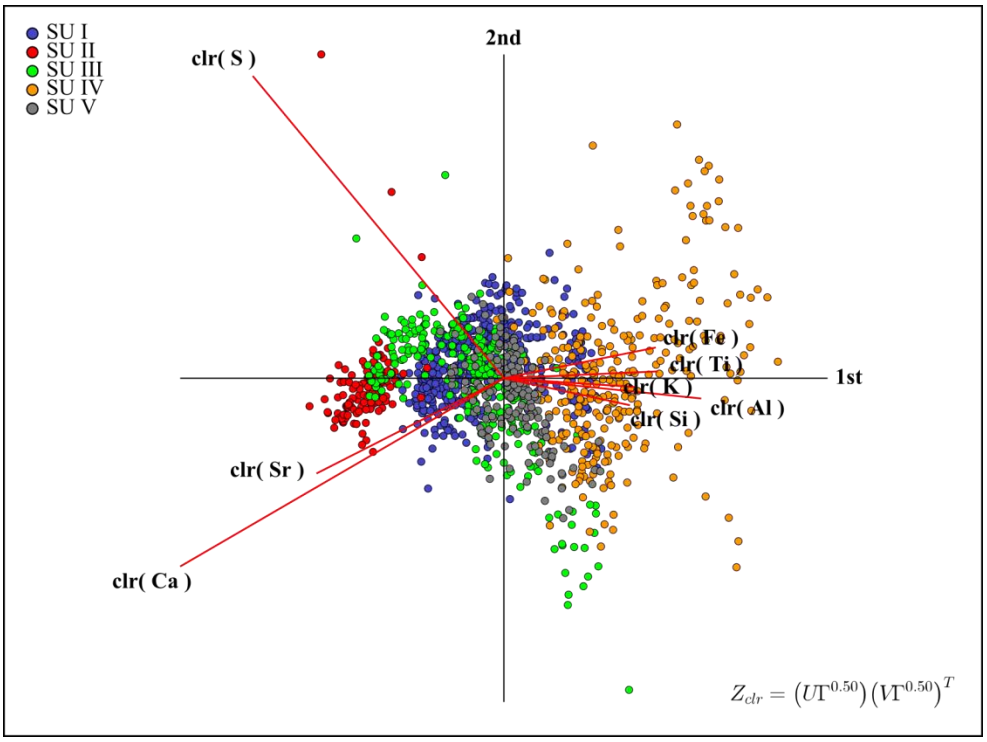

Figure 6.1: (1^{st} vs. 2^{nd}) projection of clr-biplot for subcomposition (Al, Si, S, K, Ca, Ti, Fe, Sr). Data obtained from the Itrax core scanner (1 cm resolution, i.e. sample size 1316). The cumulative explained proportions by the principal components underlying the biplot are PC1(0.8012), PC2(0.9482), and PC3(0.9722).

Furthermore, the clr-biplot allows a geochemical differentiation between the sedimentary units (Figure 6.1). Unit II (red observations) is characterized by the carbonate and sulfur fraction, and unit IV (orange observations) is mainly characterized by the siliciclastic elements. Units I and V are equally distributed in-between the groups of elements. Unit III (green observations) is partly characterized by the carbonate phase, (sample points within the 4^{th} quadrant). Furthermore, unit III sample points are spatially distributed along the direction of the sulfur ray.

6.3.1.2) Major elements and trace elements

From the discrete samples the determined major elements are C, S, N, Si, Al, Fe, Mn, Mg, Ca, Na, K, Ti, and P (Table 6.1). For the carbon content, total inorganic carbon (TIC) and total organic carbon (TOC) fractions were separately determined. From the measured trace elements, the selected elements for CoDa analysis were V, Cr, Co, Ni, Cu, Zn, Ga, As, Rb, Sr,

Y, Zr, Nb, Ba, W, Pb, Th, and U (Table 6.2), as for these elements less than 10% of data is below the detection limit[11].

The logratio approach is not suitable if the data set contains spots of missing data or zeros. If the zeros are of the type *rounded zeros* – which is the case when measurement of a determined element is below the detection limit, imputation techniques can be used to replace those zeros. It is practical to replace them by small, non zero, values. If the data set has less than 10% (of the complete matrix) of values below zero, a non-parametric replacement is appropriate, and the threshold 0.65 of the detection limit is a reasonable option (Martín-Fernández et al., 2003). This was the case for uranium.

Table 6.1: Average concentrations (geometric) for major elements along profile IZN09/LC2&LC3. Concentrations in weight percent [wt.%] (section 3.9.1)

SU	TOC	TIC	S'[12]	N	Si	Al	Fe	Mn[13]	Mg	Ca	Na	K	Ti	P
sc	1.93	2.89	0.38	0.22	17.81	6.80	3.57	0.07	1.25	10.20	0.50	1.45	0.36	0.04
I	1.30	2.58	0.50	0.15	18.65	7.08	3.73	0.07	2.16	8.67	0.55	1.60	0.37	0.05
II	2.25	5.26	0.66	0.19	12.65	4.36	2.34	0.05	1.33	17.42	0.44	0.94	0.23	0.04
III	0.91	3.18	0.54	0.11	18.48	6.48	3.62	0.08	1.38	10.76	0.67	1.52	0.34	0.04
IV	0.68	1.03	0.25	0.12	23.34	8.54	4.73	0.12	1.46	3.79	0.78	1.96	0.43	0.05
V	0.79	2.48	0.33	0.11	20.77	7.56	4.07	0.09	1.32	8.19	0.73	1.68	0.39	0.05

Table 6.2: Average concentrations (geometric) for selected trace elements along profile IZN09/LC2&LC3. Concentrations in parts per million [ppm].

Sed. Unit	V	Cr	Co	Ni	Cu	Zn
sc	108.07	73.11	14.86	47.17	30.05	72.10
I	111.94	81.24	16.16	54.39	30.13	76.21
II	70.99	45.15	10.33	29.61	19.00	49.42
III	104.57	71.16	15.30	46.00	27.33	69.59
IV	134.33	93.75	18.84	61.06	32.47	89.18
V	117.65	84.31	17.15	56.22	30.94	79.91
Sed. Unit	**Sr**	**Y**	**Zr**	**Nb**	**Ba**	**W**
sc	386.64	19.88	110.54	7.43	335.34	13.48
I	329.17	21.45	116.54	8.23	338.82	13.95
II	571.03	14.16	73.80	4.60	270.20	8.56
III	381.26	20.22	111.84	7.53	349.37	13.53
IV	163.31	25.54	144.61	10.13	355.98	18.23
V	299.20	22.59	125.83	8.72	360.17	15.00

The elementary composition for discrete measurements (5 cm depth resolution, sample size ca. 330) was computed for the compositional statistical summary. The variation matrix for the overall composition of the profile IZN09/LC2&LC3 is given in Appendix 6A.1. As expected,

[11] Further trace elements were not considered herein because they have scattered information, more than 10% of values under the detection limit (rounded zeros), or the rounded zeros appear grouped, which require a different approach to replace the zeros.

[12] S' refers to sulfur concentrations obtained with purge and trap chromatography. Details for methods in section 3.9.2 and comparison to additional sulfur measurements in section 8.2.3

[13] Manganese concentrations were preferred from measurements from fused discs

the sedimentary phases, siliciclastic, carbonate and organic are deduced from the clr-biplot of the wider element selection (Figure 6.2), representing the same phases as observed from the Itrax data. However, S shows a high variance with regard to the organic phase.

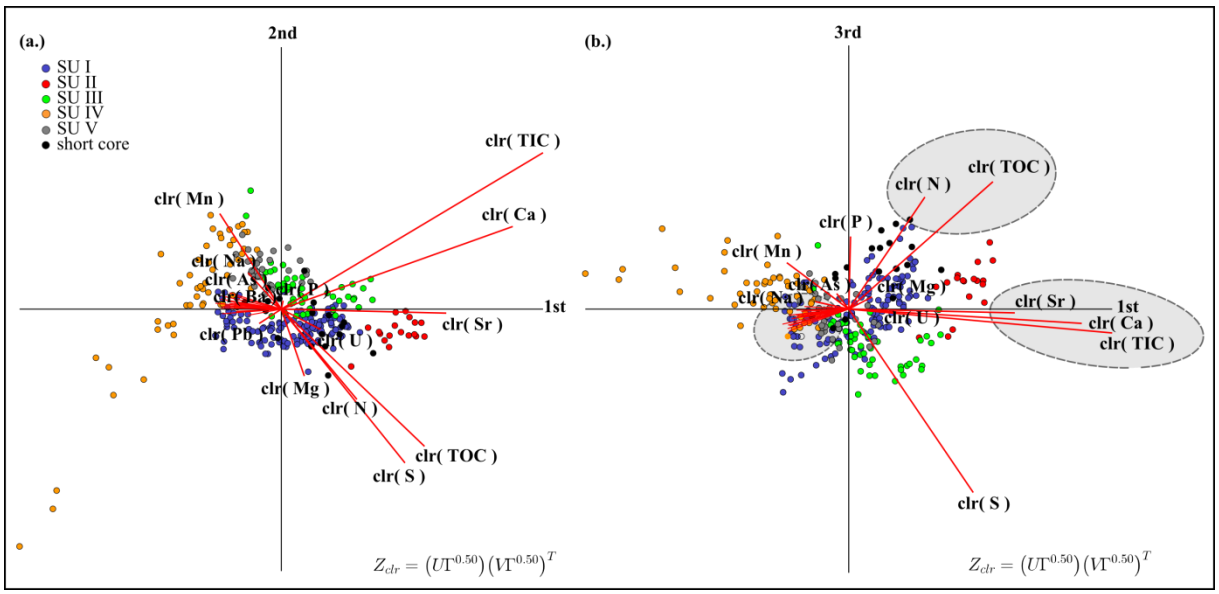

Figure 6.2: (1^{st} vs. 2^{nd}) and (1^{st} vs. 3^{rd}) projections of the clr-biplot for composition (TIC, TOC, S, N; Si, Al, Fe, Mn, Mg, Ca, Na, K, Ti, P; V, Cr, Co, Ni, Cu, Zn, Ga, As, Rb, Sr, Y, Zr, Nb, Ba, W, Pb, Th, U). The cumulative explained proportions PC1 (0.6828), PC2(0.7915), PC3(0.8499). Gray circle in the 3^{rd} and 4^{th} quadrant refers to (Si, Al, Fe, K, Ti, V, Cr, Co, Ni, Cu, Zn, Ga, Rb, Y, Zr, Nb, W, and Th) - element symbols were omitted from figure for simplicity.

The siliciclastic elements have nearly coincident vertices within the clr-biplot. The elements which have very low variance as siliciclastic fraction, and hence strong correlation, are Si, Al, Fe, K, Ti, V, Cr, Co, Ni, Cu, Zn, Ga, Rb, Y, Zr, Nb, W, and Th. The carbonate group is given by the low to intermediate variance between TIC, Ca, and Sr. U shows small variance to the carbonate and organic groups. The organic group is given by the low to intermediate variances between TOC, and N. Notably, Mg shows very small variance to the organic group, especially to nitrogen. But Mg also has low variance to Si, Al and Fe. Elements which are not associated directly to one of the three identified groups are S, Mn, Na, P, As, Pb, and U, hence their rate of supply, and/or fixation into the sediments is further controlled by additional processes than just the siliciclastic fraction. For instance, authigenic mineral formation can remobilize Pb and As to sulfides (e.g. arsenopyrite), P to phosphates (e.g. vivianite) and Mn to carbonate (e.g. rhodochrosite). The investigation of a further biplot, in which solely the trace elements are considered (not illustrated herein), leads to the same conclusions. Additional information from such a trace element clr- biplot is that Ba, as alkaline element, has intermediate variance to carbonate phase, and Unit III is further characterized by As.

One property of the clr-biplot (strictly speaking, of the *covariance* biplot) is that perpendicular links indicate that the involved log-ratios have nearly zero correlation, i.e. are independent (Aitchison and Greenacre, 2002). For example, the link connecting Mn and U, and the link connecting TIC and a siliciclastic element (e.g. Ti), are nearly at a right angle (Figure 6.2 a). Hence, the processes related to log(Mn/U) fixation in the sediments, which are influenced by oxygenation state, are primarily not related to the processes that control log(Ca/Ti), i.e. calcium accumulation.

The variation matrix (Appendix A6.1) allows some further observations: (1) TOC, Mg, P, Cu, Sr, Ba, Pb, U have low variance to nitrogen; (2) N, and Sr, have the lowest variance to TOC and hence are strongly correlated; (3) from the trace elements with lowest variance to the major siliciclastic elements, Y has the lowest variance to (Si, Al); and Rb has lowest variance to K.

Again, the sedimentary units can be differentiated geochemically (Figure 6.2). Hence, the dominant process controlling sedimentation is changing over time. For instance, the groups of elements which are most striking in characterizing the units can be summarized as follows. Unit I: organic, carbonates, siliciclastics. Unit II: carbonates, and organic. Unit III: S, carbonates, As and P. Unit IV: siliciclastics, and Mn. Unit V: siliciclastics, carbonates, and organic. Note that circa one third of the samples from Unit III behave geochemically similar to samples from Unit II.

Ternary diagrams further depict the relation between the carbonate and siliciclastic groups (represented by Ca and Ti) to selected elements. The Holocene deposition – sediment units I, II and the short core – is characterized by changes in alkaline earth metal, Mg, and alkali metal, Na, as well as the organic sedimentation. Mg increases towards unit I, conversely the short core has similar Mg/Ti ratio as the other units (Figure 6.3 a). Interestingly, Na values are reduced for unit I and the short core (Figure 6.3 b).

Total organic carbon values are the highest for units II, I and the short core. For the subcomposition (TOC, Ca, Ti) the variability is equally distributed among the components (Figure 6.3 c). Regarding the carbonate phase, unit IV is distinct. For instance, the Ca/Sr ratio, for unit IV differs of that for all the other sedimentary units (Figure 6.3 d). Regarding redox sensitive elements, when considering the subcomposition (Ti, Mn, U) the data plots along the boomerang like curve, which resembles the linear relationship within the simplex (Figure 6.3 f). Herein, Ti stays for a geochemically immobile element, and the variability within the subcomposition is given by Mn and U, which present soluble mobile forms under reducing

and oxic conditions, respectively (Bonotto and Silveira, 2006; Davison, 1993). Notably, the extremities are again marked by units II and IV. Moreover, Mn accumulation is strongly correlated with unit IV (Figure 6.3 e).

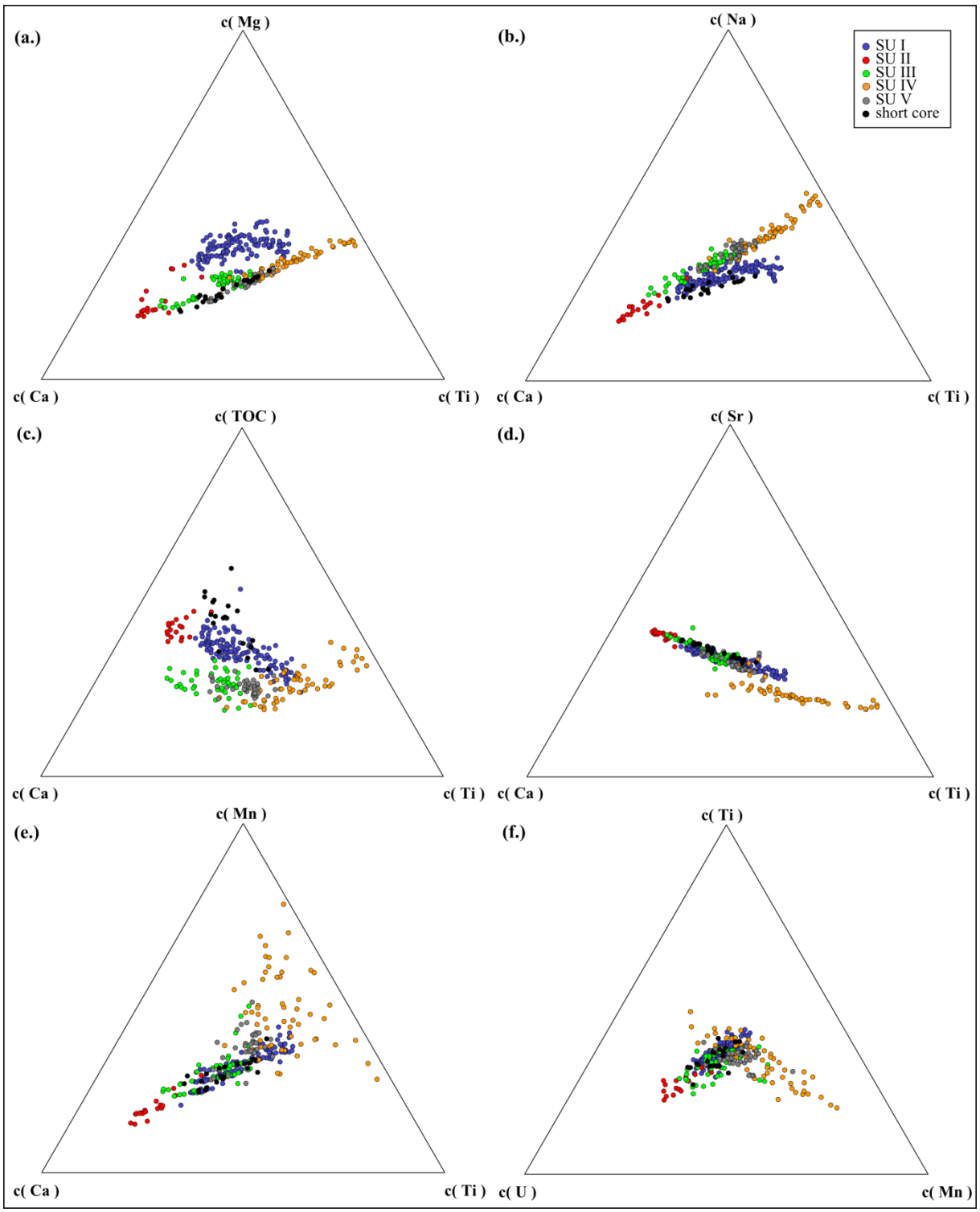

Figure 6.3: Selected ternary plots for the major and trace elements

6.3.2) Stratigraphic changes

The stratigraphic changes for the three major sedimentary components (siliciclastic, carbonate and organic) are given in Figure 6.4. Black curves show the data from the Itrax corescanner (1 cm resolution), and the gray curves show the concentrations for the discrete samples (5 cm resolution). Despite the lower resolution, the curves from discrete samples and scanner covariate exceptionally well. Due to the nature of the data, the siliciclastic (Si, Ti) and carbonate (Ca, TIC) phases are clearly complementary. Stratigraphic changes for additional elements and/or ratios are inserted in the respective discussions.

Starting from the base, unit V defines a constant background value for the three sedimentary components. Two cycles of carbonate and organic increase, are identified (16.5, and 17.5 mcd). Unit IV has the lowest percentages for organic carbon, inorganic carbon, and calcium accumulation (Ca/Ti). However, three recurring peaks are identified for the Ca/Ti (14.2, 14.5, and 15.29 mcd); and for TIC (14.2, 14.5 and 15.39 mcd) marked as gray horizontal bars in Figure 6.4. The Y2 Tephra, at 13.89 mcd, is outlined by an increase in Si and retreat in Ti values. Furthermore, the interval between 13.5 and 14 mcd is characterized by the nearly absence of Ca and TIC. The samples from this interval correspond to most extreme values for unit IV (clr-biplot, 3rd quadrant, Figure 6.2 a).

Unit III also shows a constant calcium accumulation (Figure 6.4), from 13 mcd to circa 11 mcd, with values similar to unit V. From 11 mcd upwards, Ca/Ti increases – oscillating in high amplitudes, towards unit II, where it reaches its maxima. Additionally to the highest calcium accumulation, unit II is characterized by the abrupt rise in TOC concentrations, which peak in the highest values for the profile. Note that the samples from unit III with higher Ca/Ti ratio, are those which in the clr-biplot behave like samples from unit II (Figure 6.2). Hence, it becomes meaningful to subdivide unit III at approximately 11mcd.

The transition between units II and I is marked by the simultaneous decrease in Ca/Ti, TIC and TOC values, being accompanied by the increase in siliciclastic elements. The carbonate and organic components behave parallel from unit II towards the top profile, with similar amplitudes. One observed exception is the TIC peak at 6.62 mcd.

Further detrital elements have been illustrated stratigraphically along with the lithological descriptions in chapter 4. For example, the behavior of Fe (Figure 4.2) is close to the siliciclastic elements Si, and Ti; except for unit IV, where Fe is enriched at distinct spots.

Moreover, the ratio between two siliciclastic elements K and Ti (Figure 4.2) outlines their nearly coincident information, i.e. nearly constant ratio. Nevertheless, slight shifts might be associated to changes in grain size and/or mineralogic composition.

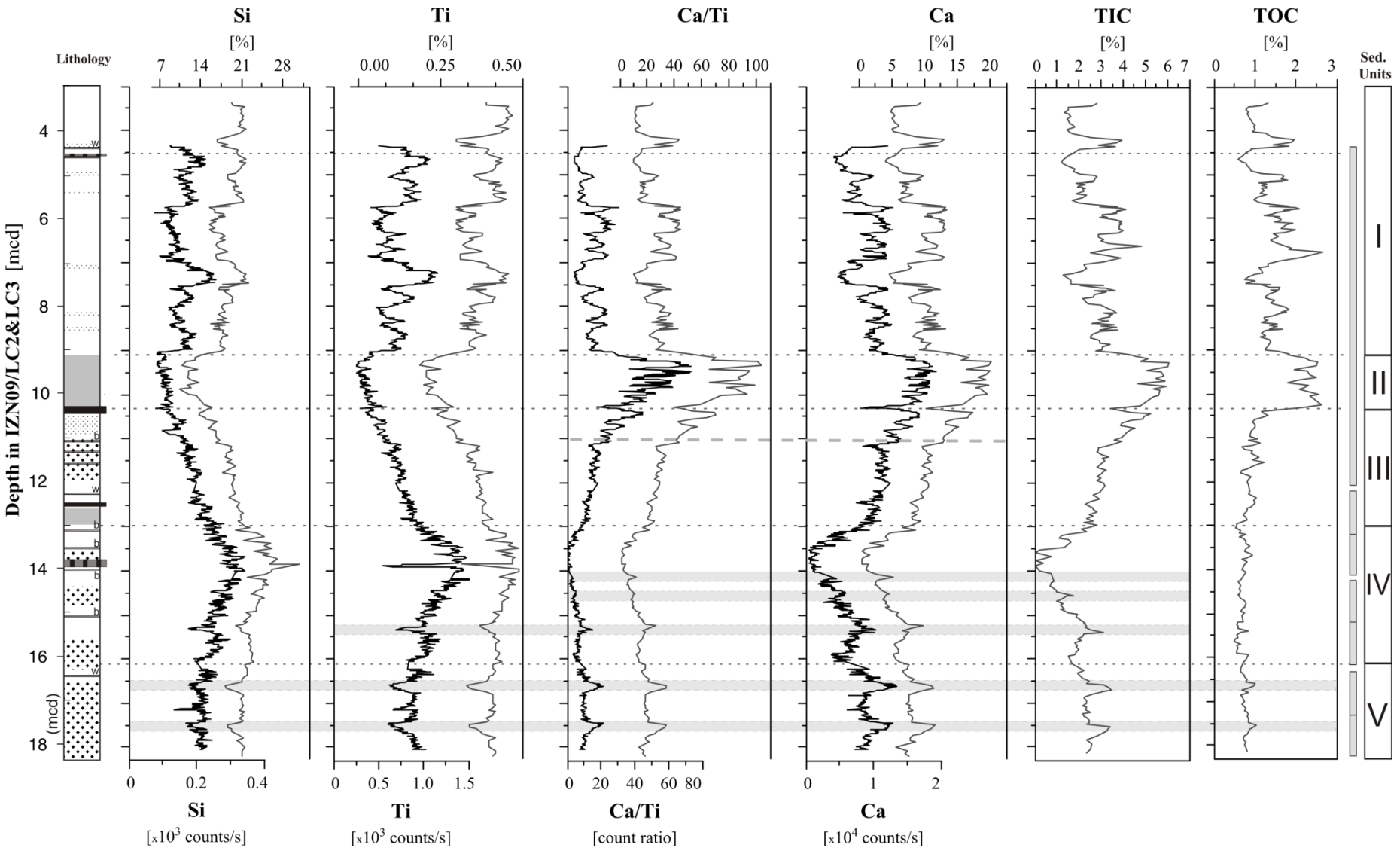

Figure 6.4: Stratigraphic changes for representative elements of the main sedimentary components: siliciclastic (Si, and Ti), carbonate (Ca/Ti, Ca, and TIC), and organic (TOC). Black curves stand for Itrax Corescanner data (1cm resolution), and gray curves stand for measurements on discrete samples (5 cm resolution).

6.4) Bulk Mineralogy

The major minerals that compose the bulk mineral assemblage of Lake Iznik sediments are quartz, feldspar (plagioclase), kaolinite/chlorite, muscovite/illite, and the carbonate polymorphs calcite and aragonite (Franz et al., 2006; Ülgen et al., 2012; Viehberg et al., 2012). The Iznik sediments are well sorted silty-clays, but some of the minerals are enriched in one or the other size fraction.

Muscovite – $KAl_2(Si_3Al)O_{10}(OH,F)_2$, and illite – $(K,H_3O)(Al,Mg,Fe)_2(Si,Al)_4O_{10}[(OH)_2 H_2O)]$, are identified in the bulk sediments, and illitic material is also abundant in the clay size fraction. The identified feldspar is the sodium end member of the plagioclase series, albite ($NaAlSi_3O_8$).

The concomitant presence of kaolinite ($Al_4Si_4O_{10}(OH)_8$) and chlorite in the bulk sediment is well delineated by the double-peak appearance at the 7Å region, allowing for good separation in between them. The chlorite type was identified as clinochlore – $(Mg,Fe^{++})_5Al(Si_3Al)O_{10}(OH)_8$, for which the dominant cation in the octahedral sites is magnesium (Moore and Robert C. Reynolds, 1997). In the clay size fraction chlorite is present rather in smaller amounts (section 6.4.3). The hitherto identified smectite could not be confirmed in oriented slides, and the respective reflection in the bulk random powder mounts is most likely due to chlorite and/or vermiculite (see section 6.4.3).

6.4.1) CoDa analysis

The seven identified mineral phases were quantified downcore means rietveld analysis, which results in a closed data vector for each depth. Because the identified trace minerals occur only in specific depths, they were not included in the rietveld analysis, so that the major composition remains uniform for the complete profile (Table 6.3).

Table 6.3: Average concentrations (geometric) for major mineral assemblage along profile IZN09/LC2&LC3. Concentrations in [w%]

SU	Quartz	Albite	Muscovite /Illite	Clinochlore	Kaolinite	Calcite	Aragonite
SC	17.2	9.2	15.0	13.4	15.3	5.3	22.6
I	18.2	8.5	18.0	13.7	15.5	6.9	16.5
II	12.5	7.7	10.0	8.4	10.2	6.2	43.0
III	19.7	11.1	15.3	12.9	10.6	9.3	17.5
IV	25.7	13.0	19.9	16.2	12.7	5.8	1.5
V	21.9	12.07	17.8	13.3	11.9	5.2	16.7

The clr-biplot of the closed mineralogical data set shows that variability of the mineralogical information is retained in the carbonates; at the same time as aragonite and calcite also have high variance in between each other. The near perpendicular links of log(aragonite/quartz) and log(calcite/albite), enlighten that the processes related to the mineral ratios originating the links have low correlation, or are independent (Figure 6.5). Similar independent processes can be found in the biplot for other ratios, although always in relation to the carbonate minerals. The ternary diagram with amalgamated coarse siliciclastic minerals (quartz, and albite), clays (kaolinite, chlorite, and illite) and carbonates (calcite, and aragonite) also shows how the carbonates retain most of variability of the mineral composition (Figure 6.6 a). Regarding the sedimentary units, aragonite retains most variability among the carbonate phases, as unit II and IV are the extremes with the highest and lowest relation to aragonite, respectively (Figure 6.5). In addition, the samples of unit IV are dispersed in the direction of the calcite ray. Notable is that for unit III (green observations), part of the samples are related to calcite, whilst a smaller part relates to aragonite, together with unit II. Aragonite is nearly absent from unit IV, accordingly unit IV retains the highest calcite variability (Figure 6.6 b). Moreover, calcite is more abundant in units III, and IV, and less abundant in unit V, whereas the calcite/quartz ratio is fairly constant for units II, I and the short core.

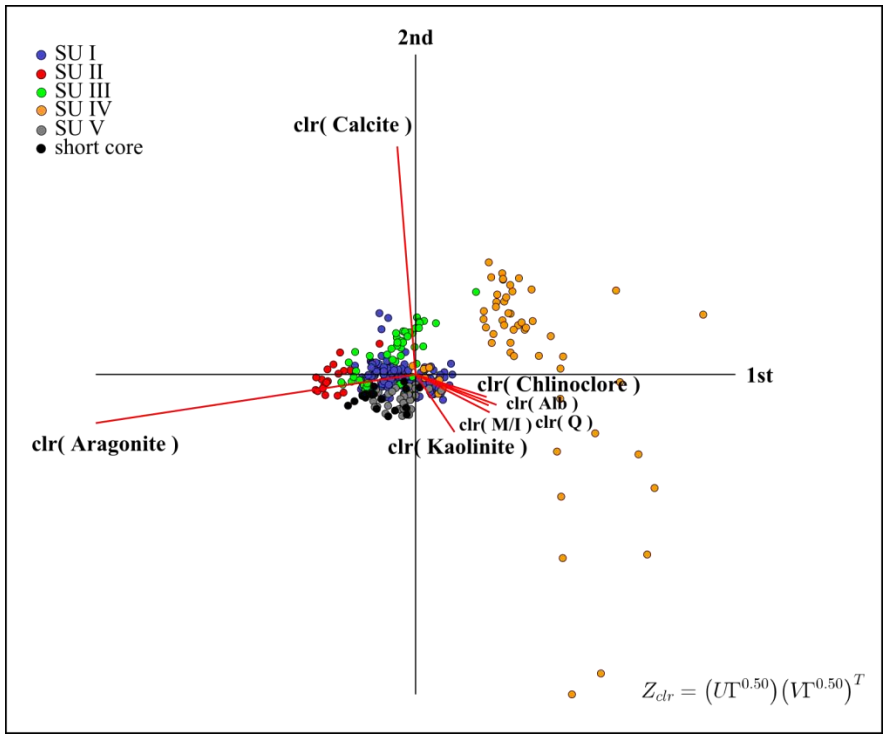

Figure 6.5: Compositional clr-biplot for major mineral assemblage. Cumulative explained proportions are PC1 (0.7588), PC2(0.9377), PC3(0.9784).

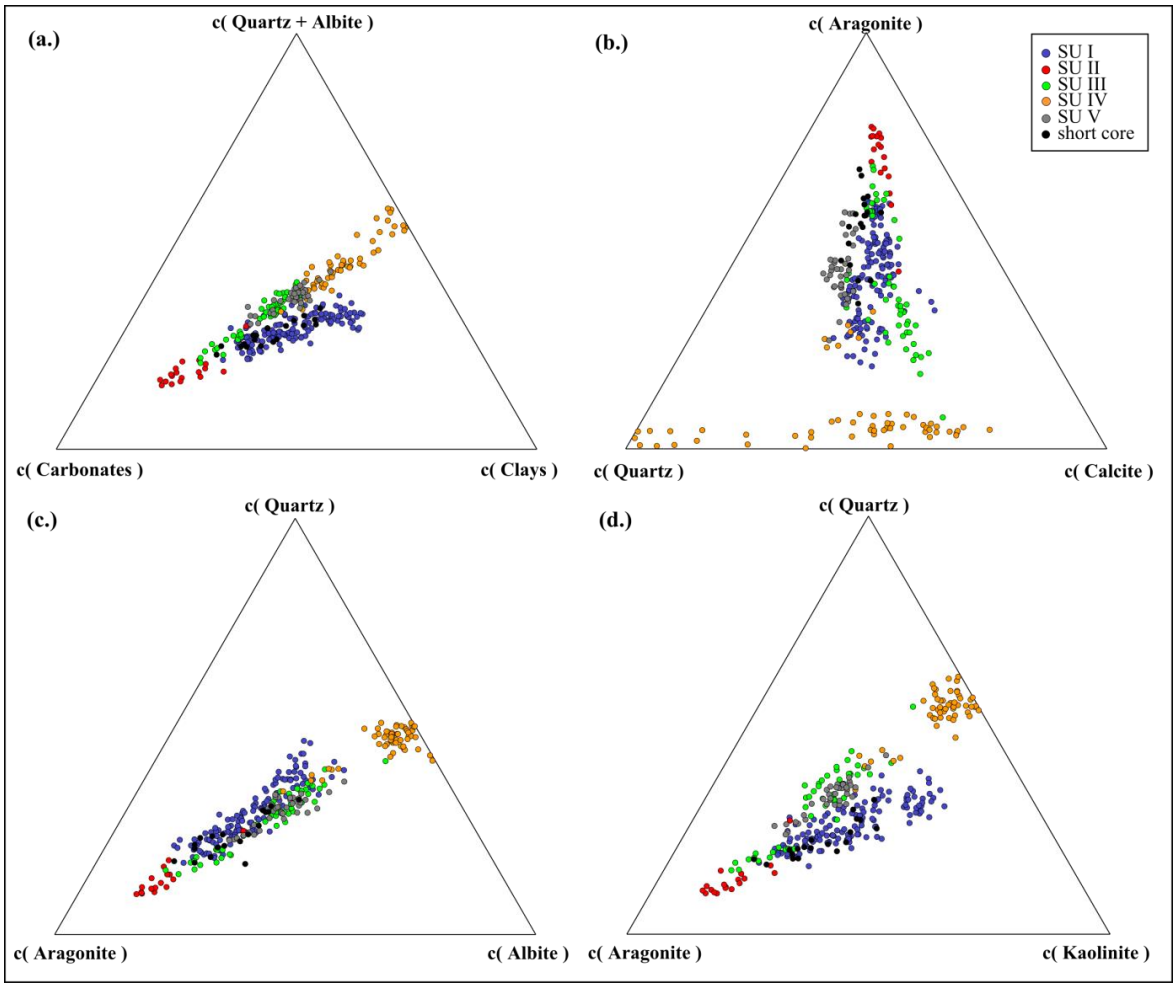

Figure 6.6: selected ternary diagrams for the major mineral assemblage.

The siliciclastic assemblage carries amounts of redundant information given the nearly coincident vertices of quartz and the silicates (Figure 6.5). Notably, kaolinite shows the higher variance to the other siliciclastic minerals. Moreover, a change in the ratio between 'coarse' (quartz, and albite) and 'fine' (clays) detrital minerals marks the transition from Pleistocene (units V, IV III) to Holocene (units II, I and sc) (Figure 6.6 a). In fact, a shift of unit I, from albite towards kaolinite is observed in the correspondent subcompositions (Figure 6.6 c, d). Kaolinite is related mainly to unit I, whereas albite relates to units III and V. These observations are in agreement with the further projections of clr-biplot (not illustrated), and the variation matrix (Appendix A6.1), which show a general pattern of low variances in between the clay assemblages with/and quartz, whereby kaolinite is the clay mineral with generally highest variance.

6.4.2) Stratigraphic changes

The mineralogy of profile clearly correlates to the pre-defined sedimentary units V to I. In the most basal unit V, the abundance of all mineral is nearly constant (Figure 6.7). Aragonite presents a fairly constant background at circa 15%, but shows two defined maxima of circa 26% (16.5 mcd, and 17.5 mcd). In unit IV, the silicates remain at constant values and quartz reaches a maximum for the entire core of 30%. At the upper and lower limits of unit IV carbonate fraction is subject to abrupt reversals of dominance between calcite and aragonite. Moreover, aragonite concentrations are very low for the entire unit IV (2%). Within units III and II, the abundances of quartz, muscovite/illite and albite are decreasing upwards, whereas clinochlore and kaolinite are constant. Calcite presents a 'step-decrease', at 11 mcd, and above and below this shift rather constant concentrations. Also at 11 mcd, aragonite concentrations increase abruptly, and continue increasing upwards in the profile to reach its highest abundace within unit II.

The transition from unit II to I is marked by the retreat of aragonite concentrations from nearly 50% to ca. 20%, which is accompanied by a slight increase from all the other minerals.

Unit I is characterized by nearly constant calcite concentrations, and increase in the average kaolinite concentrations. Aragonite is the mineral with the highest amplitude changes within the entire profile. Notable is a concomitant increase of calcite and aragonite at circa 4.3 mcd.

The sediment fraction <63 µm (wet-sieved) was also investigated for its mineralogy (red curves within Figure 6.7). The striking mineralogical changes in Unit IV cannot be caused by the occurrence of shells, as they are rather sparse - and large fragments had been removed manually in the bulk fraction. However, quartz and the silicates are enriched in the finer or coarser size fractions. Regarding this aspect, a subdivision for unit IV is proposed at a depth of circa 15 mcd. Below that, quartz is equally distributed in the bulk and <63 µm fraction, albite is enriched in the <63 µm fraction, and clinochlore is enriched in the coarser fractions. Above the depth of 15 mcd, quartz and muscovite/illite are more concentrated in the silt-clay fraction, whilst kaolinite and clinochlore are enriched in the coarser fraction.

6.4.3) Clay size fraction

The clay fraction was analyzed in a resolution of approximately 20 cm (section 3.8.2). The samples distributed along the profile are homogeneous regarding the minerals present in the clay fraction. In other words, the qualitative clay composition is similar among the

sedimentary units. The identified mineral phases belong to the four main clay groups (with 001 reflections at ~7Å, ~10Å, and ~14Å for air dried slides). The respective mineral phases are kaolinite, illite, chlorite, and most likely vermiculite. Interstratified clay minerals are present to some degree, mainly regarding the illite and vermiculite phases. Some brief observations on the identification follow.

In general, there was small response for the ethylene glycol solvation for the almost complete range of $^{o}2\theta$ positions of the diffractograms. No expansion to 17Å is observed; therefore, highly expandable smectite was not detected in the complete profile. Instead, a slight expansion is observed for the 14Å reflection to circa 15Å. This minor response to solvation, followed by stepwise collapse after heating to 350^{o}C and 550^{o}C degrees, can classify the mineral phase as intermediate to high charge vermiculite (002 and 003 reflections are also present). To make a conclusive statement towards vermiculite, further procedure would be necessary, e.g. Mg saturation and glycerol solvation (Moore and Robert C. Reynolds, 1997). On the other hand, for some depths presence of vermiculite is clear by the additional 4.80Å reflection, moreover indicating no Fe substitution for Mg in the octahedral sites.

Illite is outlined by its characteristic 001, 002 and 003 reflections, maintained after solvation and heating. At some depths its 002 reflection is asymmetric indicating some degree of interstratification. After heating for 550^{o}C, the collapsed vermiculite aggregates partly as ‘step like’ shoulders texture in the illite 001 and 003 reflections.

Regarding kaolinite and chlorite, the expected double peak at 7Å, is clearly observed in the bulk measurements, and not well delineated in the clay size fraction. At some depths however, the 7Å reflection is asymmetric. Also the doublet 3.58Å /3.54Å (002 and 004 reflections for kaolinite and chlorite respectively) indicates that only minor amounts of chlorite are present in the clay fraction, hence it is enriched in the silt.

There is interference of the kaolinite, vermiculite and chlorite patterns (001 chlorite with 001 vermiculite, 002 vermiculite and 001 kaolinite, and 004 chlorite with 002 kaolinite and 003 vermiculite), which difficult the semi-quantifications for single phases. Nevertheless, the intensity of the chlorite diagnostic phase of 4.74 Å (003 reflection) (Moore and Robert C. Reynolds, 1997), allowed inferences on the relative variations of this mineral in the clay size fraction.

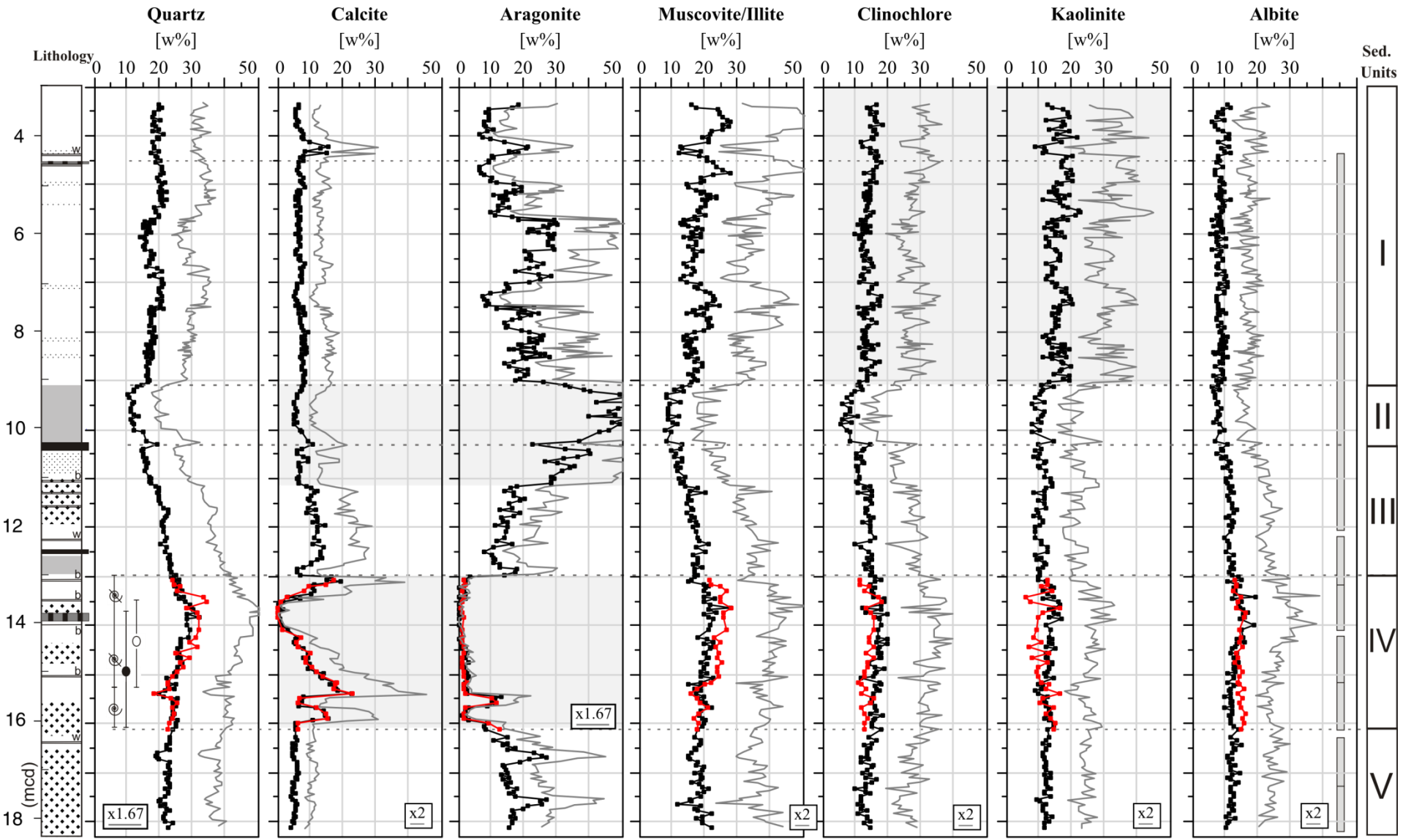

Figure 6.7: Stratigraphic changes in bulk mineralogy for the composite profile. Gray lines are multiplication by a factor indicated for each mineral, solely for visualization purposes. Red curves indicate bulk mineralogy for the fraction < 63µm. (Legend for lithology is given in Fig. 4.1)

6.4.4) Other minerals

Besides the major assemblage and minerals in the clay size fraction, some of the trace minerals were successfully identified. Birefringent needle crystals of less than 3 µm were optically recognized in some samples after carbonate removal. The needles were identified as gypsum ($CaSO_4.2H_2O$) based on X-ray diffractograms of freeze dried samples. Further trace minerals, identified via XRD diffraction and irregularly distributed over the sedimentary profile where pyrite (FeS_2), hematite (Fe_2O_3) and rhodochrosite ($MnCO_3$). Pyrite was also identified in corresponding smear slides. Rhodochrosite was clearly identified via XRD at depth 15.69 mcd, by a relative high intensity peak at its characteristic reflection in the diffractogram. The broad shape of the peak indicates that the mineral is present in a rather low crystalline form. Accordingly, an optical analysis the smear slide did not allow the finding of crystals, but rather cluster like 'massive' agglomerates with the expected greenish-brown appearance, which are only identified for this depth. However, for several other depths a 'texture- perturbance' on the diffractograms at the same $^{o}2\theta$ interval indicates that there is a mineral phase that is present in very small amounts and very low crystallinity, which is possibly related to occurrence of rhodochrosite (Table 6.4). For the depth with identified gypsum, within unit II it composes up to 4% of the mineral assemblage. Rhodochrosite at 15.39 mcd makes up ca. 2% of the mineral assemblage. The trace minerals are brought into discussion in the respective chapters.

Table 6.4: Trace minerals identified with X-ray diffraction for profile IZN09/LC2&LC3. Capital letters indicate well crystallized phases; small letters indicate depths with small XRD reflections, with or texture changes in the diffractograms that correlate to the mineral phase.

Mineral	Corresponding depths in profile IZN09/LC2&LC3 [mcd]
Gypsum (G) [a]	0.02, 0.86, 8.66, 8.96, 9.73, 10, 10.25, 10.3, 10.44, 10.54, 10.59, 10.64, 10.84, 10.96, 11.06, 11.16, 11.2, 11.7
Gypsum (g) [a]	0.26, 0.56, 0.96, 1.12, 8.36, 8.56, 9.04, 12.07
Hematite (H) [b]	15.18, 15.94 and 16.06
Pyrite	8.52, 9.28, 9.43, 9.57, 9.73 and 10.54
Rhodochrosite (R) [b]	15.39
Rhodochrosite (r) [b]	5.22, 12.91, 12.96, 13.01, 13.29, 13.34, 13.68, 13.83, 14.55, 14.57, 14.97, 15.05, 15.18, 15.19, 15.24, 15.29, 15.34, 15.39, 15.74, 15.79, 15.99, 16.65, 16.90, 17.20, 17.44, and 18.14

[a] *depicted in chapter 9, Figure 9.5*
[b] *depicted in secion 8.3.1, Figure 8.5*

6.5) Discussion – Detrital deposition

According to the exploratory CoDa results, and the identified sedimentary components, four aspects should be considered within this study: (a) the importance or weight for each sedimentation process, i.e. carbonate production, siliciclastic deposition and organic load (b) the supply of silicates and associated elements, (c) the carbonate production and associated elements (d) re-mobilization of elements resulting from changes in the oxidation potential. The investigation of each aspects and associated interpretation is supported by the CoDa balance dendograms (Appendix A6.1).

Although absolute concentrations of elements show that in average silicium is more abundant than calcium in Iznik sediment, data show that great amount of geochemical variability is retained by calcium, and in the mineralogy by aragonite. Hence, Lake Iznik is unique for its carbonate accumulation, which is favored by distinctive water chemistry of the lake. The carbonate accumulation is discussed with regard to limnological aspects in chapter 9. The organic and redox processes, which retain high variability within the data set as well, are discussed within chapter 8. Herein, the siliciclastic deposition is depicted.

6.5.1) Major cations - sources and sinks

Major cations, specially the alkaline (earth) metals, i.e. Na, K, Mg and Ca, are crucial in determining waters' salinity, and participate as important nutrients in biological cycles. These elements enter the sediment load either as detritus or after being recycled within lacustrine bio-geochemical processes (Cronan, 2009).

Regarding these elements' sources in the Iznik basin, the catchment consists of Paleozoic metamorphic shale interbedded with marble and dolomite; and Tertiary to Permian limestone, conglomerate, sandstone and marl, intercalated with volcanics (e.g. andesite, spilite and basalt), see Figure 2.2 (Franz et al., 2006). Geochemistry from the catchment of Lake Iznik shows that Ca is enriched in the carbonate rocks (limestones, marls and dolomites). K is enriched in the metamorphic rocks, which are composed of phyllites, mica schists, cherts and slates. Na and Mg are enriched in the mafic volcanic outcrops (basalts and spilites), which are composed of feldspars, pyroxenes and their alteration products chlorite and kaolinite (Viehberg et al., 2012). Further major sources of Mg are the carbonate units of dolomitic nature. Aspects regarding the sedimentary sinks for each of these elements are considered in sequence, based on the observations from the profile IZN09/LC2&LC3.

Generally, lacustrine mineral sinks for alkaline (earth) metals are mainly carbonates and silicates, from either which these elements make out the structure or adsorb to crystal surfaces. As previously stated, in the Iznik sediments Ca concentrations retain large amount of the variability of the sedimentary data. The behavior of K has a very low variability to the siliciclastic phase (e.g. Ti, Figure 6.1), while the ratio between the detrital phase (e.g. Ti) and Na or Mg sedimentary sinks changes significantly at the onset of the Holocene (Figure 6.3).

The outstanding covariance between Ca and TIC (Figure 6.4), and the small variance in between them (Figure 6.2) strongly indicate that most of calcium is in the carbonate phase. As a matter of fact, an estimation in which all inorganic carbon is assumed to be bound as calcium carbonate shows that 99.5% of the deposited Ca is explained by $CaCO_3$. This is confirmed by high quality regressions between Ca and TIC, r^2=0.975, as well as between Ca and (calcite+aragonite), r^2=0.978. Occurrences of more than 1% of Ca bound in other minerals, e.g. plagioclase or sulfates, are rather punctual (11.8 mcd, 1.2%; 12.91 mcd, 1.9%; 15.29 mcd, 2.2% and 15.99 mcd, 5.6%).

Potassium in the surficial Iznik sediments is associated to illitic material (Viehberg et al., 2012). Accordingly, K-feldspar was not identified as a major mineral in the sediments. For the sedimentary profile, K-feldspar would be expected as minor constitute, rather within units III and IV where there is a small offset between amplitudes of K and muscovite/illite curves. Since among the feldspars it has low degree of weatherability (Ray E. Ferrell et al., 2010), it is expected to be uncommon in the catchment as well. Therefore, muscovite/illite lattices are bearing major part of K.

The major sink of detrital Na for the Iznik sediments is the albite structure. Albite ($NaAlSi_3O_8$), as one end-member of the plagioclase solid solution, can contain up to 10% of anorthite ($CaAl_2Si_2O_8$) (Moore and Robert C. Reynolds, 1997). Accordingly, the estimated albite percentages for the profile are almost entirely explained by the sum of feldspar amounts calculated from the respective percentages of Na, and Ca within feldspar. The portion remaining unexplained is of 1.5%, in average for the Holocene, and 3% for the Pleistocene. It might be explained by measurement uncertainties, or presence of K-feldspars.

The 2:1 clay mineral chlorite most commonly bears Mg^{+2}, Fe^{+2}, Al and/or Fe^{+3}, in its octahedral substitution sites. Its origin might be diagenetical or from igneous and metamorphic rocks, and – similar to illite – it might present a mixed-layered nature. During weathering, chlorite and mica ‘open’ to form interstratified chlorite/vermiculite or illite/vermiculite, which in turn form vermiculite (Ray E. Ferrell et al., 2010), hence

explaining the vermiculite observed in the clay fraction. Chlorite bears approximately twice as much Mg as vermiculite[14]. Furthermore, Mg co-precipitates with rhombohedral carbonate phases, e.g. calcite (Füchtbauer et al., 1988). Additionally, Mg, as well as the other alkali (earth) metals, can be incorporated by lake biomass during the productive growing seasons (Cronan, 2009). Major Mg accumulation in the Iznik has low variance to the organic sedimentary phase (Figure 6.2), and accordingly, in the sedimentary profile it covariates with total organic carbon and nitrogen concentrations (Figure 6.8), and for the Holocene interval also with the $CaCO_3$ content. Punctual divergences from this trend (e.g. 10.33 mcd) are in accordance to a higher content of chlorite in the clay size fraction of the sediment, and therefore most likely related to diagenetical changes or detrital influxes.

Among the mineral deposition with detrital origin, there is an outstanding decrease of sedimentary albite concentrations, towards the Holocene within Iznik sediments (Figure 6.6 c, and Figure 6.7). Because plagioclase is the feldspar with the highest weatherability, i.e. lowest resistance to chemical alteration resulting from weathering (Ray E. Ferrell et al., 2010), it is sound to state that the diminishment of albite concentrations in the Holocene might be resulting from increased weathering of this mineral. To test this hypothesis, weathering indicators are discussed in the sequence.

6.5.2) Constraints on the use of conventional alteration indexes

An estimation of the chemical alteration of sediments and their mineralogical maturity is given by the chemical index of alteration (CIA) and its counterpart, the mineralogical index of alteration (MIA) (Nesbitt and Young, 1982; Rieu et al., 2007), which are expressed by:

$$CIA = \left[\frac{Al_2O_3}{(Al_2O_3 + CaO^* + Na_2O + K_2O)}\right].100 \qquad \textit{(Eq. 6.1)}$$

And

$$MIA = \left[\frac{quartz}{quartz + plagioclase + Kfeldspar}\right].100 \qquad \textit{(Eq. 6.2)}$$

where CaO* stays for the calcium contained within feldspars.

The calculation of CIA, for Lake Iznik sediments is constrained by the carbonate nature of the sediments, and the virtual absence of calcium feldspars in great part of the profile. Meaningful CIA values were obtained only punctually, for samples with some siliciclastic character[15]. For

[14] based on molecular weight (www.webmineral.com)
[15] i.e. samples for which more than 1% of calcium is retained in feldspars (n=8 out of ca. 330).

such samples, a trend of increase in the chemical alteration index is observed from Pleistocene (70<CIA<75), towards the Holocene (75<CIA<80)[16]. An 'alternative' calculation of CIA, not considering the CaO* parameter, results in a curve which reflects mainly the variations of Na accumulation. However the absolute values for the index calculated in such a manner, are meaningless in regard to the reference values from literature. Hence, the Na/Ti ratio is favored in this study (see next section).

Since the main feldspar quantified in the Iznik sediments is albite, the MIA equation is reduced to the proportion of quartz in relation to the sum (quartz + plagioclase), thus the index as expressed herein shows enrichments or losses of quartz in relation to the plagioclase albite.

In order to interpret these indexes as a result of weathering, issues such as grain size sorting, diagenetical alteration and provenance must be considered (Fedo et al., 1995; Rieu et al., 2007). However, the virtual absence of Ca-feldspars and K-feldspars further constrain the analysis of the conceptual 'ideal' weathering pathways within the appropriate ternary diagrams.

6.5.3) Alternative indexes and weathering evolution

To overcome the limitation on application of the conventional alteration indexes to the carbonatic Iznik sediments, further geochemical and mineral relations are proposed and discussed for this sediment record.

Sodium accumulation can be expressed by the ratio from Na to either K or Ti, which behave the same for the sedimentary record under investigation. A trend of sodium loss in Iznik sediments, expressed by K/Na, explains increased weathering trends in the catchment for the last 80 years (Franz et al., 2006). Regarding the Pleistocene to Holocene transition, the Na accumulation, expressed by Na/Ti, behaves constantly throughout units V to III, when it shortly increases (unit IIIa) and afterwards decreases towards unit I (Figure 6.8, note reversed axis scale, and Figure 6.3 b).

Generally, the 1:1 clay kaolinite can form by diagenesis (Velde, 1985; Weaver, 1989), or by crystal growth from the weathering decomposition products of primary minerals (Berner, 1971; Velde, 1985). In a weathering profile, kaolinite can form from the plagioclase series

[16] CIA reference values are, for intense chemical alteration, between 80 and 100, and for initial weathering stages between 50 and 60 (Rieu, et al. 2007).

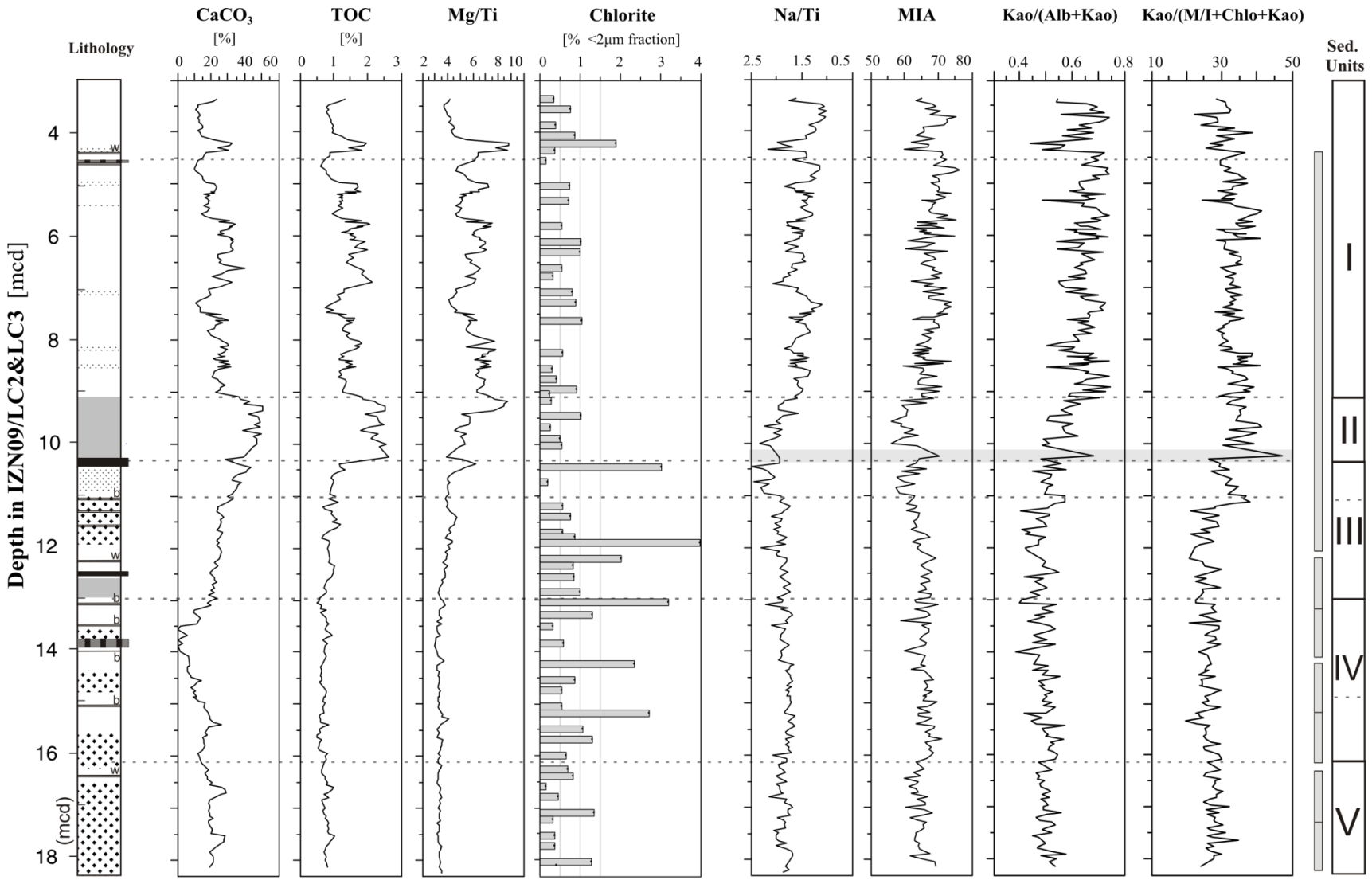

Figure 6.8: Profile for carbonate and organic phases in IZN09/LC2&LC3, aside of selected major cations (Mg, Na), their sedimentary sinks and weathering indicators.

(albite, and anorthite), from K-feldspar (microcline), as well from pyroxene (augite) or mica (biotite). In the pathway through albite, microcline, or biotite decomposition, the generated co-products are silicic acid (H_4SiO_4) and the cation(s) from the primary mineral – Na^+, K^+, or K^+ and Mg^{2+}, respectively (Berner, 1971; Ray E. Ferrell et al., 2010).

Formation of kaolinite occurs in rather neutral to acidic environments, with pH values of circa 5 to 7 (Garrels and Christ, 1965). Due the alkaline nature of Lake Iznik waters, it is reasonable to assume that the depositing kaolinite is originated mainly from alteration profiles in the catchment. Given this consideration, the high variance of kaolinite in relation to quartz and the further silicates (Figure 6.5) indicates that among the silicates it has the most dominant weathering signature. Surely illite and vermiculite are also originated from weathering processes. However, illite and its primary mineral muscovite are in practice not separable within diffractograms, as they have the same pattern. Therefore, the quantified muscovite/illite carries the amalgamated information of the primary mineral and its weathering product. Regarding chlorite and vermiculite the issue is similar. Moreover chlorite amounts in the clay size fraction of the sediments are minor (section 6.4.3, Figure 6.8). Chlorite enrichment in the silt size fraction (section 6.4.3, Figure 6.7) points towards additional physical weathering origin for this mineral.

Therefore, within the Iznik catchment, additional indicator for alteration resulting from chemical weathering is the combined analysis of the enrichment of kaolinite in relation to albite and additionally, the enrichment of kaolinite in relation to the other clay minerals. These indicators express the kaolinite accumulation in relation to the silicates (Figure 6.8), and will be used to support the interpretation of the MIA index, and the Na/Ti ratio as follows.

When MIA is applicable as a weathering index, in general, high MIA values reflect a high sediment maturity, i.e. enrichment in quartz due to chemical alteration of the sediment. Curiously, the MIA values within Pleistocene are somehow elevated, and would express chemical alteration levels similar to those of the Holocene, in unit I. However, for unit IV the high MIA values are possibly related to a higher detrital input associated with enrichment in quartz during the glacial due to enhanced physical weathering. Whilst in the Holocene, the increase in the MIA value is related to a retreat in albite accumulation.

For a parallel behavior of the MIA and the kaolinite accumulation in relation to albite, as expressed by Kao/(Kao+Alb), both indexes are reflecting the enrichments and losses in albite. The fluctuations and parallelism are more pronounced for the Holocene and are also in synchrony with the fluctuations expressed by the Na/Ti ratio. Therefore, especially for the

Holocene part of the profile, the ratio Na/Ti can be linked to the degree of alteration of albite in the catchment. Note that an increased chemical alteration of albite, i.e. a smaller Na/Ti accumulation in the sediment, results in more Na^+ in solution.

Hence, the long term trend from the Pleistocene to Holocene is outlined by an increase in weathering as observed from the Na/Ti ratio, and its synchroneity to MIA and to the index Kao/(Alb+Kao). However, for punctual lacks in synchrony within unit II and for nearly complete unit IV, the MIA is expressing enrichment in quartz, possibly detrital.

Similar conclusion can be drawn when comparing the MIA to the index which delineates the kaolinite accumulation in relation to the clay mineral assemblage, as expressed by Kao/(M/I+Chlo+Kao). In general, kaolinite forms in more humid conditions, than the clay mineral phases with 2:1 structure, and is common in pedogenic profiles where drainage is efficiently lixiviating most of the present ions. Hence, a parallel increase of both indexes related to kaolinite accumulation, will be indicating more humid conditions. Note that a synchrony between the two kaolinite indexes is clearly achieved with similar amplitudes within unit I. The accumulation of kaolinite in relation to the 2:1 clay mineral phases is nearly constant for the bottom profile (units V, IV and IIIb).

There is a lack of correspondence between Kao/(Alb+Kao) and Kao/(M/I+Chlo+Kao) within unit II and IIIa. Hence, the abrupt increases of Kao/(M/I+Chlo+Kao) in units IIIa and II are related to a higher detrital component during this phases. For instance, the sharp increase of kaolinite accumulation at the base of unit II (10.3 mcd) is in synchrony with an increase in Mg/Ti, chlorite, and a gradual increase of MIA values, opposed to the Na/Ti ratio.

Summarizing, the co- interpretation of the MIA index with the proposed parameters indicates that the MIA can be interpreted as loss in albite due to chemical weathering in exchange of a gain in kaolinite accumulation, with the prevailing of more humid conditions. For unit IV the index is imprinted by a detrital character, as well as punctually within the sedimentary profile. Notably, within units I, II, III, and V increased carbonate accumulation is related to periods of less chemical weathering, i.e. less humidity (Figure 6.8).

7.) Grain size composition and its implications for the paleo-record

7.1) Introduction

Grain size can retain valuable information on the depositional environment, in terms of the environment's energy during deposition. For instance, at deep ocean it is possible to infer on current intensity during deposition, especially from the siliciclastic fraction <63 µm, which can display size sorting in response to hydrodynamic processes (Franz and Tiedemann, 2002; McCave et al., 1995). In limnological settings grain size patterns have been applied for a variety of paleoenvironmental reconstructions, for example in association to changes in precipitation patterns, Milankovitch insolation cyclicity, or for the identification of past earthquakes (Inouchi et al., 1996; Kashiwaya et al., 1988; Peng et al., 2005; Schwab et al., 2009). In specific glacial catchments fine grained material corresponds to high magnetic material, and can estimate detrital glacial flour input (Reynolds et al., 2004; Rosenbaum and Reynolds, 2004). Furthermore, grain size analysis can be incorporated into lacustrine studies for a better understanding of geochemical evidence, since it is related to other sedimentary physical properties. Also, preferential concentration of elements in a specific grain size fraction might influence the bulk geochemistry, if elemental proportion within grain size fractions is changing.

For lakes in general a relation between the grain size of the sediments deposited within the lake and the distance from the margins is expected (Sly, 1978). Relative coarser material is expected to be deposited at shore near sites, and clayey material is expected to accumulate in the most distal/central sites, where the system's physical energy level diminishes. Depending on basin morphology, such a relation can imply a correlation between the grain size distribution and the depth of the water column.

When intending to measure the siliciclastic or detrital fraction of lacustrine sediments, a possible interference of diatom grain size should be considered (Reynolds et al., 2004; Vaasma, 2008), since diatoms dimensions range from fine to coarse silt size (Conley and Scavia, 1991).

For this reason, two distinct grain size profiles were obtained for the Iznik sedimentary record. The construction of the first profile removed solely organic material and carbonates,

and for the construction of the second grain size profile, to address the subject of diatom removal, a further step was applied to the pre-treatment procedure (section 7.2).

7.2) Evaluation in between pre-treatment methods

In freshwater system silica (SiO_2) is present either dissolved, as silicic acid (H_4SiO_4) e.g. resulting from weathering reactions, or in particulate form. Particulate silica is found (1) built in biogenic material – mainly diatoms – and (2) adsorbed to inorganic particles or forming organic complexes (Wetzel, 2001). The particulate fraction corresponds to the amorphous (or opaline) fraction, and hence encloses the biogenic material. Silica can form complexes with Fe or Al hydroxides, however for lakes in general, the biogenic precipitation is the most important sink of silica, and an inorganic precipitation is minor in relation to the quantities transported to lake floor by diatoms (Wetzel, 2001).

Diatoms – when preserved in lake sediments – can be quantified as the biogenic silica content, potentially indicating past bio-productivity (Brauer et al., 1999; de la Rocha et al., 1997; Fortin and Gajewski, 2009; Leng and Barker, 2006; Prokopenko et al., 2001). However, with the aim to obtain a solely siliciclastic granulometric distribution for sediments, biogenic silica can interfere with the measured grain size especially for mesotrophic to eutrophic lakes.

Generally there are few publications considering the interference of amorphous and/or biogenic silica in the grain size distribution in lakes. Considering the issues of the year of 2012 of the Journal of Paleolimnology (January to October), circa 9% of the publications deal with grain size in their methodology and apply laser particle size analysis. And from these only in one investigation the biogenic silica is removed prior to grain size analysis, that is less than 2% from all the considered articles.

To assess the siliciclastic grain size distribution of Lake Iznik sediments, and moreover to assess the effect of the opaline silica on grain size distribution, two different protocols of leaching pre-treatment for sediments were applied systematically. The first pre-treatment, PT1, removes carbonates and organic material leaching in sequential steps, with diluted HCl prior to H_2O_2. The second pre-treatment, PT2, adds an alkaline leaching step to the protocol of PT1, with diluted KOH, to remove the amorphous silica fraction (section 3.6.3.2).

For comparison in-between methods, i.e. to evaluate the influence of amorphous silica in the grain size, circa 150 samples (10 cm resolution) were taken along the profile which encompasses the Pleistocene-Holocene transition. Protocol PT1 was applied to these samples, and then they were measured for their grain size. The remaining sample material was subject

to the additional alkaline leaching hence completing protocol PT2, and afterwards grain size was measured again.

The final grain size profile – describing solely the distribution of the siliciclastic portion, was improved in resolution (5 cm) for selected intervals, i.e. the transition from unit III to unit II, complete unit II, and the transition from unit V to unit IV. This generated additional 100 samples. For this second batch of samples grain size measurements were undertaken after protocol PT2. In order to control reproducibility of measurements without the interruption in between protocols – as was the case for the first batch – replicates of selected samples previously measured were included in the second sample batch (section 3.6.3.3). The control replicates generated the same results when treated directly to PT2, like when treated for PT1, measured, centrifuged, and further treated for PT2.

7.2.1) Removal and estimation of opaline silica

The removal of amorphous silica from the sediments using the alkaline leaching method, as applied within PT2, has a general constraint which regards the estimation to what extend clay minerals are affected by the treatment. However, this limitation is state of the art also when the leaching method is applied to quantify the biogenic silica (Boyle, 2001; Conley, 1998; Mortlock and Froelich, 1989; Ohlendorf and Sturm, 2008). The pre-treatment applied herein was of much shorter duration and lower temperatures, when compared to the quantification methods.

In order to assess the removal of opaline silica after the alkaline leaching, the following is considered. A comparison is built for silica concentrations modeled from mineralogy, concentrations obtained from geochemical measurements, and the amount of material removed through leaching, as estimated from the laser size analysis.

Knowing the variations between the silicate minerals during the Pleistocene-Holocene transition (section 6.4.2, Figure 6.7), and given that each silicate has its characteristic Al:Si ratio, it is possible to calculate the expected variations for Si/Al for the bulk sediment downcore, which result solely from changes in the mineral assemblage. For this, the mineral assemblage was closed for silicates – in the form of a normalized mass balance. Afterwards, Al and Si concentrations were calculated for each depth. The following minerals and corresponding Al:Si relations were considered: quartz 0:1, albite 1:3, muscovite/illite 1:1, kaolinite 1:1, chlorite 2:3. This generated a predicted (or modeled) Si/Al value (Figure 7.1). Possible ionic substitutions are not accounted for.

The Si/Al predicted value, using the mass balance approach on mineralogy, covariates with the ratio determined by direct geochemical measurements on bulk sediment (Figure 7.1). Regarding the absolute value of the ratio, the measured ratios are higher than the modeled values expected solely from mineralogy. This evidences that in the bulk sediment, a portion of silica is in excess in relation to the minerals, i.e. this excess silica is not bound to the mineral phase. Given the nature of the method applied for geochemical measurements, this might have two origins: dissolved silica contained in the pore water, or the opaline silica – which includes the biogenic fraction. The relative excess in the measured Si/Al is represented by the parameter Δ(Si/Al) (Figure 7.1).

To assess the portion of material removed means the alkaline method, the following is considered. The integrate sum of the difference between grain size distributions measured after application of protocol PT1 and after protocol PT2, is expressed by the parameter $\Sigma[\Delta GS_{(PT2\text{-}PT1)}]$. Numerically it is equal to the sum of the differences measured for each size fraction (from clay upon very coarse silt). Hence, its value is an expression in percentages of the volumetric difference in particulate material, i.e. the amount of material 'removed' from the sediment after alkaline leaching. The parameter $\Sigma[\Delta GS_{(PT2\text{-}PT1)}]$ is represented in Figure 7.2 by the gray bars. Noteworthy is that this parameter has perfect correlation to another characteristic parameter of the grain size distribution, the kurtosis, which gives a measure for the shape of the distribution curve. Note that this is the kurtosis of the distributions before the alkaline leaching. The reasons for the positive covariance in between these parameters are illustrated in the next section. Herein, the kurtosis (after PT1) is considered an additional representation for the portion of material removed with the alkaline leaching.

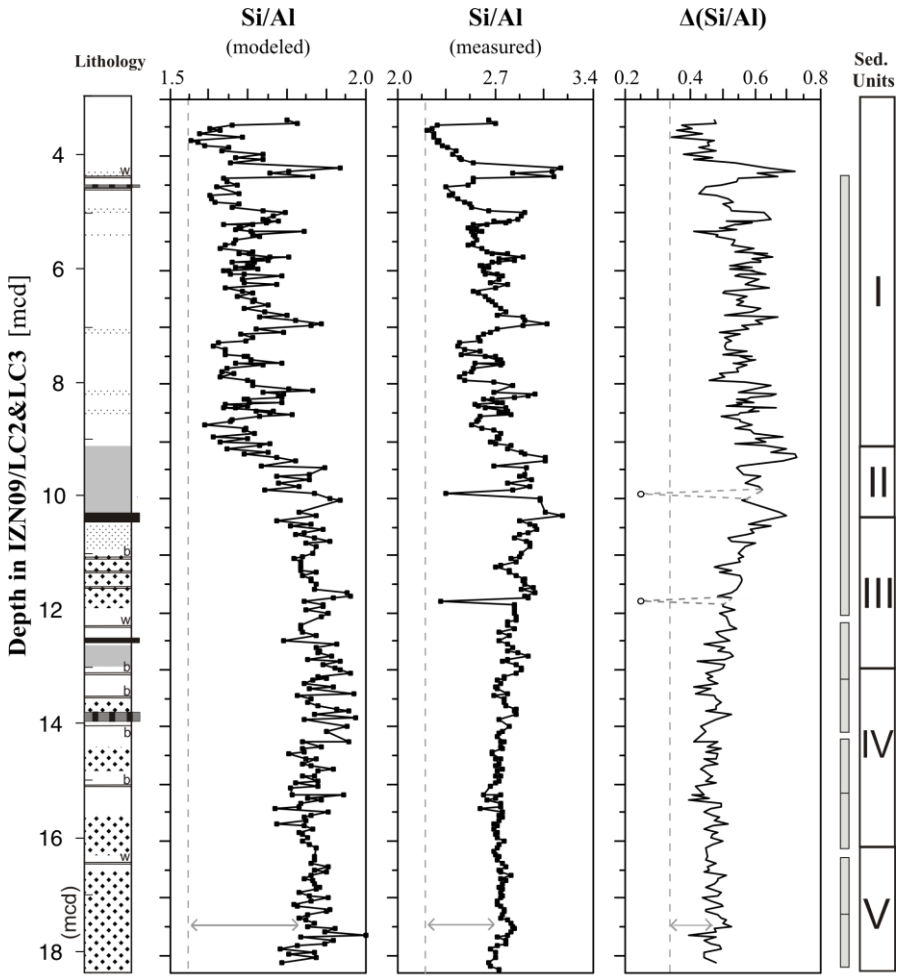

Figure 7.1: Different Si/Al ratios for the Iznik sedimentary profile (Predicted or modeled, measured and relative difference in between them).

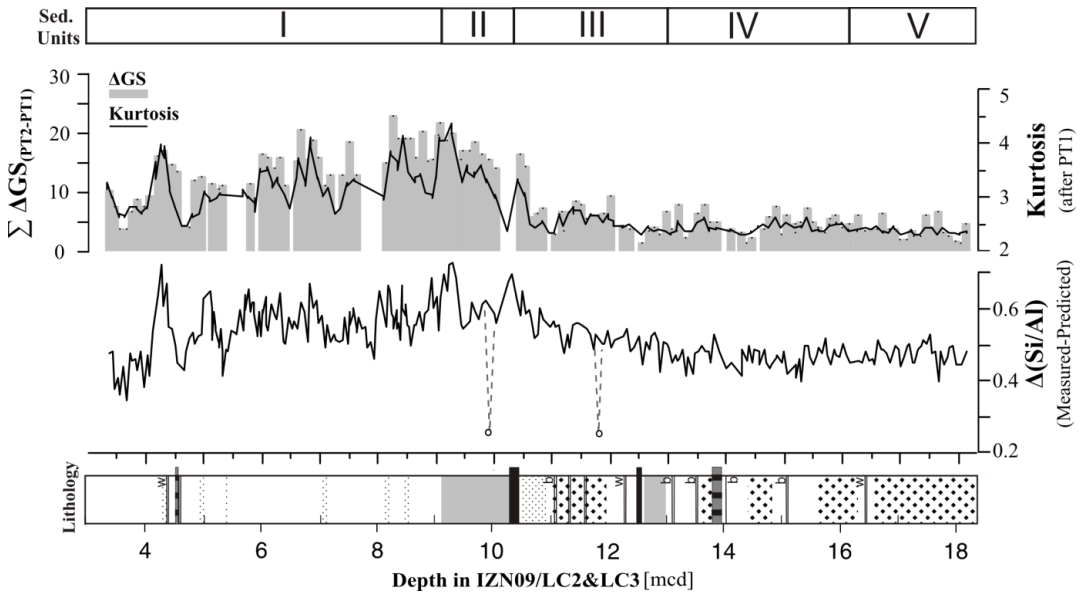

Figure 7.2: Concordance between the silica fraction removed from sediments via alkaline leaching ($\Sigma\Delta GS_{(PT2-PT1)}$), and the silica fraction not bound in mineral structure ($\Delta(Si/Al)_{(predicted-measured)}$).

An evaluation of the covariance between these parameters and Δ(Si/Al) strongly indicates that, as expected, the pre-treatment PT2 is efficient in removing the silica excess - which is not bound to the mineral phase. The positive covariance also implies that Δ(Si/Al) largely represents material which prior to leaching was in particulate form, and not dissolved, i.e. amorphous silica.

As discussed earlier, the particulate amorphous silica includes the biogenic silica and the silica fraction adsorbed to mineral surfaces. However, consider that in order for silica to adsorb on clay mineral surfaces, the concentration in solution needed is higher than 30 ppm for kaolinite (at pH = 8) and even higher for two layered clay minerals such as illite (Siever and Woodford, 1973). Because Lake Iznik waters are far more diluted, with dissolved silica values in the order of 0.1 to 0.4 mg l^{-1} (Yagci and Ustaoglu, 2012), it is reasonable to assume that the main particulate silica form in Iznik sediments is due to the biogenic silica.

7.2.2) Nature of Iznik grain size distributions

Lake Iznik sediments consist mainly of clayey silts, counting ca. 20% clay. The silt fraction is more or less equally distributed from very fine silt to coarse silt. The very coarse silt fraction highly fluctuates between 0 to 10%. The fine sand and very fine sand fractions are only sporadically present, and together, account for less than 2% of the sedimentary texture.

Grain size distributions can be clustered into two groups. Those that are distinct for pre-treatments PT1 and PT2, as exemplified in Figure 7.3 (a), and those that remain fairly constant between PT1 and PT2, as exemplified in Figure 7.3 (b). Broadly, the latter group refers to Pleistocene deposition, and the first to Holocene deposition.

The distribution of the Holocene samples (Figure 7.3 a) presents negative skewness and high kurtosis after PT1 (blue and black curves). When further treating with PT2, the cumulative frequency distribution gets significantly shifted towards clay and fine silt (red and pink curves). This striking change is expressed by a general decrease in silt content, and consequently diminishment of kurtosis. A negative skewness is mantained for both pre-treatments.

The distribution of the Pleistocene samples (Figure 7.3 b) presents gaussian form after PT1, with a small negative skewness (blue and black curves). After further applying PT2, the grain size distribution shifts towards clay (red and pink curves), however to a much lesser extend than for the Holocene samples. There is no significant change in the values of kurtosis or skewness in response to PT2 for the Pleistocene samples.

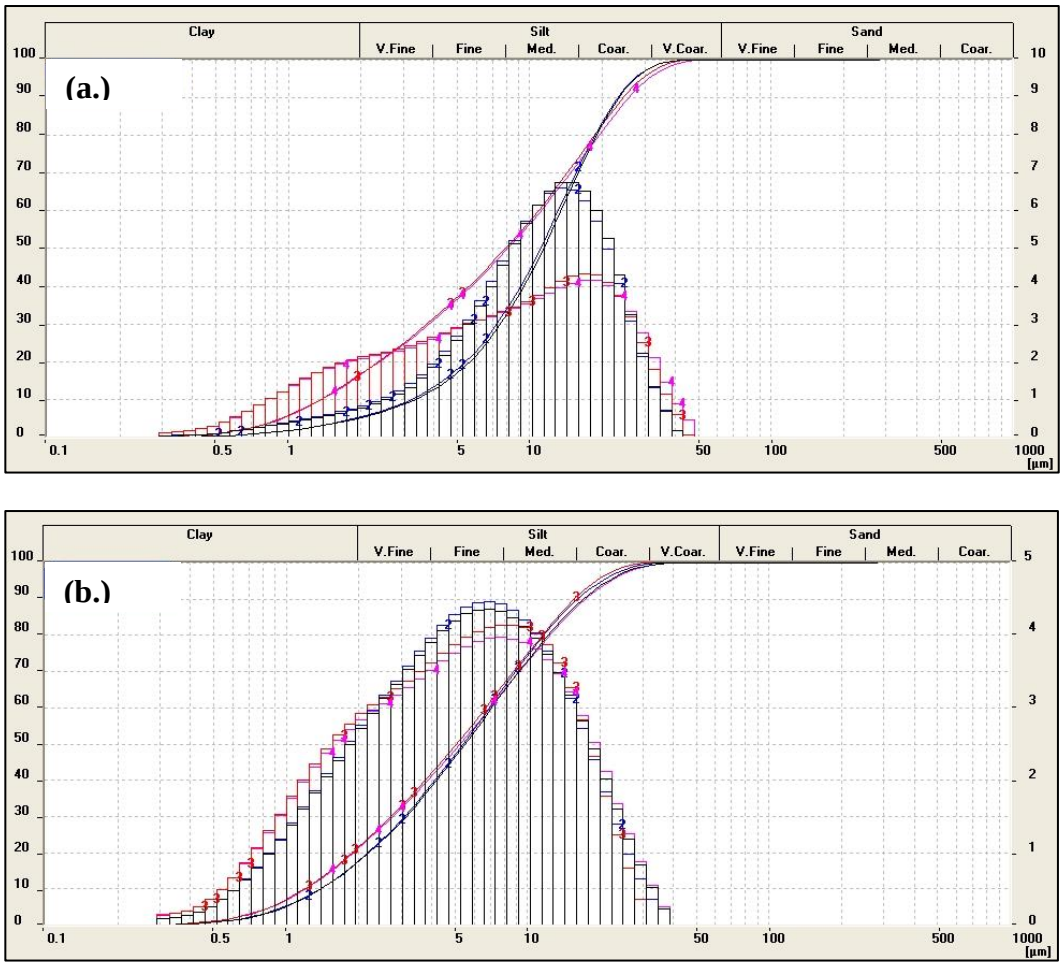

Figure 7.3: Grain size distributions for two Iznik samples. (a) One sample from unit II; and (b) one sample from unit V. Comparison on the effect of pretreatment on the same sample on each case (double measurements are shown): PT1 (black and blue, nr. 1 and 2, respectively) and PT2 (pink and red, nr. 3 and 4, respectively). Frequency distributions (bars) and cumulative frequency distribution (lines) are scaled on left and right axis respectively, i.e. $dq_3(x)$ and $Q_3(x)$. The bottom x-axis represents the grain size intervals and classes in µm.

Kurtosis provides a comparison of the spread in the central part of the distribution curve, in relation to the spread in the tail (Folk, 1966; Sly, 1978). As discussed in the previous section, the kurtosis of the distributions for Iznik sediments after PT1, is an additional measure to the amount of biogenic silica. The value of kurtosis is highly variating within units I and II, which represent the Holocene (Figure 7.2). This is a result of the leptokurtic shape of the grain size distributions for the Holocene samples before the alkaline leaching, as presented in Figure 7.3a (blue and black curves). After PT2 is applied, and the amorphous silica removed, the grain size distributions of Holocene and Pleistocene samples are platykurtic, with values ranging between 2 and 2.5 (Figure 7.4).

The kurtosis and skewness are calculated geometrically using the method of moments (Blott and Pye, 2001). The relationship between these two parameters long has been recognized to be typical for distincts sedimentation processes, e.g. dune sand deposition (Folk, 1966), and in

marine and lacustrine environs they are closely related to the hydrodinamic energy during deposition (Sly, 1978). This aspect is further explored in section (7.3.2).

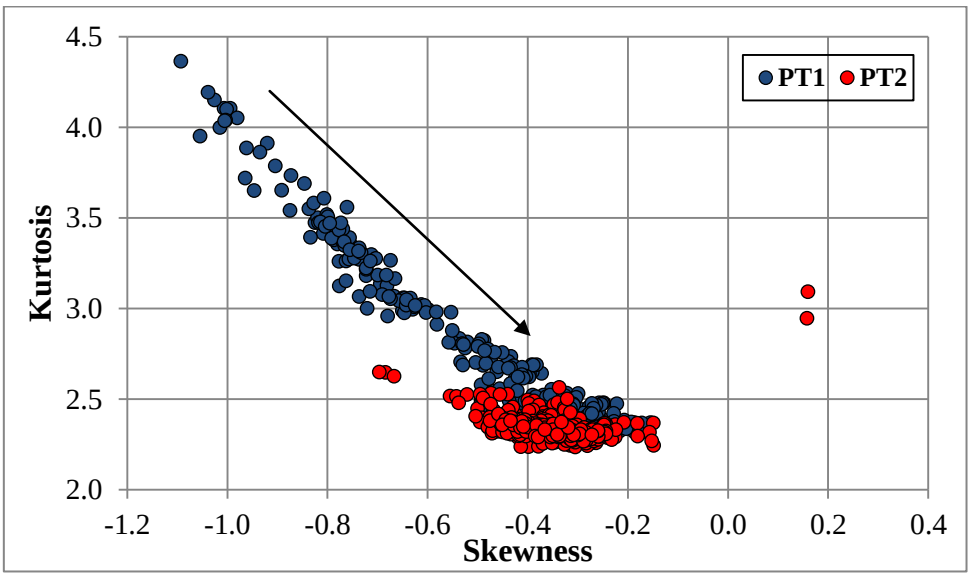

Figure 7.4: Relationship between kurtosis and skewness for Iznik sediments grain size distributions. All samples are presented for the two pre-treatments. Arrow indicates direction of pre-treatment dynamics.

Summarizing, both Holocene and Pleistocene samples respond to the alkaline leaching in similar manner, but to distinct degrees. Generally, there is a shift towards fine clay at the expense of medium silt. The distinct degree in response to the alkaline treatment is also reflected in the clr-biplot (Figure 7.5). For the calculation of the clr-biplot (Aitchison, 1982, 2003a; Aitchison and Greenacre, 2002), the first and second principal components explain 98.5% of the grain size distribution, and adding the third principal component, 99% of the variations in grain size are explained.

In Figure 7.5 the blue observations represent all of the Holocene and Pleistocene samples after PT1, and the red observations represent all of the Holocene and Pleistocene samples after the additional alkaline leaching. Hence, the red observations correspond to the distribution of the solely siliciclastic portion of Lake Iznik sediments (PT2). The blue observations correspond to the distribution of the sediments containing amorphous silica, and present much higher variability. Observe that some of the blue observations (i.e. before the alkaline leaching), are already in the variability range of the red observations. These correspond to the Pleistocene samples. After the alkaline leaching, the minor variability in between red observations stays for a uniform character of the siliciclastic fraction, which is consistent with one depositional environment.

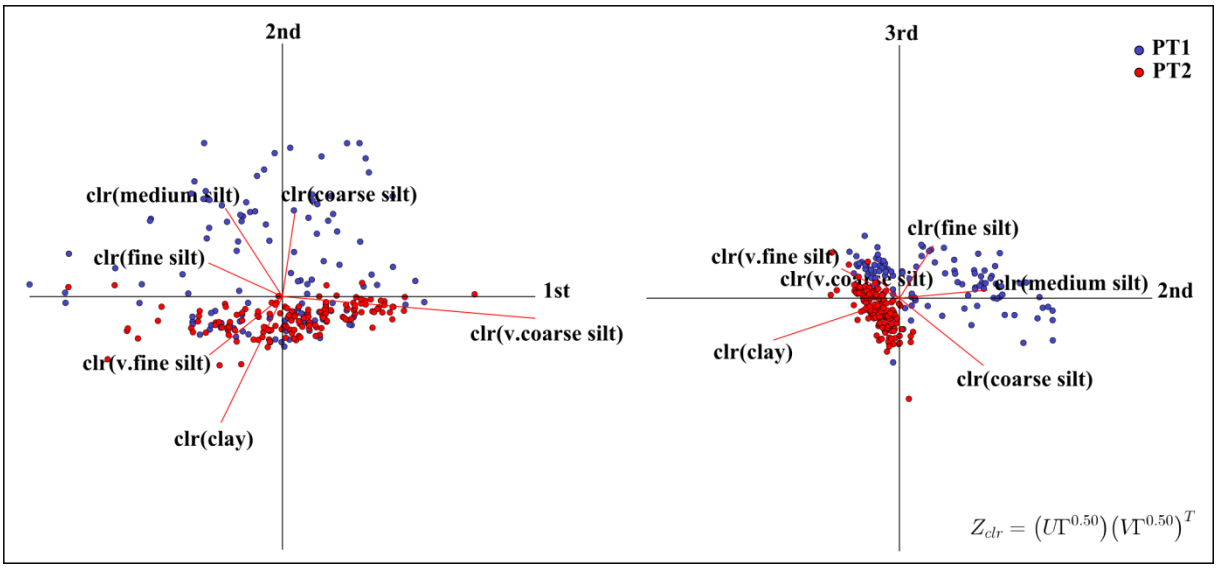

Figure 7.5: clr-biplot for the grain size fractions comparing the observations of grain size distribution for the two pre-treatment methods. PT1: blue and PT2: red.

Similar conclusions can be drawn from ternary diagrams for selected sub-compositions of the grain size distributions. Furthermore, the response to amorphous silica removal can be attributed to changes of specific ratios between grain size classes (Figure 7.6). For example, the general loss in medium silt and consequent gain of clay is supported by the shift from the blue observations towards the red observations in the sub-composition in Figure 7.6 b. The same applies to other ratios, e.g. (fine silt/very fine silt) (Figure 7.6 c) and (fine silt/clay) (Figure 7.6 d). The sub-composition of the relative coarser material behaves as a compositional line within a ternary plot for both protocols, PT1 and PT2 (Figure 7.6 a). The compositional line implies that the very coarse silt fraction retains the variability for this sub-composition, and the relation (coarse silt/medium silt) is fairly constant. Further noticeable in this ternary is that the relation (coarse silt/medium silt) remains relatively unaffected after PT2. Hence, the data shows that the removed biogenic silica is mainly concentrated in the medium silt and fine silt size fractions, and to a lesser extent in the coarse silt.

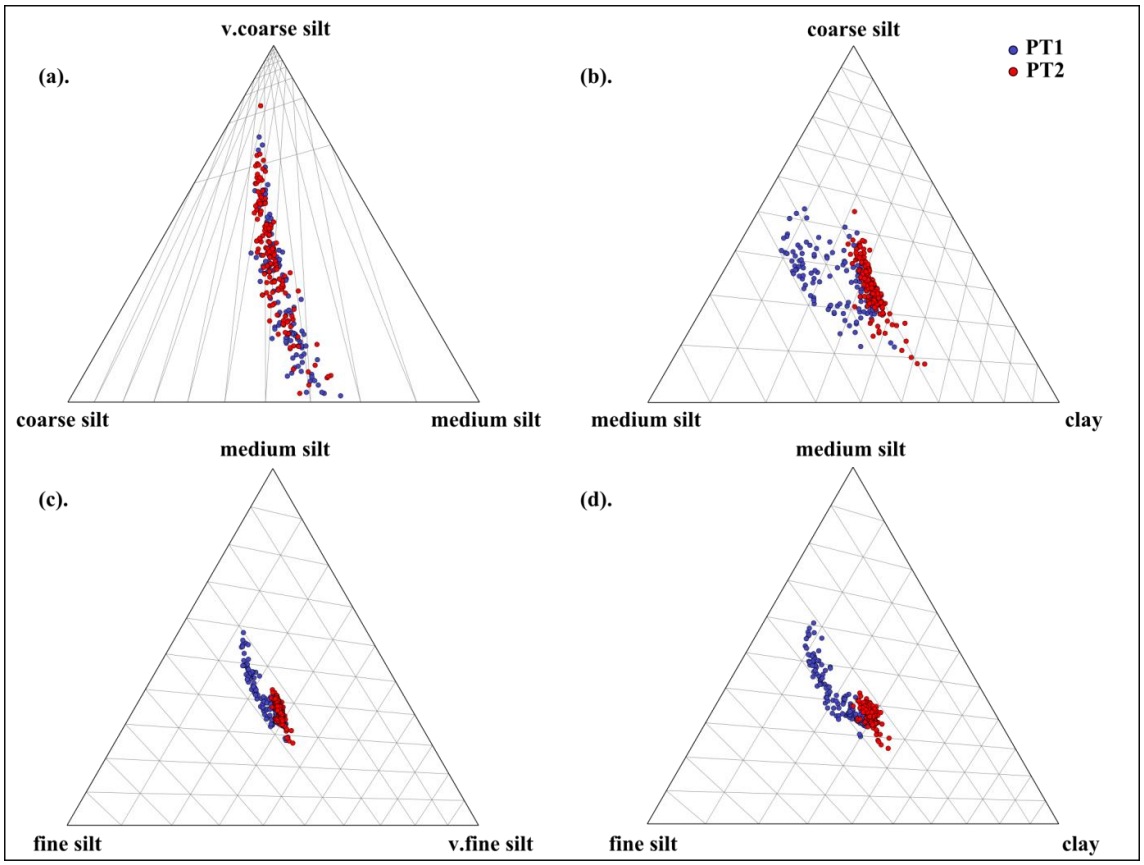

Figure 7.6: Selected ternary diagrams comparing the observations of grain size distribution for PT1 (blue) and PT2 (red).

7.2.3) Stratigraphic changes

Initially, the stratigraphic changes in grain size are evaluated through a comparison between the grain size profile which contains amorphous silica – generated after PT1, and the solely siliciclastic grain size profile – generated after PT2 (Figure 7.7). Generally, as previously outlined in section 7.1.1, the major changes in grain size distribution after removal of the amorphous silica occur for the Holocene part of the profile (units I and II). The reduction in the different silt fractions, favors an increase in the clay concentration – from ca. 10% to 20%, a value that is typical for the deeper parts of the core (Figure 7.7). The coarse silt fraction (light gray area) remains rather unaltered for all units, with punctual exceptions. The very coarse silt (black area) has its trends maintained and reinforced for the siliciclastic profile, especially for units III, II and I. For units IV and V the changes are more subtle, e.g. the very coarse silt fraction rather diminishes in unit V, from profile PT1 to profile PT2.

The siliciclastic profile is considered to retain the depositional variability which is originated solely from physical processes, whilst profile PT1 includes the influence of a productivity factor, which is tied to the amorphous silica displayed by the grain size distributions.

Hence, assessing the siliciclastic profile and the changes within it most likely gives clues about the evolution of the depositional environment from a sedimentological point of view. Noticeable for the siliciclastic profile, PT2, (Figure 7.7) is the relative constant clay proportion of ca. 20%. Especially for unit IV, the uniformity of the clay content is outstanding, and constantly at high levels. Further noticeable is the occurrence of relatively coarser material recurrently within units II and III, indicating the higher energy levels of the system during the Pleistocene-Holocene transition, and early Holocene. This is in accordance with punctual occurrences of fine sand that despite accounting for less than 2% when present, stress the higher hydrodynamic energy during deposition.

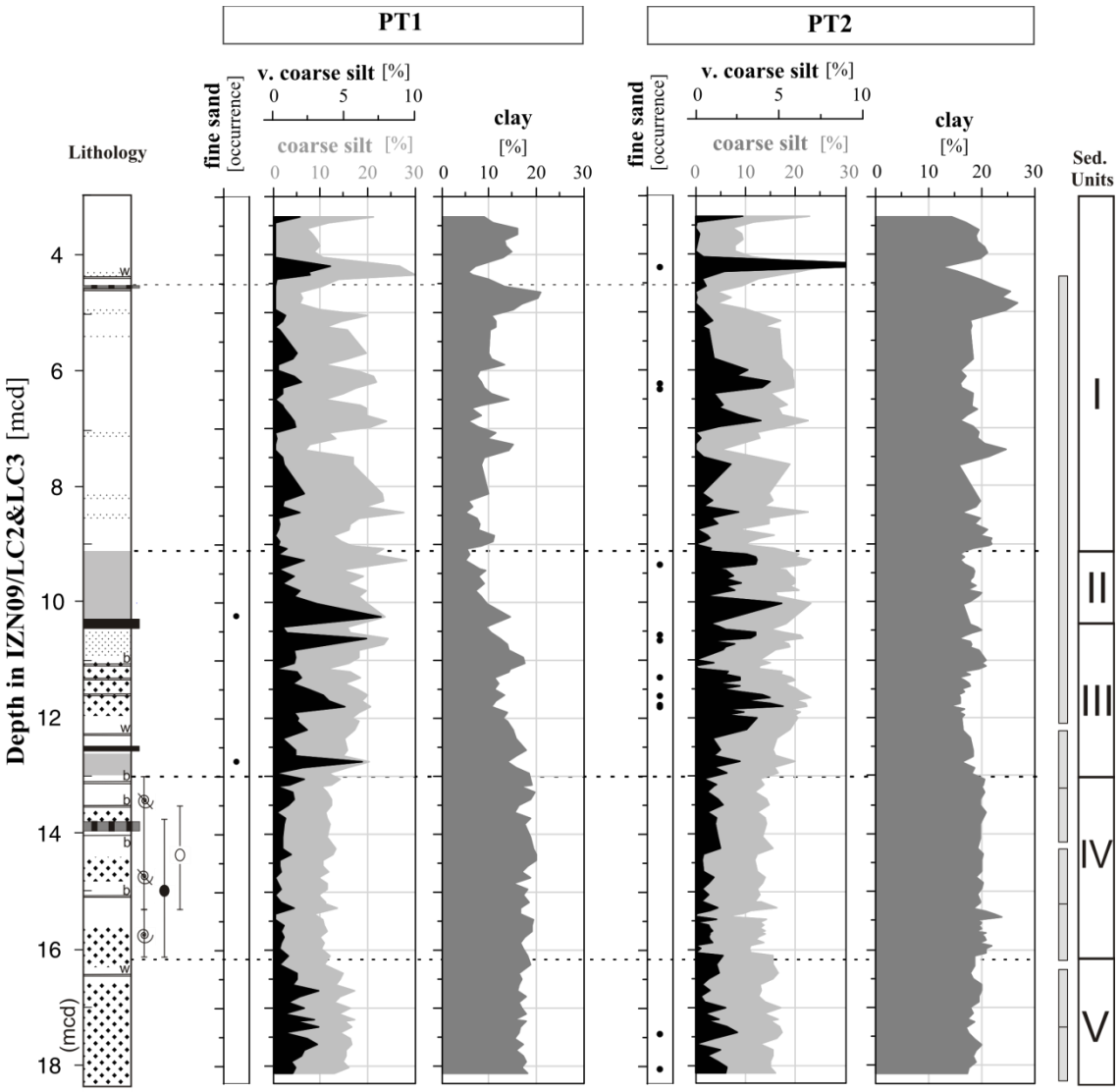

Figure 7.7: Comparison between coarse and clay distribution for PT1 (on the left) and PT2 (on the right). Represented values are averages of at least two measurements each. 'Fine sand' column includes very fine sand, and the represented occurrences account for less than 2% of total distribution. Observation: grain size analysis for tephra or sulfide layers are not represented. Legend for lithology see Fig 4.2.

7.3) Discussion: Lake level variations

7.3.1) Modern sedimentation and water column depth: a compositional model

In order to further interpret the observed past variations in grain size distribution in relation to the depositional environment, it is essential to set frames for the modern sedimentation. The grain size distribution of surface sediments for Lake Iznik over three cross profiles along different water depths shows that the sand fraction is major constitute of shoreline region, reflecting fluvial input as well as wave and current activity; whilst clay fraction distribution is influenced by fluvial inflow (Viehberg et al., 2012).

Within lakes, the major factors controlling deposition are the action of waves or currents. Lake currents are dependent largely on the basin and shoreline configuration, and wave action is more related to bathymetry and the water levels (Sly, 1978). Turbidity currents gain importance especially in stratified lakes (Sturm and Matter 1978).

Intending to further investigate a correlation of Iznik surface sediments' grain size distribution with water depth, a compositional approach is chosen. This has the main advantage that in a compositional analysis all the variables – in this case the grain size classes – are considered for the computations. Furthermore, given the closed nature of the data, the transformation to log based data, avoids the problem of dealing with the intrinsic negative bias. The correlation between modern grain size deposition and water depth is further explored means a mathematical model, which is built within the framework of compositional data analysis (Aitchison, 1982, 2003b; Aitchison and Egozcue, 2005).

For constructing the model, six grain size classes were accounted for (from clay up to very coarse clay). For this specific model, the underlying assumption is that the expected dependence of the grain size distribution to water depth is linear within the compositional approach. The information of the six grain size classes, or variables, is ilr-transformed using a default basis. Given the knowledge of the actual water depth from which the samples were taken, the obtained ilr-transformed variables are used as response variable to the known water depths, via linear regressions as a fit, returning r2=0.6 each. Based on these regressions, grain size distributions were predicted for different hypothetical water depths, from 5 to 90 meters in 5 meter intervals. After calculation of predictions for each hypothetical water depth, the ilr-variables of surface data and predictions were back transformed to the simplex. The robustness of the model in relation to the surface sediment data is illustrated for two 3 sub-compositions (ternaries) in Figure 7.8.

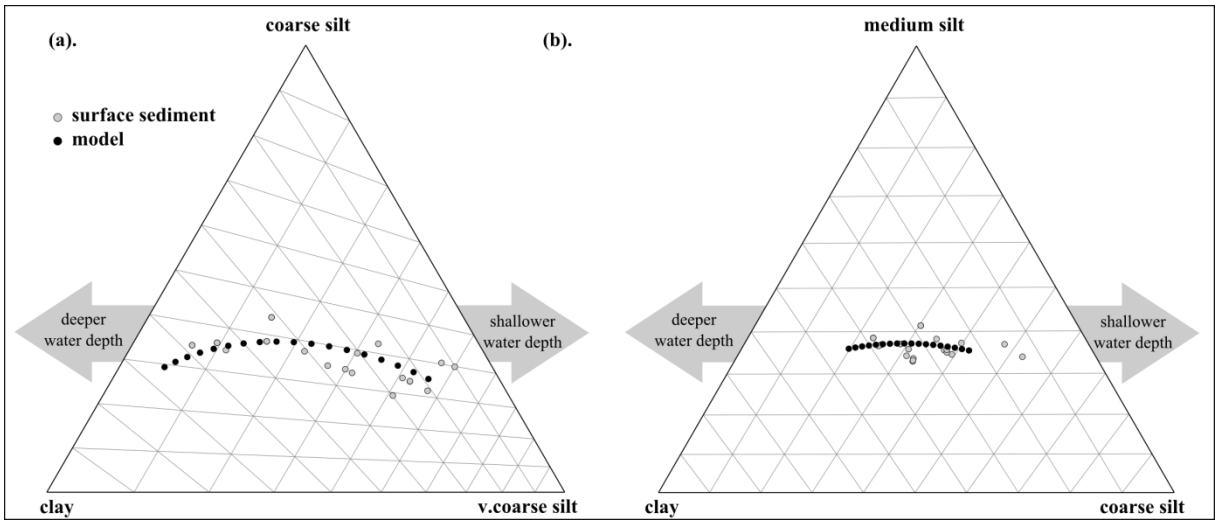

Figure 7.8: Calculated compositional model represented by two possible 3-subcompositions, outlining relationship of modern grain size distribution with water depth. Predicted grain size values were calculated for water depths from 5 to 90 meters in 5 m intervals.

Despite the fact that for the Iznik sediments the 3-sub-composition c(clay, coarse silt, v. coarse silt) retains the highest variability (section 7.2.2), the model fits very well also for this ternary composition (Figure 7.8 a). A further possible ternary composition c(clay, medium silt, coarse silt) is given in Figure 7.8 b. Surface sediment outliers at the right extreme of the model correspond to water depths of 15 meters or less, which might be influenced by two factors, which cannot be differentiated by the model. Either they originate from samples in deltaic regions, and are therefore highly influenced by fluvial input, or the observed bias is due to intense wave reworking of the material. The wave basis of Lake Iznik sediments can be calculated to be of about 20 meters depth (S. Franz, personal communication).

The presented compositional model clearly shows that there is an interdependency of the grain size deposition to the depth of the water column.

7.3.2) Consequences for ‘paleo’ water column depth

Once it is established that de grain size distribution responds to water depth, it becomes a powerful tool to analyze past lake level variations, and it becomes meaningful to evaluate the stratigraphycally established sediment units in relation to the model.

Assessing the sedimentary units in a compositional analysis, they are clearly grouped in relation to their grain size distribution. When evaluated in relation to the established model, the sedimentary units can be assigned to different energy levels in the depositional system. Clearly units II and III are influenced by high energy environ, most likely shallow water

depths, whilst unit IV and V present low energy depositional environment (Figure 7.9). Unit I, on the other hand, is highly dynamic and has some scattered data points. It is not excluded that observed outliers might be related to timely punctual events, for example, turbidity currents. Assuming that the variations observed for the sedimentary units result from changes in the water depth, they outline an evolutional history of relative higher lake levels for units V and IV, at end of Pleistocene – from which unit IV stands out for its very uniform clayey deposition. The transition to the Holocene is marked by a high energy environment, as units III and II tend towards shallower water depths.

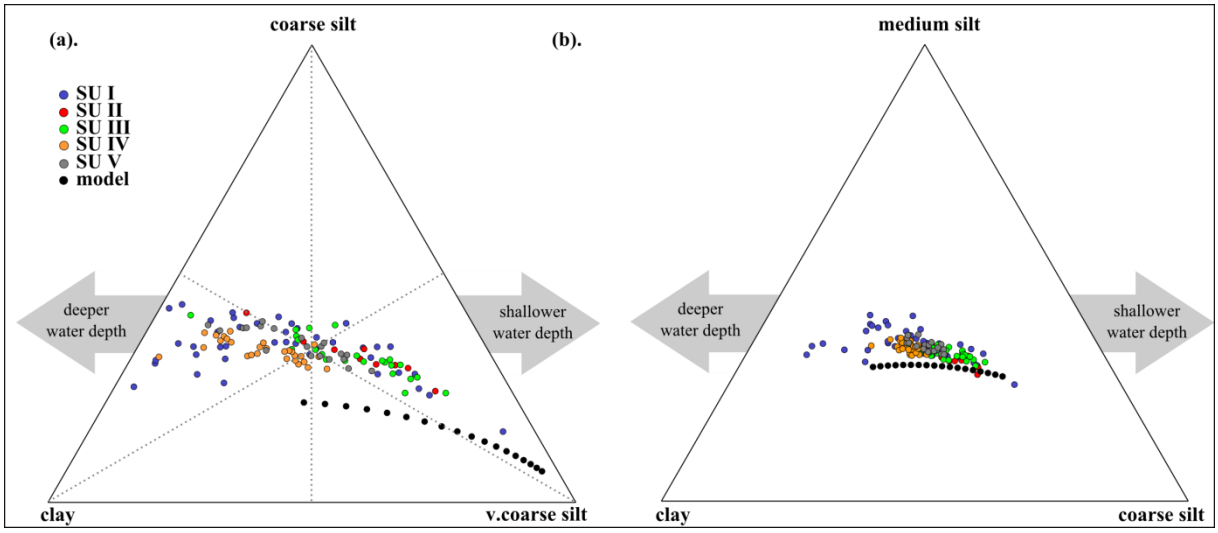

Figure 7.9: Calculated compositional model in relation to the evolution of the paleo-record, i.e. sedimentary from V to I.

Even the 3-sub-composition which retains the highest variability, c(clay, coarse silt, very coarse silt), shows the trends for the different energy levels of the units (Figure 7.9 a). Note that this is the same 3-sub-composition for which the grain size profile is illustrated in relation to its stratigraphic changes (Figure 7.7).

As discussed earlier, the favored profile within this study is the siliciclastic, obtained after PT2, to investigate the energy levels of the deposition millieu. Surface sediments where treated with an equivalent of protocol PT1. In order to get an evaluation of this issue, the model was also assessed in relation to the grain size profile which was treated solely for protocol PT1. Overall, the observations are similar. The paleo-profile data after PT1 is biased and scattered by the medium silt grain size fraction. Still, the same clusters and trends as presented in Figure 7.9 can be outlined. It is likely, that a more precise model can be constructed if PT2 is also applied to the surface sediments in future.

Analyzing the relationship between kurtosis and skewness for the sedimentary units, also a distinct clustering is formed (Figure 7.10). Again, the extreme situations are represented by

units IV and II. Intermediate states are given by units V and III, at different levels. Unit I is again the most dynamic. Considering that the relationship between kurtosis and skewness can be regarded as an adimensional measure of the depositional energy of the lacustrine environment (Sly, 1978), this distinct clustering for the units further supports the conclusions drawn from the compositional model.

Summarizing, the most important conclusions are that the existing sediment units for the Pleistocene-Holocene deposition within Lake Iznik have outstanding and distinct clustering within its grain size classes. Furthermore, the sedimentary units can be assigned to different energy levels in the depositional system.

Hence, the data analysis strongly indicates an evolution of deposition from a low energy environment, towards a high energy environment, during the Pleistocene to Holocene transition, and returning to an intermediate and highly fluctuating state at the Holocene.

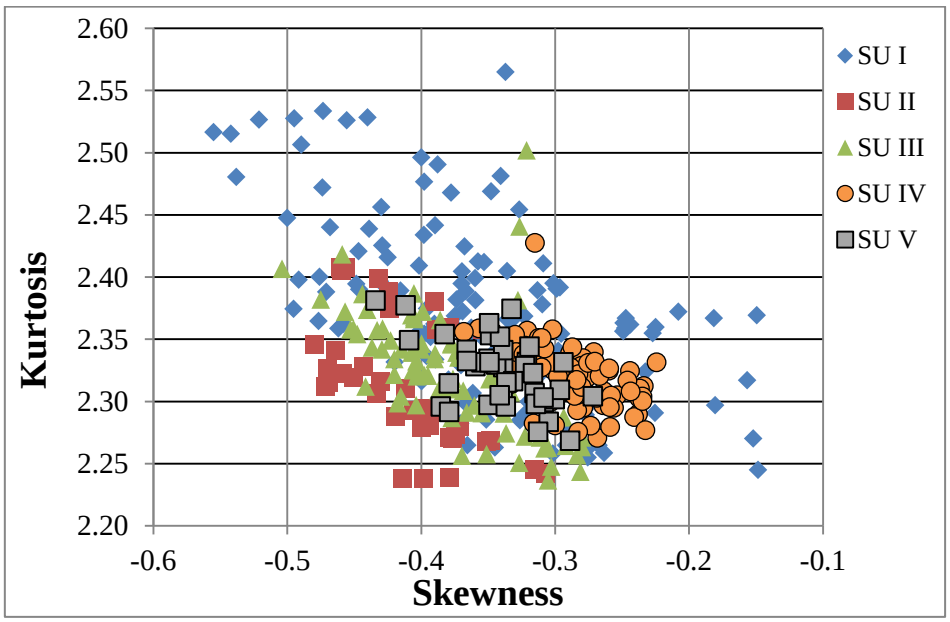

Figure 7.10: Relationship between kurtosis and skewness for Iznik sedimentary units I to V, after PT2.

7.3.3) Remark on Turbidites

Unit II presents some interbedded sequences of no more than 4 cm with sharp bottom color boundaries (Roeser et al., 2012). One of those interbedded sequences – sampled in 1cm resolution within this study, does present inverse grading, which is typical for high density fluxes. Also the 2 cm thick iron monosulfidic layer (Sf2, at 10.33 mcd, see Roeser et al, 2012) was sampled in high resolution, and the grain size distribution shows that the Sf2 layer (10.31 mcd) presents inverse grading, and up to 25 % fine sand and very fine sand accounted

together. Specifically this layer can be traced back to the core IZN09/LC3 (F. Viehberg, personal communication).

However, given the location of this specific core in the central ridge within the lake, the trigger process of the turbidites observed as interbedded sequences remains unclear. On one hand the Lake Iznik is subject to drastic changes its hydrological regime at the time (small water column depths for units II and III), on the other hand, given the regional geological setting, and that earthquakes potentially trigger the occurrence of turbidites within lakes (Inouchi et al., 1996), the very high concentration of sand observed in the layer, might possibly indicate that the mass movement from which it represents a distal deposition had a structural geological trigger. In order to further investigate these aspects, it would be meaningful to sample transects of cores, especially in the marginal regions of the lake, e.g. southern basin.

8.) Paleolimnological considerations

8.1) Introduction - Productivity and early diagenesis: prevailing processes

Organic matter cycling within lakes occurs in particulate and mainly in the dissolved form (Wetzel, 2001). It is composed of a complex mixture of biochemicals (e.g. lipids, proteins, carbohydrates), which are derived to a large extend from plants. Organic matter originates either from the watershed, i.e. terrestric, or is produced within the lake, e.g. phytoplankton (Meyers and Lallier-Verges, 1999), and the rate of which organic matter is supplied to or by the lake, is referred to as trophy (Wetzel, 2001). A high biological productivity in lakes is characterized by increased algae production and other aquatic plants, in response to a higher supply and availability of nutrients (Braga et al., 2002). In our days Lake Iznik is characterized by mesotrophic to eutrophic state, and anthropogenic enhanced nutrient load has been inducing eutrophication for the past two decades (Franz et al., 2006).

Generally, most of the organic matter is decomposed by aerobic microorganisms and only part of it gets buried in the sediments, and the deposited matter can undergo early diagenetical changes (Berner, 1981). Hence, important metabolization or decomposition reactions for organic matter in lake waters and sediments include biological respiration in aerobic waters, and, for reducing environs: denitrification, sulfate reduction, iron reduction, manganese reduction, and methanogenesis (equations 8.1 to 8.7) (Berner, 1971; Boehrer and Schultze, 2008).

$$C_6H_{12}O_6 + 6O_2 \rightarrow 6CO_2 + 6H_2O \qquad (8.1)$$

$$5CH_2O + 4NO_3^- + 4H^+ \rightarrow 5CO_2 + 2N_2 + 7H_2O \qquad (8.2)$$

$$2CH_2O + SO_4^{--} + 2H^+ \rightarrow 2CO_2 + H_2S + 2H_2O \qquad (8.3)$$

$$CH_2O + 4Fe(OH)_3 + 8H^+ \rightarrow CO_2 + 4Fe^{++} + 11H_2O \qquad (8.4)$$

$$CH_2O + 2MnO_2 + 4H^+ \rightarrow CO_2 + 2Mn^{++} + H_2O \qquad (8.5)$$

$$4CH_3OH \rightarrow 3CH_4 + CO_2 + 2H_2O \qquad (8.6)$$

$$CH_3COOH + H_2O \rightarrow CH_4 + CO_2 + H_2O \qquad (8.7)$$

The net sedimentation of organic matter is a result from a positive balance between the production, load to the sediments, and the early diagenetical processes (Wetzel, 2001). Despite early diagenetical losses of organic matter, the bulk indicators of organic matter

undergo minimal alteration after sedimentation, preserving evidence of past environmental changes (Meyers and Lallier-Verges, 1999). Elements associated to lake biologic productivity, and that can be quantified from the bulk sediment fraction, include carbon, nitrogen, silica and sulfur. The bulk content of these elements was estimated and is presented for the Iznik sediments in the present section, first carbon and nitrogen, afterwards silica – which has been discussed in chapter 7 – is briefly correlated to the organic sedimentation, and finally sulfur is evaluated. The stratigraphic changes in the behavior of these elements are then interpreted in association to the evolution of Lake Iznik's trophic status.

8.2) Bulk parameters

8.2.1) Organic carbon and nitrogen

Typically, about half of the organic matter in sediments is composed of organic carbon. The amount of total organic carbon (TOC) within sediments corresponds to the fraction of organic matter that escaped remineralization during burial (equations 9.1 to 9.7), and it includes different origins, delivery routes, depositional processes and degrees of preservation (Meyers and Lallier-Verges, 1999). Algal derived organic matter is characterized by nitrogen rich proteins, whereas vascular plants have higher carbon contents, therefore the atomic ratio between organic carbon and nitrogen becomes interesting value to identify the sources of organic matter in sediments (Meyers and Lallier-Verges, 1999; Meyers and Teranes, 2001). During diagenesis, the chemistry of nitrogen is typically dominated by nitrogen being bound in organic molecules, as this form is commonly more abundant than its inorganic species (as dissolved NO_3^- or N_2); specially in anaerobic sediments (Berner, 1971).

In general, allochthonous organic matter, as vascular plants (cellulose rich and protein poor) have C/N ratios of 20 or higher (e.g. 29 for red oak leaves, or 42 for white pine needles). In contrast, autochthonous organic matter, e.g. plankton, has low C/N ratios, typically below 12 (Meyers and Teranes, 2001; Wetzel, 2001). For most lakes an unequal mixture of these sources is expected, however, some lakes can present predominantly algal or land-derived source (Meyers and Lallier-Verges, 1999).

Sediments buried in the modern Lake Iznik contain approximately 4% of total organic carbon, and TOC/N atomic ratio between 8 and 12, as shown in this study (Figure 8.1, short core) and others (Franz et al., 2006; Ülgen et al., 2012). The observed TOC/N ratios are typical for catchments in which the watershed is relative small in relation to lakes' size, and the algal and zooplankton input of organic matter prevail. Additional biomarkers, such as *n*-alkanes, *n*-

alcohols, *n*-carboxylic acids, and lipids, further evidence the autochthonous character of deposited organic matter in Lake Iznik (Franz et al., 2006). The changes in TOC/N ratios are controlled by (1) algal deposition, (2) allochthonous organic carbon delivery, and/or (3) early diagenetical preferential removal of nitrogen from organic matter.

Evaluating the organic carbon content and quality of organic matter for the composite IZN09/LC2&LC3 and the distinct sedimentary units (Figure 8.1), a wider range of TOC values, as well as of TOC/N ratio, than for the surface sediments is observed. The deposition from the sediment-water interface (uppermost centimeters of the short core), is characterized by the highest organic carbon content, which reflects the early diagenetical stages of the fresh material (Franz et al., 2006). The sedimentary units are well clustered, and especially the Holocene units, I and II, are separable from each other, and from the Pleistocene units III, IV and V (Figure 8.1 a). For instance, sedimentary unit II presents the highest amount of allochthonous material, whereas sedimentary unit IV has the lowest degree of terrestric input (Figure 8.1 b). Furthermore, the grouping of the deposition into Pleistocene units and Holocene units allows the identification of distinct gradients between the amount of organic matter and its quality.

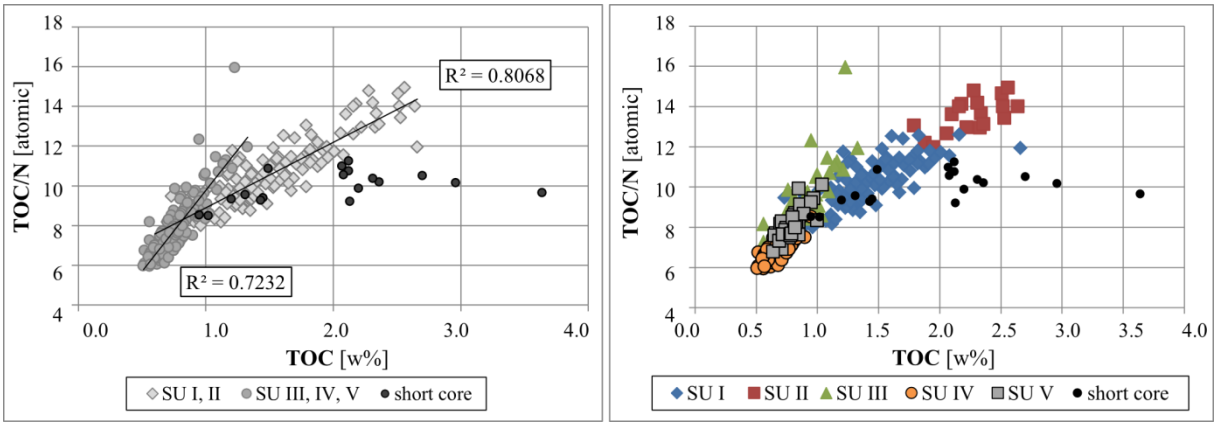

Figure 8.1: Relationship between TOC [w%] and TOC/N ratios for the different sedimentary units from composite profile IZN09/LC2&LC3

These observations strongly indicate that the organic matter within Lake Iznik has not only different prevailing origin during time, but that different processes are responsible for the maintenance of its quality during the Pleistocene than during the Holocene. Preferential diagenetical removal of nitrogen, as well as differentiated detrital supply can lead to the observed changes in the TOC/N ratios. Again, units II and IV are observed as 'extreme' millieus in the data set, likewise within the grain size profile (chapter 7).

Finally, one conclusion that can be drawn for organic carbon and its relation to nitrogen, is that the transition from Pleistocene to Holocene is marked not only by changes in the degree

of the prevailing processes, but that the onset or cease of one or more processes that interfere in the TOC/N ratio takes place. Furthermore, such processes must be related to rates of productivity or metabolization of organic matter that change the relative proportion between nitrogen and organic carbon.

8.2.2) Amorphous silica

Silica is an essential element of plant growth within terrestrial ecosystems, and within natural waters it sustains the growth of organisms such as diatoms and sponges (Conley and Struyf, 2009), therefore being closely related to lake trophic status. Availability of silicic acid is strongly connected to weathering intensities. Parameters which potentially represent the fraction of amorphous silica calculated for Iznik sediments were obtained within this study (section 7.1.1). Such parameters are in positive correlation to the organic matter of sediments quantified as the total organic carbon content (Figure 8.2), and are also increasing towards the Holocene. Sediment unit II is again observed with the highest values, whereas Pleistocene units are grouped, with low amorphous silica and low organic carbon content. Unit I and the short core present values scattered in between Pleistocene deposition and unit II.

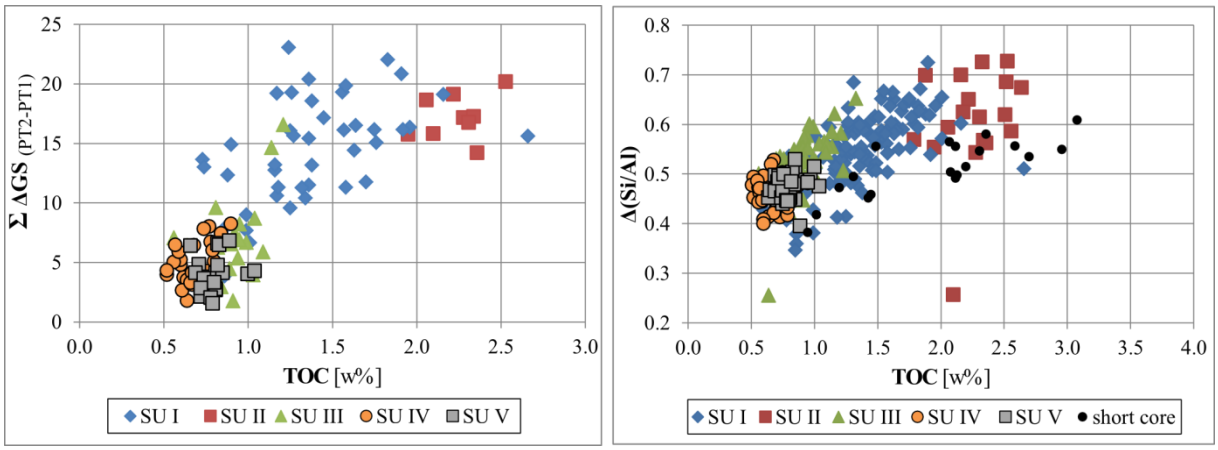

Figure 8.2: Relationship between TOC [w%] and selected parameters that stand for amorphous silica ($\Sigma\ \Delta GS_{(PT2-PT1)}$ and Δ(Si/AL) for the different sedimentary units from composite profile IZN09/LC2&LC3.

8.2.3) Sulfur

A major part of the sulfur geochemical cycle takes place in sedimentary processes. It is part of biogeochemical cycle, mineral precipitation, and diagenetical processes (Berner, 1971; Braga et al., 2002). Broadly, potential sources for sulfur for lakes are the geological background of the basin (e.g. from rocks and soils as free sulfur or sulfides, or from sedimentary rocks), decomposition of proteins from organic matter, deposition from atmospheric load (dry or wet;

volcanic or anthropogenic), and possible anthropogenic sources are fertilizers or sewage discharges (Schönborn, 2003; Wetzel, 2001). It is added to the sediments in two forms, as organic sulfur compounds and/or dissolved SO_4^{--}, and the subsequent diagenesis is strongly dependent on the oxic conditions (Berner, 1971). The limnological sulfur cycle is largely mediated by bacteria (Mackereth, 1966; Schönborn, 2003), and the main uptake path for sulfur by microorganisms is its sulfate inorganic form (Braga et al., 2002). Major part from the up taken sulfur gets mineralized via decomposition processes, generating H_2S and HS^-. Under aerated conditions this is rapidly oxidized to elemental sulfur or sulfate, or under anaerobic conditions the oxidized forms can be promptly reduced (Braga et al., 2002; Schönborn, 2003). Further under anaerobic conditions, particularly at the water-sediment interface H_2S can bind to Fe^{+2}, or other metals in solution (e.g. As, Cu, Zn and Pb), forming sulfides which are insoluble at alkaline or neutral pH (Berner, 1969; Berner et al., 1979; Schönborn, 2003; Wetzel, 2001). Sulfur can also be retained as sulfate in gypsum.

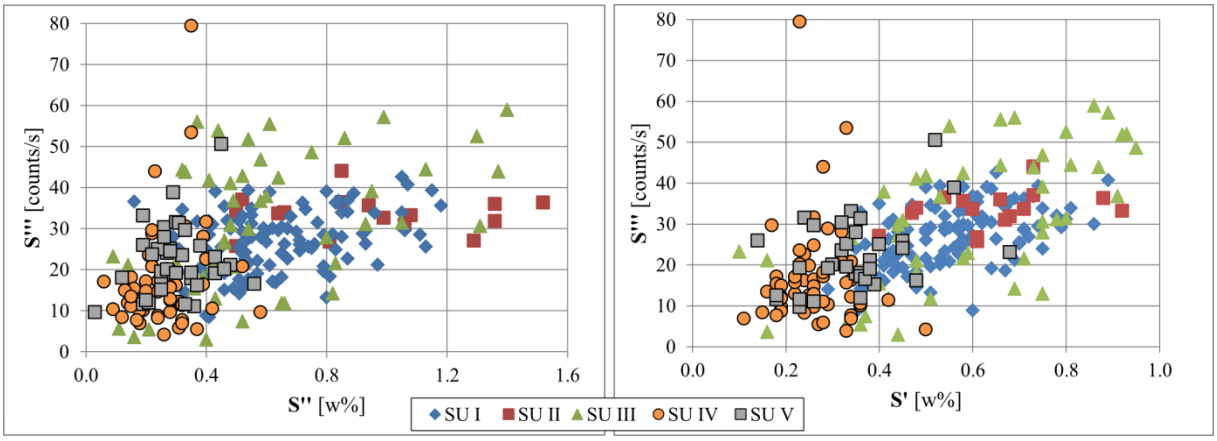

Figure 8.3: Correlation between sulfur abundances measured from independent analytical methods. S':originated from the vario el cube; S'':originated from XRF measurements on fused discs; S''': XRF measurements on humid core halves with ITRAX scanner. Note: outlier value for the Sf2 iron sulfidic layer is not presented.

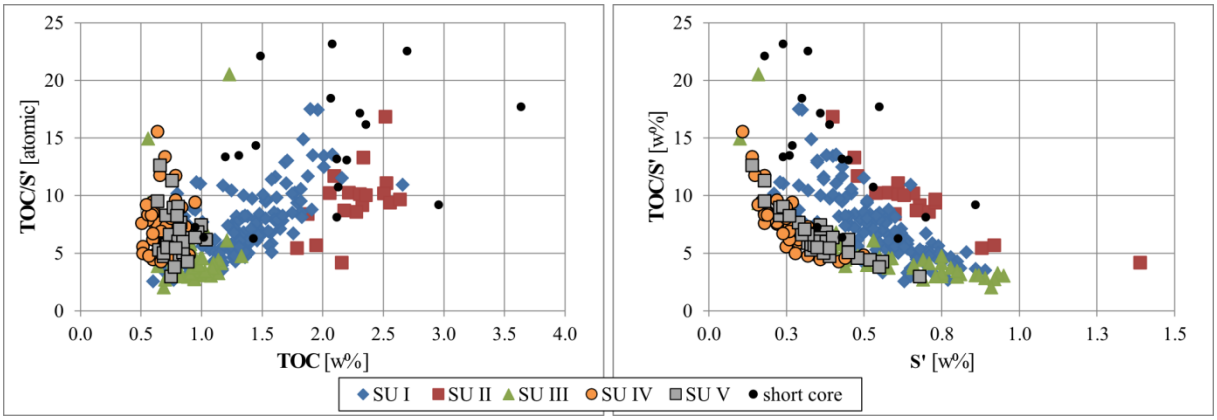

Figure 8.4: Relationship between TOC [w%] and TOC/S ratios for the different sedimentary units from composite profile IZN09/LC2&LC3.

Sulfur values for the Iznik sediments were obtained with three different methods (section 3.7). Herein they are referred to as S' – obtained from the vario el cube elementar analyser (purge

and trap chromatography), S'' – measured via XRF on fused discs, and S''' – measured with a XRF core scanner on humid core halves. Overall the results from the three methods are in good agreement, and lead to the same observations (Figure 8.3). The slight offset in absolute values for S' and S'', both in weight percent, is an effect from the different methods, given that S' refers to the bulk sediment, and S'' refers to the remnant fraction after burning at 1100^{o}C (mineral matter). The core scanner results are presented in counts per second. Because of the higher resolution of the core scanner measurements, they are preferred for representation of stratigraphic changes (section 8.3) to better depict the small scale diagenetical sulfur migration.

Given that the limnological processes participating in sulfur precipitation are largely bio-geochemical, via sedimentation of algae material or bacterial mediation reducing sulfate to sulfides (Mackereth, 1966), sulfur concentration is correlated also to lakes' productivity. Furthermore, the sulfide in sediments depend largely on the original concentration of sulfate in the pore water (Berner, 1971). Evaluating the sulfur concentrations of Lake Iznik sediments in comparison to the organic carbon (Figure 8.4), it is noticeable that sulfur has behavior consistent with TOC for all units, except unit III. In other words, sulfur has higher concentrations for the Holocene deposition (units II, I) than for Pleistocene (units IV and V). As well does the total organic carbon. However, unit III is an exception, because it has low organic matter concentrations, but the highest sulfur values. Considering the TOC/S ratios, all units have similar distribution of its values, and unit III is clearly again an exception, for it presents the lowest TOC/S ratios. The uppermost short core presents scattered values, as it is influenced by fresh sedimented material with high water contents.

The TOC/S ratio of sediments is affected by three aspects: (1) the portion of organic carbon that is metabolized in the water column, (2) the fraction of metabolized organic carbon that is metabolized via sulfate reduction (equation 9.3), and (3) the fraction of reduced sulfide that is not re-oxidized and is buried in sediments as pyrite or sulfides (Morse and Berner, 1995). For instance, the decomposition of organic matter through sulfate reduction, would favor a decrease in the TOC/S ratio. Also, an increased oxidation of organic matter in the water column (equation 8.1) would favor the reduction of the TOC/S ratio, given the sulfur load to sediments remains unchanged.

Noteworthy is also the change in the relationship between TOC/S and TOC from the Pleistocene to the Holocene (Figure 8.4 a). While the Pleistocene deposition presents a negative gradient for TOC/S vs. S, after onset of the Holocene this gradient becomes positive

– i.e. TOC/S increases with increasing TOC values. The negative gradient for units IV and V, reflects that sulfate reduction is one key process governing maintenance of TOC values for these units, and that produced sulfide gets fixed in the sediments. However, for the Holocene units I and II, as well as for the short core, the relationship is positive, reflecting an increased organic carbon load to the sediments. Unit III, as previously outlined, is somehow an exception and for now will be considered a transition state.

Concluding, an increase in the accumulation of organic carbon in relation to sulfur is taking place (Figure 8.4 b), from the Pleistocene towards the Holocene. Also, sulfate reduction and following sulfide become less important for Holocene deposition.

8.3) Bottom water oxic/anoxic conditions – behavior of iron and manganese

Iron and manganese states in lakes are largely influenced by lake mixing (i.e. oxygenation conditions), trophic status and water chemistry (Giblin, 2009). Iron and manganese are not expected to be in solution under oxidizing conditions, where Fe^{+3} and Mn^{+4} are found as precipitated forms of oxides, hydroxides, and/or oxy-hydroxides. Under reducing conditions Fe^{+2} and Mn^{+2} may get into solution – manganese more readily than iron, or when anoxic conditions are stable they might precipitate to form sulfides, carbonates, or phosphates. (Davison, 1993; Giblin, 2009; Mackereth, 1966). Therefore, mechanical erosion and transport from the basin is not expected to bring separation between iron and manganese, and a parallel sedimentary behavior of these elements usually indicates erosion as the dominating process. In that case the iron manganese ratio should be similar to the lithosphere (Mackereth, 1966). A considerable separation between their behaviors might be expected when transported within the sedimentary column in their reduced forms (Mackereth, 1966).

Generally, large fraction of the iron in sediments is present in clay minerals, or unreactive oxides which remained not reduced. Less than 10% of the iron concentration entering lakes is affected by redox transformations. The behavior of manganese, on the other hand, tends to be dominated by such processes. And periodic benthic anaerobic conditions in the lake can lead to the reduction of the iron, manganese and other metals in the sediment itself (Lerman et al., 1995; Schaller et al., 1997). According to a conceptual model for the redox cycling of elements in lakes the soluble form of the metal is more concentrated at the redox boundary, from where it diffuses upwards and downwards, and eventually becomes re-oxidized (Davison, 1993). Oxidation of Mn^{+2} is a rapid process, and oxidations rates of one day or less are common (Giblin, 2009). Periodic bottom anoxia leads to reduction of the sedimentary

manganese (Mackereth, 1966). Assuming that the supply remains constant, changes in the Mn and Fe behavior can be attributed to variations in the redox conditions at the lake bottom (Mackereth, 1966).

For the Iznik sediments in general, the overall behavior of iron is very close to that from the detrital elements, as was shown in clr biplot (chapter 6). However, the early diagenetical, vertical mobilization of Fe^{+2} gets evident from the peaks in the Fe/Ti ratio, which occur in coincidence with the Mn excursions within unit IV (Figure 8.5). The Fe/Ti excursions are also present in unit V, and to a lesser extend unit III. The sharp outlier value at the base of unit II (10.33 mcd) refers to the iron sulfidic layer Sf2 (Roeser et al., 2012). Manganese presents a 'flat' type distribution for units III, II and I (Figure 8.5). Within unit IV it fluctuates in high amplitudes, and to a lesser degree within the basal unit V. The Mn peaks are mostly coinciding with the peaks in Fe/Ti and also Fe – occasionally a little shifted in relation to iron, which indicates that the reduced Mn got further transported vertically within the sediment. Calculating the metals on a carbonate free basis (Schaller et al., 1997), the same observations apply (see gray curves in Figure 8.5).

The flat manganese distribution for the uppermost units III to I, reflects loss from the sediment via diffusion to the water possibly followed by export from the lake due to periodic mixis (Berner, 1980; Davison, 1993; Mackereth, 1966). This illustrates the lake system as it operates today, mixing once a year, with the onset of an oxic-anoxic boundary in the water column, which moves to the water-sediment boundary during the mixis. In the modern and Holocene lake, even with the prevalence of seasonal anoxic conditions at the sediment-water interface, iron is not being mobilized in the sediments or fixating into sulfides, despite the presence of available sulfur.

8.3.1) Authigenic and detrital minerals

Fe and Mn bearing minerals are good indicators for the oxygenating conditions from the milieu, because of the well-known stability fields (e.g. pH, Eh) of the involved metal species. In sediments containing enough Mn^{+2} in interstitial solution to be supersaturated with respect to rhodochrosite ($MnCO_3$), this carbonate can form as an authigenic precipitate (Berner, 1980). Hematite (Fe_2O_3) can be originated as detrital input, or can be formed during diagenesis of goethite (FeOOH) (Berner, 1971), and it is stable under oxic conditions. During the transition of unit V to IV, these minerals were found in alternating layers.

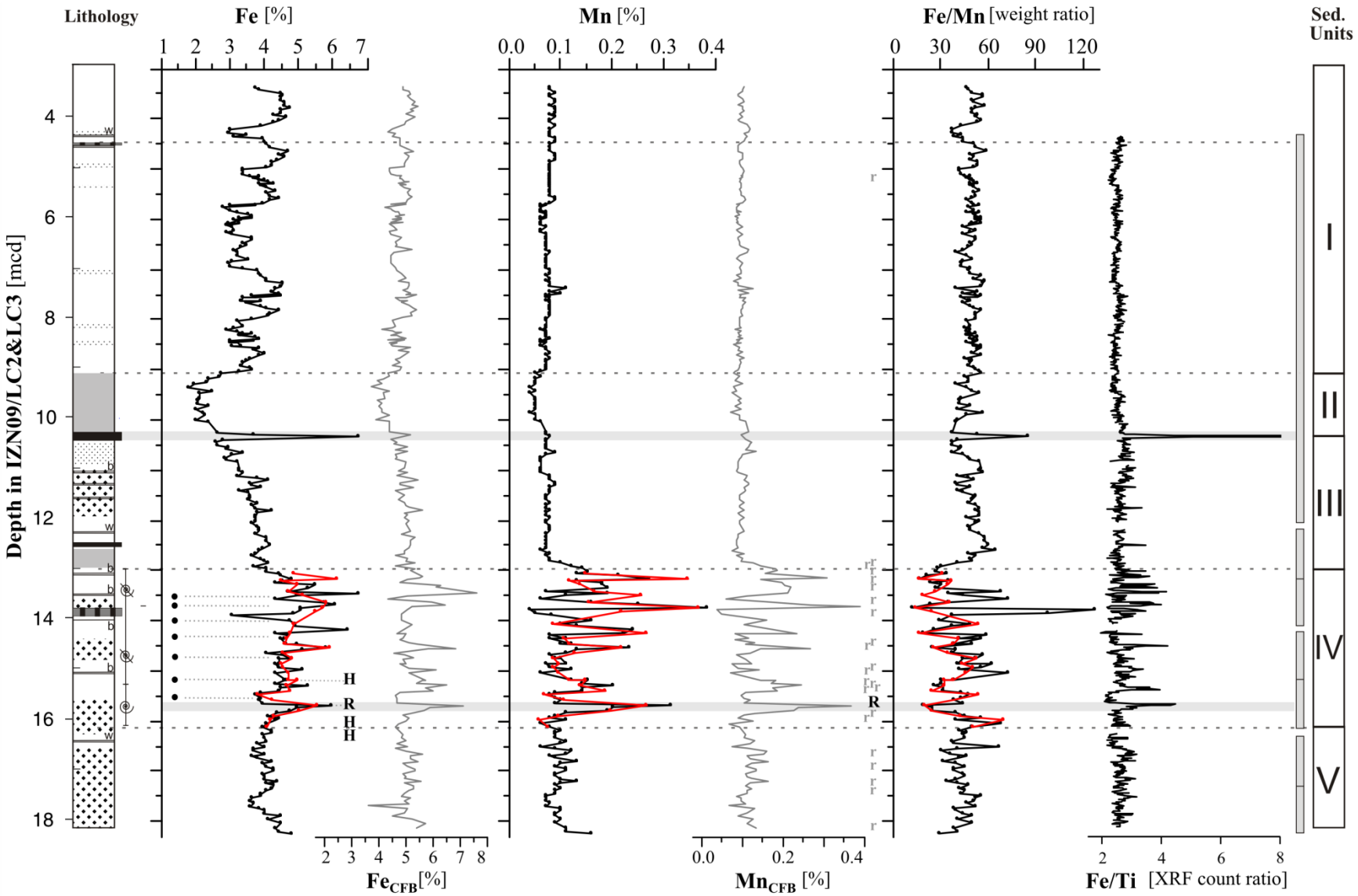

Figure 8.5: Black curves: behaviour of Fe, Mg, Fe/Mn, and Fe/Ti ratio. Red curves stand for measurements in the fraction <63µm. Gray curves Fe and Mn calculated on a carbonate free basis (CFB).Note that for CFB values, the Sf2 layer at 10.33 mcd is not included. "H" stays for hematite and "R" stays for rhodochrosite, please see text for discussion. Black dots next to iron vertical scale refer to the depths of dropstine occurrence.

Rhodochrosite is found at 15.69 mcd (section 6.4.4), which corresponds exactly to the first Fe and Mn maximum value, on the onset of unit IV (capital letter ‘R’ within Figure 8.5). Its texture in the X-ray diffractogram stresses its low crystallinity due to authigenic origin. The retreat of the Fe/Mn ratio at this depth indicates that Mn has been proportionally more accumulated than iron during diagenetical mobilization. Furthermore, for several depths slight textural changes have been found within the X-ray diffractograms (section 6.4.4), which would match position of the rhodochrosite reflection (small letter ‘r’ within Figure 8.5). This textural identification is solely on a visual basis; however it is noteworthy how well its occurrence matches observed manganese diagenetical mobilization. The respective mineral phase is not concentrated or crystalline enough to be well characterized in the diffractograms. It could refer to a very low concentration, or mineral instability. For example, dissolved organic matter interferes with the nucleation and growth of rhodochrosite (Berner, 1980).

Hematite occurrences intercalate with the rhodochrosite occurrence (capital letter ‘H’ within Figure 8.5). Its stability within the sedimentary column speaks for relatively oxic conditions. Hematite is clearly identified by a phase with good crystallinity in the diffractograms, indicating its detrital origin. This mineral is likely deposited in an environment which is oxygenated enough to maintain the load of oxides stable until deposition, and/or the reducing conditions at deposition where not ‘strong’ enough to bring Fe into solution.

8.4) Discussion

8.4.1) Evolution of trophic status

In general, the main sources for eutrophication are nitrogen and phosphates (Braga et al., 2002). The increase in total organic carbon, nitrogen and sulfur for Lake Iznik towards the Holocene (Figure 8.1 and Figure 8.4), is consistent with the classic evolution of a lake system from a status of low trophic status, during colder climate and less productive phases, towards a system with a relative higher degree of trophy, in which the organic matter is not completely metabolized and starts accumulating within the sediments. Also the manganese profile (Figure 8.5) supports the evolution of an oligotrophic towards a more productive lake (Mackereth, 1966). Besides the low organic matter production, an oligotrophic lake also favors higher retention rates of manganese. Given a lack of organic matter in the water column, the flux of oxides that reaches the deeper parts of the lake increases, and more Mn can be reduced in deeper parts of the lake, given reducing conditions prevail (Giblin, 2009).

Lake Iznik today has a trophy somewhere between a mesotrophic and a eutrophic stage, as nutrient load has been enhanced by anthropogenic activity during the past two decades (Franz et al., 2006). During the 60's the distant sight of the lake has been described as oligotrophic, due to its deep transparent blue color (Nümann, 1960), resultant from a very low algal production. However, a closer investigation on its nutrient load reveals a higher productivity in the modern lake (Franz et al., 2006; Nümann, 1960).

Table 8.1: Simplified summary of the parameter evolution that are related to redox situation, productivity and early diagenetical processes. Arrows up indicate occurrence, or high values; arrows down indicate significant reduction, or low values; a minus (-) indicates intermittent character, i.e. rapidly changing, or interruption. Intensity of shades of gray is associated to intensity of process or absolute values.

Sed.Unit	TOC	N	S	ASi	TOC/S	TOC/N	Mn accumulation	Monosulfide precipitation
Unit I	↑	↑	↑	↑	↓↑	↑	↓	↓
Unit II	↑	↑	↑	↑	↑	↑	↓	↓
Unit III	↓	↓	↑	↑↓	↓	↓↑	↓	↑↑
Unit IV	↓	↓	↓	↓	↑↓	↓	↓-↑	↑-
Unit V	↓	↓	↑↓	↓	↑↓	↓↑	↑↓	↑

The steep gradient in preservation of total organic carbon and nitrogen concentrations in the transition between units III and II (Figure 8.6, Table 8.1), could indicate an abrupt onset of eutrophia. However, for hard water lakes, internal processes such as co- precipitation of phosphorous with carbonates, can highly influence the trophic status and the onset of organic accumulation can occur abruptly (Wetzel, 2001). Natural eutrophia is most likely occurring gradually, as a slow process associated to ecosystem evolution (Braga et al., 2002). Such steep gradient is pointing towards changes in the metabolization of organic matter between units III and II.

Interpreting TOC/S as an inverse measure of sulfate reduction and sulfide fixation, unit III is marked by organic matter highly metabolized by this means, and as consequence of high sulfide production, abundant iron monosulfides are fixed in the sediment. Furthermore, as a consequence of a lower lake level (section 7.3.2), and increase in ionic concentrations, more sulfur is available. The higher sulfide production is registered by an increase in the precipitation of black iron monosulfides, also as thin black layers.

In unit II, again high TOC/S values in unit II indicate that sulfur is less pronounced as a metabolization route for organic matter. Less organic matter is metabolized and its burial rate increases. Furthermore the almost coincidence of the TOC and N gradient, with the increase in amorphous silica indicates that there is an increase in organic load. Silicic acid is

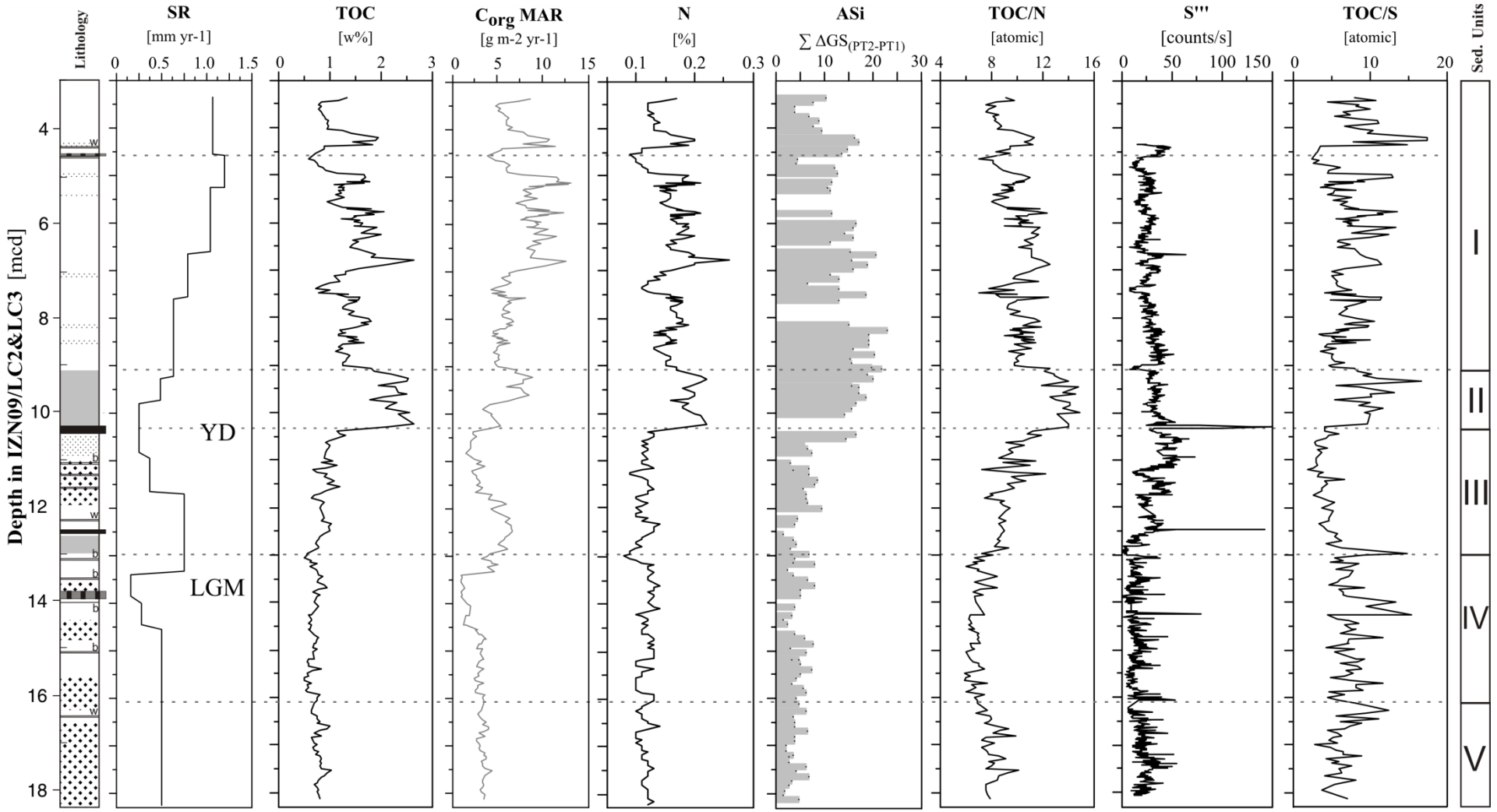

Figure 8.6: Sedimentation rate (SR) derived from the age model (chapter 5), concentrations of total nitrogen (N) and total organic carbon (TOC) both in [w%], mass accumulation of organic carbon (C_{orgc}MAR) derived from SR and TOC in [$g.m^{-2}yr^{-1}$], amorphous silica (ASi) represented by the parameter $\Sigma GS_{(PT2-PT1)}$ (section 7.1..1), sulfur (S''') derived from Itrax scanner, and atomic ratios for TOC/N and TOC/S. (Legend for lithology see Fig 5.1)

originating from higher weathering rate in the catchment (section 6.5.3), which is also reflected by the higher TOC/N ratios, indicating that the detrital character of organic matter is increasing with the onset of the Holocene.

Despite the uncertainties related to the mass accumulation rate calculation, it is notable that the organic carbon accumulation (C_{org}, derived from TOC and sedimentation rate) outlines a steady and gradual increase after the Younger Dryas (YD) towards the Holocene. Interestingly the Younger Dryas and the Last Glacial Maximum (LGM) present the lowest, if any, accumulation of organic carbon (Figure 8.6).

Summarizing, the late Pleistocene Lake Iznik evolves gradually from a status of low bio-productivity, most likely oligotrophic, towards a status of increased aquatic productivity, during the late Pleistocene to Holocene transition. This accompanies changes in the catchment, i.e. weathering and terrestric organic load.

8.4.2) Lake mixing and water column stratification

One significant aspect that remains to be explained are the striking changes in bottom oxygenation conditions as outlined by the manganese accumulation, associated to the precipitation of sulfides during the Pleistocene.

Usually the production of sulfide is expected to be higher in more eutrophic than oligotrophic lakes, because the eutrophia typically leads to the developments of an anoxic hypolimnion in which sulfate is potentially reduced (Wetzel, 2001). As previously outlined, the ‘modern’ Lake Iznik develops an annual anoxia, however it is subject to sulfide fixation in a much lesser extent, which is unlikely a result of sulfur limitation. The Holocene and the modern lake present higher sulfur load than the Pleistocene lake. Alternatively, there is less available soluble iron. However, soluble iron, and sulfides would be expected to be rather ‘increasing’ with the onset of eutrophication, and not decreasing (Wetzel, 2001). A reasonable explanation for the mentioned discrepancies, is that the Pleistocene oligotrophic lake was subject to periodic meromixis, i.e. an onset of a stratified layer of bottom water with singular oxygenation (anoxic) and chemical characteristics (Boehrer and Schultze, 2008). The establishment of a bottom water layer which is not mixing with the overlaying water column for prolonged periods of time could explain the relative high precipitation of iron monosulfides in a lake which has otherwise good oxygenated water column. Also, prolonged periods of bottom water stagnation explain the accumulation of other dissolved metal species in the anoxic bottom layer.

A density stratified system which maintains clay plumes distributed as interflows, as conceptualized for an oligotrophic system (Sturm and Matter, 1978), it is a plausible explanation for the uniform clay deposition within unit IV. Furthermore, it also explains the recurrent presence of shell fragments, which could be carried by such interflows. Still, even if the increases in Fe and Mn are related to such plumes of clayey material, the preferential accumulation of manganese and the vertical Fe displacements, stress the chemical character of the accumulation of these elements.

As previously observed, in modern conditions of seasonal anoxia manganese is not accumulating in the sediments. Consider the formation of FeS layer at the base of unit II. It represents the punctually highest Fe and S accumulation, but no Mn accumulates. On one hand Mn participates much less in sulfide precipitation, on the other hand it is being exported from the sediments. Consequently, during the onset of unit II, the lake was subject to recurrent mixis between the anoxic phases – opposed to the meromixis stages within unit IV.

Further observation regards the pebbles that occur in unit IV, which lie within the bindy-clay matrix (section 4.1.4). Given a first interpretation of low lake level for unit IV, based on lower carbonate production (Roeser et al., 2012), they were associated to fluvial input. However, the clayey matrix clearly outlines that the pebbles are dropstones, and their precise occurrence is depicted by the black dots near the vertical iron axis in Figure 8.5. Intriguingly the dropstones coincide rather with periods of low or retreating iron and manganese contents.

Hence, given the presented sedimentological and geochemical evidence, it is reasonable to state that the accumulation of elements which are mobile under reducing conditions is consequence of periods of bottom water anoxia, which were more pronounced as in the modern lake.

The stages of bottom water anoxia are characterized by the Fe/Ti and Mn excursions, and further by iron precipitated as monosulfides (FeS). The accumulation of manganese at least for one depth reaches supersaturation with respect to rhodochrosite, indicating that as during these anoxic stages, there is an impediment of the export of the solubilized elements from the lake.

Processes that can maintain a meromixis are manifold. For instance they can be biologic in origin (Boehrer and Schultze, 2008). In this case, the bottom layer is maintained by the chemical gradient resultant from metabolization of organic matter (equations 9.1 to 9.7). However, this is an unlikely situation for Lake Iznik since the lake is interpreted to have oligotrophic state at the time. This does not mean these metabolization routes do not take

place, but they are unlikely responsible for maintaining the bottom water anoxia. Further processes known to influence bottom water renewal are presented within a climatic context.

9.) Carbonate accumulation in response to changes the limnological system

9.1) Introduction

In the past decades, much knowledge has been gained on lakes mixing processes, stratification, sediment dynamics (Boehrer and Schultze, 2008; Kaden et al., 2010; Lerman et al., 1995; Sturm and Matter, 1978) and geochemical cycling (Davison, 1993; Last and Smol, 2001; Leng and Marshall, 2004; Meyers and Ishiwatari, 1995), specially for carbonate producing lakes (Gierlowski-Kordesch, 2010; Ito, 2001; Kelts and Hsü, 1978; Last, 1982; Ohlendorf and Sturm, 2001).

In general, phase relationships for carbonates are documented in detail for high pressure and high temperature systems, and the extrapolation of stability boundaries to sedimentary temperatures indicates that only magnesite, dolomite and low magnesium calcite would be expected to be stable (Tucker and Wright, 1992). For low pressure and low temperature conditions there is vast literature, however, precise conditions that maintain aragonite 'stable' in the sedimentary environment are at best approximated. Specially the ratio Mg/Ca has influence on the stable carbonate phase, as Mg has been invoked to function inhibiting calcite precipitation due to surface adsorption processes (Berner, 1975; Füchtbauer et al., 1988; Katz, 1973; Katz and Nishri, 2013; Kelts and Hsü, 1978; Last, 1982; Müller et al., 1972; Stein et al., 1997).

This chapter focuses on the relation between aragonite preservation in the sediments and limnological processes. The aim lies in generating understanding of how changes in the limnological system, are related to the preserved carbonate phases. Lake Iznik is an ideal natural laboratory to this type of investigation, given its singular characteristics in primary carbonate precipitation and preservation in the sediments. For the present thesis, this knowledge is essential in order to use carbonate accumulation as an additional tool for a paleoenvironmental reconstruction and climatic forcing (chapter 10). To attend the objective of the present chapter, the carbonate mineral phases are herein presented in their absolute concentrations, along with determined mineral structural parameters, and eventually additional parameters. Elements which have affinity with the carbonate phases are also presented. The meaning of the data is discussed in the light of selected geochemical and sedimentological evidence, which speak for limnological processes and their evolution.

9.2) Stratigraphic changes

9.2.1) Carbonate phases

The dominant carbonate phases present in the Iznik sediment profile IZN09/LC2&LC3 are aragonite and calcite. Stratigraphic changes of the carbonate phases have been depicted along with the detrital mineral contribution in section (6.4.2). Aragonite and calcite together explain more than 99% of the carbonate phase for the overall record (Figure 9.1).

Generally, the aragonite concentrations are higher than calcite for all units, except unit IV, in which aragonite is present in trace amounts. Calcite is present at a practically constant background value of circa 7% of the bulk sediment for most of the sediment profile (Figure 9.1). The main exception is unit IV in which calcite concentration reaches up to 20% punctually. Furthermore, carbonate minerals are virtually absent at circa 13.9 mcd (unit IV a). This depth represents the LGM and is also coincident with the deposition of the well dated Y2 tephra. Within unit III b, both, aragonite and calcite concentrations are of circa 10%, whereas starting in unit III a, towards unit II, aragonite accumulation increases up to 50% of the bulk mineralogy. At circa 4.3 mcd, within unit I, both carbonate phases increase simultaneously.

Remarkably, the aragonite concentrations within units V, III, II and I are never lower than calcite concentrations, and even during the aragonite minima, the values for aragonite concentrations refer to nearly the calcite background values (e.g. at the depths 4.4, 5.5 and 7.4 mcd, Figure 9.1).

Unit IV is peculiar since calcite rather than aragonite is the prevailing carbonate mineral phase. The calcite and aragonite concentrations invert promptly at the boundaries of the unit. Interestingly, despite the abrupt nature of the changes in dominant carbonate phase, the total carbonate concentration is fairly constant at the boundaries of unit IV, even during the observed inversions. Therefore, these events cannot be observed from the Ca/Ti, or $CaCO_3$ record (Figure 6.4 and Figure 6.8, respectively). The observed aragonite and calcite concentrations make out the carbonate matrix of the bulk sediment, and their quantification is not affected by shells present in the unit. This is confirmed by XRD analysis from the wet sieved fraction <63µm, i.e. without any shells. All carbonate is in the silt and clay size fraction as shown by the coincidence between black and red curves for aragonite and calcite percentages in Figure 9.3 (and Figure 6.7). For some depths data indicates that other carbonate phases than aragonite and calcite might be present in trace amounts (sections 6.4.4 and 8.3.1), for instance rhodochrosite.

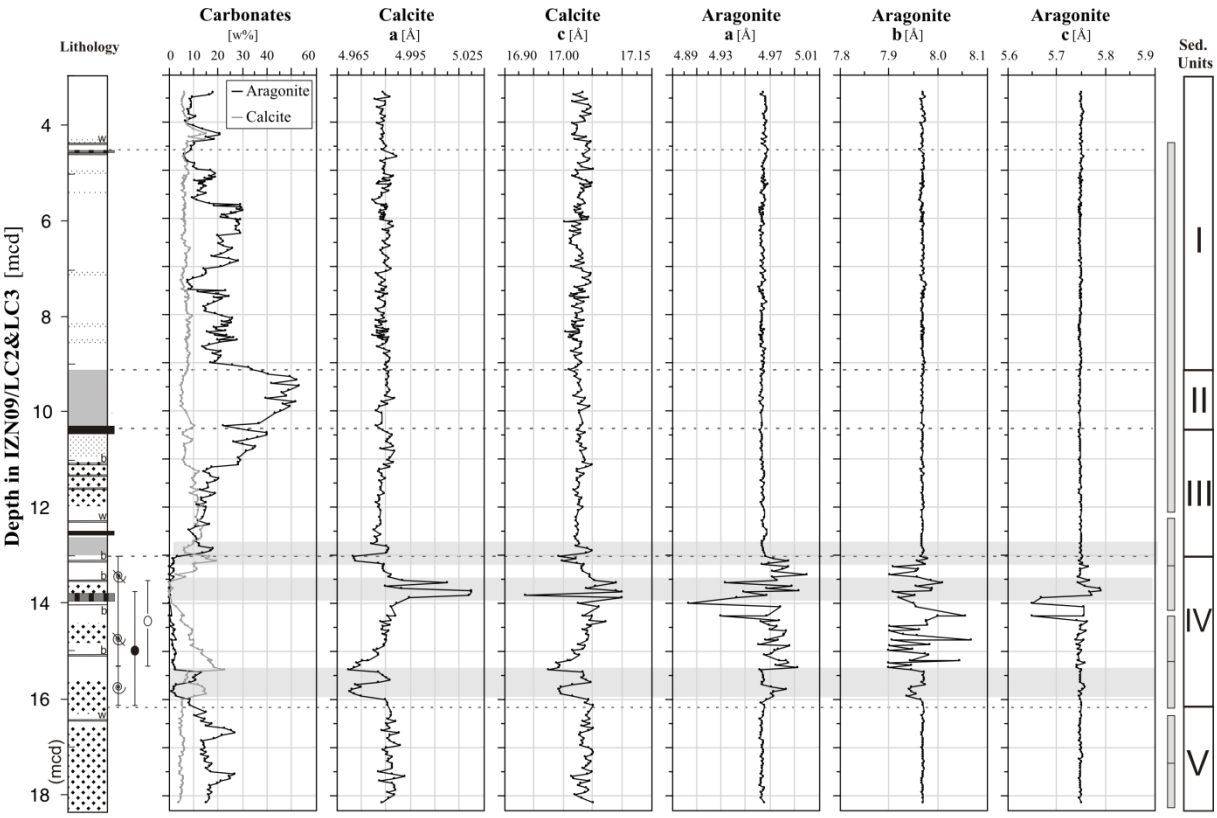

Figure 9.1: Stratigraphic changes in the concentrations (w%) of calcite and aragonite in the bulk sediment, alongside their respective lattice parameters (angstroms).

9.2.2) Mineral structure

The change in prevailing bulk carbonate phase in unit IV is accompanied by significant variations in the carbonate mineral lattices. For instance, calcite lattice parameters reflect a smaller cell volume size at the upper and lower boundaries of the unit (e.g. lattice parameter *a* shifts from 4.9853 to 4.9716 Å)[17], whereas aragonite lattice parameters reflect instability for unit IV. Remarkably, aragonite lattice parameters do not present any change at all for the other units V, III, II and I (*a*=4.96 Å, *b*=7.97 Å, *c*=5.75 Å)[18]. And yet, calcite shows slightly different cell volume size for unit V (*a*=4.990 Å, *c*=17.04 Å)[18], than for unit III (*a*=4.980 Å, *c*=17.02 Å)[18], whereas for units II and I the values fluctuate in between these observations.

If on one hand the lattice parameters can indicate slight changes in the cell volume size, on the other hand interpretation of the lattice values obtained from textural information of XRD diffractograms requires care, especially if the investigated mineral phase has low concentration. For instance, at the depth of complete absence of carbonate phases, at circa 14

[17] The standard deviation of the calculated lattice parameters lies on the last two decimals, out of four to five decimals. Hence, also a conservative plot, including the possible measurement deviation, leads to the same conclusions.
[18] rounded values

mcd, the high excursions for the lattice parameters are rather meaningless. Similarly, some of the excursions for aragonite lattice parameters cannot be interpreted. Nevertheless, some aspects remain to be noted.

For example, between 15.7 and 16 mcd there is a covariance between the increase in aragonite *a* index, decrease in aragonite *b* index (Figure 9.1), and, an correlated increase in Fe/Ti, and increased Mn accumulation (Figure 9.3). Moreover, for the same depth interval, calcite cell volume size is reducing (Figure 9.1).

The reducing calcite volume size possibly corresponds to a high magnesian calcite, and the described shift in the volume cell size, would correspond to an addition of circa 5% mol $MgCO_3$ in relation to the already existing calcite. However, to confirm this, direct measurements on single crystals need to be undertaken. The calcite lattice parameters for the units V, III, II and I, reflect that the sediment profile generally contains a low magnesium calcite (circa 2.5% mol $MgCO_3$). These values are approximated using the calculated lattice parameters (Goldschmidt et al., 1961), which is equivalent to using the position of the d_{104} peak from calcite (Tucker, 1996).

Interestingly, the values for the calcite lattice parameters within the short core (i.e. present day lake) resemble those from unit V. The fluctuating values for calcite lattice parameters reflect also the variety of calcite sources.

9.3) Origin of the carbonates

In order to reach the objectives of this study, it is crucial to understand the origin of the distinct carbonate minerals that occur in the sedimentary record. The definitions on the ‘quality’ of carbonate as used herein are (a) endogenic referring to the primary precipitation in the water column, and (b) authigenic, formed in situ by early diagenesis (Ito, 2001; Jones and Browser, 1978; Last, 2001a). In the literature, the latter term is often applied to both - minerals formed primarily in the water column, as well as minerals formed from pore waters whilst distinction between these processes is often not explicitly stated. Detrital refers to the material which is originated outside the lake, i.e. catchment.

9.3.1) Aragonite

In Lake Iznik, aragonite is expected to be the endogenic carbonate phase forming from primary precipitation in the water column. Chemical precipitation reactions from solution are of complex nature. Despite the stable carbonate phase being controlled primarily by the

concentration of Mg, several molecules (e.g. leucine, urea), minerals (e.g. oxides, silicates), ions (e.g. uranyl), and elements (e.g. Sr, Mg) can interact with the carbonate phases, potentially affecting the morphology and chemistry of the precipitate (Bischoff, 1968a; de Leeuw and Parker, 1998; Lin et al., 2009; Morse, 1986; Nehrke, 2007; Thompson et al., 2011). Detailed studies on material of sediment traps for the Lake Iznik are pending. Nevertheless, the preservation of aragonite in the sediments is confirmed by XRD measurements, as well as analysis of smear slides for the core IZN09/LC2 (10 cm resolution) and illustrated herein by REM images from two selected white laminae from the investigated profile (Figure 9.2). These white laminae represent preserved, undisturbed, events of endogenic carbonate precipitation. Similar yellowish laminae are also found when coring the water sediment interface (Nümann, 1960, and field observation).

The white laminae are largely composed of aragonite. The preserved aragonite needles in Iznik sediments have typical morphology of primary crystals, being acicular, with irregular outlines and pointed terminations (Last, 2001b; Macintyre and Reid, 1992), presenting different needle length (Figure 9.2). Aragonite needles size is diverse throughout the profile (Figure 9.1). The crystal length reaches its maximum (12 µm) in unit V and the transition towards unit IV. Within units II and III aragonite crystals have medium size (reaching 9 µm), and in unit I aragonite needles upper length is the smallest (3 µm). For the lower laminae, aragonite often occurs as twinned or multiple crystals (Figure 9.2 d). There is no evidence for overgrowth of aragonite on other mineral phases. For the same laminae it is possible to identify patterns of crystal growth on the crystal faces (Figure 9.2 c), as well as crystals with rounded edges, likely indicating partial dissolution (Figure 9.2 e). Additionally, the holes observed on the crystal structure (Figure 9.2 e) indicate that precipitation might be mediated biogenically by cyanobacteria (Matter et al., 2010).

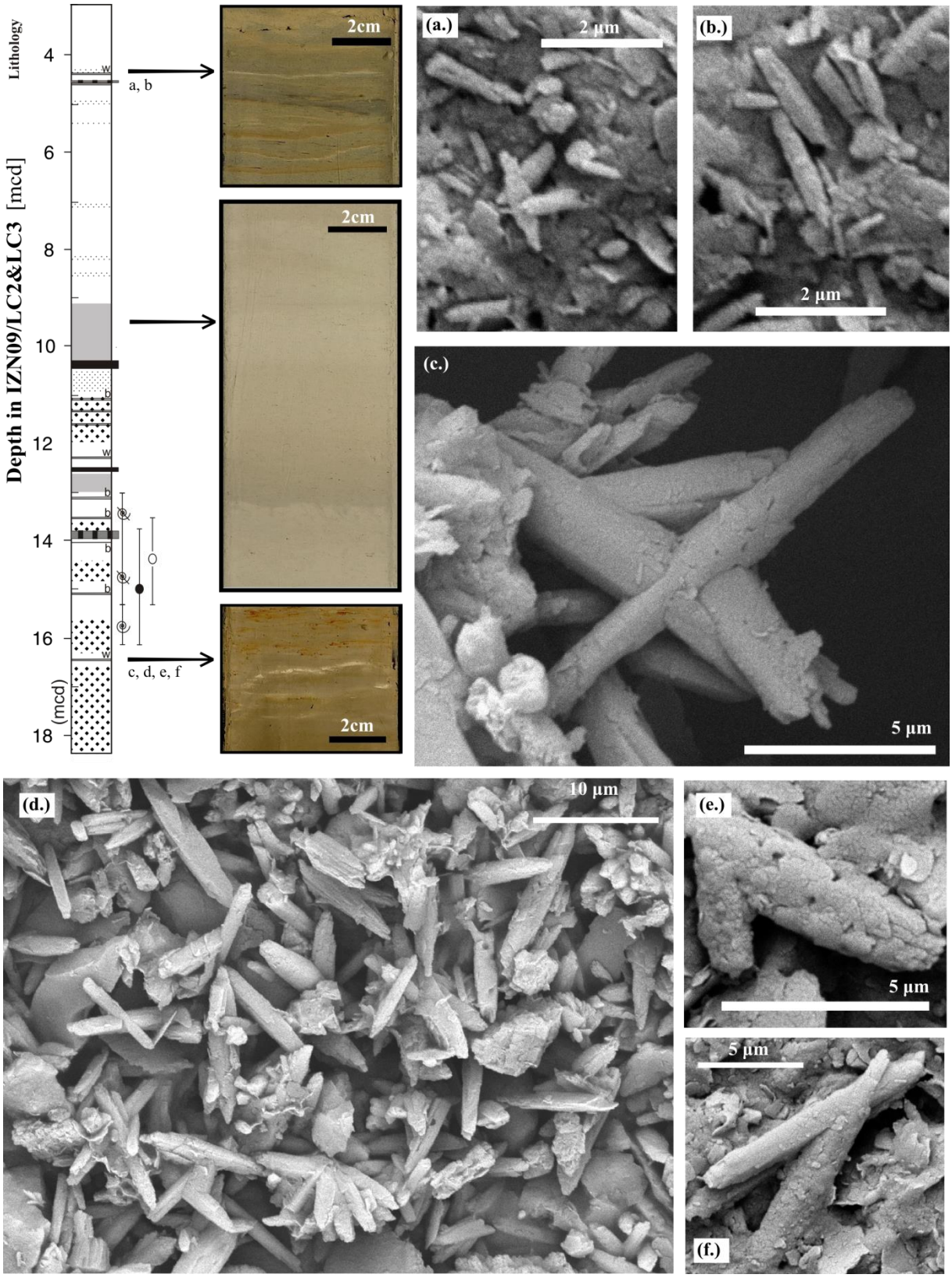

Figure 9.2: Lithofacies of endogen carbonate precipitation, and scanning electron microscope images of two selected white laminae at 4.38 and 16.36 mcd, showing aragonites with distinct needle length (a, b and c, f), and slightly differentiated morphology (e). In the bottom laminae, which is bioturbated to some extent, hexagonal clay crystals are also present (d) as well as one calcite rhombohedra (d upper left).

Table 9.1: Size of the aragonite needles within the sediment profile

Sed. Unit	Depth or depth interval [mcd]	Aragonite needle length (n_L)	Obs.[a]
Unit I	at 4.38	$n_L < 3$ µm	SEM
Unit II	from 9.12 to 10.31 x	3 µm < n_L < 6 µm, some n_L ~ 9 µm	SS
Unit III	from 10.31 to 13.02	3 µm < n_L < 9 µm	SS
Unit IV	from 13.06 to 13.29; from 13.41 to 15.39; at 14.65; from 15.49 to 16.27;	3 µm < n_L < 6 µm; absent; Few needles with n_L = 12 µm; 6 µm < n_L <12 µm;	SS
Unit V	at 16.36 mcd	10 µm < n_L <12 µm, some ~ 6 µm	SEM

[a] *origin of the observations. SEM: scanning electron microscope; SS: smear slides.*

9.3.2) Calcite

The origin of lacustrine calcite is not as straight forward to establish as the origin of lacustrine aragonite. As stable carbonate phase, calcite can have any of the general four sources for calcium carbonate in lakes (Jones and Browser, 1978; Tucker and Wright, 1992). Calcite can for instance originate from detritus of the catchment (Kelts and Hsü, 1978), or from biological shells (e.g. ostracodes). Calcite can as well precipitate as primary carbonate from the water column, or moreover form as an authigenic mineral phase.

The compositional analysis of Iznik geochemical data, clearly identifies three groups of elements, (1) the siliciclastic group (associated to detrital input), (2) the carbonate group (associated to endogenic carbonate precipitation), and (3) the organic group (associated to primary productivity, section 6.3.1.2, Figure 6.2). Interestingly, the compositional analysis of Iznik mineralogical data also identifies three groups of minerals, (1) the detrital group (2) aragonite, and (3) calcite (section 6.4.1, Figure 6.5). Remarkably, calcite presents high variance, i.e. relative low correlation, to both the detrital and the endogenic carbonate group. In analogy to the geochemical distribution, it is reasonable to state that calcite is representing the third group; thus overall calcite is closely related to the organic phase, i.e. lake productivity.

As previously noted, most of the calcite from the sediment profile IZN09/LC2&LC3 is made of low Mg calcite. However, such a calcite does not precipitate from the same waters that precipitate aragonite, but, in such environment low Mg calcite is formed and maintained stable in the shells of ostracodes (Ito, 2001). Therefore, the investigations of the calcite

mineral lattice, support the conclusions from CoDa analysis, indicating that calcite is contained to large amounts in the shells of ostracodes. In fact, when wet sieved, Iznik sediments retain significant amounts of ostracodes in different size fractions. Further investigation of ecological aspects of these biogenic carbonates is not focus of this study. However, a detrital origin of calcite is also possible (Franz et al., 2006; Viehberg et al., 2012). Therefore, concerning the profile under investigation, for units I, II, IIIa and V, the calcite percentages are made out of a mixture of ostracodes shells, and possibly some detrital calcite. Although CoDa analysis indicates that the biogenic origin predominates for the overall data.

Unit IIIb and unit IV are an exception for the previous statement. For these two units calcite has an additional origin, other than biogenic. This is based on the observations that (a) calcite concentrations are higher than 10%, (b) calcite mineral structure is slightly different, (c) and the samples belonging to the units cluster distinctly within the mineral compositional biplot (Figure 6.5). Thus, calcite is also present, either as primary (endogen) or authigenic (diagenetic) mineral phase.

Given the multiple sources of calcite, it should be stressed that also the calcite phase in the XRD diffractograms represents a mixture signal of the different sources as well. Hence, the calculated lattice parameters for calcite do not stay for the exact lattice structure from the encountered minerals, but rather their variations reflect the tendency of the major calcite type present. This is consequence of the reflections of different calcite types being very close to one another within X-ray diffractograms.

Yet, there are the boundaries of unit IV to be considered. At these depths (13 and 16mcd) the changes in calcite structure are the most prominent (Figure 9.1) and the observed reduce in cell volume size the occurrence of a high magnesian calcite (section 9.2.2). Such a mineral phase would be expected to precipitate chemically from similar water chemistry as aragonite, or form as authigenic phase (Ito, 2001). However, the Ca position in calcite can be substituted by different elements. For instance, Mn and Fe are expected to be part of the rhombohedral solid solution state, substituting in the calcite lattice (Tucker and Wright, 1992). As further investigation would be required to resolve the issue, for practical purposes herein the calcite phase will be assumed to be a high magnesian calcite which is the most common phase in aqueous milieus.

9.3.3) Rhodochrosite

In lacustrine settings, rhodochrosite has authigenic origin, and precipitates when interstitial waters become oversaturated in dissolved, reduced, Mn^{+2} (Berner, 1980; Jones and Browser, 1978; Last, 2001a). The events of changes in lake mixing which result in Mn excursions are potentially associated to authigenic formation of rhodochrosite (Figure 9.3). The authigenic changes are also characterized by slight increases in the inorganic carbon values, as well as positive excursions in the signature of stable carbon and oxygen isotopes from the carbonate phase (Figure 9.3).

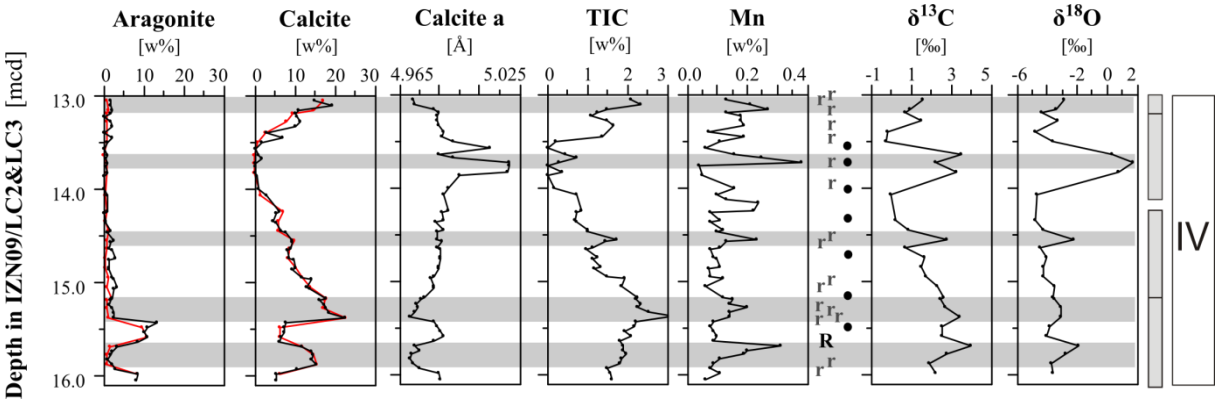

Figure 9.3: Aragonite and calcite concentrations for unit IV (black curves: bulk, red curves: fraction <63m), along with total inorganic carbon and manganese concentrations, as well as stable isotopes measured on bulk carbonates. Black dots on left scale indicate depths of dropstone occurence. Letters 'R' and 'r' indicate rhodochrosite, for discussion see sections 6.4.4 and 8.3.1.

9.3.4) Virtual Carbonate Absence

Between 13.5 and 14 mcd, the sedimentary profile is unique for the complete absence of aragonite and calcite. However, total inorganic carbon is detected up to 0.5% (Figure 9.3). Assuming it to be bound in calcium carbonate, it would mean there is up to 4% of $CaCO_3$ present. Assuming that this inorganic carbon is forming rhodochrosite, it would mean that up to 5% manganese carbonate is present in this depth interval. In the case of a pure magnesium carbonate it would be making out 3.5% of the bulk sediment. Notably at this depth the stable carbon and oxygen isotopes measured on the carbonate phase, present the heaviest values in relation to the entire profile, and thus most likely reflect the isotopic signature of the authigenic phase.

This interval corresponds to the Last Glacial Maximum, chronologically outlined by the deposition of the Y2 tephra. A complete absence of carbonates could be resulting from (a)

minor carbonates precipitation, and/or (b) complete dissolution of carbonates. On one hand, during the glacial primary aquatic productivity is reduced – and consequently also bio-induced carbonate accumulation. On the other hand, the occasional aragonite needles preserved in trace amounts within unit IV indicate that at least this carbonate phase is precipitating. Hence it is likely that some kind of dissolution leading to the virtual absence of carbonate is occurring. Therefore, is reasonable to assume that the absence of carbonates in the interval corresponding to the LGM is a combination of both, low carbonate productivity coupled to early diagenetical changes. Moreover, within unit IV such processes are more pronounced during the interval of the LGM, resulting in the complete absence of calcium carbonate in unit IVa.

9.4) Elements with affinity to the carbonate phase

Alkaline or alkaline earth elements (e.g. Ba, Sr, Mg) and other elements (e.g. Mn, U, Cu), can interact with carbonates, either by co-precipitation or by surface adsorption effects (Morse, 1986). For co-precipitation processes, the incorporation of the elements in the carbonate lattice is expected to be directly proportional to the element availability (concentration) in the water which is precipitating the mineral phase, and therefore the investigation of co-precipitating elements can be used to obtain information about past lake chemistry (Ito, 2001; Lemcke and Sturm, 1997). Alongside Ca, elements that may substitute in the rhombohedral calcite structure are Mg, Mn, Fe, Co, Zn and Ni. Whereas, elements that can substitute for Ca in the orthorhombic aragonite lattice include Sr, Eu, Pb and Ba (Tucker and Wright, 1992).

Beside the alkali earth elements, correlation of carbonates to distinct trace elements could be identified in the data[19]. From elements that undergo adsorption on carbonate surface, U is inserted in the discussion, as it was also identified as one of the elements with low variance to the carbonate phase in the Iznik sediments (see section 6.3.1.2, Figure 6.2). In the present investigation Sr and Mg are chosen, because the interaction of these elements with carbonates, and cycling of endogen lacustrine carbonates have been investigated (Berner, 1975; Goldschmidt et al., 1961; Katz, 1973; Katz and Nishri, 2013; Stein et al., 1997).

[19] For the Iznik sediments, correlations are observed for the Eu, Pb and Ba elements with the aragonite phase. For example, Ba/Ti is positively correlated to units II and III; Pb/Ti to unit II, and Eu punctually to aragonite (not illustrated herein)

9.4.1) Strontium

For the Iznik sediments Sr is strongly correlated to aragonite (Figure 9.4 a, b), with exception to sedimentary unit IV in which it is correlated to both carbonate phases, aragonite and calcite. In unit IV the linear relationship of Sr with aragonite is marked by a distinct gradient (Figure 9.4 b)[20]. For unit IIIb, Sr has a 'negative' linear association to calcite. For the units I, II, IIIa and V, there is no clear association between Sr and calcite. Hence, bulk sedimentary Sr abundances are primarily controlled by aragonite precipitation.

To obtain an approximation on the past $(Sr/Ca)_{lake}$ ratios from the waters of Lake Iznik, a distribution coefficient for Sr between aragonite and the lake water would be needed. Considering that the carbonates at the sediment water interface have the imprint of the present day water chemistry, with the available data it is possible to approximate a distribution coefficient for Sr and the carbonate phase for the Iznik sediments. Different methods can be applied to calculate distribution coefficients (Katz and Nishri, 2013; Lemcke and Sturm, 1997). Herein, to obtain a first approximation, the bulk method was applied, as given by the equation:

$$D = \frac{(Sr/Ca)_{bulk}}{(Sr/Ca)_{water}} \qquad (Eq.10.1)$$

The underlying assumption is that the sedimentation of all bulk Sr is being controlled by the total carbonate phase. The interpretation of the absolute value for such a coefficient is obviously constrained by the presence of two carbonate phases. Alternatively a distribution coefficient could be calculated using the Ca contained in aragonite. However, to maintain the distribution coefficient applicable to all sedimentary units in the profile, including unit IV, the total carbonate phase is favored. The result is an estimation of a rough, but 'Iznik specific' coefficient. This value is preferred over the usage of values of distribution coefficients for different carbonate phases as available from literature. Once the distribution coefficient is approximated, the same equation (10.1) can be used to estimate the $(Sr/Ca)_{lake}$, using the data from the sediment profile.

The distribution coefficient calculated by the described means, is around 1.39. This value is not far from, but slightly more elevated than, the expected distribution coefficient for Sr in relation to aragonite, which lies near unity (Kinsman and Holland, 1969; Stein et al., 1997).

[20] The conclusions for Sr accumulation, i.e. Sr/Ti, are the same for calcite and aragonite, as the graphics are nearly the same as or Sr abundances in [ppm]. Herein, Sr concentrations are preferred because of possible inferences on the diagenetical milieu.

The calculated $(Sr/Ca)_{lake}$ values are in general smaller for higher aragonite concentrations (Figure 9.4 f), and nearly constant for aragonite concentrations higher than circa 20%. The value of the $(Sr/Ca)_{lake}$ ratio increases when aragonite concentrations are smaller[21]. Samples from sediment unit I with less than 15% aragonite, show the highest $(Sr/Ca)_{lake}$ values.

9.4.2) Magnesium

Magnesium concentration in waters is one key factor controlling the morphology of the precipitating carbonate phase (Berner, 1975; Bischoff, 1968b; Cooke, 1977; Sawada et al., 1990). This is clear from stability diagrams, where a perpendicular line to the log(Mg/Ca) axis delineates the distinct carbonate phases (e.g. dolomite and calcite, or aragonite and calcite) (Garrels and Christ, 1965; Tucker and Wright, 1992). This is a consequence of Mg acting as inhibitor of calcite precipitation (Kelts and Hsü, 1978). Also, Mg^{+2} participates in the rhombohedral solid solution (Tucker and Wright, 1992). The Mg/Ca (eq) values for Lake Iznik waters favor aragonite stability (~4.4, after Table 2.1).

As previously discussed, possible sedimentary sinks for Mg are the clay minerals, plankton, and rhombohedral carbonates, i.e. calcite. The ratio Mg/Ti expresses the Mg accumulation relatively to the detrital phase (Figure 6.8). The Mg accumulation is somehow correlated to the carbonate phases in units I, II and III (Figure 9.4 c, d). Calcite is positively correlated to Mg especially in unit I. For unit II, Mg expresses no clear correlation to calcite. For unit III, there is a 'negative' correlation between Mg and calcite (Figure 9.4 c). Magnesium is not expected to build into the aragonite structure, hence the observed positive correlation to aragonite within units I, II and III (Figure 9.4 d) is inferred to be indirect, due to (a) Mg incorporation into plankton, given a biologically induced aragonite precipitation, and/or (b) Mg incorporation into calcite, in which case for unit I calcite and aragonite are both primary precipitates.

The Mg/Sr ratio, in general, tends to diminish with higher aragonite concentrations (Figure 9.4 e). Moreover, the samples of sedimentary unit IV present a distinct gradient. The samples from unit I are 'shifted' to higher Mg/Sr ratios in relation to the samples from units III, V, and the short core. For aragonite concentrations higher than circa 40%, the Mg/Sr ratio is nearly constant.

[21] The same conclusions are obtained on the relative changes of $(Sr/Ca)_{lake}$ calculated using Ca_{total} or $Ca_{aragonite}$. The different calculations would result in distinct absolute values for the $(Sr/Ca)_{lake}$, with difference in the order of (0.003).

For the sedimentary record, the compositional data investigation shows a correlation of Mg to the organic phase (Figure 6.2). As previously discussed, the calcite concentrations are related to the organic phase, as well (section 9.3.2). Hence, it is likely that the distinct changes in the sedimentary behavior of Mg for the Holocene, sedimentary unit I, are related to changes in the 'quality', or type, of calcite, and/or of the organic phase of sediments.

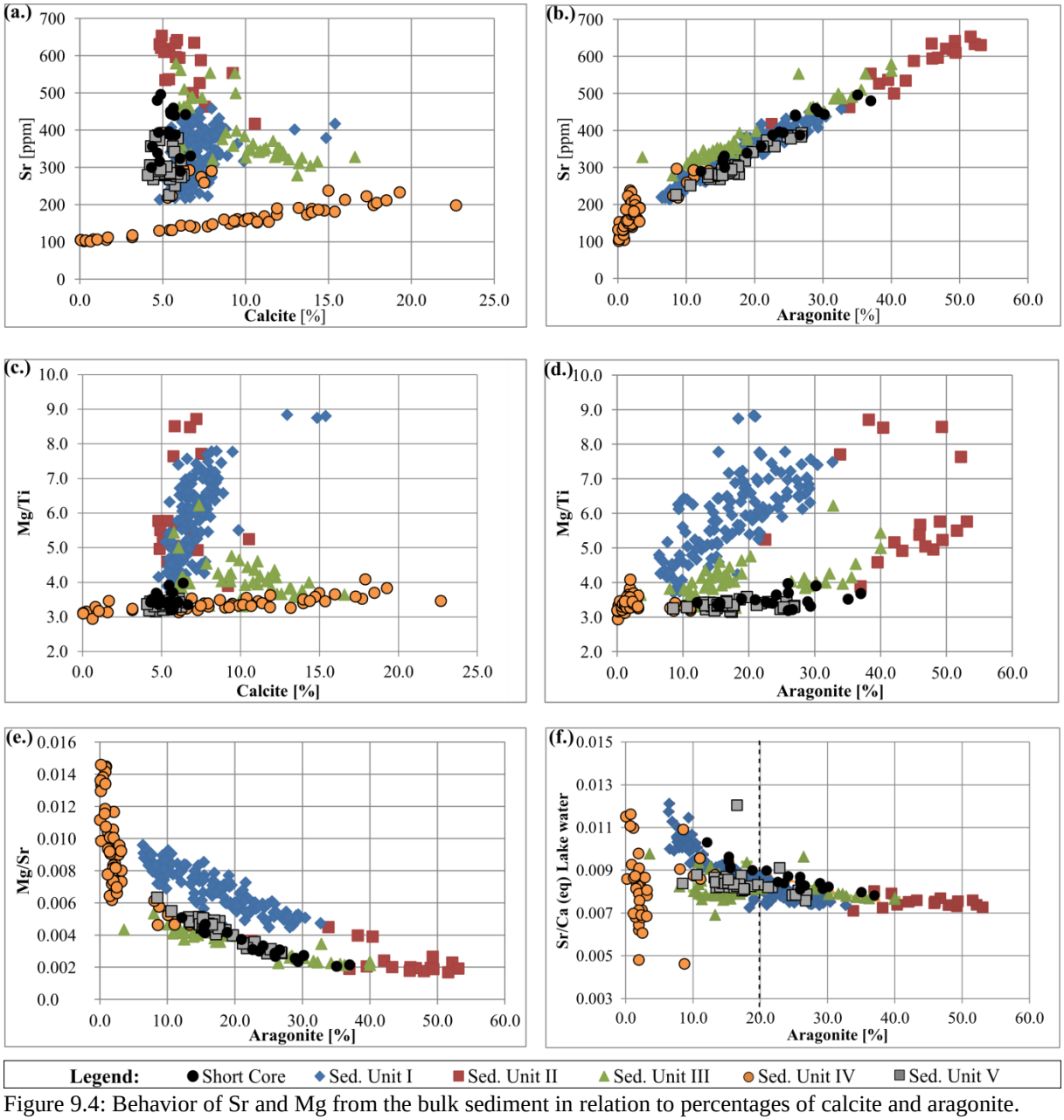

Figure 9.4: Behavior of Sr and Mg from the bulk sediment in relation to percentages of calcite and aragonite.

9.5) Discussion: relationship between carbonates and limnology

9.5.1) Water chemistry

The chemistry of the aqueous solution from which the mineral phase precipitates, defines its crystal structure, morphology, and moreover the content of trace minerals (Ito, 2001; Lemcke and Sturm, 1997; Morse, 1986). Therefore, the endogen mineral phases, their stability, and factors controlling the chemistry of lake water are intimately related. Thermodynamic calculations of carbonate saturation state for epilimnetic waters of Lake Iznik were not feasible given a lack of appropriate alkalinity data (Table 2.1). Still, the seasonally measured elemental concentrations in epilimnion and hypolimnion waters (Viehberg et al., 2012) indicate that Ca and Sr concentrations are depleted from Iznik epilimnion waters during summer as a result of carbonate precipitation. During winter the Ca and Sr concentrations in the hypolimnion are slightly enriched (Viehberg et al., 2012). Such enrichment is observed in hardwater lakes as a result of downward transportation of elements which co-precipitate with the carbonate phases (Katz and Nishri, 2013). Interestingly, the behavior of Mg in Iznik waters differs from Ca and Sr. During summer, Mg is slightly enriched in the hypolimnion in relation to the epilimnion. Towards the winter, as stratification gets stronger, Mg gets depleted in both the epilimnion and the hypolimnion as well. On one hand, such depletion can indicate that Mg cycle in Lake Iznik is not controlled by a purely chemical precipitation, and possibly supports the evidence for its biogenic association, to the benthic ostracods. On the other hand, it could be stated that the co-precipitation of Mg in endogen carbonates is of such ‘low’ order, that the absolute concentrations of Mg in water remain nearly unaffected by the co-precipitation process.

The sedimentary record holds different geochemical and mineralogical indications for changes in the water chemistry for the past 31.5 ka calBP.

For instance, sulfides and sulfates are present in different sections of the sediment profile. Monosulfidic minerals predominate as ‘dots’ in the lower core (units V and IV), and are more concentrated in unit IIIb, where accordingly sedimentary sulfur concentrations increase (Figure 8.6). Additionally, in the depth interval of units II and III, gypsum is encountered in the profile. Gypsum can be formed by the oxidation of pyrite after sampling, as for instance observed for some Mediterranean cores (B. Ryan, personal communication). In a classic evaporite sequence, the first endogen precipitates are carbonates (from waters with a minimum salinity of 0.12g/kg), which are then followed by the calcium sulfates - anhydrite

and gypsum – at high salinities (Wenk and Bulakh, 2004). For the hypersaline Lake Lisan, gypsum precipitation is associated to moments of lake turn over, after sulfate had accumulated in the epilimnion (Stein et al., 1997). Given Lake Iznik's low salinity, primary gypsum precipitation in the upper water column is very unlikely. However, gypsum may also form in early diagenesis (Muza and Wise, 1983). The specific nature of gypsum in the Iznik sediments remains open. Still, it is remarkably that gypsum occurrences are in agreement with the phases of lower lake levels, i.e. units II and III, according the coarse silt/clay ratio (Figure 9.5). Hence, it can be concluded that sulfur is enriched in the lake waters for the time of deposition of sedimentary units III and II.

Moreover, during most of the Holocene neither sulfides nor sulfates are observed in the sediments, but for punctual samples of the short gravity core, again gypsum has been found, as well as for surface sediments (not illustrated).

The latter observations, along with the observations of the calcite mineral lattice, and the observations for the alkaline elements (Mg and Sr), strongly indicate that the water chemistry, alongside with the carbonate system within Lake Iznik, are undergoing a geochemical cycle, starting from unit V (=SC) → unit IV → units (III, II) → unit I → SC (= unit V).

Therefore, we can conclude that changes in the water chemistry of Lake Iznik took place during the Pleistocene Holocene transition. Apparently such changes occurred in a specific range that maintained aragonite precipitating continuously. Hence, it is crucial to distinguish whether the observed changes are related to the chemistry of the entire water body, or to distinct water masses.

9.5.2) Epilimnion: Insights from aragonite morphology and crystal size

Endogen carbonate crystal size and form are influenced by the degree of carbonate saturation from the aqueous solution or lake water (Kelts and Hsü, 1978; Tucker and Wright, 1992). For instance, high supersaturation leads to high nucleation rates, which favor the formation of fine-micrite grains, with 1 to 4µm in size (Kelts and Hsü, 1978). Also, the length and morphology of aragonite crystals can be interpreted in relation to the depth of the chemocline. Crystal length is associated to the depth of the supersaturated water column, i.e. the thickness of the chemocline, or supersaturated epilimnion from which endogen aragonite is forming (Last, 2001b). Aragonite crystals with ellipsoidal morphology, i.e. rice like crystals, with rounded edges, are most likely affected by partial dissolution during settling through the

undersaturated hypolimnion, different than acicular crystals, i.e. with pointed edges, which are more preserved (Last, 2001b).

The sedimentary control of Sr by aragonite concentrations (Figure 9.4); and the depletion of both, Ca, and Sr in the epilimnion during the carbonate precipitation (Viehberg et al., 2012), are strong indications for the epilimnetic origin of aragonite. Therefore the previous observations on aragonite crystals for Iznik sediments can be interpreted accordingly. Generally, the length of the aragonite needles decreases from the Pleistocene towards the Holocene (Table 9.1). Thus, indicating a progressively increasing supersaturation state of the epilimnetic waters. Moreover, the bigger crystals precipitating in Pleistocene are most likely originating from an epilimnion which is deeper, i.e. thicker, than in the Holocene.

The underlying assumption for these interpretations is that the aragonite crystals are not undergoing diagenetical growth. This is very reasonable, since as metastable carbonate phase, aragonite would rather dissolve completely or partially during early diagenesis, e.g. likewise calcite in undersaturated waters (Kelts and Hsü, 1978).

9.5.3) Aragonite concentration and lake level (water column depth)

Once there is understanding in the functioning of endogen carbonate precipitation, the fluctuations in quality, i.e. type and abundances of endogen carbonate phases can be associated with changes in past hydrological conditions, and have been brought together with relative changes in lake level, or groundwater inflows (Digerfeldt et al., 2000; Grimm et al., 2011; Tucker and Wright, 1992; Ülgen et al., 2012). For late Holocene Lake Iznik, a relationship was suggested between higher aragonite concentrations and lower lake levels, based on the insertion of the lake in a broad regional context (Ülgen et al., 2012). Thorough evaluation of the Lake Iznik geochemical and sedimentological data, especially in relation to changes in siliciclastic grain sizes, confirms this mode of endogen carbonate production for the Holocene. Moreover, it shows that the nature of the interaction between the endogen carbonate production and the variation in water column depth as inferred from grain size might change over time.

Considering the coarse silt/clay ratio as indicator for the depth of the water column for Lake Iznik – as outlined by a compositional model (section 7.3.2), a direct synchronic correlation is observed between the coarse silt/clay ratio, and the concentrations of the endogen aragonite, for the Holocene sedimentary units I and II (Figure 9.5). This correlation shows that lower lake levels (increase in the coarse grain size fraction) are coupled with an increase in

aragonite concentrations. It is astonishing how the magnitude of changes in the siliciclastic coarse silt/clay ratio, and amplitudes in aragonite concentrations, are the same within unit I (Figure 9.5). The pairing of these two independent lines of evidence is strongly pointing towards an evaporative trigger to the aragonite precipitation for the Holocene. Note that, this statement is not excluding that water supersaturation in relation to carbonate is biologically mediated.

The Pleistocene phase for which aragonite is absent or present in trace amounts (unit IV) is discussed in the section (9.5.4). Considering the Pleistocene sedimentary units for which aragonite is stable (III and V), interestingly, the correlation between the coarse silt/clay ratio and the aragonite concentrations seems to be inverse. And, for the Pleistocene, generally high lake levels are followed by increase in the aragonite concentrations (Figure 9.5). This is observed for the transition from unit IIIb towards unit IIIa (11 mcd), and also observed for the two cycles observed within unit V (~16.5 mcd and ~17.5 mcd).

The modern Lake Iznik precipitates endogen carbonate during the summer season, during periods of reduced or no rainfall associated to high temperatures (Viehberg et al., 2012). For the Holocene, relative drier climatic phases might drive a lowering in lake level (Ülgen et al., 2012), which will result in an accumulation of ions in the epilimnion. Consequently, higher degrees of supersaturation lead to pronounced precipitation of endogen carbonate phases during the summer, which are observed for the higher sedimentary aragonite concentrations during the lower lake levels. The increase in supersaturation during Holocene is also reflected by the reduced aragonite needle size for this epoch.

To better understand the long term change in the functioning of endogen carbonate production and its reaction to climatic forcing, further investigation is needed, e.g. using indicators which are sensitive to record the signal of epilimnion waters, and the distinct water sources from the catchment.

Still, for the purposes of this thesis, the obtained data clearly shows that aragonite is a sensitive indicator for changes in paleohydrology. Moreover, the climatic forcing of aragonite precipitation is of distinct nature for Holocene and Pleistocene. During the Holocene (11 to ca. 2 ka calBP), given an evaporative trigger, higher aragonite concentrations are directly related to lower lake levels, and hence relatively more dry periods. During the Pleistocene (31 to 11 kacalBP), increases in aragonite concentrations correlate to prior increased lake levels. This distinction further stresses the importance of independent evidence for interpretation of

paleo-endogen carbonate production, such as the generated herein (e.g. grain size versus mineralogy).

9.5.3.1) Further Observations

During the Holocene, one singular phase for the synchronous evolution of coarse silt/clay ratio and aragonite is the depth of 4.35 mcd, in which the increase in the coarse grain size component exceeds by far the amplitude of increase in aragonite concentrations. However, at the same depth, calcite concentrations are increasing concomitantly with aragonite, which is a unique situation for the sediment profile. The precise origin for calcite in this depth remains a matter of further investigation, and can possibly give an answer on the nature of the observed event. Preferential Ca removal from water due to carbonate precipitation might lead to higher Mg/Ca ratios. With increasing Mg/Ca ratio of water, higher degrees of supersaturation of the solution are needed to precipitate calcite along with the formerly precipitating aragonite (De Choudens-Sanchez and Gonzalez, 2009). Hence, if calcite at this depth is chemically precipitated, it supports that the observed event is one of extreme dryness, leading to a very shallow lake, as outlined by the highest inputs of coarser material. The age of this event is well defined by the almost synchronic deposition of the Vesuvius tephra (AP2), at nearly 3.5 ka cal BP.

9.5.4) Carbonate phase stability and lake mixing

The sediment profile IZN09/LC2&LC3 holds two extreme situations for aragonite deposition. On one hand, aragonite is virtually absent within unit IV, and on the other hand, aragonite concentrations are the highest within units II and IIIa. Both situations correspond to distinct limnological conditions, and are discussed in the sequence.

Lake Iznik passes through periods of prolonged bottom water anoxia, in the period delineated by sedimentary unit IV, i.e. prior and during the Last Gacial Maximum (section 8.4.2). Remarkably, the most prominent feature of reversal in the dominant carbonate phase occurs during the same interval, in direct association to the excursions of Mn abundances and Fe/Ti ratio (Figure 9.5).

For hardwater lakes which mix once a year, during the stratification the epilimnion is supersaturated in relation to the carbonate phase; while the hypolimnion becomes progressively undersaturated, as well as progressively enriched in Sr and Mg, given the partial dissolution of settling carbonate phase (Katz and Nishri, 2013).

Hence, it is reasonable to state that, the longer the bottom water remains chemically isolated from the upper water mass, the more pronounced the chemical gradient will develop, e.g. due to the mentioned enrichment in Sr and Mg, as well as the mobilization of reduced metal species in the anoxic bottom waters.

Unit IV holds a few preserved aragonite needles (chapter 4), indicating that aragonite is still the endogen carbonate precipitating from the epilimnion. Given the prolonged periods of lake stratification, most likely aragonite is being dissolved during settlement through a chemically distinct bottom water. Only few aragonite needles reach the sediment and get preserved. Since calcite accumulation is maintained for the same interval in which aragonite is being dissolved, the hypolimnion is most likely still supersaturated in respect to carbonates, with exception for the LGM, where complete carbonate dissolution takes place. Therefore, aragonite absence and calcite accumulation within unit IV is a direct consequence of the stable chemocline that is prevailing for longer time periods.

For units II and IIIa, the high aragonite concentrations are in correlation with the U/Ti ratio. The mobility of U in water is controlled in first order by its oxidation potential (Bonotto and Silveira, 2006). Uranium is soluble at relatively oxic conditions in the +6 oxidation state, as the ion uranyl (UO_2^{2+}), which in neutral to alkaline environments can form complexes with CO_3^{2-} (Bonotto and Silveira, 2006; Langmuir, 1978). Uranium can also form complexes with organic matter (Bonotto and Silveira, 2006). However, for units II and III Uranium is rather associated to the carbonate phase (section 6.3.1.2, Figure 6.2), as observed stratigraphically from unit IIIa (Figure 9.5). Given U mobilization in rather oxygenated milieu, most likely a good mixed water column is prevailing for units II and IIIa, which is also be expected according to the lower lake levels. Moreover, periodic lake mixing maintains low degrees of undersaturation for the hypolimnion. Therefore aragonite is preserved during settlement through the water column, and higher concentrations are accumulated in the sediments.

A periodically mixed lake does not exclude that the sediment-water interface develops anoxia, likewise the functioning of Lake Iznik today.

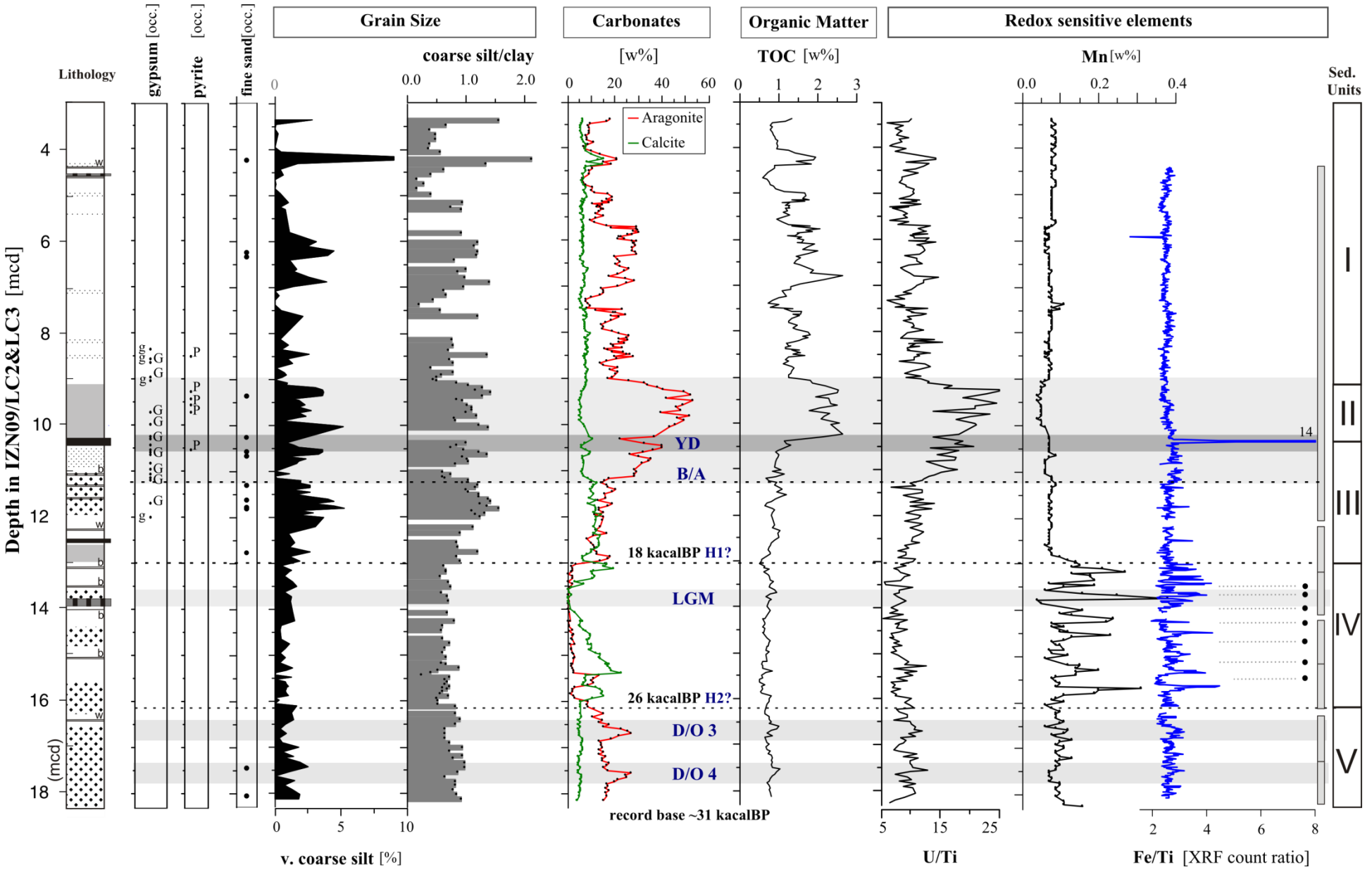

Figure 9.5: Aragonite and calcite [w%] in the profile IZN09/LC2&LC3 in relation to grain size composition, total organic carbon [w%], and redox sensitive elements uranium (U/Ti), manganese [w%] and iron (Fe/Ti). On the left column, gypsum and pyrite occurrences (capital letters indicate well crystalized phase, small letter indicate poor crystallization).

9.5.4.1) Periodicity of mixing

The geochemical behavior of Ca^{+2}, Sr^{+2}, and Mg^{+2}, for hardwater lakes was investigated in detail on the hardwater Lake Kinneret, during a full mixing-stratification cycle (Katz and Nishri, 2013). As these three elements participate in the cycling of endogen carbonate production, their concentrations in the water body clearly characterize chemical gradients within Lake Kinneret during the stratified season. Whereas, during the period (days) of annual lake mixing the homogeneity of the water column also shows a singular geochemical imprint (Katz and Nishri, 2013).

Herein, it is proposed to apply the findings for one full mixing-stratification season of Lake Kinneret (Katz and Nishri, 2013), to further interpret the data obtained for the Pleistocene profile of Lake Iznik. For this, similar plots of the ratios Mg/Ca and Sr/Ca are applied (Figure 9.6). During lake mixing periods the samples are expected to plot in one distinct area of the graphic. During stratified periods the geochemical gradient is characterized by the 'separation' of samples along a regression line (Katz and Nishri, 2013). The pattern of the stratified season is a result from the cation removal from epilimnion, due to carbonate precipitation, downwards transport in the water column, and partial carbonate dissolution in the hypolimnion (Katz and Nishri, 2013). Assuming that the calculated ratios for Lake Iznik Mg/Ca (M), and Sr/Ca (eq) retain information of past water chemistry preserved in the carbonate phase, their relative changes can be interpreted accordingly. The ratio Mg/Ca is calculated on a molar basis for the bulk sediment[22]. The Sr/Ca (eq) ratio for past Lake Iznik waters is calculated as discussed in section (9.4.1).

A first general and interesting conclusion is that, the pattern observed for Lake Kinneret water chemistry during one complete annual mixing-stratification cycle (Katz and Nishri, 2013), is reflected in analogy by the sedimentary Iznik carbonates for a millennial time scale (Figure 9.6). On one hand, unit IV which is subject to prolonged periods of stratification, has the highest gradient of concentrations between Sr/Ca and Mg/Ca (Figure 9.6 a), and on the other hand, unit II which has been inferred to be subject to recurrent mixing, presents smaller gradients between Sr/Ca and Mg/Ca (Figure 9.6 d). This analogy in an annual cycling pattern for the longer time frame under investigation is interpreted as follows.

[22] For Mg, calculation of distribution coefficients would be less meaningful with the available data, given that Mg is also retained in other sinks, e.g. clay minerals, for which stoichiometric approximations are not straightforward. Hence, the usage of the Mg/Ca ratio herein assumes that the differences in Mg accumulation due to changes in the carbonate phase are prevailing over other sinks.

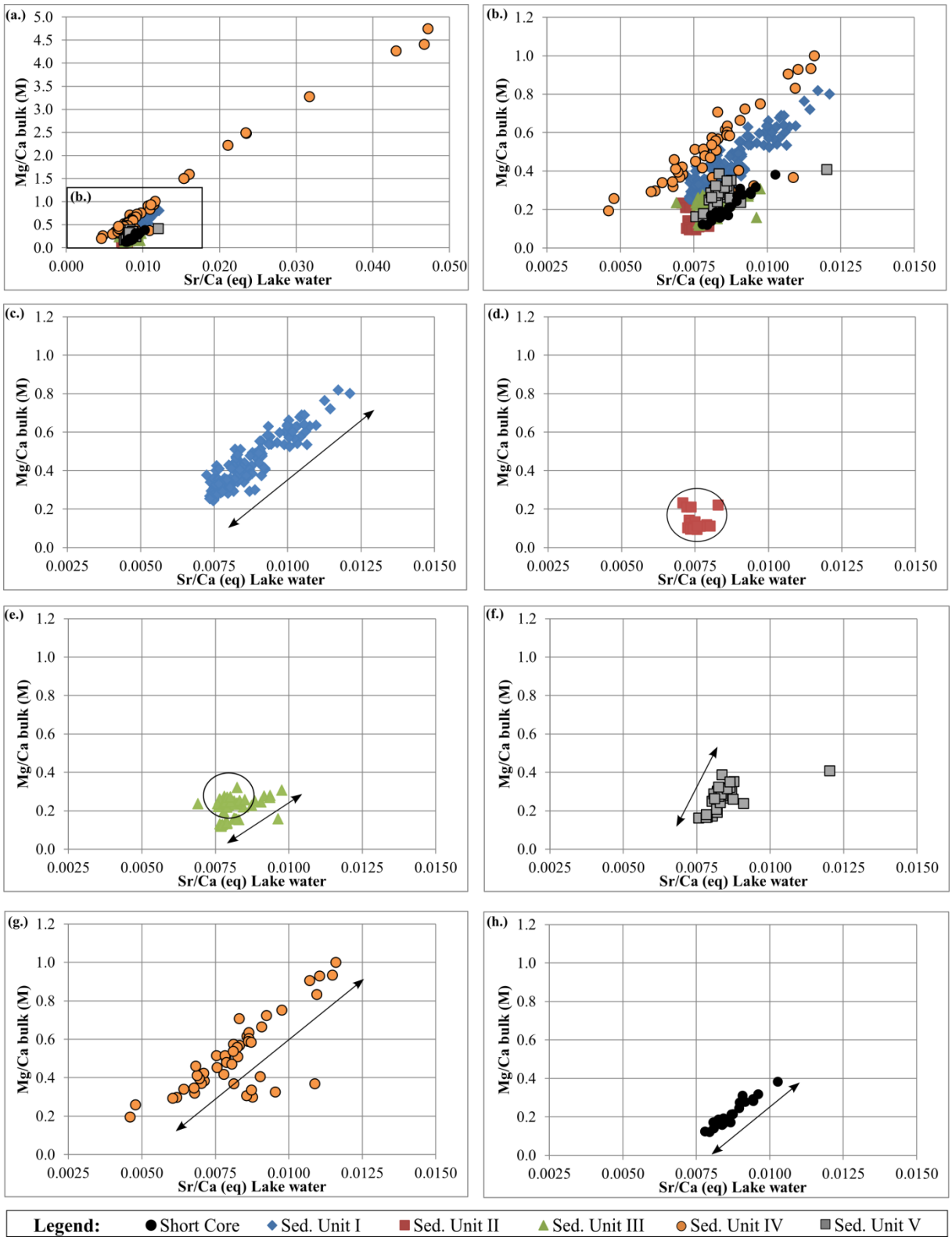

Figure 9.6: Relationship between the ratios Mg/Ca (M) for the bulk sediment, and the Sr/Ca (eq) for the water chemistry, as deduced from sedimentary bulk values, based on the Iznik specific distribution coefficient (discussion in section 9.4).

In the graphics Sr/Ca versus Mg/Ca for the sediment profile each sample represents a homogeneous geochemical signature of some decades. The precipitating aragonite is

recording the water chemistry from epilimnion. Since calcite behaves as a nearly constant background, for the sediment profile, aragonite is mainly controlling the relative changes in Ca concentrations for samples from units V, III, II, I and the short core.

During water column stratification, the hypolimnion gets progressively enriched in cations transported downwards due to the carbonate precipitation, which are partially dissolved. If the stratification season is persistent over longer time periods, the hypolimnion becomes more enriched, and the chemical gradient of the water column is higher, i.e. the gradient of enrichment is proportional to stratification time.

Whereas, the epilimnion continues to be replenished by surface water runoff, and new endogen carbonate precipitates. Once the lake undergoes complete mixing, the 'new' homogeneous lake water chemistry is the result of mixture from epilimnion waters with chemically distinct hypolimnion waters. When the new stratification sets on, the precipitating carbonates will carry the 'signal' from the mixture lake as a starting point, and the cycle restarts.

Therefore, on a long time frame, the hypolimnion works as a 'sink' of cations, and prolonged periods of stratification, could lead to concentration of ions in the lake as a whole - assuming that surface water replenishment is continuous. It is assumed that the geochemical gradient between epilimnion and hypolimnion waters is proportional to the duration of chemocline stability, i.e. to the periodicity of lake mixing.

The geochemical gradients from Figure 9.6 reflect the stability of the lake stratification, which can be interpreted as 'time', in the sense of periodicity of lake mixing.

Note that for the 'recurrent mixing' state, the pattern plots nearly at the same position (ca. Sr/Ca eq = 0.0075), and as the lake stratifies, the samples move upward right in the graphic. For instance, considering the short core to be reflecting the modern lake, it shows what would be the 'gradient' for one yearly lake turnover ($0.0075 < Sr/Ca < 0.01$). This interval is exactly the same for unit IIIb and somewhat smaller for unit V. Interestingly, the gradient for unit I is nearly the double of this value. Whereas units II and IIIa are phases of lower lake level and more intense mixing.

Also, it is interesting to note that for all units the slope of the linear relationship is similar, despite vertical offsets (Figure 9.6 b). Hence, for all units the same major processes are governing the distribution of Mg and Sr in relation to Ca. However, the vertical shifts in position of the line, indicate that either Mg or Sr concentrations are prevailing.

10.) Paleoenvironmental reconstruction for Lake Iznik during the Late Pleistocene and Holocene and regional context

This chapter aims to reconstruct the environmental setting for Lake Iznik during the time interval until circa 31.5 ka cal BP. The reconstruction (a) concerns the history of the lake (section 10.1) according to the geochemical and sedimentological evidence extensively discussed within this thesis, and (b) places Lake's Iznik history in the paleoclimate context. Focus is given on climate variability over a millennial time scale, and the relation between Lake Iznik and geographically adjacent regions, e.g. Aegean region, Pontic Coast, southern Balkans and Anatolian Plateau; as well as northern Hemispheric connections.

Firstly, the reconstructed time interval is divided into the timing of corresponding sedimentary units. Notably, the boundaries of the defined sedimentary units coincide with either the timing of (a) the transition between Marine Isotope Stages, or (b) distinct millennial scale climatic events, thus reinforcing that for Lake Iznik, the lithology – the most basic sediment characterization –reacts sensitively to climatic forcing.

10.1) Lake evolution

From the evidence documented within this thesis, specific proxies are selected to reconstruct the history of Late Pleistocene to Holocene Lake Iznik. These are summarized within Figure 10.1, and provide a set of independently generated sedimentological, geochemical and mineralogical evidence for the evolution of the lake.

Grain size information of the siliciclastic fraction is interpreted in relation to lake level changes according to a compositional model (chapter 7), which is calibrated with the present day surface sedimentation. Interpretation for organic productivity for the lake-catchment ecosystem is provided by the combined information of total nitrogen (N), total organic carbon (TOC), the atomic ratio TOC/N (chapter 8), the mineralogical index of alteration (MIA) (chapter 6), and the parameter that approximates amorphous silica (ASi), as calculated from distinctly treated grain size measurements (chapter 7). Oxic/anoxic conditions of the bottom water are inferred from manganese concentrations (chapter 8), and the association to changes in carbonate accumulation allows interpretation on the status of lake mixing.

The endogen carbonate production within Lake Iznik is mainly aragonite (Figure 10.1), and despite early diagenetical changes during and prior the LGM, the carbonate accumulation

proves to be the most climatic sensitive indicator in the Iznik sediment profile. The factors affecting the carbonate accumulation are depicted in relation to lake internal processes and climatic forcing in the following sections.

A summarizing view on Lake Iznik evolution is given in Figure 10.2. Grain size ratio coarse silt/clay, aragonite concentrations and manganese concentrations are depicted, along with the main inferred tendencies of variations in the water column depth, i.e. changes in lake level. Given an average sedimentation rate of 1 $mm.yr^{-1}$, the smoothed curves correspond to an average of 500 years, thus millennial variability in the data is highlighted.

10.1.1) Unit V - from ~ 31.5 to ~ 27 ka cal BP

The time period for deposition of Unit V corresponds to the end of MIS 3. Low aquatic bio-productivity of Lake Iznik yields very low values of nitrogen and total organic carbon (TOC). Also relative low amorphous silica (ASi) are in agreement with the independently measured TOC content (Figure 10.1), indicating (a) low aquatic bio-productivity, as well as (b) reduced delivery of Si from the catchment, as a result of low chemical weathering rates. The low load of terrestrial organic material, additionally indicated by small TOC/N values, results from the scarce vegetation cover in the catchment. Small TOC/N also indicates enhanced metabolization of organic matter, and sulfate reduction is occurring as shown by abundant monosulfides.

The precipitation of iron monosulfides in the aquatic early diagenetical milieu results from available H_2S and Fe, and indicates that the lake bottom passed through phases of anoxia. Through comparison to the modern lake, it can be inferred that these phases must lasted longer than today. The present lake bottom becomes annually anoxic; however there is nearly no accumulation of monosulfides in the sediments, despite sulfur availability.

At the end of MIS 3, the detrital load is high, but the sedimentation rates at this time are very low. Thus, the high percentages of detritus are also consequence of low carbonate accumulation. The relative fine grain size suggests a low energy deposition environment, and consequently a deeper water column for the lake.

In a lake with low organic production, the sediments and minerals delivered to the lake settle through a ‘thicker’ oxygenated upper water column, as consequence higher load of Fe oxides reach the deep parts of the lake, where they go into solution in the bottom anoxic waters. Also the profile of Mn concentrations points towards the same processes, due to its similar geochemical behavior to Fe. The Mn concentrations are slightly enriched at the end of MIS 3

in relation to the Holocene (Figure 10.1). The relative bigger size of aragonite crystals indicates a ‘thicker’ epilimnion with possibly lower supersaturation (section 9.5.2).

10.1.2) Unit IV - from ~ 27 to ~ 18 ka cal BP

For the period prior and during the Last Glacial Maximum (LGM) the indicators of lake and catchment productivity are still low, likewise at the end of MIS 3. Very low values for the sedimentary bulk TOC/N ratio indicate that nearly no organic matter is being delivered from the catchment, and/or organic matter decomposition is enhanced (Figure 10.1). The overall detrital load is maintained constant in the form of a clayey matrix, accumulating in low sedimentation rates. The grain size ratio coarse silt/clay has the most homogenous and lowest observed values of the profile, and likewise MIS 3 indicates that sediment deposition at the water sediment interface is occurring in a low energy milieu.

Shell fragments are present during this complete time span, and their size diminishes with time (shell size fining upwards, section 4.1.4). This observation leads to the inference that the shells are continuously reworked at coastal regions by wave activity, and the lake level is maintained fairly constant throughout this time period. The reworking of the shells, points towards high energy coastal environment, in agreement with observations of sedimentary beach rocks environment (Erginal et al., 2012b). A high energy coastal millieu, in synchrony with low energy deposition in the middle lake, are potentially explained by a deep water column.

Lake Iznik catchment holds evidence for several past high lake level stands or transgressions (Ikeda et al., 1991a), e.g. wave cut scarps in the northern margins of the lake (Figure 1.1). A mollusc deposit occurs in association with the lowermost wave cut scarp, which is inferred to have been formed during the last high lake level stand (Ikeda et al., 1991).

During this time interval drastic changes are observed in the accumulation of elements mobile under anoxic conditions, herein represented by Mn. Also the carbonate accumulation within this time period is unique, given that aragonite is nearly completely absent (Figure 10.1). Such changes are related to a response of geochemically ‘independent’ carbonate accumulation and redox cycling, to the same process affecting the limnological milieu.

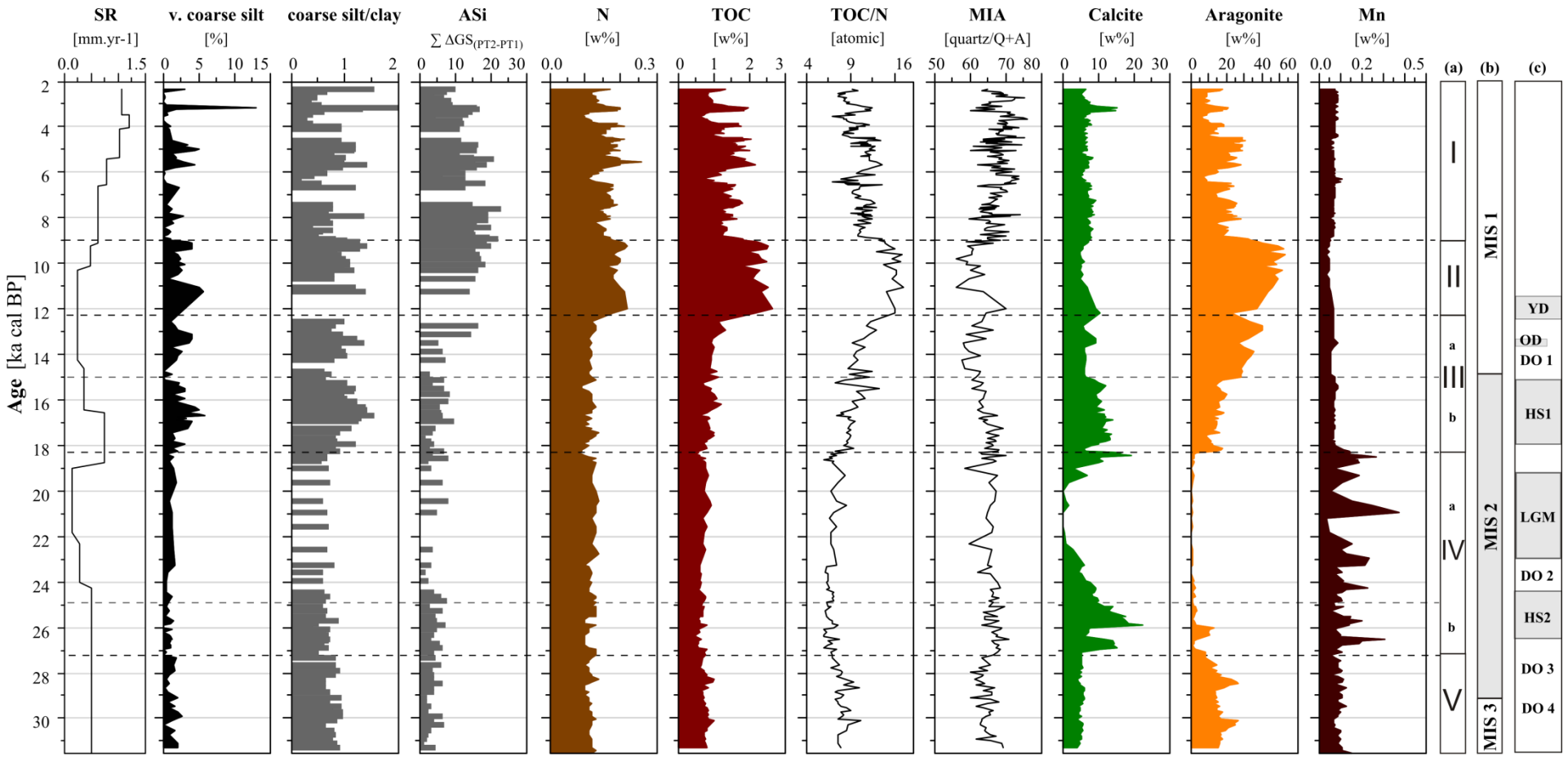

Figure 10.1: Selected parameters for mineralogy, geochemistry and sedimentology of Lake Iznik history, plotted to time: Sedimentation rate (SR) [mm.yr^{-1}], very coarse silt [%], coarse silt/clay ratio, amorphous silica, ASi [$\sum\Delta GS_{(PT2\text{-}PT1)}$], (which contains also the biogenic fraction) details in section 7.2.1, nitrogen [w%], total organic carbon [w%], TOC/N [atomic ratio], mineralogical index of alteration (MIA) as [quartz/(quartz + albite)] details in section 6.5.2, calcite [w%], aragonite [w%], manganese [w%]. Columns on the right label (a) the sedimentary units and subunits for the profile, (b) chronological limits of the corresponding Marine Isotope Stages after (Sanchez-Goni and Harrison, 2010) and (c) millennial scale climate event-stratigraphy. Timing of Younger Dryas (YD) and Older Dryas (OD) after (Brauer et al., 1999; Litt et al., 2001); timing of Heinrich Stadials (HS) after (Sanchez-Goni and Harrison, 2010); timing of Last Glacial Maximum after (Tzedakis, 2007); timing of Dansgaard-Oeschger (DO) interstadials after (Wolff et al., 2010). Gray shadows on right hand columns indicate relative cold phases over the Northern Hemisphere.

The accumulation of Fe and Mn – as it cannot be explained by the homogeneous grain size or by the relatively constant minerogenic matter – is related to mobilization of these elements under prolonged anoxic conditions. Geochemical analysis of the fraction <63 µm, confirms that these elements are concentrated in the fine sediment fraction (section 8.3.2).

The presence of few aragonite crystals indicates this carbonate phase continues precipitating in the epilimnion. Its near absence in the sediments is interpreted as aragonite dissolution in the lower body mass, pointing towards changes in the carbonate equilibrium within the water column, e.g. undersaturation, and/or increase in the pH, due to accumulation of CO_2 from metabolization of organic matter under anaerobic conditions. Compositional data analysis shows that calcite for this time period has very high variability, i.e. low correlation to quartz – and it is interpreted to be early diagenetical or endogen. Mineralogical analysis of the size fraction <63 µm shows that the carbonate phases are contained in the clay-silt matrix (section 6.4.2, Figure 6.7).

Hence, it is suggested that the mixing of Lake Iznik is confined to the upper water column for extended periods of time originating a stagnant bottom water layer which develops unique chemistry (Figure 10.3).

Such a change in lake mixis is responsible for the enhanced reservoir effect observed for sedimentary unit IV (section 5.2.1), which results from the vertical isolation of the lower water column, that leads to disequilibrium of the radiocarbon with the atmosphere (Stein et al., 2004). Moreover, as the sinking aragonite crystals become unstable in the chemical distinct bottom water, the dissolution of carbonates further increases concentrations of dissolved inorganic carbon, potentially contributing to a hard water effect.

Thus, the established chemically stratified stagnant bottom water acts as a sink for the trace elements liberated by the dissolving carbonates, as well as for elements mobile under anoxic conditions. A further consequence of the establishment of such a bottom water layer is that anaerobic metabolization of organic matter is enhanced, e.g. via sulfate reduction, and/or iron and manganese reduction. Despite the precipitation of monosulfides, the sulfur concentrations in the Pleistocene are relative low, which results of a reduced organic load, as well as a more dilute water body, as soon as complete mixing occurs.

The changes of Lake Iznik mixing intensity are potentially related to two independent or coupled processes. (1) For temperatures near to 4^{o}C, chemical stratification affects the vertical mixing of freshwater lakes (Imboden and Wüest, 1995; Wetzel, 2001). (2) An increase in lake

level suppresses deep water renewal in closed lakes where stratification is controlled by salinity gradients, e.g. Caspian Sea (Peeters et al., 2000), or Lake Van (Kaden et al., 2010).

In other words, for the period between 27 ka cal BP and 18 ka cal BP, the vertical density stratification of the Lake Iznik seems to be controlled by salinity, triggered either by (1) colder temperatures during this entire time span, and/or (2) increase in lake level, given the fulfillment the system is closed.

The generated evidence sustains the pairing of both processes as, alongside to the inferred deep water column, dropstones are deposited within the clay matrix indicating the occurrence of at least partial ice cover, e.g. in the deltaic regions.

The subdivision of unit IV at circa 25 ka cal BP is related to the timing of the LGM, when the changes in mixing intensity become more pronounced. The LGM is marked by the complete absence of carbonates, due to early diagenetical changes at that time. Also the anoxia becomes more pronounced during this phase, whereas Fe and Mn are slightly enriched in the sediment fraction <63 µm.

The end of the LGM is marked by an abrupt increase of sedimentary mass accumulation, i.e. sedimentation rates, in Lake Iznik (Figure 10.1). Also magnetic susceptibility reflects an increase in detrital input at this time resulting from input of sediment material that had accumulated in the catchment during glacial times, and the still low vegetation cover during the post glacial.

10.1.3) Unit III - from ~ 18 to ~ 12 ka cal BP

After the LGM, the increase in carbonate deposition starts gradually as calcite, when at circa 18 ka cal BP the dominant mineral carbonate phase inverts promptly to aragonite, at first for a short period of centennial time scale (ca. 200 years), followed by an again short period of calcite dominance (Figure 10.1). From ~ 18 to circa ~ 15 ka cal BP, calcite and aragonite maintain concentrations around 15%. Aragonite concentrations are similar to the ‘background’ values observed for the end of MIS 3. Calcite concentrations are slightly higher than for the interval from ~ 15 to ~ 12 ka cal BP. Calcite is interpreted to be related either to an enhanced detrital input, or to have an additional endogen origin. A significant shift of aragonite towards higher concentrations happens at circa 14.7 ka cal BP, coinciding with the subdivision of unit III (chapter 6). Notably this is the transition from MIS 2 towards MIS 1 (Figure 10.1, Figure 10.2).

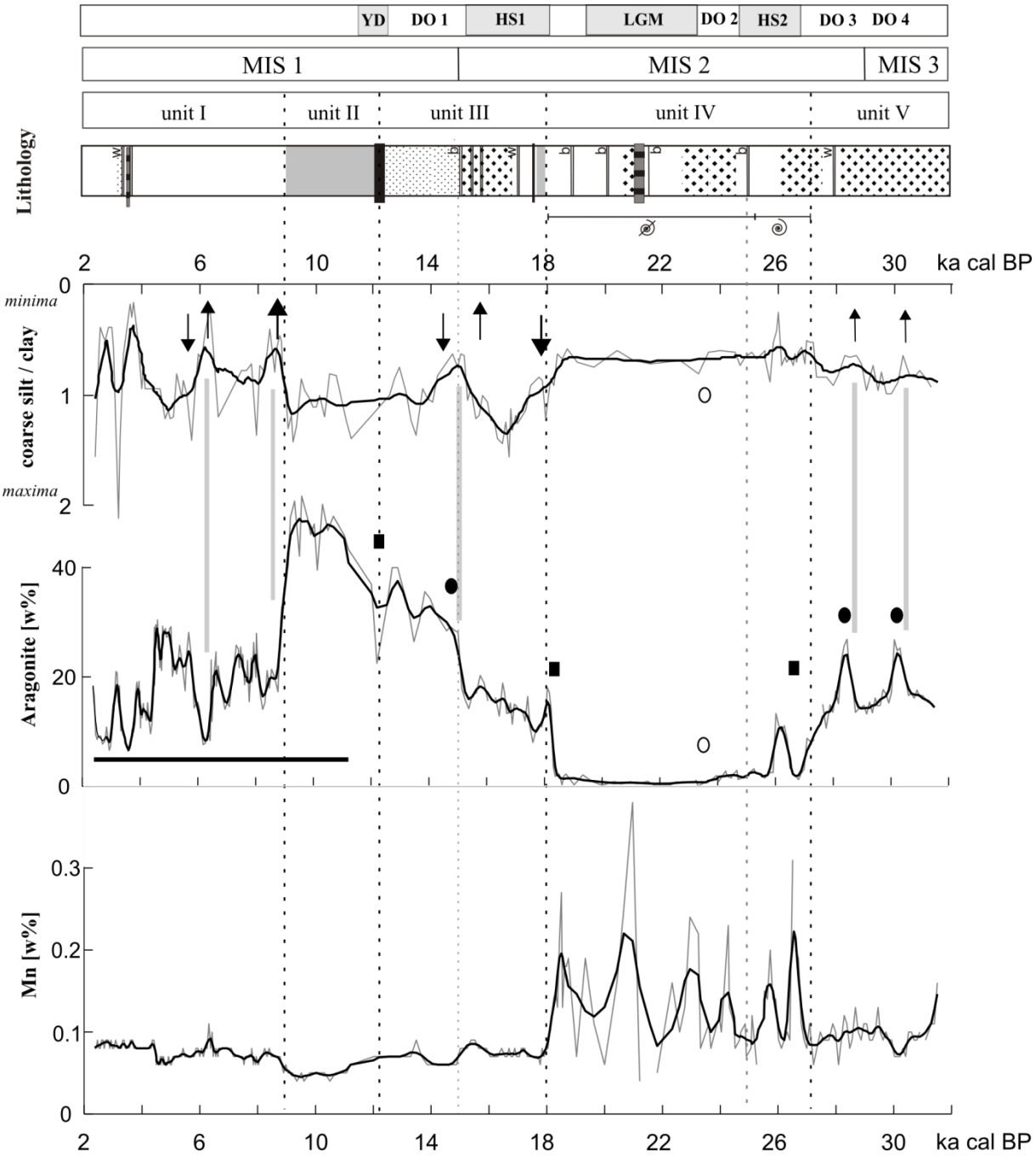

Figure 10.2: Lake Iznik lithology within a time scale, alongside with grain size ratio coarse silt/clay, aragonite concentrations and Mn concentrations. Arrows indicate inferred lake level tendencies and are discussed in section 10.1. Further symbols mark event-stratigraphy discussed in section 10.2. Black circles indicate correlation to interstadials. Black squares indicate correlation to stadials. White circle indicates expected interstadial. Black bar outlines the Holocene epoch. Gray data curves delineate measured data in 5 cm resolution (or higher for selected intervals). Black curves averages to millennial scale variability: (a) for Aragonite and Mn concentrations in a six point running average; (b) for coarse silt/clay ratio in a ten point running average to account for high Holocene variability and high sedimentation rates.

Mass accumulation rates are high during the deglaciation, until the onset of MIS 1, when they become again reduced (Figure 10.1). With the onset of MIS 1, an increase in ASi and TOC/N atomic ratio indicates enhanced weathering and organic load from the catchment; however,

sedimentary preservation of organic matter is still very low (Figure 10.1). Grain size ratio coarse silt/clay is highly fluctuating in the timeframe between 18 to 12 ka cal BP pointing towards a dynamic lake level history.

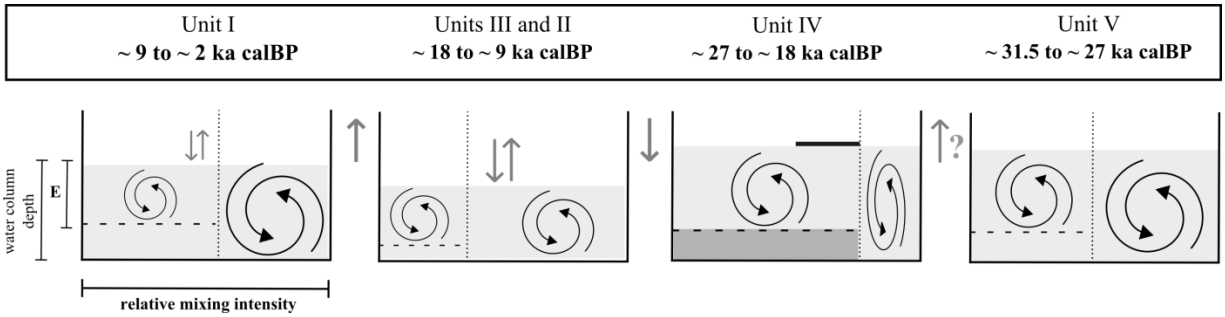

Figure 10.3: Model for Lake Iznik in terms of water column depth, epilimnion thickness (E) and lake mixing for the different sedimentary units. Changes in mixing intensity and stratified periods are indicated by the position of the vertical dotted line. Gray arrows indicate inferred lake level tendencies. Within unit IV, chemical stagnated bottom water is highlighted in dark gray, and possible ice cover is indicated by black bar.

The onset of aragonite accumulation at ~18 ka cal BP happens abruptly, subsequent to the abrupt depletion of Mn accumulation, both indicating the geochemical response to the reestablishment of a complete mixing of the water column within shorter periods of time (Figure 10.3). Such scenario is accompanied by a reduce in lake level, which starts at ~18 ka cal BP (Figure 10.2). Despite a regular lake overturn, the anoxic stages are still marked by monosulfide precipitation, and at ~17.5 ka cal BP during a stagnant phase of water column depth and mixing a fine FeS layer is precipitated.

From ~ 16.5 towards ~ 14.7 ka cal BP a lake level increase follows, as outlined by grain size (Figure 10.2). During the deepening of the water column, sulfate reduction is a prominent process of metabolization of organic matter, as monosulfides precipitate as black bands. However, the anoxic stages do not last long enough to develop distinct water chemistry in the bottom water layer, as aragonite is preserved in the sediments.

The described period of lake level lowering between ~ 18 and ~ 16.5 ka cal BP, followed by an increase during ~ 16.5 towards ~ 14.7 ka cal BP, is supported also by different geochemical indicators previously discussed in this thesis, e.g. sulfur values. The lake level lowering is associated to an increase in sulfur values (Figure 8.6, page 108), possibly pointing towards an increase in salinity of a closed system? Alternatively, the shrinking water column potentially triggers an increase of trophic conditions, due to an increase in nutrient concentrations.

After ~14.7 towards ~12 ka cal BP, with the onset of MIS 1, abrupt increase in aragonite concentrations, slight reduce in Mn accumulation, and relative coarser grain size, indicate a

general scenario of a lowering in lake level and periodic mixing of the complete water column (Figure 10.2, Figure 10.3). Sulfate reduction is still taking place however the size of precipitated monosulfides diminishes considerably. Catchment detrital load and sedimentation rates are low, and reflect establishment of vegetation in the catchment. Availability of silicic acid shows that chemical weathering becomes pronounced after the onset of MIS 1. Geochemically, this subunit of unit III behaves likewise unit II, as has been shown from different perspectives, e.g. mixing conditions according to Sr/Ca and Mg/Ca (Figure 9.6, page 135). Such a geochemical correspondence shows that after the onset of MIS 1, the limnological system enters a different functioning, triggered by climatic conditions.

10.1.4) Unit II - from ~ 12 to ~ 9 ka cal BP

At the onset of the Holocene, mass accumulation rates within Lake Iznik are still very low. The dynamic lake level fluctuations lead to instabilities of marginal slopes and turbidite deposition reached the central portions of the lake sporadically. The transition from unit III towards unit II, at ~ 12 ka cal BP, is marked by the precipitation of a prominent iron monosulfide layer. Iron and sulfur were remobilized in the sediment (under anoxic conditions) towards a previously deposited sandy layer which corresponds to a distal deposition of a turbidite (section 7.3.3). Such a geochemical remobilization is also a result of the sharp gradient in total organic carbon concentrations, and possibly a period of lake mixing stagnation at the beginning of the Holocene.

Between ~12 and ~ 9 ka cal BP, grain size shows that the deposited siliciclastic material is relatively coarse, indicating a shallower water column, whereas endogen carbonate accumulation in Lake Iznik represents at least 50% of total mineralogy. Aragonite crystal size indicates a ‘small’ epilimnion, and high supersaturation in relation to carbonates. This scenario is inserted in a time of early Holocene maximum in summer insolation, thus a more pronounced thermal lake stratification is expected during the summer. Still, complete lake mixing occurs periodically, as indicated by several lines of evidence. For instance, Mn does not accumulate aside with the prominent FeS layer at ~ 12 ka cal BP. Also the ratios Sr/Ca of lake water and Mg/Ca of the sediments, are homogenous (chapter 9), reflecting a rather homogen chemistry of the complete water column.

The TOC/N ratio indicates the highest load of terrestric organic matter for this time frame, in consistency with the shallow water column and previous expansion of vegetation (Figure 10.1). The organic load from the Iznik catchment has direct influences on primary aquatic

productivity, as outlined by high ASi content and abundant diatoms. The sedimentary preservation of organic matter starts abruptly, after the deposition of the FeS layer. Following the increase in ASi, which starts already at ~13 ka cal BP. But, as outlined by the TOC/N ratio and ASi values, the increase in terrestric organic load was rather slow, and an increase in lake trophic conditions is inferred to have followed this gradual pattern. Therefore, the observed sharp gradient in TOC is most likely resulting from a rapid change in the early diagenetical metabolization routes of organic matter, resulting from changes in the lakes' mixing dynamics.

10.1.5) Unit I - from ~ 9 to ~ 2 ka cal BP

Sedimentation rates increase from 9 ka cal BP towards the middle Holocene, indicating a general higher load of sediments which is partially attributed to the higher organic load in the postglacial, and also results from an increased input of detrital material from the catchment. The grain size ratio coarse silt/clay expresses highly dynamic variability; whereas the overall tendency in the middle Holocene is towards finer grain size deposition between 9 and 6 ka cal BP and relatively coarser siliciclastic material from 6 towards 2 ka cal BP (Figure 10.1).

In comparison to the early Holocene unit II, the organic indicators show that aquatic productivity is enhanced from 9 towards 2 ka cal BP, as reflected by the TOC/N values. Generally, the indicators of lake productivity and endogen carbonate production fluctuate in synchrony for this time interval, mainly in response to changes in the water column depth, i.e. in parallel variation to the grain size ratio coarse silt/clay.

Smaller aragonite crystals point towards a relative high supersaturation state of the epilimnion. Additionally, (a) an increase in Mg accumulation, (b) the maintained high ASi, and (c) a increase of kaolinite accumulation in the expense of albite, are all evidencing an increase of ionic load to the lake, as a result of increased weathering rates, i.e. higher temperature and humidity. This is consistent with the highest values for the mineralogical index of alteration (MIA) (Figure 10.1) which shows relative high sediment maturity – despite the constraints in the interpretation of this index for the prior time frames (for discussion see section 6.5.2).

Given this overall scenario for the postglacial, particular time frames deserve special attention. The most prominent feature during the early Holocene is a slow increase in lake level, starting at circa 9.5 ka cal BP and lasting towards circa 9 ka cal BP, which was first

described on the basis of changes in the Ca/Ti ratio (Roeser et al., 2012). This increase in lake level is synchronously indicated by several further lines of evidence.

Lake Iznik endogen carbonate accumulation, i.e. aragonite, is marked by a sharp retreat at this time, resulting from a gradual dilution in ionic concentrations. This is accompanied by a parallel decrease in depositing grain size, i.e. decrease of the ratio coarse silt/clay, as well as diminishing terrestrial organic load, as shown by the lowering of the TOC/N ratio. These observations are consistent with a deepening of the water column. During the 500 years of lake level increase, also TOC and N values retreat, resulting from the dilution of nutrient concentration in the deepening water column.

The amplitude of the lake level increase during 9 and 9.5 ka cal BP is best explained by the magnitude of changes of the grain size ratio coarse silt/clay, or the ratio TOC/N, which are similar since both result from physical processes related to the distance of the sampling point towards the shore. The sharp retreat in aragonite concentrations is resulting from a reduce in geochemical processes, and the apparent abrupt nature of the retreat is related to its (bio)geochemical triggering.

A further lowering in aragonite production potentially associated to an increase in lake level occurs at circa 6.5 ka cal BP, when aragonite has concentrations of circa 10% of the mineralogical assemblage (Figure 10.2). At this time, grain size deposition is fine, and Mn abundances slightly increase, indicating that potentially the bottom water renovation is again affected by surface freshwater inputs. Afterwards, from 6.5 towards 5.5 ka cal BP, the synchrony between grain size, carbonate accumulation and organic production, continues indicating a response to the same processes, and water column is slowly becoming shallower (Figure 10.2).

Starting at circa 5.5 towards 2 ka cal BP, an increase in mass accumulation takes place. Sedimentation rates are up to one third higher than those observed during the deglaciation (Figure 10.1). Moreover, a change takes place regarding the proportions of very coarse silt percentages in relation to the ratio coarse silt/clay. Generally, for the Iznik sediment profile a coarse silt/clay ratio of about 1.5 would correspond to circa 5% of very coarse silt. However, at 5 ka cal BP, the percentages of very coarse silt reach 5% for a ratio of circa 1, and at 3 ka cal BP, the percentages of very coarse material are considerably higher than expected in relation to the earlier profile.

10.2) Paleoclimatic and regional context

Long term global climate patterns, delineate alternation of glacial and interglacial cycles, in response to orbital forcing, i.e. the Milankovitch cycles. Such cycles of orbital time scale (precession, 23 ka), or Marine Isotope Stages (MIS), are for example recorded by $\delta^{18}O$ in benthic marine foraminifera (Lisiecki and Raymo, 2005). Superimposed on these long term fluctuations, the last glacial cycle (comprising MIS 4, MIS 3 and MIS 2) is marked by climatic variability of sub-orbital scale, the Dansgaard-Oeschger (DO) oscillations, with hemispheric extent (Dansgaard et al., 1993; Johnsen et al., 1992; Martinson et al., 1987; Sanchez-Goni et al., 2008; Voelker, 2002). The interstadial phases of the DO fluctuations are associated to recurring episodes of relatively mild climate conditions for the Northern Hemisphere, i.e. increase in temperature, which are known from the northern ice core records as Greenland Interstadials (GI's), related to inflow of melting ice, i.e. fresh water into the North Atlantic, affecting oceanic thermohaline circulation (Voelker, 2002; Wolff et al., 2010).

The counterparts of such warm phases in the Northern Hemisphere – also in a millennial time scale – are the Heinrich Stadials (HS). During Heinrich stadials, the air surface cooling in the northern Hemisphere, is accompanied by massive iceberg discharge to the North Atlantic (Broecker, 2003; Liu et al., 2009), hence the associated Heinrich event layers (HE) deposited in the North Atlantic, result from northeast Atlantic major ice raftings (Heinrich, 1988; Hemming, 2004; Sanchez-Goni and Harrison, 2010). These events were first described through changes in foraminifera assemblages which are best represented by abrupt increase in *N. pachiderma* (s) concentration (Heinrich, 1988). For each Heinrich stadial there is a deposition of an Heinrich event layer (HE), either during its entire time span, or at the end of the HS (Sanchez-Goni and Harrison, 2010). The HS can be correlated to minimum values in the stable oxygen isotope composition from Greenland sheet ice cores during the last 75 ka (Bradley, 1999).

During the Pleistocene to Holocene transition, i.e. during the last deglaciation, a striking feature in climatic event-stratigraphy for the Northern Hemisphere is the pattern of cold Heinrich Stadial 1, followed by warm Dansgaard-Oeschger 1.

The modeled surface air temperature for Heinrich Stadial 1 (HS1), exhibits a bipolar seesaw, with a cooling pattern for the North Atlantic, that reached the east Mediterranean (Liu et al., 2009). Following the HS1, the Dansgaard-Oeschger event 1 (at ~ 15 kaBP), which is equivalent to the European Meiendorf/Bølling/Allerød (B/A) complex (Litt, 2007), had a global warming effect with a maximum warming relative to HS1 exceeding 20^{o}C in the North

Atlantic (Liu et al., 2009; Timmermann and Menviel, 2009). DO1 event was triggered by changes in the North Atlantic realm (Severinghaus and Brook, 1999), and simulations using a coupled atmosphere-ocean circulation model, suggest that the resulting enhanced warming, is a superimposition of climate response to increased atmospheric greenhouse gases, and recovery of the Atlantic Meridional Overturning circulation after the end of HS1 (Liu et al., 2009; Timmermann and Menviel, 2009).

The millennial scale stadials and interstadials as observed from the Northern Hemisphere ice core and oceanic records, are also expressed in the Eastern Mediterranean geological record. For example, Heinrich stadials were associated to aridity over the Levant, expressed by retreats in the lake levels of Pleistocene Lake Lisan (Stein et al., 2010; Torfstein et al., 2013), and reduced rainfall in the western Pontic Coast (Kwiecien et al., 2009). The climate trigger mechanisms are related to abrupt cooling of Eastern Mediterranean atmosphere and sea surface temperatures, expected to lead to reduced cyclogenesis, which is one of the main humidity sources for the region (Kwiecien et al., 2009; Torfstein et al., 2013).

The onset of the Holocene, at 11.7 ka BP, happens after the end of a further cooling phase of the Northern Hemisphere (Walker et al., 2009): the Younger Dryas (YD) event, which triggered by a massive inflow of freshwater into the northern Atlantic, weakening the formation of north Atlantic deep water (Broecker, 2003). The YD event lasted circa one millennia and presents a slightly reduced time for an eastward gradient. For example it lasted circa 1300 years over Greenland (Mayewski et al., 1993), and at maximum 1150 years over Europe (Brauer et al., 1999; Litt et al., 2001), whereas the duration of the YD in Eastern Anatolia is of circa 1100 years (Litt et al., 2009). The transition from the YD towards the Holocene is inferred to have occurred in a decadal period, of circa 40 years over Greenland (Taylor et al., 1997), and 10 to 50 years in Eastern Anatolia (Litt et al., 2009; Wick et al., 2003)). The transition from YD towards milder Holocene is generally marked by reduce in wind speeds, increase in rainfall and increase in temperatures throughout the Northern Hemisphere (Mayewski et al., 1993; Taylor et al., 1997).

During the Holocene, millennial to centennial scale relative cold phases – also related to freshwater inputs in the North Atlantic – are associated to changes in solar forcing, and potentially transmitted to other regions, e.g. inferred hydroclimatic changes in northern Anatolia and the northern Red Sea (Bond et al., 2001; Lamy et al., 2006). However the trigger mechanisms for such Holocene cycles are of complex nature, and remain in debate (Wanner and Butikofer, 2008).

10.2.1) Late Pleistocene

Overall, Lake Iznik carbonate accumulation and the coarse silt/clay ratio can be clearly correlated to the existing regional geological record (Figure 10.4, Figure 10.5). The well-established oxygen isotope record from the NGRIP Greenland ice core expresses changes in atmospheric temperature over Greenland and the Northern Hemisphere (e.g. Wolff et al., 2010). The region of Sofular cave receives humidity from the Black Sea, which is expressed along with changes in the ecosystem productivity by determined $\delta^{13}C$ from the speleothem record (Fleitmann et al., 2009). For the sediments depositing within the Black Sea, at the Pontic Coast margins, the carbonate accumulation during MIS 2 is mainly detrital and indicates the rainfall on the catchments in the borderlands, e.g. the detrital load originated from the Sakarya river basin (Kwiecien et al., 2009), which is adjacent to the Iznik basin (Figure 10.4). After the onset of MIS 1, carbonate production in the Black Sea is activated (Shumilovskikh et al., 2012).

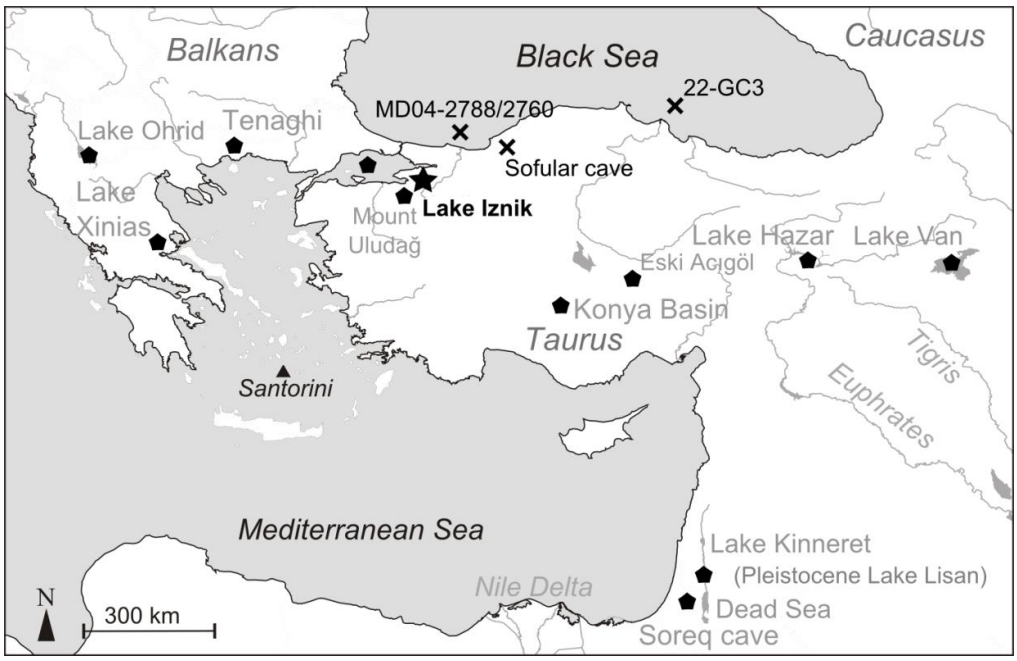

Figure 10.4: Lake Iznik (black star) inserted in the regional context and correlated to the geological record. (a) sites marked with black 'x': correlation undertaken to a direct age scale, for data see Figure 10.5; and (b) sites marked with black polygon: inserted in the according time frame within regional discussion.

From the good correspondence between long term changes in aragonite concentrations within Lake Iznik and the summer insolation curve (Figure 10.5), it is inferred that long term changes in endogen aragonite production are closely related to atmospheric temperature. Additionally, from the previous correlation between aragonite and grain size changes, it is

inferred that aragonite variations are superimposed by relative short term changes in the hydrologic balance, especially during the Holocene.

Main warm and cold phases expected for event-stratigraphy for the past 31.5 ka cal BP are marked within Figure 10.2, as circles and squares, respectively. Black circles mark the Dansgaard-Oeschger interstadial phases as correlated to the Sofular and NGRIP records (Figure 10.5). Black squares mark correlation to the Heinrich stadials and the Younger Dryas event. Each of these groups of events, i.e. interstadials and stadials, has a distinct pattern within the Iznik record, and are discussed in the next sub-sections.

A correlation between the Lake Iznik event-stratigraphy as constructed from aragonite concentrations with the Sofular cave $\delta^{13}C$ record shows that for the interval between 25 and 31 ka cal BP there is an offset of maximum 1,500 years. This issue is limited to the lowermost core, resulting from a generally higher reservoir effect for radiocarbon datings due the bottom water stagnation. From the LGM upwards the age depth model of the Iznik record is solidly established, on the basis of tephrocronology and radiocarbon determinations (also on terrestric plant material, details in chapter 5).

Regarding the orbital time scale, generally the late Pleistocene is outlined by a decrease in temperatures and an increase in aridity over Anatolia (Akçar and Schlüchter, 2005; Tzedakis, 2007). The time period between MIS 4 and MIS 2 is a relative drier phase, presenting cold and stable conditions from the southern Balkans towards the Aegean and Anatolia, with prevalence of steppe biome, low plant density and low microbial soil activity (Fleitmann et al., 2009; Müller et al., 2011; Wagner et al., 2009). Accordingly, Lake Iznik shows low bio-productivity, and weathering is reduced in the catchment. However, for the period just before the LGM a slow transgression is inferred towards the beginning of MIS 2. According to the pollen record of the Sea of Marmara, precipitation/evaporation rates were high enough to allow the persistence of oro-Mediterranean forest vegetation (Mudie et al., 2002).

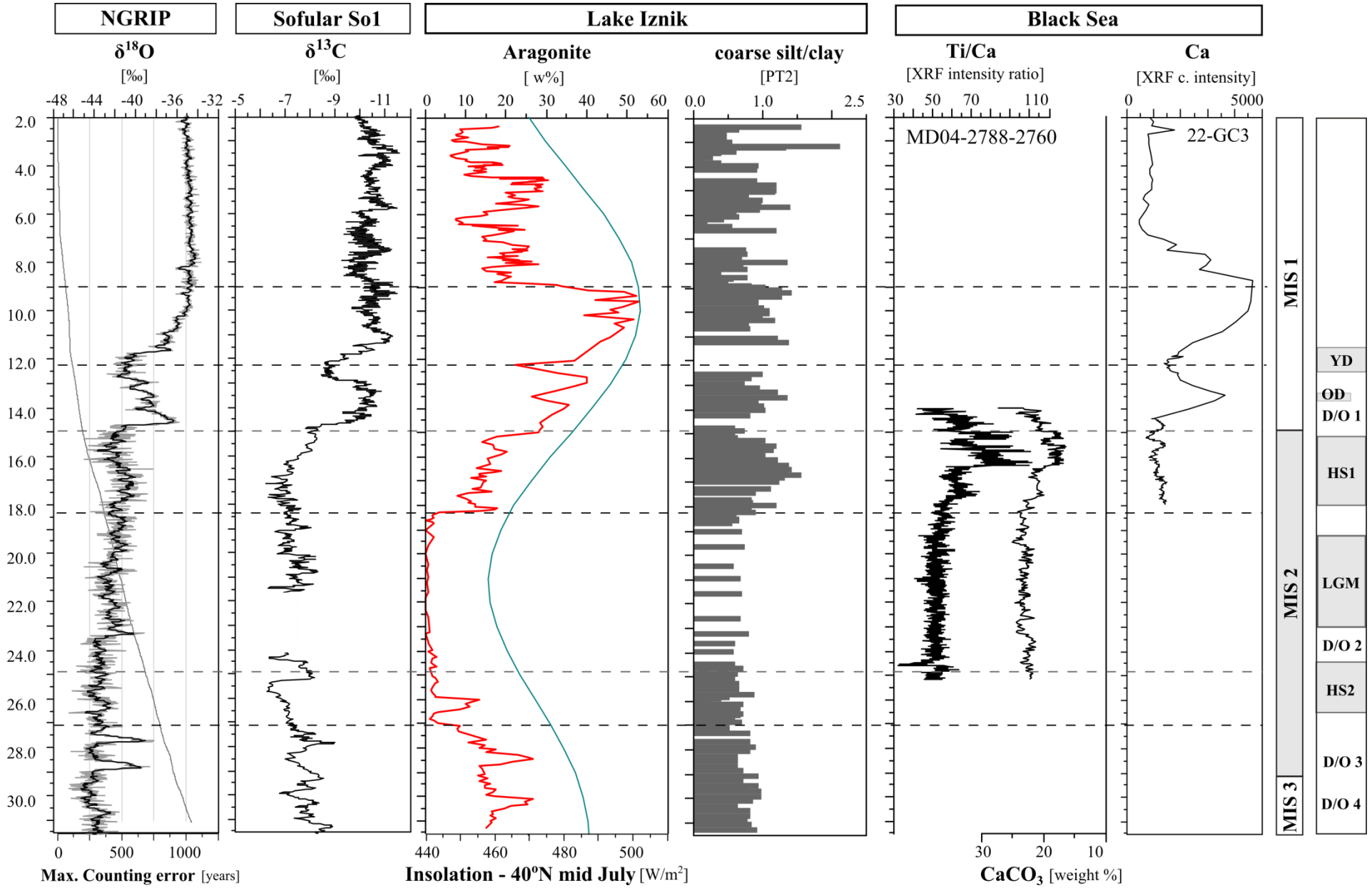

Figure 10.5: Legend on next page.

Legend for Figure 10.5: Lake Iznik aragonite concentrations and coarse silt/clay ratio inserted in the regional geological record. Data for summer insolation at 40°N (Berger, 1978; Berger and Loutre, 1999) and regional and global climate records. NGRIP record $\delta^{18}O$ [‰] (black curve represents 100 year running average) and associated uncertainty of ice core age model (Maximum counting error) (Wolff et al., 2010). Sofular cave $\delta^{13}C$ [‰] record So1, after (Fleitmann et al., 2009). Black Sea data for core MD04-2788-2760, after (Kwiecien et al., 2009); and Black Sea data for core 22-GC3, after (Shumilovskikh et al., 2012). All records are plotted on independently generated age models. Age scale is in [ka cal BP]. The NGRIP record is given in [b2k] scale (the resulting 50 year shift does not affect the millennial correlation for the given data resolution). Right hand columns highlight climate stratigraphy (for references on chronology see legend of Figure 10.1).

10.2.1.1) Last Glacial Maximum

The Last Glacial Maximum (LGM) is clearly identified within the proposed age-depth model (section 5.2) by the deposition of the Y2 tephra, originating from the Cape Riva eruption of Santorini (Figure 10.4). During the LGM the low lake productivity is coupled to low catchment ecosystem productivity, reduced weathering and condensed sedimentation rates (Figure 10.1). This is a timely continuation of the previous described scenario for MIS 2, and in consistent to a regional low vegetation cover and low pollen influxes over the Sea of Marmara (Mudie et al., 2007; Tzedakis, 2007).

As discussed, for MIS 2 a high lake level stand is conceivable for Lake Iznik based on the constant and homogeneous clayey grain size, and prolonged maintenance of an unmixed bottom water layer. According to the existing evidence, the lacustrine physical and geochemical conditions prevailing at the beginning of MIS 2 were most likely intensified during the LGM. Thus, between 22 to 20 ka cal BP neither calcite nor aragonite are present, due to early diagenetical dissolution, possibly in combination to very low carbonate precipitation rates. Moreover, the continuous shell reworking at the coastal areas, strongly suggests that a lake level stand is sustained for the time period between ~ 27 and 18 ka cal BP. It is conceivable that the inferred high lake level is maintained through lower evaporation rates, due to colder climate. Supra regional correlation to further lacustrine records show a general picture of elevated lake levels during or shortly prior the LGM, e.g. Lake Van (Landmann et al., 1996), the Konya Basin (Roberts et al., 1999) , or Pleistocene Lake Lisan which presents a high stand until circa 24 ka cal BP (Bartov et al., 2007).

10.2.1.2) Correlation to Dansgaard-Oeschger Interstadials

During the investigated time frame, four warm interstadials are observed in the northern Hemisphere event-stratigraphy (Fletcher et al., 2010; Wolff et al., 2010), correspondent to DO oscillations DO1 to DO4, or the respective Greenland Interstadials (GI's).

The interstadials (black circles in Figure 10.2) are indicated by the increase in magnitude of aragonite concentrations, i.e. relative height of peaks, comparable for the magnitude in variability for the NGRIP $\delta^{18}O$ record (Figure 10.5), suggesting that aragonite production is related to the rising temperature.

Also the grain size ratio expresses changes in a millennial time scale at the timing of each interstadial (marked by gray vertical bars in Figure 10.2). Hence carbonate production and lake level variations respond to interstadial milder climate. A slight time lag is observed between coarse silt/clay ratio minima (marked by gray vertical bar) and aragonite concentrations maxima (black circles).

From the Lake Iznik record, a typical 'interstadial pattern' is clearly identified for the pronounced DO1. At the onset of DO1, at circa 15 ka cal BP the water column is deep (Figure 10.2). During the development of the interstadial lake level decreases, followed by an increase in aragonite concentrations.

This suggests that at the onset of the DO's lake levels are high and decrease during their development, whereas aragonite concentrations increase. Such observation can be related either to the internal dynamics of the lacustrine system, as well as to a differential onset of climatic forcing.

For the Marmara region and the Pontic Coast, the milder climate at the onset of the DO1 is associated with the fast expansion of vegetation, and primary ecosystem productivity in response to regional increase in effective moisture (Fleitmann et al., 2009; Mudie et al., 2007). Such conditions most likely enhanced chemical weathering and ion supply to Lake Iznik, and additionally reducing physical erosion in the catchment, i.e. the clastic sediment supply.

In general, the period between MIS 4 and MIS 2 is marked by summer warmth for the Aegean, given the presence of summergreen *Quercus*, and most likely recurrent winter frosts, due to the absence of evergreen *Quercus* (Müller et al., 2011). Also for the Aegean, rainfall increases in this phases allowing the growth of tree populations (Müller et al., 2011). In the Levant, the Pleistocene Lake Lisan presents high lake level stands associated to the DO events

(Torfstein et al., 2013), with one exception for the B/A, which is accompanied by extreme aridity at circa 14 ka BP (Stein et al., 2010). Hence, there is a general consensus for supra-regional elevated effective moisture at the DO interstadials, ranging from the Pontic Coast at the north, towards the Levant at the south.

Within the Lake Iznik record, during the end of MIS3, the interstadials DO3 and DO4 present similar pattern as DO1, with deeper water columns at the onset of the DO's, and followed by aragonite concentration maxima after a time lag of less than a decade.

DO2, which immediately precedes the LGM is less pronounced for this time interval (see NGRIP record Figure 10.5). This DO is not evident the Iznik aragonite record because of the early diagenetical change in the carbonate system in response to the changes in lake mixing dynamics (section 9.3.4). For the timing in which DO2 would be expected a slight response from grain size is tentatively correlated (white circle within Figure 10.2). Given the low sedimentation rates at the time, the resolution for the grain size data-set is too low to resolve this interstadial.

10.2.1.3) Correlation to Heinrich Stadials

Within the investigated time frame, two Heinrich stadials are documented in the northern Hemisphere event-stratigraphy: HS1 with duration from ~ 18 to 15.6 ka cal BP, and HS2 with duration from ~ 26.5 to 24.3 ka cal BP (Sanchez-Goni and Harrison, 2010).
However, neither the total carbonate abundances, nor the total calcium accumulation (Ca/Ti) of Iznik sediments, show clear or stand alone evidence for a 'type pattern' for HS1 or HS2. However, for the timing in which HS1 and HS2 are expected, a particular and unique pattern can be recognized in changes of the depositing carbonates within Lake Iznik. Such changes are given by rapid inversions in the dominant carbonate mineral phase (Figure 10.6). Such inversions or 'reversals' have short term duration and are expressed as an abrupt increase in calcite concentrations in expense of aragonite concentrations. The latter 'recover' shortly after the first increase in calcite (marked by black squares within Figure 10.2). The nature of calcite deposited at these events is unique in relation to the sedimentary profile, as it has the lattice characteristics of a magnesian calcite, and is therefore interpreted to be endogen in origin (section 9.3.2). Different factors might lead to favored production of magnesian calcite (chapter 9), e.g. changes in the molar Mg/Ca of the solution (De Choudens-Sanchez and Gonzalez, 2009), and/or a lowering in temperatures (Kinsman and Holland, 1969).

After the inversions of magnesian calcite precipitating in the expense of aragonite, slightly enhanced calcite concentrations (higher than ~8%) are maintained throughout the time interval of each HS (Figure 10.6). These are interpreted as either (a) slightly elevated detrital component, resulting from enhanced mechanical erosion during cold periods or (b) endogen calcite production along with aragonite.

Also the grain size ratio responds to the Heinrich stadials; however the grain size changes for HS1 are much more pronounced than for HS2. During the development of HS1 there is a clear lake level decrease from 18 towards ~ 16.5 ka cal BP (Figure 10.2).

This stadial is in outstanding stratigraphic correlation to the record of the Black Sea (Kwiecien et al., 2009) (Figure 10.5). Slight chronological offsets of circa one thousand years are unlikely related to time lags. Rather they are attributed to issues on reservoir effect of radiocarbon dating, for either one, or both the archives.

For the eastern Pontic Coast, between 18 and 14.5 ka cal BP, the dominance of *Artemisia* indicates aridity, which was not extreme, given the relative high percentages of grass pollen and the presence of arboreal vegetation (Shumilovskikh et al., 2012). The cooling and aridity associated to the HS's extends over the Levant (Bar-Matthews et al., 1999; Torfstein et al., 2013).

Past glacial activity of the Marmara region is inferred from moraine deposits at Mount Uludağ situated 30 km south from Lake Iznik, in the vicinities of the city of Bursa (Figure 10.5). Besides the LGM, three additional phases of glacier advances are documented for this region, at 16.1 ± 1.2 ka BP, 13.3 ± 1.1 ka BP and again at 11.5 ± 1.0 ka BP (Sarikaya et al., 2011). The first one is related to the timing of HS1. Besides the calcite increases during the Heinrich stadials, the regional glacial activity can be linked to increases of calcite concentrations within Lake Iznik, due to the expected increases in detrital calcite load from the catchment (Figure 10.6).

Moreoever, the moments in which magnesian calcite is deposited within Lake Iznik, resulting from colder temperatures, correlates with enhanced dust deposition over Greenland (Figure 10.6).

Generally in the Northern Hemisphere the cold stadials are characterized by a higher atmospheric dust load. The two characteristic events at the timing during and after the HS2 (or GS3) correspond to the highest atmospheric dust load to Greenland over the past circa 100 ka cal BP (Rasmussen et al., 2008; Ruth et al., 2007). The dust deposition over Greenland has its major source in eastern Asia (Biscaye et al., 1997), and has been shown to be intimately

linked with periods of enhanced loess deposition, and is therefore used as an indication of storminess and dust formation in association with the east Asian monsoon system (Ruth et al., 2007). A direct influence of the mentioned monsoon system to the Mediterranean in the form of dust deposition is not expected, given that the influence of the westerly winds carrying humidity sets on from Indochina eastwards (Yihui and Chan, 2005). In the modern setting of atmospheric circulation, the Mediterranean climate and the Asian monsoon climate share an atmospheric teleconnection during summer (Sanchez-Goni et al., 2008), and based on similar patterns of enhancement of Mediterranean type climate and Asian Summer monsoons during precession minima, Sanchez-Göni et al. (2008) had proposed that Mediterranean climate responds to changes in the Asian monsoon intensity.

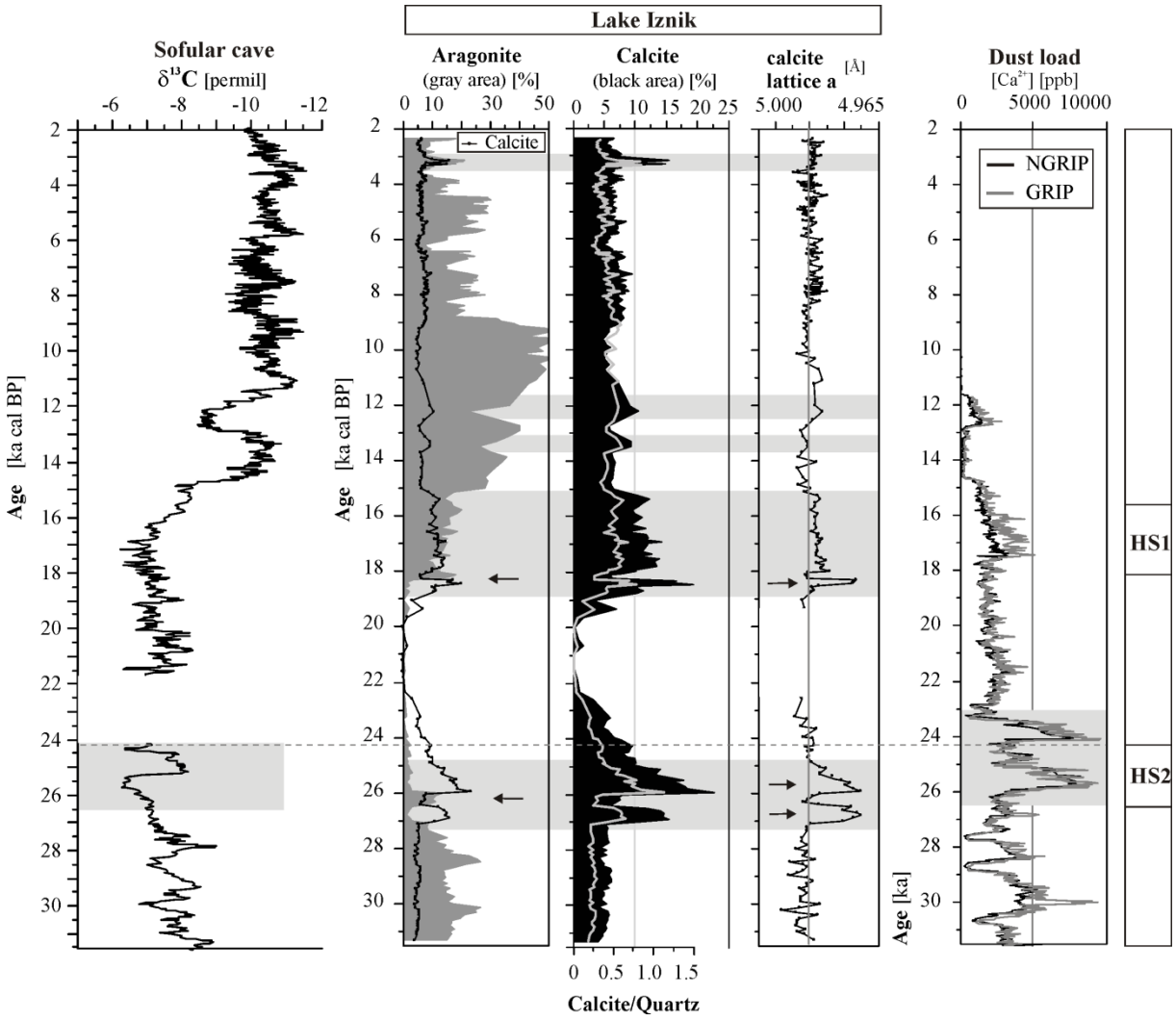

Figure 10.6: Lake Iznik variability for aragonite and calcite concentrations. Calcite/quartz ratio is provided along with the lattice parameter of calcite. Sofular $\delta^{13}C$ record is provided as age control for Iznik bottom profile between 25 ka cal BP to 31.5 ka cal BP. Dust distribution over NGRIP expressed by $[Ca^{+2}]$, data from (Bigler, 2004). Timing of the Heinrich Stadials on the right bar, after Sanchez-Goni et al. (2010). Gray horizontal bars are defined for periods with calcite concentrations higher than approx. 8%.

10.2.1.4) Younger Dryas event

For the time period between the deglaciation and the onset of the Holocene sedimentation rates in Lake Iznik are again very low, of about 0.5 $mm.yr^{-1}$, comparable to those from the glacial times. Aragonite concentrations maintain the increasing trend towards the Holocene, and are punctuated by rapid retreats, in favor of a gain in calcite concentrations, at ~ 13.6 and 12.5 ka cal BP. The latter refers to the occurrence of the Younger Dryas (YD) (marked with a black square in Figure 10.2), whereas the former is tentatively related to one of the short temperature retreats within DO1, i.e. in-between GI1abcd (Walker et al., 2009). According to the interpretation of the coarse silt/clay ratio for Lake Iznik, these cold events are inserted in a general phase of shallow water column (Figure 10.2), possibly a low lake level stand, lasting from ~ 14 towards ~9 ka cal BP. Lake Iznik margins are steep and become unstable for this time frame, and sporadically turbidite deposition reaches the lake center.

The timing of the YD is punctuated by the early diagenetical precipitation of a prominent iron sulfide layer. The geochemical remobilization of iron under anoxic conditions, for this time is believed to be a result from the sharp gradient in organic matter concentrations. In association sulfur concentrations are increased as a result from the lower lake level. Hence, the lake mixing dynamics is inferred to have presented a stagnation phase during the YD event.

In the Aegean, the Greenland Stadials (GS) are marked by dry steppe to desert biomes (Müller et al., 2011). During the Younger Dryas, or GS1, the Sea of Marmara had a still stand, whereas it was disconnected from Mediterranean and Black Sea (Cagatay et al., 2003; Vidal et al., 2010). At this time the Pontic Coast is marked by a decrease in vegetation, accompanied by increasing soil erosion, increased aridity and climatic cooling, especially during winter (Shumilovskikh et al., 2012). However, the YD in northern Anatolia was relatively mild, and not as dry and cold as the Pleniglacial (Shumilovskikh et al., 2012). Also in eastern Anatolia the YD is characterized by a drier climate, resulting in lower lake levels in Lake Van (Wick et al., 2003), and Lake Hazar (Eriş, 2013). Conversely, in the Levant the YD is characterized by a wet phase, resulting in an increase in lake level, prior to the deposition of a distinct salt layer in the early Holocene (Stein et al., 2010).

10.2.2) Holocene

The Holocene is formally defined to begin after the end of the Younger Dryas event, at 11.7 ka cal BP (Walker et al., 2009). Within Lake Iznik, beginning deposition of this warm epoch (marked with a black horizontal bar in Figure 10.2) is reflected by a further slight increase in

aragonite concentrations. The time interval reconstructed herein reaches from the end of the YD event towards circa 2 ka cal BP. Comparisons to the modern lake state, i.e. short core and surface sedimentation, were undertaken within this thesis when necessary, and the sediment history of the past century and the past four millennia are presented elsewhere in detail (Franz et al., 2006; Ülgen et al., 2012).

At the early Holocene, i.e. from circa ~ 11 to ~ 9 ka cal BP, the Iznik sediments show the highest concentrations of endogen carbonate which are directly associated to the maximum in summer insolation (Figure 10.5). Pronounced summer stratification of the water column is hence expected. Additionally epilimnion supersaturation is increased towards the Holocene, as a result of enhanced ionic input resulting from chemical weathering. Despite pronounced summer stratification, the lake mixes recurrently (chapter 9), most likely due to the shallow water column.

The high carbonate production, and its retreat, is in excellent correlation with the endogen carbonate production in the Black Sea (Figure 10.5) (Shumilovskikh et al., 2012). During this time, a sapropel is formed in the Sea of Marmara, immediately following the Younger Dryas event, as a consequence of enhanced aquatic productivity (Vidal et al., 2010). Also the Aegean shows a tendency of relative warmer/drier summers in the early Holocene. For northern Greece, pollen investigations from three different sites, deliver evidence for expansion of the *Sclerophyllous* taxa in the period between circa 10.5 and 7.5 ka cal BP (Lawson et al., 2005). For Lake Xinias a lake lowering is recorded in the early Holocene due to favoring of aragonite precipitation in the expense of calcite (Digerfeldt et al., 2000). According to Tzedakis (2007), summer aridity might have persisted during boreal insolation maxima, i.e. minima in the precession cycle, for the Mediterranean region.

During the middle Holocene, i.e. from ~ 9 towards circa 5 ka cal BP, sedimentation rates start increasing, along with catchment weathering. For the Holocene period (marked with horizontal black bar in Figure 10.2), aragonite concentrations and coarse silt/clay ratio vary synchronously most probably in response to effective moisture. This differentiated response of aragonite production and lake levels than in the interstadials, is tentatively linked to (a) an additional and/or enhanced biological trigger of aragonite production, or (b) more elevated epilimnetic supersaturation rates.

During the early to middle Holocene, Lake Iznik sediments record two distinct increases in lake levels, resulting from increase in regional effective humidity. The first and most pronounced lake level increase lasted circa 500 years, starting at circa 9 ka cal BP, and

corresponds to the time of the last reconnection between the Black Sea and the Mediterranean (Figure 10.7). The second lake level increase occurs at circa 6.5 ka cal BP.

The hydrologic changes sensitivity of Lake Iznik was tentatively connected to Holocene Bond cyclicity for the past four millenia, based on a broad correlation to regional paleoclimatic records (Ülgen et al., 2012). Also the closest regional records of the Marmara Sea indicate a humid middle Holocene (Gokturk et al., 2011; Mudie et al., 2002) and in northern Anatolia the middle Holocene is the most humid and warm period since the last 18 ka cal BP (Shumilovskikh et al., 2012). Also in eastern Anatolia, humidity increases towards the Holocene (Litt et al., 2009). After the Younger Dryas the Sea of Marmara passed through a transgressive phase (Cagatay et al., 2003), and the Marmara region is subject to fast revegetation of trees and shrubs at circa 10.5 kyr BP (Fleitmann et al., 2009).

10.2.2.1) Human mobility in the Marmara region

Geographically enclosed by the Black Sea and the Mediterranean, the Marmara region serves as a bridge for human mobility, uniting the Asian and the European continents, and is known as '*the last human destination, before farming spread to SE Europe*' (Sagona and Zimansky, 2009), given that Anatolia was considered a source area for Neolithic cultures to Europe. Recent research shows that the picture is more complex, as a Balkano-Anatolian cultural complex emerges, and separate waves of migration for the expansion of the Neolithic are becoming recognized (Özdoğan, 2011).

At circa 5 ka cal BP, Iznik sediments record an abrupt increase of sedimentation rates, accompanied by an increase in the relative proportion of very coarse silt delivered to Lake Iznik (Figure 10.1), which are resulting from enhanced erosion due to human settling within the catchment. The first farming communities settling in the Marmara region are radiocarbon dated to ~ 8 ka cal BP, e.g. Ilıpınar within the Iznik basin (Roodenberg, 2013; Roodenberg et al., 2008). Human activity became enhanced during Chalcholithic and Bronze Age times, e.g. Barcın Höyük in the adjacent Yenişehir valley (Roodenberg, 2008, 2013).

Noteworthy, the first settlements in the Iznik basin are established shortly after the lake level increases in the early Holocene, from 9 towards 9.5 ka cal BP (Figure 10.2, Figure 10.7). This slow lake level increase is inserted into a regional scenario of increase in effective moisture (Fleitmann et al., 2009; Gokturk et al., 2011).

During most of MIS 3 and MIS 2 the Black Sea was a low saline water body (i.e. Late Neoeuxinian lake), with episodes of reopening of the Black Sea – Mediterranean water ways

(Badertscher et al., 2011; Eris et al., 2011; Yanko-Hombach et al., 2007). The last reconnection between these major water bodies, via the Sea of Marmara, is placed in the early Holocene, however the precise timing remains a matter of discussion (Badertscher et al., 2011; Eris et al., 2011; Hiscott et al., 2007; Major et al., 2006; Okay et al., 2011; Soulet et al., 2011). Also the consequences of such a major geologic event for human communities remain under debate (Ryan et al., 1997; Yanko-Hombach et al., 2007).

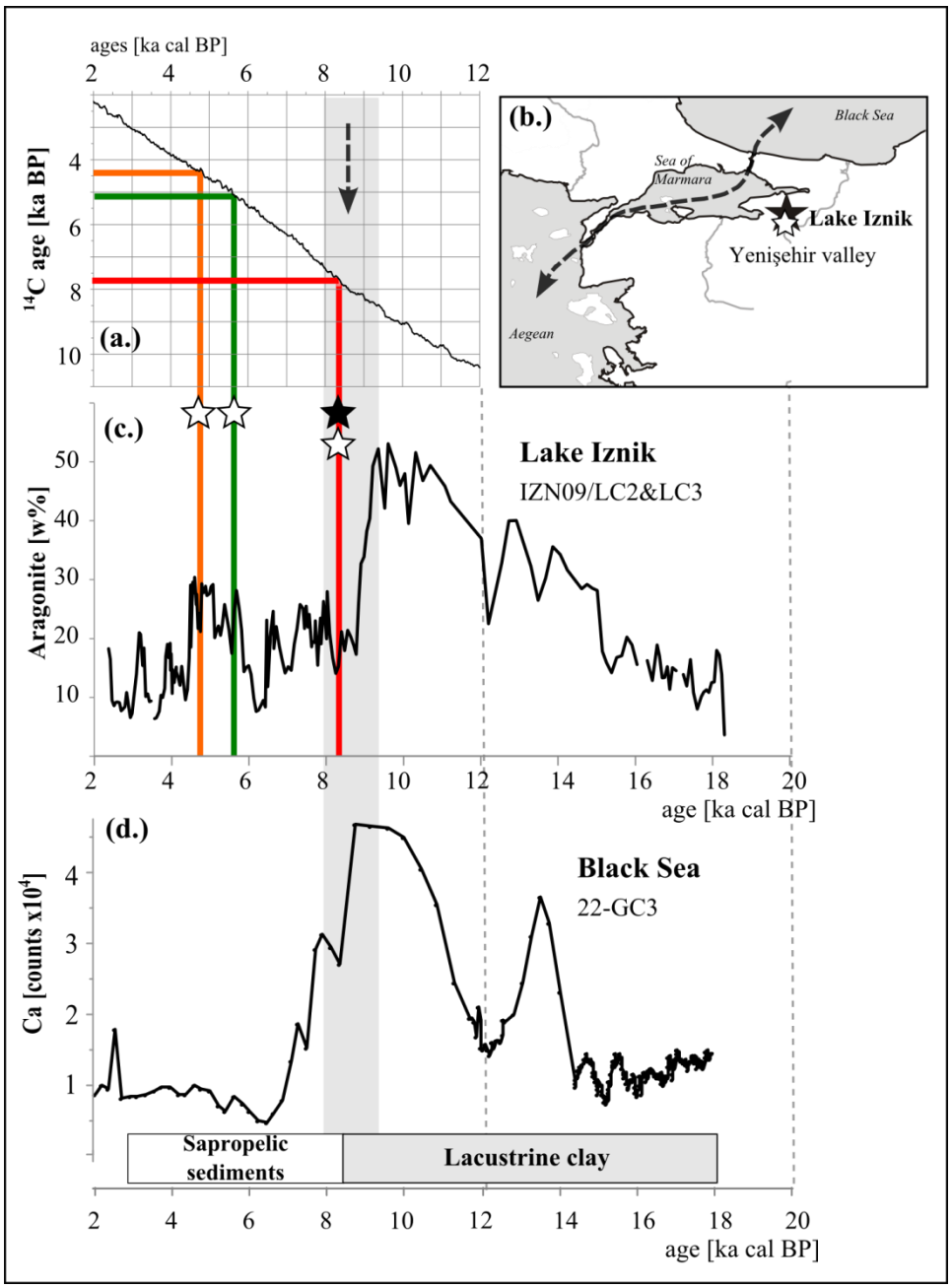

Figure 10.7: Establishment of first settlements in the Marmara region inserted in the climate context. (a) Location of settlements: Ilıpınar located in Iznik basin (black star), and Bacir located in Yenisehir valley (white star), (b) Radiocarbon determinations after (Roodenberg et al., 2008) for settling phases: Pre-pottery Neolithic (red), Chalcolithic (green) and Bronze age (orange); age calibration using Intcal09 curve (Reimer et al., 2009); (c) Lake Iznik aragonite curve highlighting changes in temperature and hydrology for the past 18 ka cal BP correlated to the (d) Black Sea carbonate production and lithology, after (Shumilovskikh et al., 2012). Gray vertical bar highlights the timing of reconnection between the Black Sea and the Mediterranean water ways.

The lake level increase as recorded in Iznik sediments correlates to the transition of a lacustrine Black Sea towards a ‘marine’ basin, also recognized by a typical change in Black Sea lithology (Figure 10.7), which reflects the reopening of the corridor Black Sea Marmara (Shumilovskikh et al., 2012). The mineralogical to geochemical signal correlation between the climatically triggered aragonite accumulation within Lake Iznik and the carbonate accumulation within the Black Sea respectively, has further implications to the regional geological and archeological pictures (Figure 10.7). In this sense this work (a) Contributes with an independent age model to the establishment of the timing of reconnection of the Black Sea – Mediterranean water ways, and (b) links the timing of reopening of the Bosphorous to the subsequent establishment of the first farming settlement in the Marmara region through archeological and geological evidence from Lake Iznik catchment.

The presented data makes it tempting to speculate on a physical barrier formed by the water corridor for at least part of the westward migrating communities. However, such inference remains speculative, and should be regarded under the light of a detailed discussion concerning the cultural exchange between coastal and inland communities, which is not in the scope of this document.

Increased humidity in a warm scenario is expected to lead to increased steppe productivity, especially grasses, including wild cereals. Probably a productive Iznik basin, with plenty freshwater supply, became more attractive for human communities, which at that time consumed pulses, specially lentils, cereals and Triticum (Roodenberg, 2013). Between ~14 and 9 ka cal BP Lake Iznik basin was probably unattractive for inhabitation, given low lake levels, relative more saline water and steep marginal lake slopes. At that time interval, settling at the nearby abundant low-saline Black Sea waters would seem much more likely. Moreover, in the Levant, the early Holocene is marked by a warm and arid phase (Litt et al., 2012), which possibly triggered northward community movements in the search of more fertile environments. The presented linkage between Lake Iznik and Black Sea evolution and the subsequent settling of farming communities in the Marmara region is one further piece of evidence for the establishment of expansion routes of the Neolithic pathways towards Europe.

11.) Summary

Lake Iznik, situated in the Marmara region (NW Turkey), is an alkaline lake with about 300 km^2 surface area, inserted in an area of typical Mediterranean climate. During the dry summer season, carbonates are precipitating from the water column. The endogen carbonate accumulation, e.g. aragonite, is expected to hold past climate information. A detailed understanding of the limnological system is required to differentiate site specific signals and responses to climatic forcing.

Geochemical and mineralogical evidence from a continuous composite profile was documented in a decadal to centennial time scale. A novel improved age model shows that the sediment record reaches up to ~31.5 ka cal BP. Compositional Data (CoDa) analysis allowed the identification of three groups of elements, and particular elements with distinct geochemical behavior, which indicate specific geochemical processes. Also, CoDa analysis allowed clear geochemical characterization of litho-stratigraphic units.

Grain size measurements were undertaken to determine the energy levels of the physical deposition environment. Detailed grain size analysis allowed the quantification of relative changes in amorphous silica. From siliciclastic grain size analysis, the ratio coarse silt/clay was identified to be a sensitive indicator to infer changes in the depth of the water column. This ratio was a calibrated to the modern depositional regime.

The endogen carbonate production proved to be a sensitive climatic indicator. Changes in carbonate concentration are timely associated to the inferred fluctuations in water column depth. The aragonite concentrations are most likely related to regional temperature, catchment hydrology and the mixing dynamics of the lake.

The physical mixing dynamics of the lake is reflected in (a) behavior of elements mobile under different oxic/anoxic conditions, and (b) geochemical patterns for carbonate bound elements in hardwater lakes, and (c) stability of various minerals.

This study established the current knowledge of the geochemical evolution of Lake Iznik. It further adds to the understanding of paleoclimate evolution in the Marmara region on a millennial time scale.

From ~31 ka cal BP until the deglaciation at ~18 ka cal BP, Lake Iznik is characterized by low productivity and higher detrital load, in association to a low carbonate accumulation. Thicker epilimnion and lower supersaturation states are inferred in association to a deeper water column. During the last glacial, i.e. from ~26 ka cal BP to ~18 ka cal BP, Lake Iznik

passes through prolonged stages of incomplete mixing of the water column, whereas the lake level is most likely maintained during that period. In addition, the crystal structure of carbonates reflects mineral instability. At the Last Glacial Maximum (~22 ka cal BP) carbonate accumulation in the lake is nearly absent.

During the deglaciation, starting at ~18 ka cal BP, dynamic and pronounced lake level variations occur. A shallow water column is inferred at ~16.5 ka calBP, and a possible low stand is identified for the period between ~14 and ~9 ka cal BP. Generally Marine Isotope Stage (MIS) 1 is marked by increased aragonite concentrations, and enhanced chemical weathering. The terrestric organic load increases gradually, and is accompanied by lake trophic conditions.

Lake Iznik climate event stratigraphy highly correlates with the regional geological record. The endogen carbonate accumulation seems to occur in phase to Northern Hemisphere climate variability, for instance warm interstadials and cold stadials are depicted. In synchrony with Dansgaard-Oeschger interstadials Iznik sediments point to a deep water column, which decreases in time. After a short time lag, geochemistry reacts with increasing aragonite concentrations. In synchrony with Heinrich stadials, the Iznik sediments underwent short phases of magnesian calcite preservation, after that generally more elevated calcite concentrations prevail. In general the cold phases are associated to a higher input of detrital calcite, likewise during the Younger Dryas cold event (~12 ka cal BP).

The early Holocene (from ~12 to ~9 ka cal BP) is characterized by pronounced summer stratification of the water column and higher epilimnion carbonate supersaturation. Recurrent stages of good lake mixing are accompanying a shallow water column. The middle Holocene is generally more humid, as indicated by enhanced chemical weathering and by two distinct lake level increases. The first of such increases occurred at ~9.3 ka cal BP and is related to the reconnection of the Black Sea to Mediterranean water ways. This geological event is followed by the settlement of the first farming communities in the Iznik basin. Moreover, at circa 5 ka cal BP a change occurs in delivery of grain size proportions – in relation to what is expected according to the inferred water column depth. This is most likely resulting from anthropic land-use within the basin.

11.1) Zusammenfassung

Der alkalische Iznik See ist in der Marmara Region (NW-Türkei), in der ein typisches mediterranes Klima vorherrscht, gelegen. Er besitzt eine Oberfläche von ca. 300 km^2. Im See selbst fallen aus der Wassersäule Karbonate hauptsächlich während des Sommers aus, wobei die hydro-geochemischen Bedingungen die Karbonatkonservierung in den Sedimenten begünstigen. Es wird erwartet, dass endogene Karbonate, besonders Aragonit, Informationen über die vergangenen klimatischen Bedingungen speichern.

Die geochemische und mineralogische Zusammensetzung der Sedimente wurde für ein kontinuierliches Kompositprofil untersucht. Ein neu erstelltes Altersmodell zeigt dass dieses Kompositprofil ~31.5 ka der Klimageschichte der Marmara Region aufzeichnet. Somit ergeben die Untersuchungen eine zeitliche Auflösung von zehn bis zu hundert Jahren. Die statistische Analyse der Daten (*Compositional Data Analysis, CoDa*) identifiziert drei geochemische Hauptgruppen aus Elementen, die hydro-geochemisch ähnlich auf Umweltveränderungen reagieren. Entsprechend konnten die fünf lithostratigraphischen Einheiten auch eindeutig geochemisch erfasst werden und lassen sich im Kontext vergangener Klimazustände interpretieren.

Die siliziklastischen Korngrößenverteilungen der Sedimente deuten das Energieniveau der Ablagerungsbedingungen der Iznik Sedimente an. Besondere Einblicke hierzu liefert das Verhältnis von Grobsilt zu Ton. Der Zusammenhang zur Wassersäulentiefe wurde anhand der rezenten Sedimentation modelliert. Somit konnten die Änderungen der Seetiefe bzw. der Seespiegel für die Vergangenheit rekonstruiert werden.

Die endogene Karbonatausfällung erweist sich als äußerst klimasensitiv. Änderungen in der Karbonatakkumulation zeigen Änderungen in der Mischungsdynamik innerhalb der Wassersäule an, da der vertikale Wasseraustausch sensitiv auf Klimaveränderungen reagiert, was wiederum die Karbonatausfällung im Wasser beeinflusst. Entsprechend spiegelt sich die Dynamik der Seemischung (a) im Verhalten von redox-sensitiven Elementen (oxische versus anoxische Bedingungen), (b) in geochemischen Mustern von Elementen die sich an Karbonate binden, und (c) in der geochemischen Stabilität diverser Minerale wider.

Aus den abgeleiteten Veränderungen der Seespiegelschwankungen und Mischungsdynamik im Iznik-See lassen sich Aussagen über die regionale Klimaentwicklung der Marmara Region gewinnen, da das Klima letztlich das Mischverhalten des Sees maßgebend bestimmt.

Somit war der Iznik See in der Zeitspanne zwischen ~31.5 bis ~18 ka cal BP nur wenig produktiv und nur wenig Karbonate sind in den Sedimenten erhalten. Entsprechend war die Sedimentation zu dieser Zeit durch terrestrischen Eintrag stark geprägt. Während des letzten Glazials (~26 bis ~18 ka cal BP) traten verschiedene Phasen auf, in denen die Wassersäule nur unvollständig durchmischte. Während dieser Zeitspanne variierte die Seetiefe kaum und Karbonate sind geochemisch nur wenig stabil. Somit fehlen Karbonate während des letzten glazialen Maximums (LGM) beinahe vollständig.

Mit Beginn des finalen Rückzugs der Vereisung (~18 ka cal BP) zeigt der Iznik See ausgeprägte Seespiegelschwankungen. Tiefstände finden sich bei ~16.5 ka cal BP und zwischen ~14 und ~9 ka cal BP. Das marine Isotopenstadium 1 (MIS 1) ist im Allgemeinen durch erhöhte Aragoniterhaltung und eine höhere chemische Verwitterung charakterisiert. Der terrestrisch-organische Eintrag erhöht sich graduell und entsprechend nimmt die Trophie des Sees zu.

Die Klima-Eventstratigraphie der Sedimente des Iznik Sees lässt sich gut und eindeutig in den Kontext der regionalen Klimaentwicklung der Marmara Region integrieren. So scheint die endogene Karbonatakkumulation in Phase mit der Klimavariabilität der Nordhemisphäre zu sein. Zudem lassen sich beispielsweise anhand der Karbonatphasen die warmen Interstadiale deutlich von den kälteren Stadialen unterscheiden. Dansgaard-Oeschger-Interstadiale sind in den Iznik Sedimenten durch Aragoniterhaltung gekennzeichnet. Während der Heinrich-Stadiale wird in den Sedimenten für kurze Phasen hoch Mg-Kalzit erhalten. Außerdem, sind im Allgemeinen die kälteren Phasen mit höherem Eintrag von terrestrischem Kalzit verknüpft, so auch während der Jüngeren Dryas (~12 ka cal BP).

Zu Beginn des Holozäns zeigt die Sedimentgeochemie ein gutes Mischverhältnis des Sees an, was mit einer niedrigen Wassersäule einhergeht. Das mittlere Holozän ist generell feuchter, was anhand einer höheren chemischen Verwitterung und zwei ausgeprägten Seespiegelanstiegen zu erkennen ist. Der Erste dieser Anstiege ist zeitgleich mit der ‚Wieder‘ -Verbindung der Wasserstraße zwischen dem Schwarzen Meer und dem Mittelmeer, um ~9 ka cal BP. Im Anschluss an dieses geologische Ereignis folgte im Einzugsgebiet des Iznik Sees die menschliche Erstbesiedlung die durch Ackerbau gekennzeichnet ist. Ein zweiter ausgeprägte Seespiegelanstieg im Holozän ist bei ~6.5 ka cal BP dokumentiert. Um ~5 ka cal BP ist eine Veränderung der Verhältnisse der Korngrößen zu beobachten die auf anthropogenen Einfluss im Einzugsgebiet in Folge höherer Erosion durch Bodennutzung hindeutet.

11.2) Síntese

O lago Iznik, localizado na região de Marmara (NE, Turquia), possui águas alcalinas, área superficial de cerca 300 km2, e está inserido em uma área de clima tipicamente Mediterrâneo. Durante o verão, carbonatos são precipitados na coluna d'água. Espera-se que a acumulação de carbonatos endógenos, e.g. aragonita, retenha informações sobre o clima do passado. A fim de diferenciar entre sinais específicos do lago e respostas à forçantes climáticas, é necessário um entendimento em detalhe sobre o sistema limnológico.

Registros geoquímicos e mineralógicos foram documentados para um perfil contínuo e composto em escala de tempo decadal a secular. Um novo modelo de idades mostra que o perfil sedimentar alcança até ~31.5 ka cal BP. O uso da análise de dados composicionais (Compositional Data – CoDa) permitiu a identificação de três grupos de elementos que reagem de maneira similar às condições hidrogeoquímcias. O uso da análise CoDa também permitiu a caracterização geoquímica das unidades lito-estratigráficas.

Análises granulométricas foram realizadas a fim de determinar o nível de energia do ambiente físico deposicional. O detalhamento das análises de granulometria permitiu estimar um parâmetro que mede variações relativas da concentração de sílica amorfa. A partir da análise granulométrica siliciclástica, a razão silte coarso/argila foi identificada como indicator sensível para inferir mudanças na profundidade da coluna d'água. Esta razão foi calibrada para o regime deposicional moderno.

A produção de carbonatos endógenos se mostrou um indicator sensível para variações climáticas. Mudanças na concentração de carbonatos estão associadas temporalmente com as mudanças inferidas para a profundidade da coluna d'água. As concentrações de aragonita estão associadas à temperatura regional, hidrologia da bacia e à dinâmica de mistura do lago. A dinâmica dos processos físicos de mistura lacustre se reflete (a) no comportamento de elementos móveis em diferentes condições de oxidação/anoxia, e (b) padrões geoquímicos para elementos ligados à carbonatos em lagos alcalinos, e (c) estabilidade de diversos minerais.

Este estudo estabelece o conhecimento atual sobre a evolução geoquímica do lago Iznik. Além disso, este trabalho é uma contribuição para o entendimento da evolução paleoclimática na região de Marmara em escala temporal milenar.

A partir de ~31 ka cal BP, até a deglaciação em ~18 ka cal BP, o lago Iznik é caracterizado por baixa produtividade e grande aporte terrígeno, em associação com baixa acumulação de

carbonatos. Maior profundidade de epilímnio e menores estados de supersaturação podem ser inferidos em conjunto com uma maior profundidade geral da coluna d'água do lago. Durante o último glacial, i.e. de ~26 ka cal BP até ~18 ka cal BP, o lago Iznik passa por prolongados estágios de mistura incompleta da coluna d'água, sendo que o nível do lago provavelmente é mantido durante este período. Em adição, a estrutura cristalina dos carbonatos reflete instabilidade mineral. Durante o último máximo glacial (~22 ka cal BP) a acumulação de carbonatos no lago é praticamente ausente.

Durante a deglaciação, começando em ~18 ka calBP, se inferem variações dinâmicas e pronunciadas do nível do lago. Uma queda do nível de água é inferida em ~ 16.5 ka cal BP, e uma coluna d'água rasa é identificada para o período entre ~14 e ~9 ka cal BP. Em geral, o Estágio isotópico marinho 1 (MIS 1) é marcado por um aumento nas concentrações de aragonita, e intemperismo químico elevado. O aporte orgânico terrígeno aumenta gradualmente, e é acompanhado pelas condições tróficas do lago.

A estratigrafia de eventos climáticos do lago Iznik pode ser claramente correlacionada com o registro geológico regional. A acumulação de carbonatos endógenos ocorre em fase com a variabilidade climática do Hemisfério Norte, por exemplo é possivel diferenciar entre os interstadials quentes e os stadials frios. Em sincronia com os interstadials Dansgaard-Oeshger, os sedimentos do lago Iznik apontam para uma coluna d'água profunda, que descresce com o tempo. Após um curto intervalo de tempo, a geoquímica reage com aumento das concentrações de aragonita. Em sincronia com os stadials Heinrich, os sedimentos do lago Iznik passam por uma curta fase de preservação de calcita magnesiana, após a qual em geral teores mais elevados de calcita prevalecem. Em geral as fases frias estão associadas à maior aporte de calcita detrítica, da mesma maneira durante o evento Younger Dryas (~12 ka cal BP).

O início do Holoceno (de ~12 até ~9 ka cal BP) é caracterizado por pronunciada estratificação da coluna d'água durante o verão e elevada supersaturação do epilímnio. Estágios recorrentes de boas condições de mistura do lago são acompanhados por uma coluna d'água rasa. O Holoceno médio é geralmente mais úmido, como indicado por um aumento do intemperismo químico e por dois aumentos marcantes do nível do lago. O primeiro destes aumentos ocorreu em ~9.3 ka cal BP, e está relacionado à reconexão da via aquática entre os mares Negro e Mediterrâneo. Este evento geológico foi seguido pelo estabelecimento das primeiras comunidades na bacia do lago Iznik. Além disso, em ~5 ka cal BP nas proporções granulométricas do aporte sedimentar se deve ao uso antrópico do solo na bacia.

11.3) Özet

İznik Gölü Marmara Bölgesinde (KB Türkiye) konumlanmış, tipik olarak Akdeniz iklim kuşagi içerisinde yer alan, 300 km2'lik yüzey alanına sahip bir alkali göldür. Kuru yaz sezonu süresince su kolununda karbonat çökelmektedir. Endojenik karbonat çökelimi (örneğin, aragonit oluşumu), eski iklim hakkında bilgiler barındırır. Limnolojik sistemin iyi bir şekilde anlaşılması için, yöresel, kendine özgü sinyaller ve iklimsel etkiye olan tepkinin ayırt edilmesi gereklidir.

Sürekli, birleşik bir çökel profili boyunca bin yıllık ve yüzyıllık zaman ölçeğinde jeokimyasal ve mineralojik bulgular belgelenmiştir. Yeni geliştirilmiş yaş modeli, sediment kaydının G.Ö. 31.5 bin kalibre edilmiş yıla kadar ulaştığını göstermektedir. Çökel bileşimi (CoDa) analizleri belirgin jeokimyasal süreçleri gösteren farklı jeokimyasal davranıştaki üç element gurubu ve özel elementlerin tanımlanmasını sağlamıştır. Ayrıca, CoDa analizleri litostratigrafik birimlerin anlaşılır jeokimyasal tanımlamasını sağlamıştır.

Tane boyu analizleri çökelme ortamının fiziksel enerji düzeyinin saptanması için yürütülmüştür. Detaylı tane boyu analizleri amorf silika miktarının belirlenmesini sağlamıştır. Silisiklastik tane boyu analizlerinden elde edilen iri silt/kil oranının su sütunu derinliğindeki değişimlerin anlaşılması için hassas bir gösterge oldugu saptanmistir. Bu oran güncel çökelme ortamlarına göre kalibre edilmiştir.

Endojen karbonat üretiminin hassas iklim göstergesi olduğu kanıtlanmıştır. Karbonat bileşimindeki değişimler, su sütunu derinliğindeki salınımların zamana bağlı değişimleri ile ilişkilidir. Aragonit konsantrasyonu büyük olasılıkla yersel sıcaklık, havza hidrolojisi ve gölün karışım dinamiği ile ilgilidir.

Gölün fiziksel karışım dinamiği; (a) oksik/anoksik şartlar altında hareketli elementlerin davranışını, ve (b) sert sulu göllerde karbonat oluşturan elementlerin jeokimyasal motiflerini, ve (c) çeşitli minerallerin duraylılığını yansıtmaktadır.

Bu çalışma İznik Gölü'nün jeokimyasal evrimi ile ilgili güncel bilgilere ulaşmamızı ve ayrıca, Marmara bölgesinin bin yıl zaman ölçeğindeki eski iklimsel evriminin anlaşılmasını sağlamıştır.

G.Ö. ~31 – ~18 bin yıllari arasinda, İznik Gölü düşük karbonat birikimi ile ilişkili olarak düşük üretkenlik ve yüksek detritik girdi ile karakterize edilir. Kalın epilimnion ve daha düşük doygunluk hali daha derin su kolonu ile ilişkilidir. Son buzul döneminde, örneğin G.Ö. ~26 – ~18 bin yıl, İznik Gölü uzunyarı-karışım dönemleri geçirirken, göl seviyesi

muhtemelen buzul döneminin büyük bir kısmında değişmeden kalmıştır. Buna ilaveten, karbonatların kristal yapıları mineral duraysızlığını göstermektedir. Son Maksimum Buzul döneminde (G.Ö. ~22 bin yil) gölde karbonat birikimi neredeyse yoktur.

G.Ö. ~18 bin yılında başlayan buzul erime döneminde, dinamik ve belirgin göl seviyesi değişimi yaşanır. Sığ su derinliği, G.Ö. ~16.5 bin yılında ortaya çıkar. G.Ö. ~14 – ~9 bin yılları arasındaki dönemde, düşük su seviyesi tespit edilmiştir. Genel olarak 1. Denizel İzotop Dönemi (MIS) hızlanan kimyasal ayrışma ve aragonit konsantrasyonu ile belirgindir. Gölün trofik şartlarına uyumlu olarak karasal organik girdi kademeli olarak artar.

İznik Gölü'nün iklimsel olaylara bağlı stratigrafisi bölgesel jeoloji kayıtları ile büyük bir oranda örtüşmektedir. Endojen karbonat birikiminin Kuzey Yarım Küre iklim değişimi ile uyumlu olarak gerçekleştiği gözlenmekte, örneğin sıcak buzullararası ve soğuk buzullaşmalar tanımlanmaktadır. Dansgaard-Oeschger ısınmaları ile uyumlu olarak İznik çökelleri zaman içinde azalan derin su kolonuna işaret eder. Kısa bir zamansal gecikmeden sonra artan aragonit konsantrasyonu ile jeokimyasal tepkiyi gösterir. Heinrich soğumaları ile uyumlu olarak, İznik çökelleri kısa bir mağnezyum kalsit korunmasına maruz kalır, daha sonra genellikle daha yüksek konsantrasyonda kalsit yaygınlaşır. Genç Dryas soğuk olayında (G.Ö. ~12 bin yıl) olduğu gibi genel olarak soğuk evreler daha yüksek detritik kalsit girdisi ile bağdaştırılırlar.

Erken Holosen (G.Ö. ~12 – ~9 bin yil) bariz yaz tabakalanması ve daha yüksek epilimnion karbonat doygunluğu ile temsil edilir. Tekrarlayan iyi göl karışımı evreleri sığ su kolonu ile birlikte gelişir. Orta Holosen artan kimyasal ayrışma ve iki ayrı göl seviyesi yükselimi ile belirtildiği gibi genellikle daha fazla nemlidir. Bunun gibi ilk evre yaklaşık G.Ö. ~9.3 bin yılında meydana gelir ve bu Karadeniz'in Akdeniz ile su geçişinin sağlanması ile ilgilidir. Bu jeolojik olayı, İznik havzasında ilk tarım topluluğunun yerleşmesi takip eder. Bunun dışında yaklaşık G.Ö. ~5 bin yılında, su kolonu derinliğine bağlı tane boyu oranlarında beklenen bir değişim meydana gelir. Bu değişim büyük olasılıkla havza içinde antropojenik arazi kullanımından kaynaklanmıştır.

12.) References

Aitchison, J., 1982. The statistical analysis of compositional data. Journal of the Royal Statistical Society Series B-Methodological, 44(2): 139-177.

Aitchison, J., 1983. Principal component analysis of compositional data. Biometrika, 70(1): 57-65.

Aitchison, J., 1984a. Reducing the dimensionality of compositional data sets. Journal of the International Association for Mathematical Geology, 16(6): 617-635.

Aitchison, J., 1984b. The statistical analysis of geochemical compositions. Journal of the International Association for Mathematical Geology, 16(6): 531-564.

Aitchison, J., 2003a. A Concise Guide to Compositional Data Analysis, Lecture Notes. Available online at CoDaWeb.

Aitchison, J., 2003b. The Statistical Analysis of Compositional Data. The Blackburn Press, 416 pp.

Aitchison, J., Egozcue, J.J., 2005. Compositional data analysis: Where are we and where should we be heading? Mathematical Geology, 37(7): 829-850.

Aitchison, J., Greenacre, M., 2002. Biplots of compositional data. Journal of the Royal Statistical Society Series C-Applied Statistics, 51: 375-392.

Akbaygil, I., Inalcık, H., Aslanapa, O. (Eds.), 2003. Iznik throughout history. Ofset Yapimevi, Istanbul, 312 pp.

Akçar, N., Schlüchter, C., 2005. Glacial Geology in Turkey - A Schematic Summary - Paleoglaciations in Anatolia: A Schematic Review and First Results. Eiszeitalter und Gegenwart – Quaternary Science Journal, 55(1): 102-121.

Aksu, A.E., Jenner, G., Hiscott, R.N., Isler, E.B., 2008. Occurrence, stratigraphy and geochemistry of Late Quaternary tephra layers in the Aegean Sea and the Marmara Sea. Marine Geology, 252(3-4): 174-192.

Altinsaçli, S., 1999. The ostracoda (crustacea) fauna of Lake Iznik. IUFS Journal of Biology, 61/62: 81-105.

Badertscher, S., Fleitmann, D., Cheng, H., Edwards, R.L., Gokturk, O.M., Zumbuhl, A., Leuenberger, M., Tuysuz, O., 2011. Pleistocene water intrusions from the Mediterranean and Caspian seas into the Black Sea. Nature Geosci, 4(4): 236-239.

Bahr, A., Lamy, F., Arz, H.W., Major, C., Kwiecien, O., Wefer, G., 2008. Abrupt changes of temperature and water chemistry in the late Pleistocene and early Holocene Black Sea. Geochemistry Geophysics Geosystems, 9.

Bar-Matthews, M., Ayalon, A., Kaufman, A., Wasserburg, G.J., 1999. The Eastern Mediterranean paleoclimate as a reflection of regional events: Soreq cave, Israel. Earth and Planetary Science Letters, 166(1-2): 85-95.

Bartov, Y., Enzel, Y., Porat, N., Stein, M., 2007. Evolution of the late pleistocene-holocene dead sea basin from sequence statigraphy of fan deltas and lake-level reconstruction. Journal of Sedimentary Research, 77(9-10): 680-692.

Berger, A., 1978. Long-Term variations of daily insolation and Quaternary climate changes. Journal of Atmospheric Sciences, 35: 2362-2367.

Berger, A., Loutre, M.F., 1999. Parameters of the Earths orbit for the last 5 Million years in 1 kyr resolution, Supplement to: Berger, A; Loutre, M F (1991): Insolation values for the climate of the last 10 million of years. Quaternary Science Reviews, 10(4), 297-317, doi:10.1016/0277-3791(91)90033-Q. PANGAEA.

Berner, R.A., 1969. Migrattion of iron and sulfur within anaerobic sediments during early diagenesis. American Journal of Science, 267(1): 19-42.

Berner, R.A., 1971. Principles of Chemical Sedimentology. International Series in the Earth and Planetary Sciences. McGraw-Hill Book Company, 240 pp.

Berner, R.A., 1975. The role of magnesium in the crystal growth of calcite and aragonite from sea water. Geochimica Et Cosmochimica Acta, 39(4): 489-504.

Berner, R.A., 1980. Early Diagenesis - A Theoretical Approach. Princeton University Press, New Jersey, 241 pp.

Berner, R.A., 1981. A new geochemical classification of sedimentary environments. Journal of Sedimentary Petrology, 51(2): 359-365.

Berner, R.A., Baldwin, T., Holdren, G.R., 1979. Authigenic iron sulfides as paleosalinity indicators. Journal of Sedimentary Research, 49(4): 1345-1350.

Bertrand, S., Doner, L., Akçer Ön, S., Sancar, U., Schudack, U., Mischke, S., Çagatay, M.N., Leroy, S.A.G., 2011. Sedimentary record of coseismic subsidence in Hersek coastal lagoon (Izmit Bay, Turkey) and the late Holocene activity of the North Anatolian Fault. Geochemistry Geophysics Geosystems, 12(6): Q06002.

Bigler, M., 2004. Hochauflösende Spurenstoffmessungen an polaren Eisbohrkernen: Glaziochemische und klimatische Prozessstudien (Datensatz). University of Bern, Bern.

Biscaye, P.E., Grousset, F.E., Revel, M., Van der Gaast, S., Zielinski, G.A., Vaars, A., Kukla, G., 1997. Asian provenance of glacial dust (stage 2) in the Greenland Ice Sheet Project 2 Ice Core, Summit, Greenland. Journal of Geophysical Research: Oceans, 102(C12): 26765-26781.

Bischoff, J.L., 1968a. Catalysis, inhibition, and the calcite-aragonite problem; [Part] 2, The vaterite-aragonite transformation. American Journal of Science, 266(2): 80-90.

Bischoff, J.L., 1968b. Kinetics of Calcite Nucleation: Magnesium Ion Inhibition and Ionic Strength Catalysis. J. Geophys. Res., 73(10): 3315-3322.

Blaauw, M., 2010. Methods and code for 'classical' age-modelling of radiocarbon sequences. Quaternary Geochronology, 5(5): 512-518.

Blott, S.J., Pye, K., 2001. GRADISTAT: A grain size distribution and statistics package for the analysis of unconsolidated sediments. Earth Surface Processes and Landforms, 26(11): 1237-1248.

Boehrer, B., Schultze, M., 2008. Stratification of Lakes. Rev. Geophysics, 46.

Bond, G., Kromer, B., Beer, J., Muscheler, R., Evans, M.N., Showers, W., Hoffmann, S., Lotti-Bond, R., Hajdas, I., Bonani, G., 2001. Persistent solar influence on north Atlantic climate during the Holocene. Science, 294(5549): 2130-2136.

Bonotto, D.M., Silveira, E.G.d., 2006. Geoquímica do urânio aplicada a águas minerais. Editora Unesp, São Paulo, 160 pp.

Boyle, J.F., 2001. Inorganic Geochemical Methods in Palaeolimnology. In: Last, W.M., Smol, J.P. (Eds.), Tracking Environmental Change Using Lake Sediments: Physical and Geochemical Methods. Kluwer Academic Publishers, 2001, pp. 83-142.

Bradley, R.S., 1999. Paleoclimatology - Reconstructing Climates of the Quaternary. International Geophysics Series, 68. Elsevier Academic Press, 614 pp.

Braga, B., Hespanhol, I., Conejo, J.G.L., Barros, M.T.L.d., Jr., M.S.V., Porto, M.F.d.A., Nucci, N.L.R., Juliano, N.M.d.A., Eiger, S., 2002. Introdução à Engenharia Ambiental. Prentice Hall, São Paulo, 305 pp.

Brauer, A., Endres, C., Günter, C., Litt, T., Stebich, M., Negendank, J.F.W., 1999. High resolution sediment and vegetation responses to Younger Dryas climate change in varved lake sediments from Meerfelder Maar, Germany. Quaternary Science Reviews, 18(3): 321-329.

Broecker, W.S., 2003. Does the Trigger for Abrupt Climate Change Reside in the Ocean or in the Atmosphere? Science, 300(5625): 1519-1522.

Cagatay, M.N., Gorur, N., Polonia, A., Demirbag, E., Sakinc, M., Cormier, M.H., Capotondi, L., McHugh, C., Emre, O., Eris, K., 2003. Sea-level changes and depositional environments in the Izmit Gulf, eastern Marmara Sea, during the late glacial-Holocene period. Marine Geology, 202(3-4): 159-173.

Camara, G., Souza, R.C.M., Freitas, U.M., Garrido, J., 1996. SPRING: Integrating remote sensing and GIS by object-oriented data modelling. Computers & Graphics, 20(3): 395-403.

Canık, S.P.B., Rosen, M.R., 2004. Hydrogeology and Possible Effects of the Mw 7.4 Marmara Earthquake (17 August 1999) on the Spring Waters in The Orhangazi-Bursa Area, Turkey. Journal Geological Society of India, 63(March): 313-322.

Conley, D.J., 1998. An interlaboratory comparison for the measurement of biogenic silica in sediments. Marine Chemistry, 63(1-2): 39-48.

Conley, D.J., Scavia, D., 1991. Size structure of particulate biogenic silica in Lake Michigan. Journal of Great Lakes Research, 17(1): 18-24.

Conley, D.J., Struyf, E., 2009. Silica. In: Editor-in-Chief: Gene, E.L. (Ed.), Encyclopedia of Inland Waters. Academic Press, Oxford, pp. 85-88.

Cooke, R.C., 1977. Factors regulating the composition, change, and stability of phases in the calcite-seawater system. Marine Chemistry, 5(1): 75-92.

Cronan, C.S., 2009. Major Cations (Ca, Mg, Na, K, Al). In: Editor-in-Chief: Gene, E.L. (Ed.), Encyclopedia of Inland Waters. Academic Press, Oxford, pp. 45-51.

Croudace, I.W., Rindby, A., Rothwell, R.G., 2006. ITRAX: description and evaluation of a new multi-function X-ray core scanner. In: Rothwell, R.G. (Ed.), New Techniques in Sediment Core Analysis. The Geological Society of London, London, pp. 267, 51-63.

Dansgaard, W., Johnsen, S.J., Clausen, H.B., Dahljensen, D., Gundestrup, N.S., Hammer, C.U., Hvidberg, C.S., Steffensen, J.P., Sveinbjornsdottir, A.E., Jouzel, J., Bond, G., 1993. Evidence for general instability of past climate from a 250-kyr ice-core record. Nature, 364(6434): 218-220.

Davison, W., 1993. Iron and manganese in lakes. Earth-Science Reviews, 34(2): 119-163.

De Choudens-Sanchez, V., Gonzalez, L.A., 2009. Calcite and aragonite precipitation under controlled instantaneous supersaturation: elucidating the role of $CaCO_3$ saturation state and Mg/Ca ratio on calcium carbonate polymorphism. Journal of Sedimentary Research, 79(5-6): 363-376.

de la Rocha, C.L., Brzezinski, M.A., DeNiro, M.J., 1997. Fractionation of silicon isotopes by marine diatoms during biogenic silica formation. Geochimica Et Cosmochimica Acta, 61(23): 5051-5056.

de Leeuw, N.H., Parker, S.C., 1998. Surface Structure and Morphology of Calcium Carbonate Polymorphs Calcite, Aragonite, and Vaterite: An Atomistic Approach. The Journal of Physical Chemistry B, 102(16): 2914-2922.

Demaster, D.J., 1981. The Supply and Accumulation of Silica in the Marine-Environment. Geochimica Et Cosmochimica Acta, 45(10): 1715-1732.

Digerfeldt, G., Olsson, S., Sandgren, P., 2000. Reconstruction of lake-level changes in lake Xinias, central Greece, during the last 40000 years. Palaeogeography Palaeoclimatology Palaeoecology, 158(1-2): 65-82.

Erginal, A., Kiyak, N., Ozturk, M., Yigitbas, E., Bozcu, M., Avcioglu, M., Ozturk, B., 2012a. First note on marine-like cementation of Late Holocene beachrock, Iznik Lake (Turkey). Geochronometria, 39(1): 76-83.

Erginal, A.E., Kiyak, N.G., Ozturk, Z., Avcioglu, M., Bozcu, M., Yigitbas, E., 2012b. Cementation characteristics and age of beachrocks in a fresh-water environment, Lake Iznik, NW Turkey. Sedimentary Geology, 243: 148-154.

Eriksen, U., Friedrich, W.L., Buchardt, B., Tauber, H., Thomson, M.S., 1990. The Stronghyle Caldera: geological, paleontological and stable isotope evidence from radiocarbon dated stromalites from Santorini. In: Hardy, D.A., Keller, J., Galanopoulos, V.P., Flemming, N.C., Druitt, T.H. (Eds.), Thera and the Aegean World III, Santorini, Greece, pp. 139-150.

Eriş, K.K., 2013. Late Pleistocene–Holocene sedimentary records of climate and lake-level changes in Lake Hazar, eastern Anatolia, Turkey. Quaternary International, 302(0): 123-134.

Eriş, K.K., Cagatay, M.N., Akcer, S., Gasperini, L., Mart, Y., 2011. Late glacial to Holocene sea-level changes in the Sea of Marmara: new evidence from high-resolution seismics and core studies. Geo-Marine Letters, 31(1): 1-18.

Eugster, H.P., Hardie, L.A., 1978. Saline Lakes. In: Lerman, A. (Ed.), Lakes - Chemistry, Geology, Physics. Springer, New York, pp. 237-293.

Fedo, C.M., Wayne Nesbitt, H., Young, G.M., 1995. Unraveling the effects of potassium metasomatism in sedimentary rocks and paleosols, with implications for paleoweathering conditions and provenance. Geology, 23(10): 921-924.

Filzmoser, P., Hron, K., Reimann, C., 2009. Univariate statistical analysis of environmental (compositional) data: Problems and possibilities. Science of the Total Environment, 407(23): 6100-6108.

Fleitmann, D., Cheng, H., Badertscher, S., Edwards, R.L., Mudelsee, M., Gokturk, O.M., Fankhauser, A., Pickering, R., Raible, C.C., Matter, A., Kramers, J., Tuysuz, O., 2009. Timing and climatic impact of Greenland interstadials recorded in stalagmites from northern Turkey. Geophysical Research Letters, 36.

Fletcher, W.J., Sanchez-Goni, M.F., Allen, J.R.M., Cheddadi, R., Combourieu-Nebout, N., Huntley, B., Lawson, I., Londeix, L., Magri, D., Margari, V., Müller, U.C., Naughton, F., Novenko, E., Roucoux, K., Tzedakis, P.C., 2010. Millennial-scale variability during the last glacial in vegetation records from Europe. Quaternary Science Reviews, 29(21–22): 2839-2864.

Folk, R.L., 1966. A review of grain-size parameters. Sedimentology, 6(2): 73-93.

Fortin, M.C., Gajewski, K., 2009. Assessing the use of sediment organic, carbonate and biogenic silica content as indicators of environmental conditions in Arctic lakes. Polar Biology, 32(7): 985-998.

Franz, S.O., Schwark, L., Bruchmann, C., Scharf, B., Klingel, R., Van Alstine, J.D., Cagatay, N., Ulgen, U.B., 2006. Results from a multi-disciplinary sedimentary pilot study of tectonic Lake Iznik (NW Turkey) - geochemistry and paleolimnology of the recent past. Journal of Paleolimnology, 35(4): 715-736.

Franz, S.O., Tiedemann, R., 2002. Depositional changes along the Blake-Bahama Outer Ridge deep water transect during marine isotope stages 8 to 10 links to the Deep Western Boundary Current. Marine Geology, 189(1-2): 107-122.

French, D.H., 1967. Prehistoric Sites in Northwest Anatolia: I. The İznik Area. Anatolian Studies, 17(ArticleType: research-article / Full publication date: 1967 / Copyright © 1967 British Institute at Ankara): 49-100.

Friedman, I., O'Neil, J., Cebula, G., 1982. Two New Carbonate Stable-Isotope Standards. Geostandards Newsletter, 6(1): 11-12.

Füchtbauer, H., Heling, D., Müller, G., Richter, D.K., Schmincke, H.-U., Schneider, H.-J., Valeton, I., Walther, H.W., Wolf, M., 1988. Sedimente und Sedimentgesteine. Sediment Petrologie, Bochum.

Garrels, R.M., Christ, C.L., 1965. Solutions, Minerals, and Equilibria. Harper's Geoscience Series. Harper & Row, New York, 450 pp.

Giblin, A.E., 2009. Iron and Manganese. In: Editor-in-Chief: Gene, E.L. (Ed.), Encyclopedia of Inland Waters. Academic Press, Oxford, pp. 35-44.

Gierlowski-Kordesch, E.H., 2010. Chapter 1 Lacustrine Carbonates. In: Alonso-Zarza, A.M., Tanner, L.H. (Eds.), Developments in Sedimentology. Elsevier, pp. 1-101.

Gokturk, O.M., Fleitmann, D., Badertscher, S., Cheng, H., Edwards, R.L., Leuenberger, M., Fankhauser, A., Tuysuz, O., Kramers, J., 2011. Climate on the southern Black Sea coast during the Holocene: implications from the Sofular Cave record. Quaternary Science Reviews, 30(19-20): 2433-2445.

Goldschmidt, J.R., Graf, D.L., Heard, H.C., 1961. Lattice constants of the calcium-magnesium carbonates. The American Mineralogist, 46(3).

Grimm, E.C., Donovan, J.J., Brown, K.J., 2011. A high-resolution record of climate variability and landscape response from Kettle Lake, northern Great Plains, North America. Quaternary Science Reviews, 30(19-20): 2626-2650.

Günther, D., Pichler, H., 1973. Die Obere und Untere Bimsstein-Folge auf Santorin / The Upper and Lower Pumice Series on Satorini - Aegean Sea, Greece. Neues Jahrbuch für Geologie: 394-415.

Gürbüz, A., Leroy, S.A.G., 2010. Science versus myth: was there a connection between the Marmara Sea and Lake Sapanca? Journal of Quaternary Science, 25(2): 103-114.

Hahn-Weinheimer, P., Hirner, A., Weber-Diefenbach, K., 1995. Röntgenfluoreszenzanalytische Methoden - Grundlagen und praktische Anwendung in den Geo-, Material- und Umweltwissenchaften. Analytische Chemie. Vieweg, Braunschweig; Wiesbaden, 284 pp.

Heinrich, H., 1988. Origin and Consequences of Cyclic Ice Rafting in the Northeast Atlantic-Ocean during the past 130,000 years. Quaternary Research, 29(2): 142-152.

Heiri, O., Lotter, A.F., Lemcke, G., 2001. Loss on ignition as a method for estimating organic and carbonate content in sediments: reproducibility and comparability of results. Journal of Paleolimnology, 25(1): 101-110.

Hellier, C., 1993. Living in the shadow of history. The Middle East Journal, 227.

Hemming, S.R., 2004. Heinrich events: Massive late Pleistocene detritus layers of the North Atlantic and their global climate imprint. Reviews of Geophysics, 42(1).

Highet, J., 1999. The glory of Iznik. The Middle East Journal, 291.

Hiscott, R., Aksu, A., Mudie, P., Kaminski, M., Abrajano, T., Yaşar, D., Rochon, A., 2007. The Marmara Sea Gateway since ~16 ky BP: non-catastrophic causes of paleoceanographic events in the Black Sea at 8.4 and 7.15 ky BP. In: Yanko-Hombach, V., Gilbert, A., Panin, N., Dolukhanov, P. (Eds.), The Black Sea Flood Question: Changes in Coastline, Climate, and Human Settlement. Springer Netherlands, pp. 89-117.

Ikeda, Y., Herece, E., Sugai, T., Isikara, A.M., 1991a. Postglacial Crustal Deformation Associated with Slip on the Western Part of the North Anatolian Fault Zone in the Iznik Lake Basin, Turkey. Bulletin of the Department of Geopgraphy - University of Tokyo, 23(December): 13-23.

Ikeda, Y., Suzuki, Y., Herece, E., Şaroğlu, F., Isikara, A.M., Honkura, Y., 1991b. Geological evidence for the last two faulting events on the north Anatolian Fault zone in the Mudurnu Valley, western Turkey. Tectonophysics, 193(4): 335-345.

Imboden, D.M., Wüest, A., 1995. Mixing Mechanisms in Lakes. In: Lerman, A., Imboden, D.M., Gat, J.R. (Eds.), Physics and Chemistry of Lakes. Springer, Berlin, pp. 83-138.

Inouchi, Y., Kinugasa, Y., Kumon, F., Nakano, S., Yasumatsu, S., Shiki, T., 1996. Turbidites as records of intense palaeoearthquakes in Lake Biwa, Japan. Sedimentary Geology, 104(1–4): 117-125.

Ito, E., 2001. Applications of Stable Isotope Techniques to Inorganic and Biogenic Carbonates. In: Last, W.M., Smol, J.P. (Eds.), Tracking Environmental Change Using Lake Sediments - Physical and Geochemical Methods, Kluwer Academic Publishers, pp. 351-371.

Johnsen, S.J., Clausen, H.B., Dansgaard, W., Fuhrer, K., Gundestrup, N., Hammer, C.U., Iversen, P., Jouzel, J., Stauffer, B., Steffensen, J.P., 1992. Irregular glacial interstadials recorded in a new Greenland ice core. Nature, 359(6393): 311-313.

Jones, B.F., Browser, C.J., 1978. The Mineralogy and Related Chemistry of Lake Sediments. In: Lerman, A. (Ed.), Lakes - Chemistry, Geology, Physics. Springer Verlag, New York Berlin Heidelberg, pp. 179-235.

Jones, B.F., Deocampo, D.M., 2003. 5.13 - Geochemistry of Saline Lakes. In: Editors-in-Chief: Heinrich, D.H., Karl, K.T. (Eds.), Treatise on Geochemistry. Pergamon, Oxford, pp. 393-424.

Kaden, H., Peeters, F., Lorke, A., Kipfer, R., Tomonaga, Y., Karabiyikoglu, M., 2010. Impact of lake level change on deep-water renewal and oxic conditions in deep saline Lake Van, Turkey. Water Resources Research, 46.

Kashiwaya, K., Yamamoto, A., Fukuyama, K., 1988. Statistical analysis of grain size distribution in Pleistocene sediments from Lake Biwa, Japan. Quaternary Research, 30(1): 12-18.

Katz, A., 1973. The interaction of magnesium with calcite during crystal growth at 25–90°C and one atmosphere. Geochimica Et Cosmochimica Acta, 37(6): 1563-1586.

Katz, A., Nishri, A., 2013. Calcium, magnesium and strontium cycling in stratified, hardwater lakes: Lake Kinneret (Sea of Galilee), Israel. Geochimica et Cosmochimica Acta, 105: 372-394.

Kazanci, N., Leroy, S.A.G., Öncel, S., Ileri, Ö., Toprak, Ö., Costa, P., Sayili, S., Turgut, C., Kibar, M., 2010. Wind control on the accumulation of heavy metals in sediment of Lake Ulubat, Anatolia, Turkey. Journal of Paleolimnology, 43(1): 89-110.

Kelts, K., Hsü, K.J., 1978. Freshwater Carbonate Sedimentation. In: Lerman, A. (Ed.), Lakes - Chemistry, Geology, Physics. Spriger Verlag, New York, Heidelberg, Berlin, pp. 295-323.

Kinsman, D.J.J., Holland, H.D., 1969. The co-precipitation of cations with $CaCO_3$—IV. The co-precipitation of Sr^{2+} with aragonite between 16° and 96°C. Geochimica Et Cosmochimica Acta, 33(1): 1-17.

Koczy, F.F., 1951. Factors determining the element concentration in sediments. Geochimica et Cosmochimica Acta, 1(2): 73-85.

Kwiecien, O., Arz, H.W., Lamy, F., Plessen, B., Bahr, A., Haug, G.H., 2009. North Atlantic control on precipitation pattern in the eastern Mediterranean/Black Sea region during the last glacial. Quaternary Research, 71(3): 375-384.

Lamy, F., Arz, H.W., Bond, G.C., Bahr, A., Patzold, J., 2006. Multicentennial-scale hydrological changes in the Black Sea and northern Red Sea during the Holocene and the Arctic/North Atlantic oscillation. Paleoceanography, 21(PA1008).

Landmann, G., Reimer, A., Kempe, S., 1996. Climatically induced lake level changes at Lake Van, Turkey, during the Pleistocene/Holocene transition. Global Biogeochemical Cycles, 10(4): 797-808.

Langbein, W.B., 1961. Salinity and Hydrology of Closed Lakes - A study of the long therm balance between input and loss of salts in closed lakes. Geological Survey Professional Paper 412: 20.

Langmuir, D., 1978. Uranium solution-mineral equilibria at low temperatures with applications to sedimentary ore deposits. Geochimica Et Cosmochimica Acta, 42(6, Part A): 547-569.

Last, W.M., 1982. Holocene Carbonate Sedimentation in Lake Manitoba, Canada. Sedimentology, 29(5): 691-704.

Last, W.M., 2001a. Mineralogical Analysis of Lake Sediments. In: Last, W.M., Smol, J.P. (Eds.), Tracking Environmental Changes Using Lake Sediments. Kluwer Academic Publishers, Dordrecht, pp. 143-187.

Last, W.M., 2001b. Textural Analysis of Lake Sediments. In: Last, W.M., Smol, J.P. (Eds.), Tracking Environmental Change Using Lake Sediments: Physical and Geochemical Methods. Developments in Palaeonvironmental Research. Kluwer Academic Publishers, Dordrecht, pp. 41-81.

Last, W.M., Ginn, F.M., 2009. The chemical composition of saline lakes of the Northern Great Plains, Western Canada. Geochemical News, 141(October).

Last, W.M., Smol, J.P. (Eds.), 2001. Tracking environmental change using lake sediments Vol 2: Physical and geochemical methods. Kluwer Academic Publishers, Dordrecht, 504 pp.

Lawson, I.T., Al-Omari, S., Tzedakis, P.C., Bryant, C.L., Christaniss, K., 2005. Lateglacial and Holocene vegetation history at Nisi Fen and the Boras mountains, northern Greece. The Holocene, 15(6): 873-887.

Lemcke, G., Sturm, M., 1997. d18O and Trace Element Measurements as Proxy for the Reconstruction of Climate Changes at Lake Van (Turkey): Preliminary Results. In: Dalfes, H.N., Kukla, G., Weiss, H. (Editors), Third Millennium BC Climate Change and Old World Collapse. NATO ASI Series. Springer, Berlin, pp. 728 p.

Leng, M.J., Barker, P.A., 2006. A review of the oxygen isotope composition of lacustrine diatom silica for palaeoclimate reconstruction. Earth-Science Reviews, 75(1-4): 5-27.

Leng, M.J., Marshall, J.D., 2004. Palaeoclimate interpretation of stable isotope data from lake sediment archives. Quaternary Science Reviews, 23(7–8): 811-831.

Lerman, A., Imboden, D.M., Gat, J.R. (Eds.), 1995. Physics and chemistry of lakes. Springer, Berlin, 334 pp.

Leroy, S., Kazanci, N., Iileri, O., Kibar, M., Emre, O., McGee, E., Griffiths, H.I., 2002. Abrupt environmental changes within a late Holocene lacustrine sequence south of the Marmara Sea (Lake Manyas, NW Turkey): possible links with seismic events Marine Geology, 190(4): 531-552.

Lev, L., Boaretto, E., Heller, J., Marco, S., Stein, M., 2007. The feasibility of using Melanopsis shells as radiocarbon chronometers, Lake Kinneret, Israel. Radiocarbon, 49(2): 1003-1015.

Lin, Y., Hu, Q.N., Chen, J., Ji, J.F., Teng, H.H., 2009. Formation of Metastable $CaCO_3$ Polymorphs in the Presence of Oxides and Silicates. Crystal Growth & Design, 9(11): 4634-4641.

Lisiecki, L.E., Raymo, M.E., 2005. A Pliocene-Pleistocene stack of 57 globally distributed benthic δ18O records. Paleoceanography, 20(1): PA1003.

Litt, T., 2007. The Quaternary as a chronostratigraphical unit. Eiszeitalter und Gegenwart – Quaternary Science Journal, 56(1-2): 3-6.

Litt, T., Brauer, A., Goslar, T., Merkt, J., Balaga, K., Müller, H., Ralska-Jasiewiczowa, M., Stebich, M., Negendank, J.F.W., 2001. Correlation and synchronization of Lateglacial continental sequences in northern central Europe based on annually laminated lacustrine sediments. Quaternary Science Reviews, 20: 1233-1249.

Litt, T., Krastel, S., Sturm, M., Kipfer, R., Orcen, S., Heumann, G., Franz, S.O., Ulgen, U.B., Niessen, F., 2009. 'PALEOVAN', International Continental Scientific Drilling Program (ICDP): site survey results and perspectives. Quaternary Science Reviews, 28(15-16): 1555-1567.

Litt, T., Ohlwein, C., Neumann, F.H., Hense, A., Stein, M., 2012. Holocene climate variability in the Levant from the Dead Sea pollen record. Quaternary Science Reviews, 49(0): 95-105.

Liu, Z., Otto-Bliesner, B.L., He, F., Brady, E.C., Tomas, R., Clark, P.U., Carlson, A.E., Lynch-Stieglitz, J., Curry, W., Brook, E., Erickson, D., Jacob, R., Kutzbach, J., Cheng, J., 2009. Transient Simulation of Last Deglaciation with a New Mechanism for Bølling-Allerød Warming. Science, 325(5938): 310-314.

Lukas, S., Preusser, F., Anselmetti, F.S., Tinner, W., 2012. Testing the potential of luminescence dating of high-alpine lake sediments. Quaternary Geochronology, 8: 23-32.

Macintyre, I.G., Reid, R.P., 1992. The origin of aragonite needle mud - a picture is worth 1000 words - Comment. Journal of Sedimentary Petrology, 62(6): 1095-1097.

Mackereth, F.J.H., 1966. Some Chemical Observations on Post Glacial Lake Sediments. Freshwater Biological Association, 250: 165-213.

Major, C.O., Goldstein, S.L., Ryan, W.B.F., Lericolais, G., Piotrowski, A.M., Hajdas, I., 2006. The co-evolution of Black Sea level and composition through the last deglaciation and its paleoclimatic significance. Quaternary Science Reviews, 25(17-18): 2031-2047.

Margari, V., Pyle, D.M., Bryant, C., Gibbard, P.L., 2007. Mediterranean tephra stratigraphy revisited: Results from a long terrestrial sequence on Lesvos Island, Greece. Journal of Volcanology and Geothermal Research, 163(1-4): 34-54.

Martín-Fernández, J.A., Barceló-Vidal, C., Pawlowsky-Glahn, V., 2003. Dealing with Zeros and Missing Values in Compositional Data Sets Using Nonparametric Imputation. Mathematical Geology, 35(3): 253-278.

Martinson, D.G., Pisias, N.G., Hays, J.D., Imbrie, J., Moore Jr, T.C., Shackleton, N.J., 1987. Age dating and the orbital theory of the ice ages: Development of a high-resolution 0 to 300,000-year chronostratigraphy. Quaternary Research, 27(1): 1-29.

Matter, M., Anselmetti, F.S., Jordanoska, B., Wagner, B., Wessels, M., Wuest, A., 2010. Carbonate sedimentation and effects of eutrophication observed at the Kalista subaquatic springs in Lake Ohrid (Macedonia). Biogeosciences, 7(11): 3755-3767.

Mayewski, P.A., Meeker, L.D., Whitlow, S., Twickler, M.S., Morrison, M.C., Alley, R.B., Bloomfield, P., Taylor, K., 1993. The atmosphere during the Younder Dryas. Science, 261(5118): 195-197.

McCave, I.N., Manighetti, B., Robinson, S.G., 1995. Sortable Silt and Fine Sediment Size/Composition Slicing: Parameters for Palaeocurrent Speed and Palaeoceanography. Paleoceanography, 10(3): 593-610.

Menounos, B., 1997. The water content of lake sediments and its relationship to other physical parameters: An alpine case study. Holocene, 7(2): 207-212.

Meyers, P.A., Ishiwatari, R., 1995. Organic Matter Accumulation Records in Lake Sediments. In: Lerman, A., Imboden, D., Gat, J. (Eds.), Physics and Chemistry of Lakes. Springer, Berlin, pp. 279-328.

Meyers, P.A., Lallier-Verges, E., 1999. Lacustrine sedimentary organic matter records of Late Quaternary paleoclimates. Journal of Paleolimnology, 21(3): 345-372.

Meyers, P.A., Teranes, J.L., 2001. Sediment Organic Matter. In: Last, W.M., Smol, J.P. (Eds.), Tracking Environmental Changes Using Lake Sediments. Vol.2: Physical and Geochemical Methods. Kluwer Academic Publishers, Dortrecht, pp. 239-269.

Moore, D.M., Robert C. Reynolds, J., 1997. X-Ray diffraction and the identification and analysis of clay minerals. Oxford University Press, Oxford, 378 pp.

Morse, J.W., 1986. The surface chemistry of calcium carbonate minerals in natural waters: An overview. Marine Chemistry, 20(1): 91-112.

Morse, J.W., Berner, R.A., 1995. What determines sedimentary C/S ratios? Geochimica Et Cosmochimica Acta, 59(6): 1073-1077.

Mortlock, R.A., Froelich, P.N., 1989. A Simple Method for the Rapid-Determination of Biogenic Opal in Pelagic Marine-Sediments. Deep-Sea Research Part a-Oceanographic Research Papers, 36(9): 1415-1426.

Mudie, P.J., Marret, F., Aksu, A.E., Hiscott, R.N., Gillespie, H., 2007. Palynological evidence for climatic change, anthropogenic activity and outflow of Black Sea water during late Pleistocene and Holocene: Centennial- to decadal-scale records from the Black and Marmara Seas. Quaternary International, 167: 73-90.

Mudie, P.J., Rochon, A., Aksu, A.E., 2002. Pollen stratigraphy of Late Quaternary cores from Marmara Sea: land-sea correlation and paleoclimatic history. Marine Geology, 190(1-2): 233-260.

Müller, B., Maerki, M., Schmid, M., Vologina, E.G., Wehrli, B., Wuest, A., Sturm, M., 2005. Internal carbon and nutrient cycling in Lake Baikal: sedimentation, upwelling, and early diagenesis. Global and Planetary Change, 46(1-4): 101-124.

Müller, G., 1967. Methods in Sedimentary Petrology. Sedimentary Petrology, Part I. Schweizerbart'sche Verlagsbuchhandlung, Stuttgart.

Müller, G., Forstner, U., Irion, G., 1972. Formation and diagenesis of inorganic Ca-Mg carbonates in lacustrine environment. Naturwissenschaften, 59(4): 158-&.

Müller, U.C., Pross, J., Tzedakis, P.C., Gamble, C., Kotthoff, U., Schmiedl, G., Wulf, S., Christanis, K., 2011. The role of climate in the spread of modern humans into Europe. Quaternary Science Reviews, 30(3–4): 273-279.

Murray, M.R., 2002. Is laser particle size determination possible for carbonate-rich lake sediments? Journal of Paleolimnology, 27(2): 173-183.

Muza, J.P., Wise, S.W., 1983. An authigenic gypsum, pyrite and glauconite association in a miocene deep-sea biogenic ooze from the Falkland Plateau, Southwest Atlantic Ocean. Initial Reports of the Deep Sea Drilling Project, 71(Sep): 361-375.

Nagels, 1970. Enzyklopädie - Reiseführer Türkei. Nagel Verlag, Genf, pp. 896.

Nazik, A., Meriç, E., Avşar, N., 2012. Reply to Discussion: a critique of Possible waterways between the Marmara Sea and the Black Sea in the late Quaternary: evidence from ostracod and foraminifer assemblages in lakes İznik and Sapanca, Turkey, Geo-Marine Letters, 2011. Geo-Marine Letters, Online First.

Nazik, A., Meriç, E., Avşar, N., Ünlü, S., Esenli, V., Gökaşan, E., 2011. Possible waterways between the Marmara Sea and the Black Sea in the late Quaternary: evidence from ostracod and foraminifer assemblages in lakes İznik and Sapanca, Turkey. Geo-Marine Letters, 31(2): 75-86.

Nehrke, G., 2007. Calcite Precipitation from aqueous solution: transformation from vaterite and role of solution stoichiometry, Universiteit Utrecht, Utrecht, 133 pp.

Nesbitt, H.W., Young, G.M., 1982. Early Proterozoic climates and plate motions inferred from major element chemostry of lutites. Nature, 299(5885): 715-717.

Neumann, F., Schölzel, C., Litt, T., Hense, A., Stein, M., 2007. Holocene vegetation and climate history of the northern Golan heights (Near East). Vegetation History and Archaeobotany, 16(4): 347-347.

Niessen, F., 2010. Geologische und geochemische Entwicklung des Iznik Sees (NW-Türkei). GEPRIS - Gefördete Projekte der DFG.

Nowaczyk, N., Melles, M., Minyuk, P., 2007. A revised age model for core PG1351 from Lake El'gygytgyn, Chukotka, based on magnetic susceptibility variations tuned to northern hemisphere insolation variations. Journal of Paleolimnology, 37(1): 65-76.

Nümann, W., 1960. Limnologische Untersuchungen einiger Anatolischer Seen. Internationale Revue gesamten Hydrobiologie, 45(1): 11-54.

Ohlendorf, C., Sturm, M., 2001. Precipitation and Dissolution of Calcite in a Swiss High Alpine Lake. Arctic, Antarctic, and Alpine Research, 33(4): 410-417.

Ohlendorf, C., Sturm, M., 2008. A modified method for biogenic silica determination. Journal of Paleolimnology, 39(1): 137-142.

Okay, A.I., 1989. Tectonic Units and Sutures in the Pontides, Northern Turkey. In: Sengör, A.M.C. (Ed.), Tectonic Evolution of the Tethyan Region. Kluwer Academic Publishers, pp. 109-116.

Okay, S., Jupinet, B., Lericolais, G., Çifçi, G., Morigi, C., 2011. Morphological and stratigraphic investigation of a Holocene subaqueous shelf fan, north of the Istanbul strait in the Black Sea. Turkish Journal of Earth Sciences, 20: 287-305.

Özcan, Z., Okay, A.I., Özcan, E., Hakyemez, A., Özkan-Altiner, S., 2012. Late Cretaceous–Eocene Geological Evolution of the Pontides Based on New Stratigraphic and Palaeontologic Data Between the Black Sea Coast and Bursa (NW Turkey). Turkish Journal of Earth Sciences, 21: 933-960.

Özdoğan, M., 2011. Archaeological Evidence on the Westward Expansion of Farming Communities from Eastern Anatolia to the Aegean and the Balkans. Current Anthropology, 52(S4): S415-S430.

Öztürk, K., Yaltirak, C., Alpar, B., 2009. The Relationship Between the Tectonic Setting of the Lake İznik Basin and the Middle Strand of the North Anatolian Fault. Turkish Journal of Earth Sciences, 18: 209-224.

Pawlowsky-Glahn, V., Egozcue, J.J., Tolosana-Delgado, R., 2011. Lecture Notes on Compositional Data Analysis, Univeristy of Girona, Technical University of Catalonia, Girona, Barcelona.

Peeters, F., Kipfer, R., Achermann, D., Hofer, M., Aeschbach-Hertig, W., Beyerle, U., Imboden, D.M., Rozanski, K., Fröhlich, K., 2000. Analysis of deep-water exchange in the Caspian Sea based on environmental tracers. Deep Sea Research Part I: Oceanographic Research Papers, 47(4): 621-654.

Peng, Y., Xiao, J., Nakamura, T., Liu, B., Inouchi, Y., 2005. Holocene East Asian monsoonal precipitation pattern revealed by grain-size distribution of core sediments of Daihai Lake in Inner Mongolia of north-central China. Earth and Planetary Science Letters, 233(3–4): 467-479.

Pfannenstiel, M., 1944. Die diluvialen Entwicklungstadien und die Urgeschichte von Dardanellen, Marmarameer und Bosporus. Geologische Rundschau, 34: 342-434.

Pichler, H., Friedrich, W., 1976. Radiocarbon-dates of Santorini volcanics. Nature, 262(5567): 373-374.

Prokopenko, A.A., Karabanov, E.B., Williams, D.F., Kuzmin, M.I., Shackleton, N.J., Crowhurst, S.J., Peck, J.A., Gvozdkov, A.N., King, J.W., 2001. Biogenic silica record of the Lake Baikal response to climatic forcing during the Brunhes. Quaternary Research, 55(2): 123-132.

Pross, J., Kotthoff, U., Muller, U.C., Peyron, O., Dormoy, I., Schmiedl, G., Kalaitzidis, S., Smith, A.M., 2009. Massive perturbation in terrestrial ecosystems of the Eastern Mediterranean region associated with the 8.2 kyr BP climatic event. Geology, 37(10): 887-890.

Pross, J., Tzedakis, P., Schmiedl, G., Christanis, K., Hooghiemstra, H., Müller, U.C., Kotthoff, U., Kalaitzidis, S., Milner, A., 2007. Tenaghi Philippon (Greece) Revisited: Drilling a Continuous Lower-Latitude Terrestrial Climate Archive of the Last 250,000 Years. Scientific Drilling, 5: 44-46.

Ramsey, C.B., 2008. Radiocarbon dating: Revolutions in understanding. Archaeometry, 50: 249-275.

Rasmussen, S.O., Seierstad, I.K., Andersen, K.K., Bigler, M., Dahl-Jensen, D., Johnsen, S.J., 2008. Synchronization of the NGRIP, GRIP, and GISP2 ice cores across MIS 2 and palaeoclimatic implications. Quaternary Science Reviews, 27(1–2): 18-28.

Ray E. Ferrell, J., Aparicio, P., Forsman, J., 2010. Interstratified clay minerals in the weathering environment. In: Fiore, S., Cuadros, J., Huertas, F.J. (Eds.), Interstratified Clay Minerals - Origin, Characterization & Geochemical Significance. AIPEA Educational Series. Associazione Italiana per lo Studio delle Argille - AISA, Bari, pp. 115-140.

Reimer, P.J., Baillie, M.G.L., Bard, E., Bayliss, A., Beck, J.W., Blackwell, P.G., Ramsey, C.B., Buck, C.E., Burr, G.S., Edwards, R.L., Friedrich, M., Grootes, P.M., Guilderson, T.P., Hajdas, I., Heaton, T.J., Hogg, A.G., Hughen, K.A., Kaiser, K.F., Kromer, B., McCormac, F.G., Manning, S.W., Reimer, R.W., Richards, D.A., Southon, J.R., Talamo, S., Turney, C.S.M., van der Plicht, J., Weyhenmeye, C.E., 2009. Intcal09 and Marine09 Radiocarbon Age Calibration Curves, 0-50,000 years calBP. Radiocarbon, 51(4): 1111-1150.

Reynolds, R.L., Rosenbaum, J.G., Rapp, J., Kerwin, M.W., Bradbury, J.P., Colman, S., Adam, D., 2004. Record of late Pleistocene glaciation and deglaciation in the southern Cascade Range. I. Petrological evidence from lacustrine sediment in Upper Klamath Lake, southern Oregon. Journal of Paleolimnology, 31(2): 217-233.

Rieu, R., Allen, P.A., Plotze, M., Pettke, T., 2007. Compositional and mineralogical variations in a Neoproterozoic glacially influenced succession, Mirbat area, south Oman: Implications for paleoweathering conditions. Precambrian Research, 154(3–4): 248-265.

Roberts, N., Black, S., Boyer, P., Eastwood, W.J., Griffiths, H.I., Lamb, H.F., Leng, M.J., Parish, R., Reed, J.M., Twigg, D., Yiğitbaşioğlu, H., 1999. Chronology and stratigraphy of Late Quaternary sediments in the Konya Basin, Turkey: Results from the KOPAL Project. Quaternary Science Reviews, 18(4–5): 611-630.

Roberts, N., Meadows, M.E., Dodson, J.R., 2001. The history of the mediterranean-type environments: climate, culture and landscape. The Holocene, 11(6): 631-634.

Roeser, P.A., Franz, S.O., Litt, T., Ülgen, U.B., Hilgers, A., Wulf, S., Wennrich, V., Akçer Ön, S., Viehberg, F.A., Çağatay, M.N., Melles, M., 2012. Lithostratigraphic and geochronological framework for the paleoenvironmental reconstruction of the last ~36 ka cal BP from a sediment record from Lake Iznik (NW Turkey). Quaternary International, 274(0): 73-87.

Rolandi, G., Petrosino, P., Mc Geehin, J., 1998. The interplinian activity at Somma-Vesuvius in the last 3500 years. Journal of Volcanology and Geothermal Research, 82(1-4): 19-52.

Rollinson, H., 1993. Using Geochemical Data: evaluation, presentation, interpretation. Longman Scientific&Technical, 352 pp.

Rollinson, H.R., 1992. Another look at the constant sum problem in geochemistry. Mineralogical Magazine, 56(385): 469-475.

Roodenberg, J., 2008. Stratigraphy and Architecture - The basal occupation levels (Phases X and IX). In: Roodenberg, J., Roodenberg, S.A. (Eds.), Life and Death in a Prehistoric Settlement in Northwest Anatolia - The Ilıpınar Excavations. Nederlands Instituut voor het Nabije Oosten, Leiden, pp. 1-34.

Roodenberg, J., 2013. Change in food production and its impact on an early 6th millennium community in northwest Anatolia. The example of Ilipinar. Praehistorische Zeitschrift, 87(2): 223-235.

Roodenberg, J., As, A.v., Roodenberg, S.A., 2008. Barcın Hüyük in the plain of Yenişehir (2005-2006) A preliminary note on the fieldwork, pottery and human remains of the prehistoric levels. Anatolica, 34: 53-60.

Rosenbaum, J.G., Reynolds, R.L., 2004. Record of Late Pleistocene glaciation and deglaciation in the southern Cascade Range. II. Flux of glacial flour in a sediment core from Upper Klamath Lake, Oregon. Journal of Paleolimnology, 31(2): 235-252.

Ruth, U., Bigler, M., Röthlisberger, R., Siggaard-Andersen, M.-L., Kipfstuhl, S., Goto-Azuma, K., Hansson, M.E., Johnsen, S.J., Lu, H., Steffensen, J.P., 2007. Ice core evidence for a very tight link between North Atlantic and east Asian glacial climate. Geophysical Research Letters, 34(3): L03706.

Ryan, W.B.F., Pitman, W.C., Major, C.O., Shimkus, K., Moskalenko, V., Jones, G.A., Dimitrov, P., Gorur, N., Sakinc, M., Yuce, H., 1997. An abrupt drowning of the Black Sea shelf. Marine Geology, 138(1-2): 119-126.

Sagona, A., Zimansky, P., 2009. Ancient Turkey. Routledge World Archaeology. Routledge, London & New York.

Sanchez-Goni, M.F., Harrison, S.P., 2010. Millennial-scale climate variability and vegetation changes during the Last Glacial: Concepts and terminology. Quaternary Science Reviews, 29(21–22): 2823-2827.

Sanchez-Goni, M.F., Landais, A., Fletcher, W.J., Naughton, F., Desprat, S., Duprat, J., 2008. Contrasting impacts of Dansgaard–Oeschger events over a western European latitudinal transect modulated by orbital parameters. Quaternary Science Reviews, 27(11–12): 1136-1151.

Santacroce, R., Cioni, R., Marianelli, P., Sbrana, A., Sulpizio, R., Zanchetta, G., Donahue, D.J., Joron, J.L., 2008. Age and whole rock–glass compositions of proximal pyroclastics from the major explosive eruptions of Somma-Vesuvius: A review as a tool for distal tephrostratigraphy. Journal of Volcanology and Geothermal Research, 177(1): 1-18.

Santisteban, J.I., Mediavilla, R., López-Pamo, E., Dabrio, C.J., Zapata, M.B.R., García, M.J.G., Castaño, S., Martínez-Alfaro, P.E., 2004. Loss on ignition: a qualitative or quantitative method for organic matter and carbonate mineral content in sediments? Journal of Paleolimnology, 32(3): 287-299.

Sarikaya, M.A., Çiner, A., Zreda, M., 2011. Quaternary Glaciations of Turkey. In: Ehlers, J., Gibbard, P.L., Hughes, P.D. (Eds.), Quaternary Glaciations - Extent and Chronology A Closer Look. Developments in Quaternary Science. Elsevier, Amsterdam, pp. 393 - 403.

Sariş, F., Hannah, D.M., Eastwood, W.J., 2010. Spatial variability of precipitation regimes over Turkey. Hydrological Sciences Journal-Journal Des Sciences Hydrologiques, 55(2): 234-249.

Sawada, K., Ogino, T., Suzuki, T., 1990. The distribution coefficients of Mg^{2+} ion between $CaCO_3$ polymorphs and solution and the effects on the formation and transformation of $CaCO_3$ in water. Journal of Crystal Growth, 106(2–3): 393-399.

Schaller, T., Moor, H.C., Wehrli, B., 1997. Sedimentary profiles of Fe, Mn, V, Cr, As and Mo as indicators of benthic redox conditions in Baldeggersee. Aquatic Sciences, 59(4): 345-361.

Schönborn, W., 2003. Lehrbuch der Limnologie. E. Schweizerbart'sche Verlagsbuchhandlung (Nägele u. Obermiller), Stuttgart, 588 pp.

Schwab, M.J., Neumann, F., Litt, T., Negendank, J.F.W., Stein, M., 2004. Holocene palaeoecology of the Golan Heights (Near East): investigation of lacustrine sediments from Birkat Ram crater lake. Quaternary Science Reviews, 23(16–17): 1723-1731.

Schwab, M.J., Werner, P., Dulski, P., McGee, E., Nowaczyk, N.R., Bertrand, S., Leroy, S.A.G., 2009. Palaeolimnology of Lake Sapanca and identification of historic earthquake signals, Northern Anatolian Fault Zone (Turkey). Quaternary Science Reviews, 28(11-12): 991-1005.

Şengör, A.M.C., Tüysüz, O., İmren, C., Sakınç, M., Eyidoğan, H., Görür, N., Le Pichon, X., Rangin, C., 2005. The North Anatolian Fault: a new look. Annual Review of Earth and Planetary Sciences, 33(1): 37-112.

Severinghaus, J.P., Brook, E.J., 1999. Abrupt Climate Change at the End of the Last Glacial Period Inferred from Trapped Air in Polar Ice. Science, 286(5441): 930-934.

Shumilovskikh, L.S., Tarasov, P., Arz, H.W., Fleitmann, D., Marret, F., Nowaczyk, N., Plessen, B., Schluetz, F., Behling, H., 2012. Vegetation and environmental dynamics in the southern Black Sea region since 18 kyr BP derived from the marine core 22-GC3. Palaeogeography Palaeoclimatology Palaeoecology, 337: 177-193.

Siever, R., Woodford, N., 1973. Sorption of silica by clay minerals. Geochimica Et Cosmochimica Acta, 37(8): 1851-1880.

Sly, P.G., 1978. Sedimentay processes in lakes. In: Lerman, A. (Ed.), Lakes - Chemistry, Geology, Physics. Springer Verlag, Berlin, pp. 65-89.

Soulet, G., Menot, G., Lericolais, G., Bard, E., 2011. A revised calendar age for the last reconnection of the Black Sea to the global ocean. Quaternary Science Reviews, 30(9-10): 1019-1026.

Stein, M., Migowski, C., Bookman, R., Lazar, B., 2004. Temporal changes in radiocarbon reservoir age in the dead sealake Lisan system. Radiocarbon, 46(2): 649-655.

Stein, M., Starinsky, A., Katz, A., Goldstein, S.L., Machlus, M., Schramm, A., 1997. Strontium isotopic, chemical, and sedimentological evidence for the evolution of Lake Lisan and the Dead Sea. Geochimica Et Cosmochimica Acta, 61(18): 3975-3992.

Stein, M., Torfstein, A., Gavrieli, I., Yechieli, Y., 2010. Abrupt aridities and salt deposition in the post-glacial Dead Sea and their North Atlantic connection. Quaternary Science Reviews, 29: 567-575.

Sturm, M., Matter, A., 1978. Turbidites and Varves in Lake Brienz (Switzerland): Deposition of Clastic Detritus by Density Currents, Modern and Ancient Lake Sediments. Blackwell Publishing Ltd., pp. 147-168.

Suguio, K., 1998. Dicionário de Geologia Sedimentar e áreas afins. Bertrand Brasil, Rio de Janeiro, pp. 222.

Taylor, K.C., Mayewski, P.A., Alley, R.B., Brook, E.J., Gow, A.J., Grootes, P.M., Meese, D.A., Saltzman, E.S., Severinghaus, J.P., Twickler, M.S., White, J.W.C., Whitlow, S., Zielinski, G.A., 1997. The Holocene-Younger Dryas Transition Recorded at Summit, Greenland. Science, 278(5339): 825-827.

Telford, R.J., Heegaard, E., Birks, H.J.B., 2004. All age-depth models are wrong: but how badly? Quaternary Science Reviews, 23(1-2): 1-5.

Terrasi, L., Campajola, F., Petrazuolo, V., Roca, M., Romano, A., Brondi, A., D'Onofrio, M., Romoli, R., Monito, K., 1999. Datazione con la spettrometria di massa ultrasensibile di campioni provenienti dall'area interessata dall'eruzione delle “Pomici di Avellino”. In: Edipuglia (Ed.), L'eruzione vesuviana delle “Pomici di Avellinoe la facies di Palma Campania (Bronzo Antico), Bari, pp. 139-146.

Thompson, S.P., Parker, J.E., Street, S.R., Tang, C.C., 2011. Morphological templating of metastable calcium carbonates by the amino acid leucine. Journal of Physics: Conference Series, 286(1): 012030.

Timmermann, A., Menviel, L., 2009. What Drives Climate Flip-Flops? Science, 325(5938): 273-274.

Tjallingii, R., Röhl, U., Kölling, M., Bickert, T., 2007. Influence of the water content on X-ray fluorescence core-scanning measurements in soft marine sediments. Geochemistry Geophysics Geosystems, 8(2): Q02004.

Tolosana-Delgado, R., Otero, N., Pawlowsky-Glahn, V., 2005. Some Basic Concepts of Compositional Geometry. Mathematical Geology, 37(7): 673-680.

Torfstein, A., Goldstein, S.L., Stein, M., Enzel, Y., 2013. Rapid communication: Impacts of abrupt climate changes in the Levant from Last Glacial Dead Sea levels. Quaternary Science Reviews, 69: 1-7.

Tucker, M., 1996. Methoden der Sedimentologie übersetzt von Gerd Hitermaier-Erhard. Ferdinand Enke Verlag Stuttgart, 366 pp.

Tucker, M.E., Wright, V.P., 1992. Carbonate Sedimentology. Blackwell Scientific Publications, Oxford, 482 pp.

Türkes, M., 1996. Spatial and temporal analysis of annual rainfall variations in Turkey. International Journal of Climatology, 16(9): 1057-1076.

Tzedakis, P.C., 2007. Seven ambiguities in the Mediterranean palaeoenvironmental narrative. Quaternary Science Reviews, 26(17-18): 2042-2066.

Ülgen, U.B., Franz, S.O., 2006. The chemical and mineralogical influence of catchment geology on lake sediment composition - Preliminary results from a multi disciplinary study on Lake Iznik (NW Turkey), 17th International Sedimentological Congress, Fukuoka.

Ülgen, U.B., Franz, S.O., Biltekin, D., Çagatay, M.N., Roeser, P.A., Doner, L., Thein, J., 2012. Climatic and environmental evolution of Lake Iznik (NW Turkey) over the last ~4700 years. Quaternary International, 274(0): 88-101.

Vaasma, T., 2008. Grain-size analysis of lacustrine sediments: a comparison of pre-treatment methods. Estonian Journal of Ecology, 57(4): 231-243.

Velde, B., 1985. Clay minerals - A physico-chemical explanation of their occurence. Developments in Sedimentology, 40. Elsevier, Amsterdam, 427 pp.

Vidal, L., Menot, G., Joly, C., Bruneton, H., Rostek, F., Cagatay, M.N., Major, C., Bard, E., 2010. Hydrology in the Sea of Marmara during the last 23 ka: Implications for timing of Black Sea connections and sapropel deposition. Paleoceanography, 25.

Viehberg, F.A., Ülgen, U.B., Damcı, E., Franz, S.O., Ön, S.A., Roeser, P.A., Çağatay, M.N., Litt, T., Melles, M., 2012. Seasonal hydrochemical changes and spatial sedimentological variations in Lake Iznik (NW Turkey). Quaternary International, 274(0): 102-111.

Voelker, A.H.L., 2002. Global distribution of centennial-scale records for Marine Isotope Stage (MIS) 3: a database. Quaternary Science Reviews, 21(10): 1185-1212.

Vogel, J.S., Cornell, W., Nelson, D.E., Southon, J.R., 1990. Vesuvius Avellino, one possible source of 17th-century-bc climatic disturbances. Nature, 344(6266): 534-537.

Wagner, B., Lotter, A.F., Nowaczyk, N., Reed, J.M., Schwalb, A., Sulpizio, R., Valsecchi, V., Wessels, M., Zanchetta, G., 2009. A 40,000-year record of environmental change from ancient Lake Ohrid (Albania and Macedonia). Journal of Paleolimnology, 41(3): 407-430.

Wagner, B., Sulpizio, R., Zanchetta, G., Wulf, S., Wessels, M., Daut, G., Nowaczyk, N., 2008. The last 40 ka tephrostratigraphic record of Lake Ohrid, Albania and Macedonia: a very distal archive for ash dispersal from Italian volcanoes. Journal of Volcanology and Geothermal Research, 177(1): 71-80.

Walker, M., Johnsen, S., Rasmussen, S.O., Popp, T., Steffensen, J.-P., Gibbard, P., Hoek, W., Lowe, J., Andrews, J., Björck, S., Cwynar, L.C., Hughen, K., Kershaw, P., Kromer, B., Litt, T., Lowe, D.J., Nakagawa, T., Newnham, R., Schwander, J., 2009. Formal definition and dating of the GSSP (Global Stratotype Section and Point) for the base of the Holocene using the Greenland NGRIP ice core, and selected auxiliary records. Journal of Quaternary Science, 24(1): 3-17.

Wanner, H., Butikofer, J., 2008. Holocene Bond cycles: real or imaginary? Geografie, 113(4): 338-350.

Weaver, C.E. (Ed.), 1989. Clays, Muds, and Shales. Developments in Sedimentology, 44. Elsevier, 819 pp.

Wenk, H.-R., Bulakh, A., 2004. Minerals - Their constitution and origin. Cambridge University Press, Cambridge, 646 pp.

Wester, R., 1989. Wasserwirtschaftlicher Rahmenplan für das Izniksee-Gebiet/Türkei. Fachhochschule Rheinland-Pfalz, Abteilung Mainz I - Fachbereich Bauingenieurwesen.

Wetzel, R.G., 2001. Limnology lake and river ecosystems. Elsevier Academic Press, San Diego, 1006 pp.

Wick, L., Lemcke, G., Sturm, M., 2003. Evidence of Lateglacial and Holocene climatic change and human impact in eastern Anatolia: high-resolution pollen, charcoal, isotopic and geochemical records from the laminated sediments of Lake Van, Turkey. Holocene, 13(5): 665-675.

Wolff, E.W., Chappellaz, J., Blunier, T., Rasmussen, S.O., Svensson, A., 2010. Millennial-scale variability during the last glacial: The ice core record. Quaternary Science Reviews, 29(21–22): 2828-2838.

Wulf, S., Kraml, M., Brauer, A., Keller, J., Negendank, J.F.W., 2004. Tephrochronology of the 100 ka lacustrine sediment record of Lago Grande di Monticchio (southern Italy). Quaternary International, 122(1): 7-30.

Wulf, S., Kraml, M., Kuhn, T., Schwarz, M., Inthorn, M., Keller, J., Kuscu, I., Halbach, P., 2002. Marine tephra from the Cape Riva eruption (22 ka) of Santorini in the Sea of Marmara. Marine Geology, 183(1-4): 131-141.

Yagci, M.A., Ustaoglu, M.R., 2012. Zooplankton fauna of Lake Iznik (Bursa, Turkey). Turkish Journal of Zoology, 36(3): 341-350.

Yaltırak, C., 2002. Tectonic evolution of the Marmara Sea and its surroundings. Marine Geology, 190(1-2): 493-529.

Yaltirak, C., Alpar, B., 2002. Evolution of the middle strand of North Anatolian Fault and shallow seismic investigation of the southeastern Marmara Sea (Gemlik Bay). Marine Geology, 190(1-2): 307-327.

Yaltirak, C., Ülgen, U.B., Zabci, C., Franz, S.O., Ön, S.A., Sakmç, M., Çagatay, M.N., Alpar, B., Öztürk, K., Tunoglu, C., Ünlü, S., 2011. Discussion: a critique of Possible waterways between the Marmara Sea and the Black Sea in the late Quaternary: evidence from ostracod and foraminifer assemblages in lakes İznik and Sapanca, Turkey, Geo-Marine Letters, 2011. Geo-Marine Letters, online first DOI 10.1007/s00367-011-0270-y.

Yanko-Hombach, V., Gilbert, A.S., Dolukhanov, P., 2007. Controversy over the great flood hypotheses in the Black Sea in light of geological, paleontological, and archaeological evidence. Quaternary International, 167: 91-113.

Yavuz, V., Akcar, N., Schlüchter, C., 2007. The frozen Bosphorus and its paleoclimatic implications based on a summary of the historical data. In: Yanko-Hombach, V., Gilbert, A., Panin, N., Dolukhanov, P. (Eds.), The Black Sea Flood Question: Changes in Coastline, Climate, and Human Settlement. Springer Netherlands, pp. 633-649.

Yihui, D., Chan, J.C.L., 2005. The East Asian summer monsoon: an overview. Meteorology and Atmospheric Physics, 89(1-4): 117-142.

Yilmaz, Y., Genc, S.C., Yigitbas, E., Bozcu, M., Yilmaz, K., 1995. Geological evolution of the late-Mesozoic continental-margin of northwestern Anatolia. Tectonophysics, 243(1-2): 155-171.

Yilmaz, Y., Gokasan, E., Erbay, A.Y., 2010. Morphotectonic development of the Marmara Region. Tectonophysics, 488(1-4): 51-70.

Acknowledgements

I would like to express my deep gratitude to my research supervisors Thomas Litt and Sven Oliver Franz for offering me this fascinating subject to work with, for scientific guiding and absolute support during the past years, for independency to develop the present work and for plenty of room for discussion. I further thank Sven for sharing his knowledge on geochemistry and Thomas for his pragmatism.

I am very thankful to the paleobotany working group for support during the past years, for critical and constructive discussions in a pleasant environment. At the University of Bonn, Steinmann Institute, I further appreciated productive discussions with Tom McCann, Andreas Schäfer, and Horst Wörmann. For orientation in laboratory and discussions I thank Sven Berkau, Camilla Kurth, Bettina Schulte-van Berkum, and Rainer Schwarz. For mineralogical analysis and support in treatment of diffraction data I thank Harald Euler and Bruno Barbier. For assistance with geochemical analysis I thank Radegund Hoffbauer and Dorothee Dohle. I thank Georg Heumann, Dirk Handwerk, and Thorsten Wappler for a great and fun field campaign at Lake Iznik in September 2009. The photographs taken by Georg Oleschinsky for detailed core documentation and his assistance with REM analysis are acknowledged for. The processing and analysis of the samples referring to results presented herein - and some more - was assisted by the students Miriam Sass, Beate Hacker, and Jani Biber. I also am thankful for the help of Hannah Vossel and Manuela Rüssmann who segregated material for radiocarbon dating.

This work was financed in the framework of the *SFB 806* – Our way to Europe. I further appreciate a scholarship from DAAD (*Doktorandenkurzstipendium*) for a scientific stay at Istanbul Technical University – ITU, in the Eastern Mediterranean Centre for Oceanography and Limnology – EMCOL, from June to August 2012.

I am grateful to Namık Çağatay for receiving me as a guest at EMCOL, as well as for scientific discussions during the past years. I also thank Celal Şengör for access to a unique library from which this work also profited. From ITU/EMCOL I further thank Umut Ülgen and Sena Akçer for coordination of the 2009 field work. I thank Sena Akçer and Dursun Acar for the data generated by first core loggings. I am thankful to Umut Ülgen for several productive discussions, exchanging ideas and sharing his experience with working on Lake Iznik's sedimentary geochemistry.

From the Quaternary Geology group of the University of Cologne I appreciate the usage of the Itrax core scanner and I therefore thank Martin Melles, and the support offered by Volker Wennrich and Armine Shahnazarian. Finn Viehberg is thanked for providing geochemical data from Iznik surface sediments.

Key contributions for first data analysis came from OSL measurements and geochemical identification of selected tephra material. I respectively thank Alexandra Hilgers (Institute of Geography, University of Cologne) and Sabine Wulf (Geoforschungszentrum - GFZ, Potsdam) for sample processing, and assistance with data interpretation. Further data

contribution to this work comes from isotopic analysis by Nils Andersen (Leibniz Laboratory for Radiometric Dating and Isotope Research, Kiel). The experience and orientation of Michael Köhler (MK Factory, Potsdam) during the field campaign are deeply appreciated.

I much appreciate that during the compilation of the written part of the thesis and data interpretation several people contributed with careful reading drafts of chapters and exchange of ideas, offering room for discussion. I therefore thank Josep Antoni Martín Fernández (Dept. d'Informàtica i Matemàtica Aplicada, Universitat de Girona), Georg Heumann (Steinmann Institute, University of Bonn), Neil Roberts (University of Plymouth), Axel Schmidt (Bundesanstalt für Gewässerkunde, Koblenz), and Horst Wörmann (Steinmann Institute, University of Bonn). I am also thankful to Rolf Kipfer (Department Umweltsystemwissenschaften – ETH, Zürich) for a great amount of constructive critique.

Kürşad Kadir Eriş (Fırat University, Turkey) and Deniz Cukur (GEOMAR Helmholtz-Zentrum für Ozeanforschung Kiel) are thanked for the translation of the thesis summary into Turkish and its revision, respectively.

I thank Kurt Friese (Helmholtzzentrum für Umweltforschung – UFZ, Magdeburg), Barbara Reichert (Steinmann Institute, University of Bonn), and Wulf Amelung (INRES, University of Bonn), for being members of the examination committee for this work.

I certainly extend my deep gratitude to my family and my friends, who kept me going on the rollercoaster of writing this document. This work is dedicated to Raíssa – friend with whom I shared the experience of moving to a foreign country, and to her baby girl Lara, who saw the day of light by the time this manuscript was being submitted.

I specially thank my father, Hubert Mathias Peter Roeser, for a detailed revision of this manuscript before the final printing.

“The pursuit of ignorance”

Appendices

Table of Contents

Appendix A2.1

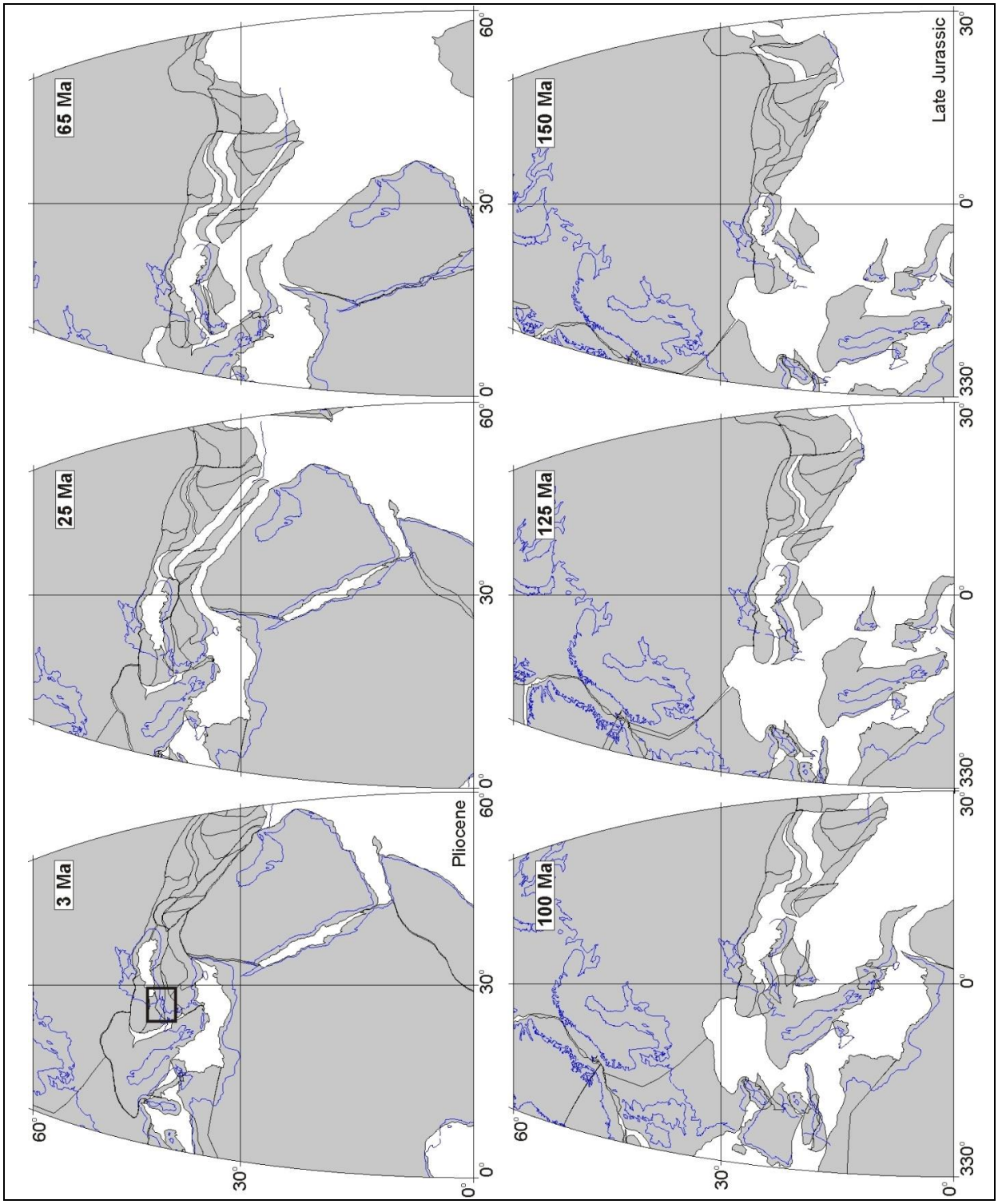

Figure: Paleogeographical evolution of the Eastern Mediterranean and adjacent regions from Late Jurassic to Pliocene. Reconstruction made using the Ocean Drilling Stratigraphic Network (ODSN) - Plate Tectonic Reconstruction Service. Plate tectonic maps and calculations are according to Hay et al. (1999), and Cox and Hart (1986); further references are given at ODSN (2011). For the reconstruction plates were moved in relation to the magnetic reference frame. Representation is in Mollweide projection. Black lines separate plate fragments and thin blue lines indicate present day shorelines. Black square in first map (3 million years before present, Ma) marks present day location of Sea of Marmara.

Appendix A2.2

Table: selected metereological information for Iznik Lake Basin[1].

Paramater	Station name, Elevation [m.a.s.l.], Observation time frame [years]	J	F	M	A	M	J	J	A	S	O	N	D	Year
Prevailing wind direction	Iznik, 88, 2	E	E	SW	E	W	W	W	W	E	E	E	E	E
Strongest measured wind, direction and strength [Beaufort]	Iznik, 88, 2	E 8	W 8	SW 8	E 5	W 7	NE 4	NE 4	W 3	E 4	NE 4	W 7	E 7	E, W 8
Number of stormy Days [6 < Beaufort < 7]	Iznik, 88, 2	1.5	1.5	0.5	-	0.5	-	-	-	-	-	0.5	3.5	8
Number of days with more than 0.1 mm rainfall	Iznik, 88, 28	12.1	12.1	11.4	9.2	8.2	5.2	3.1	2.3	4.4	7.1	9	12	96.1
Number of days with more than 10 mm rainfall	Iznik, 88, 28	2	1.7	1.6	1.4	1.3	1.1	0.7	0.3	1.2	1.1	1.5	2.2	16
Maximum Daily precipitation [mm]	Iznik, 88, 28	63.3	43.7	32.6	24.9	29.5	50.7	53.7	66	71.2	35.3	72.2	40.4	71.2
Average days with storm	Iznik, 88, 23	0.2	0.3	0.1	0.7	2.1	1.9	0.9	0.8	0.9	0.5	0.3	0.2	8.7
Average days with hail	Iznik, 88, 23	-	-	-	-	0.1	0.3	0.1	-	-	0.1	-	-	0.6
Average days with hail	Mecidiye, 550, 3	-	-	-	1	4	3	1	2	-	-	-	-	10
Average days with snowfall	Iznik, 88, 10	1.8	1.6	0.1	-	-	-	-	-	-	-	-	0.3	3.8
Average days with snowfall	Mecidiye, 550, 3	8	12	6	1	-	-	-	-	-	-	1.7	2.7	34.4
Highest measured snowcover [cm]	Iznik, 88, 22	42	70	15	-	-	-	-	-	-	-	20	20	70
Highest measured snowcover [cm]	Mecidiye, 550, 3	63	145	120	-	-	-	-	-	-	-	-	38	145
Highest measured snowcover [cm]	Haciosman, 900, 2	76	127	85	-	-	-	-	-	-	-	-	46	127

[1] compilation of data presented in Wester (1989); originated from different meteorological stations located within the Iznik Lake Basin, operated by the Turkish State Meteorological Service - DMI (Iznik) and the General Directorate of State Hydraulic Works - DSI (Mecidiye, Haciosman)

Appendix A2.3

Field campaign September/October 2009

Figure: Five piston core sections (2 m each) recovered in one day. From left to right Muhsine Kocakurt (MTA), Thorsten Wappler (Uni Bonn), Georg Heumann (Uni Bonn), Sven Oliver Franz (Uni Bonn), Dirk Handwerk (Uni Bonn), Patricia Roeser (Uni Bonn), and Ali Okkali (Iznik).

Figure: Sven Oliver Franz indicates the lake level from 2005. The present water level in Lake Iznik is controlled by a dam at the Karsak outflow. Additionally, water from the lake is used for farming in the basin.

Appendix A3.1

Sampling Strategy

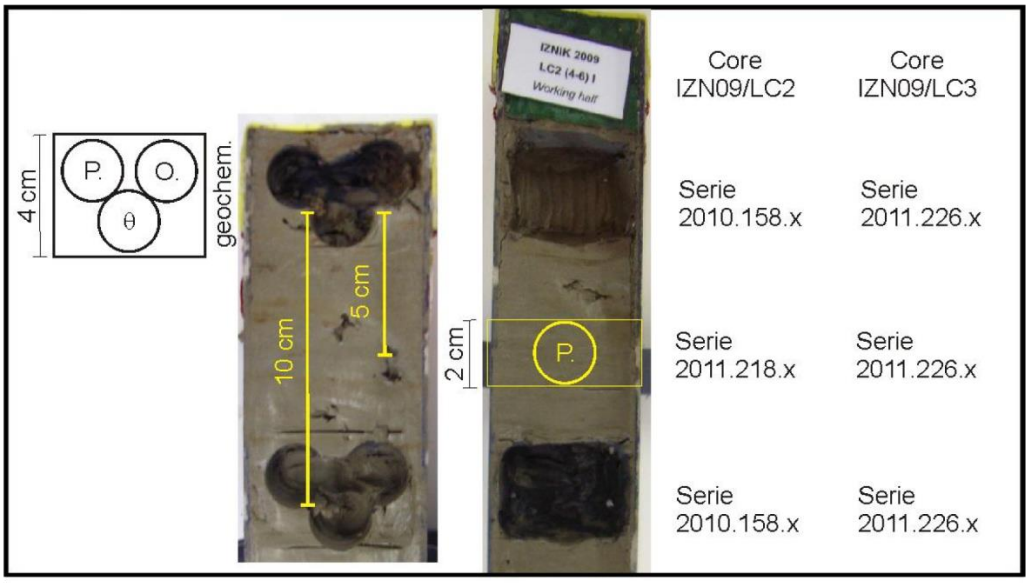

Sampling strategy for Iznik cores (tabular form) relating type of samples and sampling resolution to the sediment cores (IZN09/LC2 and IZN09/LC3), for each of the sampling series (2010.158, 2011.218 and 2011.216)

Type and volume of samples taken were
P: pollen, 4cm^3
O: ostracodes, 8cm^3
Theta: water content, 5 cm^3
and sample for geochemistry/mineralogy integrates the correspondent 4 cm or 2 cm interval.

Pollen and ostracod samples come accurately from the same depth; water content is circa 1.5 cm dislocated in relation to the former.

Sampling series 2010.158 and 2011.218 intercalate at core IZN09/LC2 generating a 5 cm resolution sampling.

Sample series 2011.226 corresponds to samples taken from core IZN09/LC3 in 5 cm resolution, alternating the same strategies applied for 2010.158 and 2011.218.

Sample depth were occasionally shifted to respect abrupt changes in lithology, or to preserve sedimentary structural facies.

Appendix A3.2

Protocol for pre-treatment of sediment samples for grain size analysis

15.06.12 – 15.08.12 (DAAD scholarship)
EMCOL Sedimentology laboratory / Istanbul Technical University

This protocol was developed according to literature references and small experiments in laboratory, and used for sediment samples of Lake Iznik, NW Turkey. For the analysis of sediments with different origin, the pre-treatment may have to be adapted, depending on the characteristics of the sediments to be analyzed. After each of the steps 1, and 2, (removal of carbonates and organics, respectively), it should be tested if samples are still reacting (production of air bubbles). Total inorganic carbon and total organic carbon measurements can be helpful to evaluate on the need of further addition of reagent. As a reference, some approximate values of parameters from the Iznik sediments are (1) maximum carbonate content circa 40%; (2) maximum total organic carbon circa 10%

One aspect of the preparation that should not be neglected is the amount of sample material to be prepared. At the end, two or three measurements are to be undertaken to have reproducible results. In general a few milliliters of sediment suspension are enough for that. Hence, one should reduce the sediment amount from the beginning, as sampling too much sediment will not only consume more of the reagents, as will also increase the pre treatment time. Circa 1 cm^3 of sampling material should be more than enough to undertake repeated measurements. It is recommended to undertake the pre-treatment on some samples first, to ensure there is enough sediment left at the end of the process to run analysis.
The sampled sediment can be deposited directly into the centrifuge tubes, in which they will be subjected to following pre-treatments:

1) **Removal of carbonates**
   Addition of 20 ml of a 10% (v/v) HCl solution, in two steps of 10 ml.
   Leave samples reacting at room temperature for two hours, and then heat up to 60^{o}C in a water bath for two hours, until no more reaction is observed.
   Centrifuge samples to remove the acid, at 3000 rpm for 5 minutes*.
   The supernatant should be discarded into the 'Acid effluents' tank.
   Wash the samples two times: add distilled water, stir up with a spatula, centrifuge at 3000 rpm for 5 minutes and discard supernatant.

Calculated centrifugation times are according to (Tanner and Jackson, 1947)

2) **Removal of organic matter**
   First Day: Addition of 20 ml 15% (v/v) H_2O_2 solution, in two steps of 10 ml.
   Leave the samples reacting at room temperature for three hours. Observe the samples during that time, as the reaction can be intense, and care should be taken that no sample material gets lost over the borders of centrifuge tube. Stirring with a spatula once in a while can break superficial tension of formed air bubbles.
   Heat up to 60^{o}C in water bath, for 2 hours.
   Leave in closed water bath with the residual heat overnight.
   Second day: Heat up to 60^{o}C in water bath for ca. 6 hours
   Leave in closed water bath with the residual heat overnight.
   Third day: Heat up to 60^{o}C in water bath for ca. 5 hours.
   Centrifuge samples to remove the residual peroxide, at 3000 rpm for 5 minutes.
   The supernatant should be discarded into the 'Acid effluents' tank.
   Wash the samples two times: add distilled water, stir up with a spatula, centrifuge at 3000 rpm for 5 minutes and discard supernatant.

3) **Removal of the amorphous silica**
   Add 10ml of a 10% (m/v) solution of KOH.

Leave samples reacting for two hours, and then heat up to 60^{o}C in the water bath for 30 minutes.
Centrifuge samples to remove the residual peroxide, at 3000 rpm for 5 minutes.
The supernatant should be discarded into the 'Alkaline effluents' tank.
Wash samples two times: add distilled water, and centrifuge at 3000rpm, 5 min.

4) Grain size measurements

Dispersion

Add 20ml of a 1% (m/v) Pirofosfat solution to the samples 12 hours before analysis.
If possible, samples should be placed on a shaker overnight.

Before measurement, centrifuge tubes containing the sample/pirofosfat suspension should be left on the magnetic stirrer for circa one hour before analysis. The cone form of the end of the centrifuges has the effect that the magnetic fish gets inclined, contributing to a good mixture. A good dispersion can be observed on the surface of the suspension through the appearance of 'current' lines, as if one is stirring paint.
Additionally, shortly before measurement each sample should be mixed with a plastic Pasteur pipette, for circa 10 times, observing that the small volume in the centrifuge, ca 20ml, gets completely homogenized each time. Applying some pressure when returning the suspension to the centrifuge tube will additionally avoid that coarser material settles at the bottom.

Measurement

Each measurement should consist of: background measurement, and sample measurement (in case of Iznik samples 3 scans of 3 seconds each). Samples should be diluted to obscuration values between 7 and 14.
For a high reproducibility of the grain size analyses, it should be undertaken under permanent dispersing conditions (Murray, 2002); therefore the equipment should be fed with the dispersing pirofosfat solution. Therefore add 30ml of the 1% pirofosfat solution directly to the tank of the grain size Analysette 22 Compact before clicking the button 'start analysis'. Note that the background measurement will be undertaken with the pirofosfat solution, and the tank should be cleaned after the analysis, otherwise the solution would be discarded before analysis.
Samples should be measured at least two times, until reproducibility is achieved.

Murray, M. R. (2002). Is laser particle size determination possible for carbonate-rich lake sediments? *Journal of Paleolimnology* **27,** 173-183.

Tanner, C. B., and Jackson, M. L. (1947). Nomographs of Sedimentation Times for Soil Particles Under Gravity or Centrifugal Acceleration. *Soil Science Society of America Journal* **12,** 60-65.

Appendix A6.1

Appendix A6.1

1.1 Concepts for application of CoDa analysis

Intrinsic characteristics of compositional data (CoDa) are: (1) compositional data are vectors of positive components which sum up to a total (or constant) sum, and c*losure* of the variables refers to their expressions as proportions of the constant sum (*k*); (2) the parts represent relative information (3) the sampling space is the *simplex.* (Aitchison, 2003b). In order to undertake compositional analysis, the requirements for the data are: scale invariance – the analysis should not depend on the closure constant (*k*), permutation invariance – the order of parts is irrelevant, and subcompositional coherence – studies on subcompositions are in agreement with those performed on the full composition (Aitchison, 1982).

The compositional geometry is completely equivalent to the standard Euclidian geometry in real space. Fundamental operations in the Aitichson geometry are *perturbation* and *powering*, which are handled formally within the simplex likewise standard vector operations *sum* and *scaling* in multidimensional real space (Tolosana-Delgado et al., 2005).

The logratio transformations, applied to CoDa in the simplex, are of three types: (1) additive log-ratio (alr), (2) centered log-ratio (clr), and (3) isometric log-ratio (ilr). Mathematical definitions of each of the transformations, and further definitions inside the Aitchison geometry, are given in appendix A6.2 (Tolosana-Delgado, 2008).

The exploratory statistical analysis of compositional data consists of the following steps: (1) compute the descriptive compositional statistics, (2) center the data for a better visualization in ternary diagrams, (3) investigate the clr-biplot to discover patterns in the data set, (4) define an appropriate representation on orthonormal coordinates, and (5) compute the summary statistics of the coordinates and represent results in a balance dendogram (Pawlowsky-Glahn et al., 2011). Each of these steps is briefly commented in the following paragraphs.

For compositional data, classical statistical summaries carry no information, due to the spurious correlation effect. Therefore, the compositional summary is used, which consists of the determination of the geometrical mean of the composition, and the investigation of the variation matrix, which describes the dispersion in the compositional data set. It is a tool to analyze the relations between the pairs of variables (geochemical elements or minerals). The total variance gives a measure of global dispersion of the composition.

Centering the compositional data, means that a perturbation is applied to shift the data set around its barycenter. For this, the samples are perturbed by the opposite of the geometric mean, $\mathbf{g}^{-1}$. Centering the data set is used for better visualization within the ternary diagrams.

A useful exploratory tool which represents at the same time the samples and the related variables is the clr-biplot, which is a projection of the variability of the data (Tolosana-

Delgado, 2012). Likewise a principal component analysis, it consists of a singular value decomposition, applied for the matrix of centered logratio transformed data (Aitchison and Greenacre, 2002). The biplot has unique mathematical properties, which are used for interpretation of results. The most striking property is that information is contained mainly in the links, i.e. distances between the apexes, or vertices (Aitchison and Greenacre, 2002). The length of links is proportional to the variance in-between the variables. Furthermore, the angles in-between links in the covariance biplot can give an estimation of the relationship between the variables (Aitchison and Greenacre, 2002). For instance, orthogonal links indicate that the associated logratios might be independent. Additionally, coincident vertices (very small variance in-between links) carry the same, or redundant, information. Whilst for collinear vertices the associated subcomposition is a one dimensional biplot, i.e. a compositional line (Aitchison, 2003a) The biplot does not allow to conclude on only one component, because as the projection refers to a clr logratio transformation (which contains the ratio to the geometric mean of the complete composition) it implies a weight of all the parts and not only a single component.

As a result of the exploratory analysis, or given *a priori* knowledge of the data set, the investigation of a certain sequential binary partition might become interesting. A graphical representation for the coordinates based on such a partition is the balance dendogram (Egozcue and Pawlowsky-Glahn, 2006; Pawlowsky-Glahn et al., 2011). CoDa balance-dendograms are not dendograms in the ‘traditional’ sense. They go beyond descriptive statistics, and represent a first step to conceptualizing the data, as the balances are defined according to reasonable interpretation approaches. The graphical display of balance dendograms are represented by structure from which we can read mainly two characteristics for each coordinate: (1) the sample variance, which is given by the ‘height’ of the vertical line (2) the sample mean, which is indicated by the contact point (Pawlowsky-Glahn et al., 2011 and references therein).

1.2 Major Elementes – Itrax Core scanner

1.2.1 Variation Matrix

Variation matrix for the subcomposition (Al, Si, S, K, Ca, Ti, Fe, Sr) obtained from the Itrax core scanner (1 cm resolution, i.e. sample size 1316). Bold values in blue fields highlight, and green fields mark the smallest variances. Reddish fields highlight high variances[1].

Variance ln(Xi/Xj)

Xi\Xj	Al	Si	S	K	Ca	Ti	Fe	Sr	clr variances
Al		0.0454	0.842	0.0434	0.9769	0.0419	0.0511	0.5538	0.1498
Si			0.6416	**0.0074**	0.7368	0.0169	0.0244	0.3605	0.0596
S				0.6413	0.3721	0.6861	0.6654	0.2663	0.3448
K					0.7627	**0.0075**	0.0165	0.3798	0.0628
Ca						0.8385	0.8448	0.132	0.4135
Ti							0.0123	0.4331	0.085
Fe								0.4469	0.0882
Sr									0.1521
								Total variance	**1.3559**

1.2.2 Balances

Possible ilr binary partition for the data of subcomposition (Al, Si, S, K, Ca, Ti, Fe, Sr). Data obtained from the Itrax core scanner (1 cm resolution, i.e. sample size 1316)

balance	Al	Si	S	K	Ca	Ti	Fe	Sr	
b1	-1	-1	-1	-1	+1	-1	-1	+1	(a)
b2	0	0	0	0	-1	0	0	+1	(c)
b3	-1	-1	1	-1	0	-1	1	0	(d)
b4	0	0	1	0	0	0	-1	0	(d)
b5	-1	-1	0	-1	0	1	0	0	(b)
b6	-1	1	0	-1	0	0	0	0	(b)
b7	1	0	0	-1	0	0	0	0	(b)

The letters in the last column, classify the balances according to the four aspects described in section 6.5, first paragraph.

The resulting balances are interpreted as:

1) importance of carbonate phase relative to detrital fraction
2) importance of strontium co-precipitation in carbonate
3) distribution of monosulfides against detrital elements
4) importance of sulfide precipitation
5) distribution of silicates and clay minerals (K, Al, Si) against Ti, i.e. evaluating if Ti is contained in clay minerals
6) distribution of micas and kaolinite against Si (which has possible biogenic influence) [2]
7) distribution of micas against kaolinite

[1] Per definition the variance matrix is symmetric, and its diagonal will contain only zeros, therefore, only the upper half is represented herein. The variances measure the dispersion of the elements within the compositional data set. Hence, smaller values for the variance of the logratio for two elements, means that their behavior is closely related (blue and green fields).

[2] Note that the interpretation of balances 5 and 6 is not without problem, since Al and Si are elements common to a variety of feldspars and clay minerals. Still, it was considered valuable to evaluate whether further conclusion can be drawn from these balances.

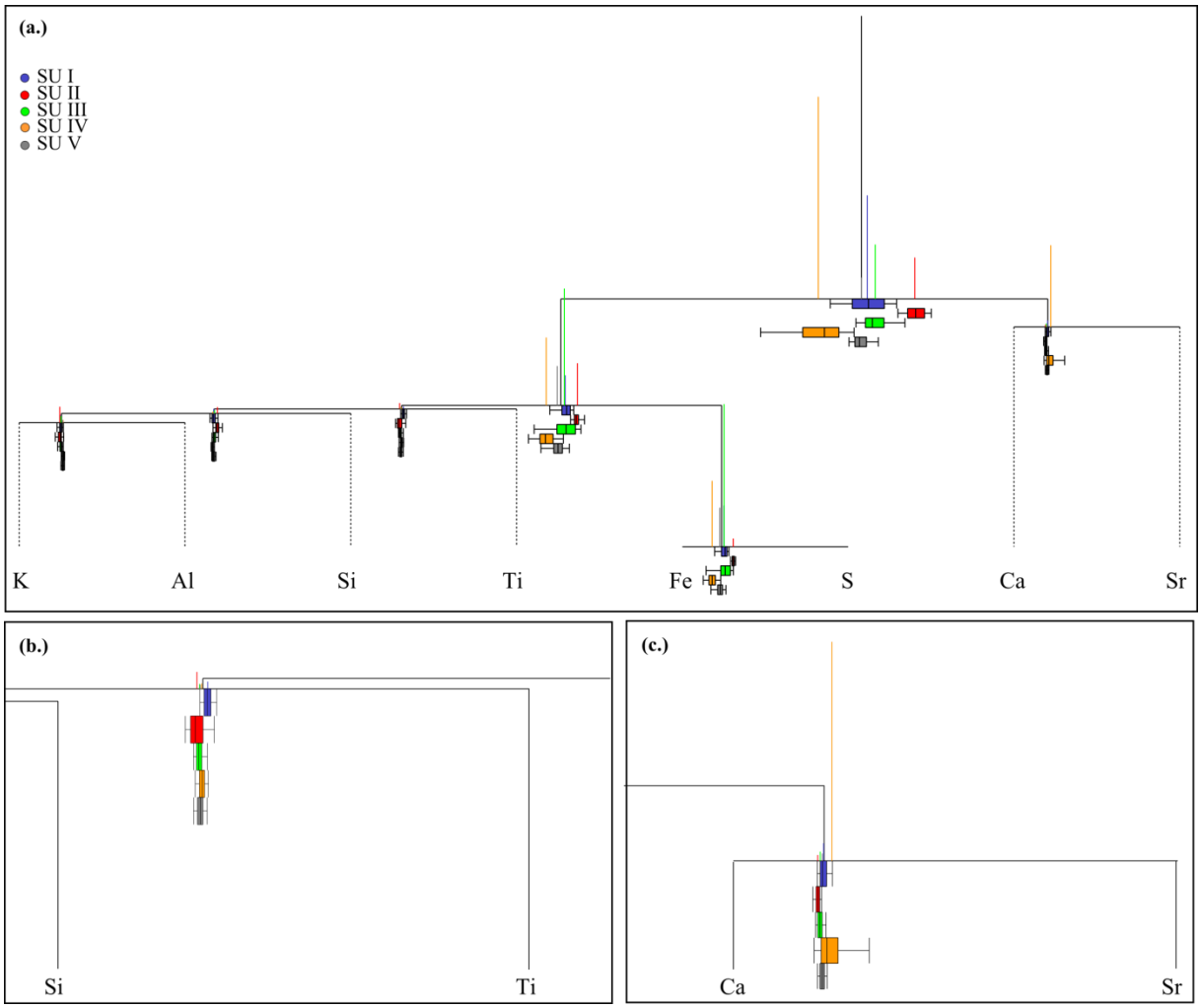

(a) Full balance-dendogram of data of subcomposition (Al, Si, S, K, Ca, Ti, Fe, Sr), using the defined balances; (b) and (c) zoomed parts of the full balance dendogram, related to balances b2 (Ca, Sr) and b3 (redox against detritals), respectively.

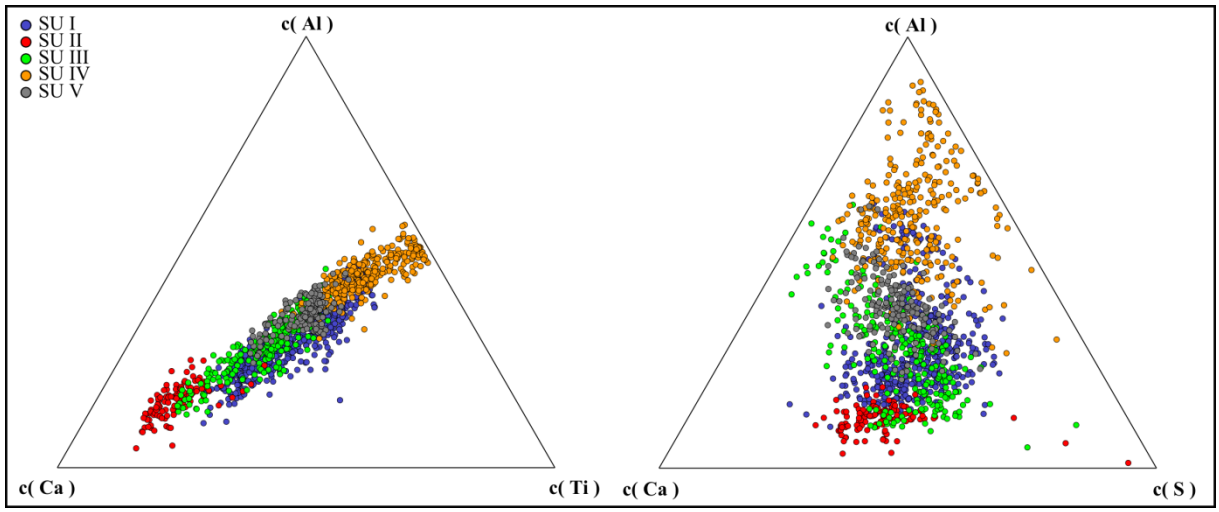

Ternary plot of centered data of subcomposition (Al, Ti, Ca).

1.3 Major and trace elements - absolute concentrations

1.3.1 Variation Matrix

Variance ln(Xi/Xj)

Xi\Xj	S	TOC	TIC	Si	Al	Fe	Mn	Mg	Ca	Na	K	Ti	P	V	Cr	Co	Ni	Cu	Zn	Ga	As	Rb	Sr	Y	Zr	Nb	Ba	W	Pb	Th	U	clr variances
N	0.192	0.041	0.402	0.140	0.153	0.158	0.246	0.098	0.261	0.159	0.174	0.142	0.097	0.143	0.171	0.144	0.172	0.122	0.136	0.159	0.161	0.166	0.117	0.136	0.150	0.181	0.101	0.175	0.103	0.152	0.075	0.082
S		0.186	0.417	0.311	0.326	0.322	0.465	0.212	0.284	0.321	0.338	0.314	0.288	0.308	0.339	0.297	0.332	0.277	0.302	0.330	0.306	0.330	0.158	0.299	0.322	0.350	0.248	0.345	0.253	0.311	0.181	0.221
TOC			0.344	0.302	0.320	0.326	0.431	0.177	0.214	0.317	0.348	0.304	0.214	0.305	0.341	0.302	0.340	0.270	0.294	0.329	0.298	0.336	0.101	0.293	0.316	0.357	0.231	0.347	0.241	0.309	0.164	0.203
TIC				0.636	0.666	0.658	0.697	0.506	0.047	0.614	0.694	0.646	0.519	0.650	0.698	0.647	0.699	0.604	0.644	0.684	0.595	0.692	0.167	0.627	0.668	0.717	0.525	0.697	0.580	0.651	0.428	0.488
Si					0.004	0.006	0.062	0.093	0.482	0.017	0.007	0.003	0.044	0.003	0.012	0.006	0.015	0.008	0.005	0.006	0.066	0.007	0.281	**0.002**	**0.002**	0.009	0.011	0.015	0.011	0.013	0.068	0.014
Al						0.005	0.068	0.093	0.512	0.032	**0.002**	**0.001**	0.058	**0.002**	0.005	0.006	0.007	0.006	**0.002**	**0.001**	0.087	**0.002**	0.305	**0.003**	**0.003**	0.005	0.016	0.012	0.015	0.012	0.082	0.019
Fe							0.052	0.100	0.509	0.028	0.006	0.005	0.052	0.004	0.010	0.008	0.012	0.010	0.006	0.006	0.079	0.007	0.308	0.004	0.005	0.009	0.018	0.008	0.016	0.016	0.081	0.020
Mn								0.188	0.586	0.069	0.068	0.068	0.089	0.067	0.078	0.075	0.085	0.083	0.073	0.070	0.127	0.072	0.403	0.064	0.065	0.071	0.085	0.062	0.081	0.072	0.157	0.084
Mg									0.368	0.129	0.102	0.086	0.073	0.086	0.093	0.085	0.088	0.074	0.082	0.096	0.162	0.097	0.206	0.081	0.092	0.100	0.073	0.114	0.073	0.105	0.095	0.057
Ca										0.459	0.540	0.494	0.378	0.496	0.543	0.490	0.544	0.453	0.489	0.527	0.447	0.535	0.061	0.476	0.510	0.560	0.378	0.543	0.426	0.497	0.282	0.350
Na											0.036	0.029	0.043	0.030	0.047	0.030	0.053	0.036	0.031	0.036	0.053	0.038	0.270	0.025	0.023	0.039	0.026	0.040	0.031	0.033	0.070	0.030
K												0.004	0.068	0.004	0.004	0.008	0.007	0.009	0.005	**0.003**	0.092	**0.001**	0.328	0.005	0.005	0.003	0.021	0.013	0.019	0.012	0.092	0.026
Ti													0.052	**0.002**	0.005	0.005	0.008	0.004	**0.002**	**0.003**	0.081	0.004	0.291	**0.002**	**0.002**	0.006	0.014	0.013	0.013	0.014	0.077	0.015
P														0.053	0.070	0.055	0.073	0.051	0.051	0.062	0.084	0.066	0.211	0.046	0.051	0.070	0.034	0.065	0.041	0.060	0.064	0.031
V															0.006	0.005	0.008	0.004	**0.002**	**0.002**	0.080	0.003	0.292	**0.002**	**0.002**	0.005	0.014	0.012	0.011	0.012	0.075	0.015
Cr																0.008	**0.002**	0.008	0.006	0.004	0.101	0.004	0.332	0.007	0.007	0.004	0.025	0.016	0.022	0.019	0.099	0.028
Co																	0.010	0.007	0.005	0.006	0.078	0.007	0.286	0.005	0.005	0.009	0.015	0.016	0.014	0.016	0.074	0.016
Ni																		0.009	0.007	0.006	0.108	0.006	0.331	0.010	0.011	0.007	0.028	0.019	0.025	0.022	0.100	0.029
Cu																			0.003	0.006	0.084	0.007	0.258	0.005	0.007	0.010	0.011	0.019	0.011	0.016	0.066	0.010
Zn																				**0.003**	0.082	0.004	0.285	**0.002**	0.003	0.006	0.013	0.014	0.012	0.013	0.073	0.014
Ga																					0.090	**0.002**	0.316	0.003	0.003	0.004	0.019	0.012	0.017	0.013	0.087	0.022
As																						0.091	0.272	0.075	0.072	0.091	0.063	0.089	0.071	0.077	0.093	0.064
Rb																							0.322	0.005	0.004	**0.003**	0.020	0.013	0.017	0.011	0.089	0.024
Sr																								0.278	0.302	0.344	0.197	0.335	0.233	0.289	0.124	0.181
Y																									**0.002**	0.007	0.011	0.012	0.010	0.012	0.069	0.012
Zr																										0.004	0.014	0.012	0.013	0.013	0.078	0.018
Nb																											0.025	0.015	0.022	0.015	0.101	0.030
Ba																												0.029	0.010	0.018	0.041	0.004
W																													0.027	0.024	0.099	0.032
Pb																														0.022	0.046	0.009
Th																															0.076	0.023
U																																0.035

Values rounded to three decimals for representation purposes; blue cells show low variance between variables.

Total variance **2.2021**

1.3.2 Balances

1.3.2.1 Major elements

Possible ilr binary partition for data of major element subcomposition (C_{org}, Na, Mg, S, Ca, Ti, Mn)

balance	C_{org}	Na	Mg	S	Ca	Ti	Mn	
b1	+1	-1	+1	+1	+1	-1	-1	(a)
b2	-1	0	+1	-1	+1	0	0	(a)
b3	0	0	-1	0	+1	0	0	(c)
b4	+1	0	0	-1	0	0	0	(d)
b5	0	+1	0	0	0	-1	-1	(b)
b6	0	0	0	0	0	+1	-1	(d)

The letters in the last column, classify the balances according to the four aspects described in section 6.5, first paragraph.

The resulting balances are interpreted as:

1) Importance of detrital phase against carbonate and organic
2) Importance of organic against carbonate
3) distribution of Mg co-precipitation with carbonates (Mg calcite)
4) importance of organic decomposition by sulfur pathway
5) importance of albite in relation to detrital
6) importance of redox processes (Mn) against immobile Ti

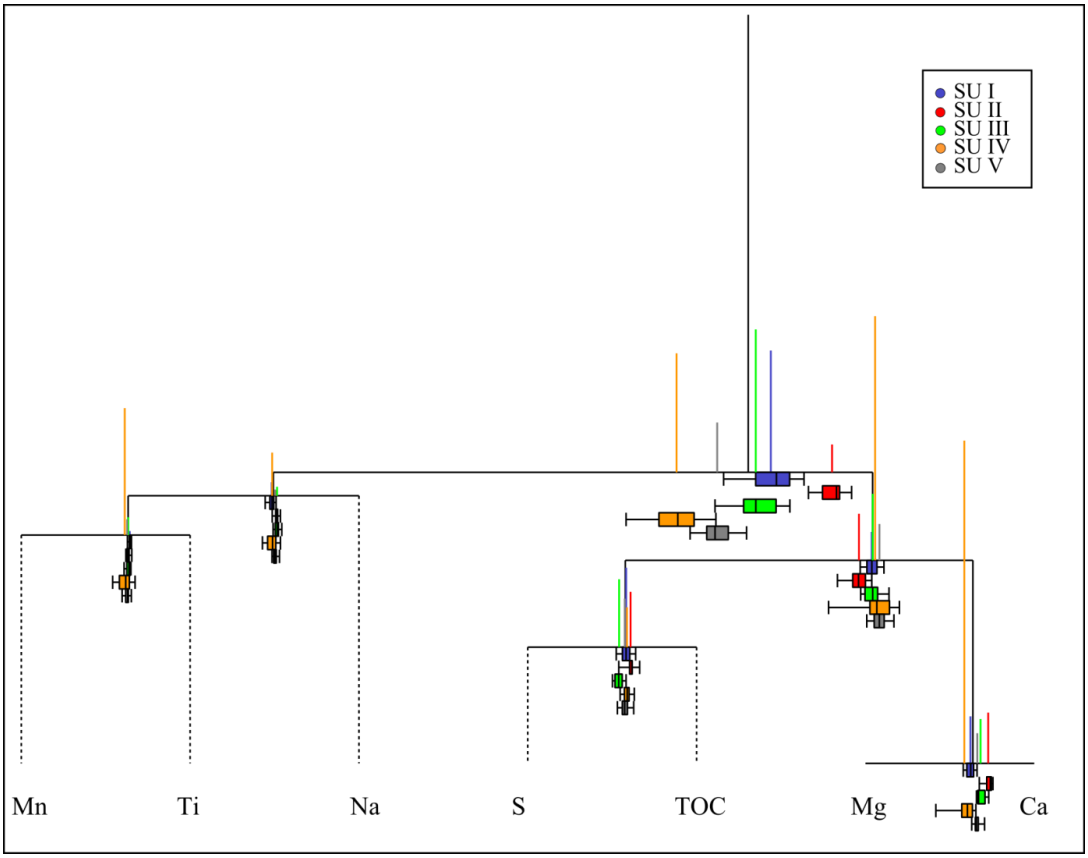

Balance dendogram for subcomposition (TOC, Na, Mg, S, Ca, Ti, Mn)

1.3.2.2 Trace Elements

Possible ilr binary partition for the data of trace element subcomposition (As, Rb, Sr, Y, Ba, Th, U)

balance	As	Rb	Sr	Y	Ba	Th	U	
b1	-1	-1	+1	-1	-1	-1	-1	(a)
b2	+1	-1	0	-1	-1	-1	+1	(a)
b3	-1	0	0	0	0	0	+1	(d)
b4	0	-1	0	-1	+1	-1	0	(c)
b5	0	+1	0	-1	0	-1	0	(b)
b6	0	0	0	-1	0	+1	0	(b)

The letters in the last column, classify the balances according to the four aspects described in section 6.5, first paragraph.

The resulting balances are interpreted as:

1) importance of carbonate phase against siliciclastic
2) organic/possibly redox against siliciclastic
3) As (possibly assoc. to sulfides) against U (mobile in oxic conditions)
4) Co-precipitation of Ba in carbonates in relation to siliciclastic

5 and 6) testing for geochemical immobility of selected detrital representatives

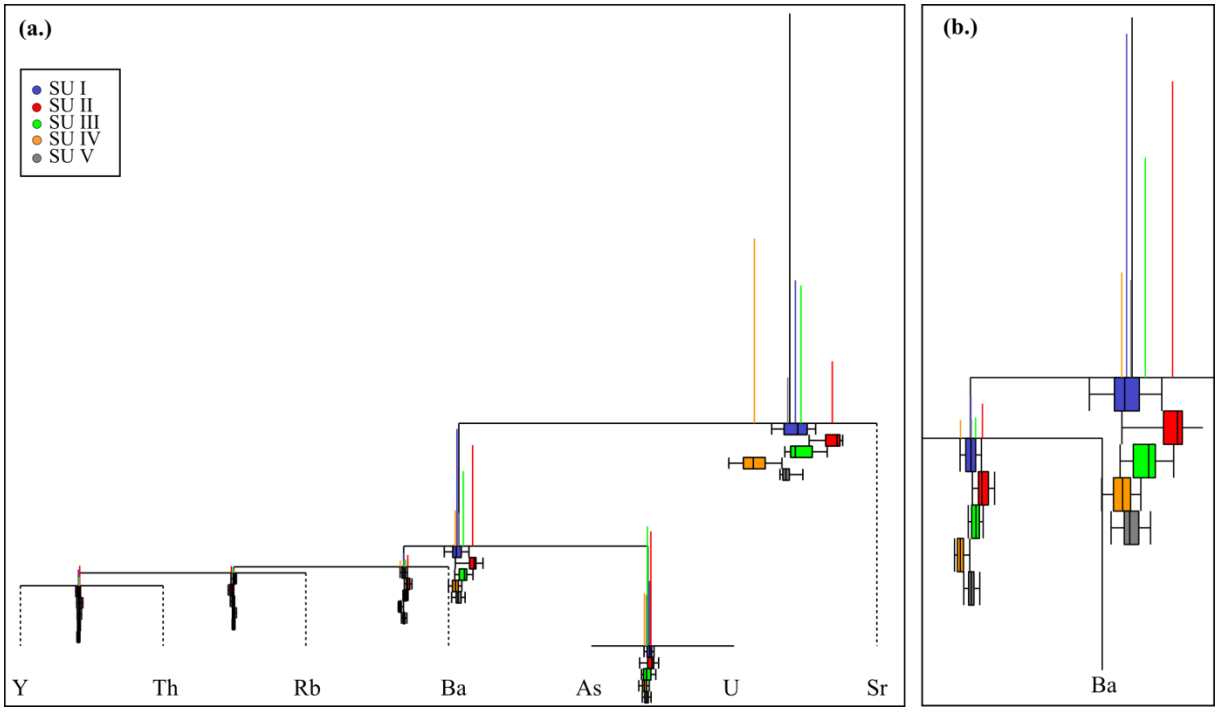

(a) Full balance dendogram for subcomposition (As, Rb, Sr, Y, Ba, Th, U) (b) zoom into balances b2 and b4

1.4 Bulk Mineralogy

1.4.1 Variation Matrix

Variation matrix for the subcomposition (quartz, calcite, aragonite, muscovite/illite, chlinoclore, kaolinite, albite). Bold values in blue fields highlight smallest variances. Reddish fields highlight high variances.

Variance ln(Xi/Xj)

Xi\Xj	Qz	Cal	Ara	M / I	Chli	Kao	Alb	clr variances
Quartz		0.4521	1.6841	0.0332	0.0258	0.0887	0.0282	0.0816
Calcite			1.3379	0.4627	0.4126	0.4749	0.4702	0.2671
Aragonite				1.6383	1.6089	1.3863	1.6447	1.0799
Musc. /Illite					0.0327	0.0579	0.0865	0.0815
Chlinoclore						0.0593	0.0611	0.0657
Kaolinite							0.1391	0.0665
Albite								0.0984

Total Variance **1.7407**

1.4.2 Balances

possible ilr binary partition for the data of major mineral composition (quartz, calcite, aragonite, muscovite/illite, chlinoclore, kaolinite, albite)

balance	Quartz	Calcite	Aragonite	Musc./Illite	Chlinoclore	Kaolinite	Abite	
b1	+1	+1	+1	-1	-1	-1	-1	(a)
b2	-1	-1	+1	0	0	0	0	(a)
b3	-1	+1	0	0	0	0	0	(c)
b4	0	-1	0	+1	+1	-1	-1	(b)
b5	0	0	0	+1	-1	0	0	(b)
b6	0	0	0	0	0	+1	-1	(b)

The letters in the last column, classify the balances according to the four aspects described in section 6.5, first paragraph.

Balances are interpreted as follows:

1) Importance of silicates, against carbonate and quartz
2) Importance of primary carbonate production (aragonite)
3) origin of calcite (detrital vs. chemically precipitated)
4) 2:1 clays against feldspar and 1:1 clay
5) K bearing against Fe and Mg bearing clay
6) Importance of weathering of alb into kao

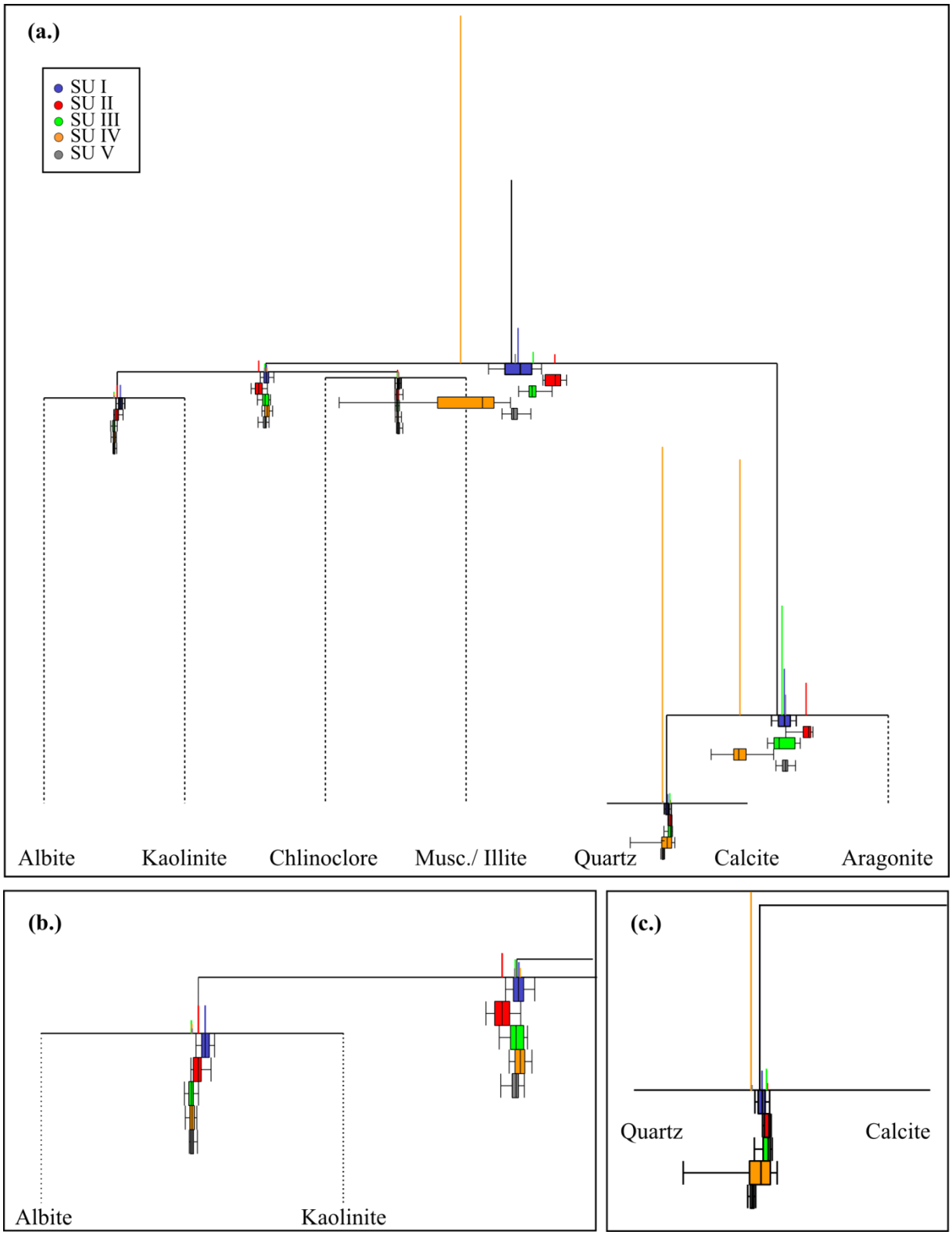

Figure 0.1: (a) full balance dendogram for the major mineral assemblage; (b) zoom into balances b4 and b6; (c) zoom into balance b3.